Liliana Patrícia dos Reis Teixeira

Master in Molecular Biotechnology

Unveiling *Geobacter sulfurreducens* electron transfer chain: probing the mechanisms of bacterial electricity production

Thesis submitted in partial fulfillment of the degree of Doctor of Philosophy in Radiation Biology and Biophysics

Adviser: Carlos Alberto Gomes Salgueiro, Associate Professor with Habilitation, Faculty of Science and Technology, University NOVA of Lisbon

Co-adviser: Marta Bruix Bayés, Full Research Professor, Rocasolano Institute of Physical Chemistry, Spanish National Research Council, Madrid

Examination Committee

Chairperson: Professor Paulo Manuel Assis Loureiro Limão-Vieira

Rapporteurs: Professor Douglas Vinson Laurents

Professor António Eduardo do Nascimento Ferreira

Members: Professor Pedro António de Brito Tavares

Professor Carlos Alberto Gomes Salgueiro

FACULDADE DE CIÊNCIAS E TECNOLOGIA
UNIVERSIDADE NOVA DE LISBOA

December, 2020

Universidade NOVA de Lisboa

Liliana Patrícia dos Reis Teixeira

Mestrado em Biotecnologia Molecular

Unveiling *Geobacter sulfurreducens* electron transfer chain: probing the mechanisms of bacterial electricity production

Dissertação para obtenção do Grau de Doutor em

Radiation Biology and Biophysics

Orientador: Carlos Alberto Gomes Salgueiro, Professor Associado com Agregação, Faculdade de Ciências e Tecnologia, Universidade NOVA de Lisboa

Co-orientador: Marta Bruix Bayés, Professor Catedrático, Instituto de Química-Física Rocasolano, Consejo Superior de Investigaciones Científicas, Madrid

FACULDADE DE CIÊNCIAS E TECNOLOGIA
UNIVERSIDADE NOVA DE LISBOA

Dezembro, 2020

Unveiling *Geobacter sulfurreducens* electron transfer chain: probing the mechanisms of bacterial electricity production

Agradecimentos

O trabalho realizado nesta teve envolveu a participação direta e indireta de várias pessoas às quais gostaria de agradecer.

Esta tese é dedicada especialmente ao Professor Doutor Carlos Salgueiro, um excelente profissional, um ótimo professor, um ainda melhor orientador e uma verdadeira inspiração. Sempre pediu o melhor de mim e fez-me querer primar pela perfeição. Obrigada por tudo o que me ensinou, por ter acreditado em mim e nas minhas capacidades, por nunca me ter deixado desistir e por ter sido mais do que um professor, por ter sido meu amigo. Obrigada por me ter dado a oportunidade de fazer o que mais gosto.

Obrigada à Professora Doutora Marta Bruix, por me ter recebido tão bem em Madrid, por me ter consigo integrar na perfeição num novo grupo, e por me ter dado o valor que nem eu acreditava ter. Obrigada por me ter cedido acesso ao RMN 800 Mz, que foi tão importante na realização de experiencias cruciais para a minha tese. Se algum dia conseguir alcançar metade da sua carreira, serei feliz.

À Professora Doutora Alice Pereia, ao Professor Doutor Pedro Tavares e ao Professor Doutor Paulo Limão-Vieira por me terem aceitado no Radiation Biology and Biophysics Doctoral Training Programme (RaBBiT) e por me terem ajudado sempre que precisei. Obrigada por terem acreditado em mim e por me terem dado oportunidade de fazer carreira na ciência.

À Doutora Cristina Cordas por me ter ensinado eletroquímica e por tanto ter contribuído na interpretação de resultados relativamente a este tema. Ao Doutor Raj Pokkuluri pelo trabalho na determinação da estrutura de raio-X dos mutantes do OmcF.

Obrigada à Doutora Leonor Morgado, por me ter passado tanto da sua experiência e sabedoria, por nunca recusar ajudar e por saber quando me chamar a atenção quando era preciso. Encontrei nela uma verdadeira amiga na qual eu sei que posso confiar tanto a nível profissional como pessoal.

Obrigada a todas as pessoas que passaram pelo Laboratório 611 que, de uma maneira ou de outra me ajudaram a tornar na profissional que sou hoje. Gostaria de fazer especial enfase às seguintes pessoas: Doutora Joana Dantas, obrigada por me teres ensinado tanto no primeiro ano da minha tese; Pilar Portela, obrigada por seres uma das pessoas mais inteligentes e bondosas que conheço; Tomás Fernandes, obrigada pela boa disposição, alegria e ensinamentos; Doutora Marta Silva e Doutora Ana Fernandes, obrigada por tudo o que me ensinaram; Marta Fonseca, obrigada por me teres aceitado como orientadora e me teres ensinado a ser uma melhor pessoa. Tenho muito a agradecer à Marisa Ferreira. Não só é uma ótima colega de trabalho, sempre pronta a ajudar e a colaborar, como se tornou uma grande amiga. Obrigada pelas nossas conversas de almoço, por me compreenderes, por trabalhares comigo e por me criticares quando é preciso.

Quero agradecer a todos os meus colegas do programa doutoral RaBBiT, por todo o companheirismo e diversão, em especial à Sara Gemelgo. Obrigada também aos meus colegas do Instituto de Química-Física "Rocasolano" no CSIC em Madrid, por me terem recebido tão bem.

À Faculdade de Ciências e Tecnologia da Universidade NOVA de Lisboa (FCT-UNL) que forneceu os recursos necessários para desenvolver este trabalho. Este trabalho foi financiado e suportado pelo Radiation Biology and Biophysics Doctoral Training Programme (RaBBiT, PD/00193/2012), pela Unidade de Ciências Biomoleculares Aplicadas – UCIBIO (UID/Multi/04378/2020) e pelo Centro de Física e Investigação Tecnológica - CEFITEC (UID/FIS/00068/2020). Agradeço à Fundação para a Ciência e Tecnologia pelo suporte e financiamento através da bolsa de doutoramento, PD/BD/114445/2016, e pelo projeto PTDC/BIA-BQM/31981/2017 (a CAS). Ao Laboratório de RMN da FCT-UNL, integrado na Rede Nacional de RMN (PTNMR) e financiado por FCT-MCTES (ROTEIRO/0031/2013 - PINFRA/22161/2016) co-financiado pelo FEDER através COMPETE 2020, POCI, e PORL e FCT através PIDDAC.

Aos meus amigos, que sempre me acompanharam por todas as etapas da minha vida, em especial à Rita Almeida, Cátia Santos e Sara Resende. Obrigada à minha família em especial aos meus pais, António e Idalina Teixeira. Obrigada por me apoiarem em tudo o que faço, por acreditarem sempre em mim, por fazerem tudo por mim e ficarem sempre orgulhosos de quem eu sou. Não seria metade do que sou sem os meus pais e sem o seu amor.

Por fim quero agradecer ao meu namorado, Flávio Mota, à pessoa que esteve comigo através de todo este processo. Quem me aturou nos meus piores momentos, que sempre esteve lá para me reconfortar. Por compreender as dificuldades e desafios do meu trabalho e por ter aceitado as repercussões que trouxe para as nossas vidas. Obrigada por ralhar comigo quando estava a trabalhar de mais ou quando sabia que eu podia fazer melhor. Obrigada.

Resumo

As bactérias do género *Geobacter* têm ganho interesse devido às suas aplicações biotecnológicas e de biorremediação. Espécies como a *G. sulfurreducens* são capazes de produzir bioenergia e de remover contaminantes de águas poluídas. *G. sulfurreducens* transfere eletrões para aceitadores extracelulares, num processo denominado por transferência extracelular de eletrões, e também aceita eletrões de elétrodos. De modo a obter melhor rendimento das suas aplicações, é necessário entender os mecanismos e as proteínas envolvidas nestes processos. O genoma da *G. sulfurreducens* codifica para mais de 100 citocromos do tipo *c*, sendo estes os principais intervenientes na transferência de eletrões. Nesta tese, alguns dos citocromos codificados por esta bactéria foram estudados: OmcF, citocromo monohémico localizado na membrana externa, PpcA, citocromo trihémico localizado no periplasma, e PccH e GSU2515, ambos citocromos monohémicos localizados no periplasma.

Espectroscopia por ressonância magnética nuclear (RMN) foi usada na atribuição dos sinais da cadeia polipeptídica e das cadeias laterais do OmcF, no estado oxidado. Estes resultados foram usados em interações moleculares com o PpcA. Apesar dos resultados das interações não serem conclusivos, a atribuição dos sinais do OmcF constitui um importante passo para determinar parceiros redox desta proteína.

O estudo eletroquímico do OmcF foi obtido através de experiências de voltametria cíclica. Ao construir estrategicamente mutantes, analisando os respetivos espectros de RMN e determinando o seu potencial redox, foi também possível determinar o centro redox-Bohr do OmcF.

Espectroscopia por RMN foi utilizada para atribuir os sinais da cadeia polipeptídica, cadeias laterais e do heme do PccH, no estado oxidado.

O citocromo GSU2515 foi caracterizado bioquímica e estruturalmente, usando técnicas como dicroísmo circular, titulações redox, espectroscopia de UV-visível e RMN. Os resultados das interações moleculares por RMN entre GSU2515 e PccH, indicam ser possível estes citocromos serem parceiros fisiológicos.

Os resultados obtidos contribuem para a compreensão dos mecanismos de transferência eletrónica da bactéria *G. sulfurreducens*.

Palavras-chave: citocromos, transferência extracelular de eletrões, ressonância magnética nuclear, eletroquímica.

Abstract

Geobacter bacteria have been gaining attention due to their biotechnological and bioremediation applications. Species like *G. sulfurreducens* are capable of bioenergy production and removal of contaminants from wastewaters. *G. sulfurreducens* is capable of transferring electrons towards extracellular acceptors, in a process called extracellular electron transfer, and it is also capable of accepting electrons in current consuming biofilms. In order to take full advantage of their applications, it is necessary to understand the mechanisms and the proteins involved in these processes. *G. sulfurreducens* genome encodes for more than 100 *c*-type cytochromes, being these the main intervenient in the electron transfer. In this thesis, some of the cytochromes encoded by this bacterium were studied: OmcF, and outer-membrane monoheme cytochrome, PpcA, a thriheme periplasmatic cytochrome, and PccH and GSU2515, both monoheme cytochromes localized at the periplasm.

Using Nuclear Magnetic Resonance (NMR) was possible to assign the backbone and side-chain of OmcF in the oxidized state, and use these results to perform molecular interactions with PpcA. Although the results of the interaction were inconclusive, the assignment of OmcF constitutes an important step to find putative redox partners of this protein.

Using cyclic voltammetry, an electrochemical study was performed on OmcF. Furthermore, by constructing strategic mutants, analyzing their NMR spectra and determining their redox potential, was possible to determine the redox-Bohr center of OmcF.

NMR spectroscopy was also used to assign the backbone, side-chain and heme substituents of PccH in the oxidized state.

A biochemical and structural characterization of cytochrome GSU2515 was carried using circular dichroism, visible redox titrations, UV-visible, and NMR spectroscopy techniques. By performing NMR molecular interactions between GSU2515 and PccH, there is a strong indication that these two cytochromes are physiological partners.

The results obtained contribute to a better understanding of the electron transfer mechanisms of *G. sulfurreducens*.

Keywords: cytochromes, extracellular electron transfer, nuclear magnetic resonance, electrochemistry

Table of contents

List of figures

1. Introduction

2. Fundaments of Nuclear Magnetic Resonance Electrochemistry

3. Backbone and side-chain assignment of the cytochrome OmcF in the oxidized state

4. Thermodynamic and kinetic properties of OmcF

5. Backbone, side-chain and heme assignment of cytochrome PccH in the oxidized state

6. Characterization of cytochrome GSU2515

7. Future perspetives

A. Appendix

List of tables

A. Appendix

Abbreviations, Symbols and Constants

1D	One dimensional
2D	Two dimensional
2xYT	2x Yeast extract – tryptone
3D	Three dimensional
A	Electrode area
AH_2QDS	Anthrahydroquinone-2,6-disulphonate
Amp	Ampicillin
AQDS	Anthraquinone-2,6-disulphonate
B_0	External magnetic field
BLAST	Basic Local Alignment Search Tool
BMRB	Biological Magnetic Resonance Data Bank
bp	Base-pair(s)
C	Concentration
CD	Circular dichroism
D	Diffusion coefficient of the electroactive species
d1, d2	Delay
DIPSI	Decoupling in the presence of scalar interactions
DNA	Deoxyribonucleic acid
dNTPs	Deoxynucleotides
DSS	4,4-dimethyl-4-silapentane-1-sulfonic acid
ΔE	Energy difference
E. coli	*Escherichia coli*
E_{app}/ E^0	Macroscopic apparent midpoint reduction potential
EDTA	Ethylenediaminetetraacetic acid
EMBL-EBI	European Bioinformatics Institute
E_p	Peak potential
FID	Free Induction Decay
FT	Fourier transformation
ΔG^o	Gibbs free energy
Gmet, GM, *G. metallireducens*	*Geobacter metallireducens*
GP, *G. pickeringii*	*Geobacter pickeringii*
GSU, GS, *G. sulfurreducens*	*Geobacter sulfurreducens*
ΔH°	Enthalpy
HMQC	Heteronuclear Multiple Quantum Coherence

HSQC	Heteronuclear Single Quantum Coherence
I	Spin quantum number
Imc	Inner membrane cytochrome
I_p	Peak current
IPTG	Isopropyl β-D-thiolgalactopyranoside
IUPAC-IUB	International Union of Pure and Applied Chemistry – International Union of Biochemistry
J	Coupling constant
k_o	Kinetics of the electrode reaction
k_d	Transport of species
K_d	Dissociation constant
KEGG	Kyoto Encyclopedia of Genes and Genomes
k_{sh}	Heterogeneous rate constant
LB	Luria Bertani
m	Magnetic quantum numbers
M	Magnetization
M. braunii	*Monoraphidium braunii*
Mac	Membrane associated cytochrome
MALDI-TOF	Matrix-assisted laser desorption-ionization time-of-flight
ME	Microbial electrosynthesis
MFC	Microbial fuel cells
MQ/MQH_2	Menaquinone/ menaquinol
NADH	Nicotinamide adenine dinucleotide
NaPi	Sodium phosphate buffer
NCBI	National Center for Biotechnology Information
NHE	Normal Hydrogen Electrode
NMR	Nuclear Magnetic Resonance
NOE	Nuclear Overhauser Effect
NOESY	Nuclear Overhauser Effect SpectroscopY
OD	Optical Density
Oma	Outer-membrane associated
Omb	Outer-membrane barrel
Omc	Outer-membrane cytochrome
PCR	Polymerase Chain Reaction
PDB	Protein Data Bank
pI	Isoelectric point

Ppc	Periplasmic cytochrome
ppm	Parts per million
rmsd	Root mean square deviation
rpm	Rotations per minute
ΔS°	Entropy
S. obliquus	*Scenedesmus obliquus*
SDS-PAGE	Sodium dodecyl sulfate – polyacrylamide gel electrophoresis
t	Evolution time
T	Temperature
T_1	Longitudinal spin-lattice relaxation time
T_2	Transversal spin-lattice relaxation time
T_m	Melting temperature
TMS	Tetramethylsilane
TOCSY	TOtal Correlation SpectroscopY
Tris	Tris(hydroxymethyl)aminomethane
UV	Ultraviolet
V	Volume
v	Scan rate
v_i	Stoichiometric numbers of species
vs	*versus*
μ	Magnetic moment
δ	Chemical shift
γ	Gyromagnetic ratio
ω	Angular frequency
υ	Larmor frequency
σ	Shielding constant
σ_0^{corr}	Standard deviation to zero value
τ_m	Mixing period
α_i	Chemical activity of the species
F	Faraday constant (96 485 C mol^{-1})
h	Planck constant ($6.63x10^{-34}$ m^2 kg s^{-1})
k_B	Boltzmann constant ($1.38x10^{-23}$ m^2 kg s^{-2} K^{-1})
R	Molar gas constant (8.314 J K^{-1} mol^{-1})
w_i	Constant that compensates the scaling differences between ^1H and ^{15}N shifts (0.102)

Amino Acid Abbreviations

Alanine	Ala	A
Arginine	Arg	R
Asparagine	Asn	N
Aspartate	Asp	D
Cysteine	Cys	C
Glutamate	Glu	E
Glutamine	Gln	Q
Glycine	Gly	G
Histidine	His	H
Isoleucine	Ile	I
Leucine	Leu	L
Lysine	Lys	K
Methionine	Met	M
Phenylalanine	Phe	F
Proline	Pro	P
Serine	Ser	S
Threonine	Thr	T
Tryptophan	Trp	W
Tyrosine	Tyr	Y
Valine	Val	V

Nucleobases Abbreviations

Adenine	a
Thymine	t
Cytosine	c
Guanine	g

1. Introduction

1.1 The exoelectrogens bacteria

Environmental problems are one of the biggest concerns nowadays. Naturally, a lot of research is directed into alternative and renewable energy sources, in opposition to fossil energy that has major consequences in global warming. Dissimilatory metal reducing bacteria have been pinpointed as viable alternatives for environmental biotechnological applications.

Dissimilatory metal reduction can be conducted by a group of microorganisms that are capable of coupling their oxidative metabolism to the reduction of extracellular electron acceptors [1]. This process is unlike other respiratory pathways since the final electron acceptor is not a freely diffusible gas (as is the case O_2) or a soluble molecule that is reducible in the cell interior. These bacteria are of great importance in anaerobic environments, being crucial in the biogeochemical cycles of some metals as iron, manganese, uranium and chromium [2]. Some of these microorganisms, denominated as exoelectrogens, can even couple their oxidative metabolism to the electron transfer toward electron surfaces. Organisms such as *Geobacter sulfurreducens*, *Geobacter metallireducens*, *Shewanella putrefaciens*, *Shewanella oneidensis*, *Desulfuromonas acetoxidans*, *Desulfobulbus propionicus*, *Rhodoferax ferrireducens*, *Enterococcus gallinarum*, among others, [3] are exoelectrogens.

Exoelectrogens have important biotechnological and bioremediations applications that are being explored in bioelectrochemical systems. These bioengineering technologies use microorganisms, or other bio-based catalysts, combined with a bioelectrochemical methods [4]. Bioelectrochemical systems such as microbial fuel cells (MFCs) and microbial electrosynthesis (ME) have been gaining a lot of attention due to their green and sustainable features [5].

Electric current can be harvested from the electron flow from the intracellular carriers to the exoelectrogens' exterior, where the acceptors are localized. This process is called extracellular electron transfer and is the basis of MFCs functioning [6]. These devices use bacteria as biocatalysts to generate current by oxidizing organic and inorganic matter. The electrodes are usually immersed in a solution or even wastewater, which contains all the reactants and products necessary. This way, MFCs couple the production of electric current with the treatment of wastewater, being this technology self-sustainable or even with a net positive energy output [6] [7].

The electrons in MFCs, which are produced by bacterial oxidation of nutrients, are transferred to the anode by direct contact through nanowires, outer membrane proteins and/or mediated by electron shuttles. Simultaneously, protons are also produced and migrate through a proton exchange membrane into the cathodic chamber. Electrons flow through an external circuit from the anode to the cathode, where they react with oxygen and protons to produce water [6] [8]. A schematic representation of a MFC is represented in Figure 1.1. *Geobacter* and *Shewanella* species have remarkable extracellular electron transfer mechanisms, which are explored in MFC

[9]. To date, pure cultures of *G. sulfurreducens* produced the highest power density levels in MFC than any other known microorganism, being the most promising exoelectrogens for biotechnological application [10].

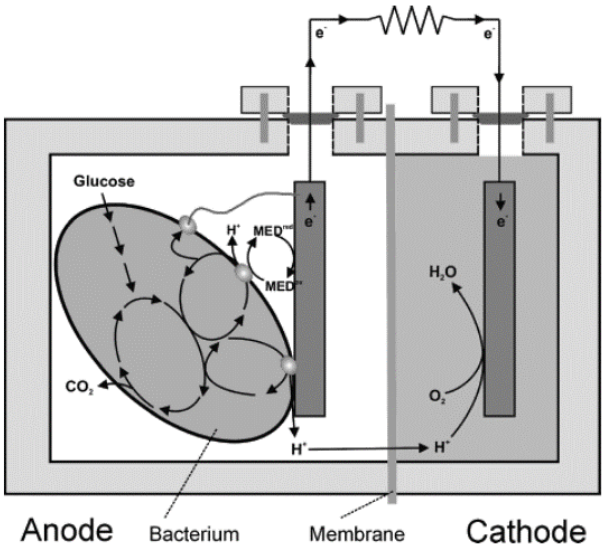

Figure 1.1 - Schematic representation of the operating principles of a microbial fuel cell. The elements are not to scale. The bacteria culture is in the anode compartment, where it transfers electrons to the electrode through direct contact, nanowires or mobile shuttles. The electrons flow from the anode, through an external resistance, to the cathode where they react with the final electron acceptor. Protons migrate through the cation exchange membrane from the anode to the cathode. Figure adapted from [6].

ME is an emerging green technology that explores the capability of a particular group of microorganisms to drive their metabolism toward the production of hydrogen or value-added chemicals from electrons supplied by electrode surfaces. Contrary to MFCs, ME takes advantage of the electron transfer from electrodes to the cell interior, a process with different mechanisms involved. In fact, the process of this technology is opposite to MFC, since the electrons are supplied to the microorganisms through the cathode [11] [12].

In ME, the reducing power is provided by an electrode, maintained at an enough negative electrochemical potential, and used by microorganisms in current-consuming biofilms. It is an extremely promising novel technology, since it is considerably less energy demanding, utilizes non-hazardous chemicals and it is a self-renewable and low-cost method for hydrogen production, for example. Electron transfer from electrodes has been mostly studied in *G. sulfurreducens* and *S. oneidensis* bacteria, being these microorganisms the most promising for this biotechnological application [11] [12].

Despite their advantages, the reliability and efficiency of MFC and ME cells are still low. The scale-up issue can be overcome by improving the architecture, electrodes and materials which constitutes these devices [13]. A biotic approach can be as well explored, which includes the selective adaptation of species [14], synthetic biology [15], and engineering of proteins involved in the electron transfer processes of exoelectrogens. Due to the promising potential of *G.*

sulfurreducens for biotechnological applications, it is crucial to functionally and biochemically characterize the proteins involved in the electron transfer mechanisms of these bacteria.

1.2 The *Geobacter sulfurreducens* bacteria

The *Geobacteraceae* family are a group of Gram-negative bacteria which belong to the *Desulfuromonadales* order in the *δ*-proteobacteria class. *Geobacteraceae* members are well-known exoelectrogens microorganisms capable of extracellular respiration toward electron acceptors that are unable to pass the outer membrane [16]. *Geobacteraceae* microorganisms are important agents in natural biogeochemical cycles and are commonly found in sediments where Fe(III) and Mn(IV) reduction is essential [17]. They are also important bioremediation agents, since they can reduce and precipitate radionuclides or toxic metals, such as U(VI), Cr(VI) or Co(III) [18]. These microorganisms also have the ability to couple the oxidation of organic matter to electricity production [19] [20]. Additionally, they generate energy by using metal ion-mediated electron transport to oxidize organic compounds to CO_2. Furthermore, *Geobacteraceae* microorganisms have the potential to interact with syntrophic partners via direct interspecies electron transfer and interspecies hydrogen transfer. In fact, it was discovered that co-cultures of *G. sulfurreducens* and *G. metallireducens* form aggregates that are electrically conductive [21]. Altogether, these extracellular respiration mechanisms opened new routes to be explored for practical biotechnological applications in the bioremediation and bioenergy fields [17] [18].

Currently, 19 species of *Geobacter* are known, being the most studied ones *G. sulfurreducens* and *G. metallireducens*. Although *G. metallireducens* was the first member of *Geobacter* to be isolated in 1987 [22] [23], *G. sulfurreducens* is the best studied species. It was firstly isolated in 1994 from surface sediments of a hydrocarbon-contaminated ditch in Oklahoma, United States of America [24]. Its genome was sequenced in 2003 [25] and a genetic system was fully developed [26]. For these reasons, *G. sulfurreducens* is considered to be a model organism for the *Geobacteraceae* family.

G. sulfurreducens is a rod-shaped bacterium, with 2 to 3 μm in length and is 0.5 μm wide. At first, it was considered to be a strict anaerobic, however analysis of its genome indicated oxidative capacity, since it codes for proteins involved in response to oxidative stress [25]. It has respiratory versatility, since it can use acetate, lactate, formate, anthrahydroquinone-2,6-disulphonate (AH_2QDS) or hydrogen as electron donors. Its electron acceptors are, to name a few, fumarate, sulphur, malate, malate, Co(III), Cr(VI), Mn(IV) oxides, Fe (III), U(VI), Tc(VII) and anthraquinone-2,6-disulphonate (AQDS) [18] [27].

The genome of the bacterium *G. sulfurreducens* encodes for 111 *c*-type cytochromes from which 73 are multiheme. Most of these cytochromes have been proved to be electron transport

proteins. Cytochromes were predicted and some proven to be localized in the periplasm, inner- and outer-membrane, ensuring the extracellular electron transfer of the bacteria [25].

1.3 Cytochromes

Cytochromes are a type of proteins involved in various biological functions that contain one or more iron-porphyrin complexes, known as heme. Their functions include electron transfer reactions, oxygen transport, storage, oxygenation of organic substrates, reduction of peroxides, gas sensing and gene regulation. These functions can be further extended when the heme groups are combined with co-factors, such as flavins or other metal ions (molybdenum and copper). This confers cytochromes the ability to couple electron transfer with other molecular processes [28] [29].

Cytochromes can be divided into different categories (represented by an italic letter), according to their heme substituents. Cytochromes are also divided into sub-categories (represented by a subscript number) which depend on their axial ligands' coordination, number of heme groups, optical and functional activities, structure and redox potential. The classifications are attributed progressively upon new characterization [30]. Cytochromes are classified into several categories, being the *b*-type the most common, from which is thought all the other heme types are derived [31] [32]. The *b*-type heme is not covalently connected to the polypeptide chain and its spatial localization is dependent on the interaction with the neighboring amino acid residues [33].

Cytochromes *c* are among the most studied type of proteins and are mainly involved in aerobic and anaerobic respiration in various life forms. A *c*-type heme is constituted by a protoporphyrin IX ring with an iron atom in the center, coordinated by four nitrogen atoms of the ring (Figure 1.).

The polypeptide chain of the cytochrome *c* binds covalently to one or more *c*-type hemes through two thioether bonds with the sulfydryl groups of two cysteine residues. The heme is additionally axially coordinated through a histidine side chain (Figure 1.2). These amino acids constitute a signature for heme attachment which is a highly conserved motif, Cys-X-X-Cys-His, where XX represents any amino acid (except for cysteine) and its length is variable. Besides the two cysteines and histidine, the heme has another ligand which is, in most cases, a methionine for monoheme cytochromes, or a histidine in the case of multiheme cytochromes. In the case of methionine as the axial ligand, the ligation atom is a sulphur, and in the case of a histidine the ligation is through a nitrogen. Asparagine and tyrosine are less common, or the distal axial ligand can even be absent [30] [29].

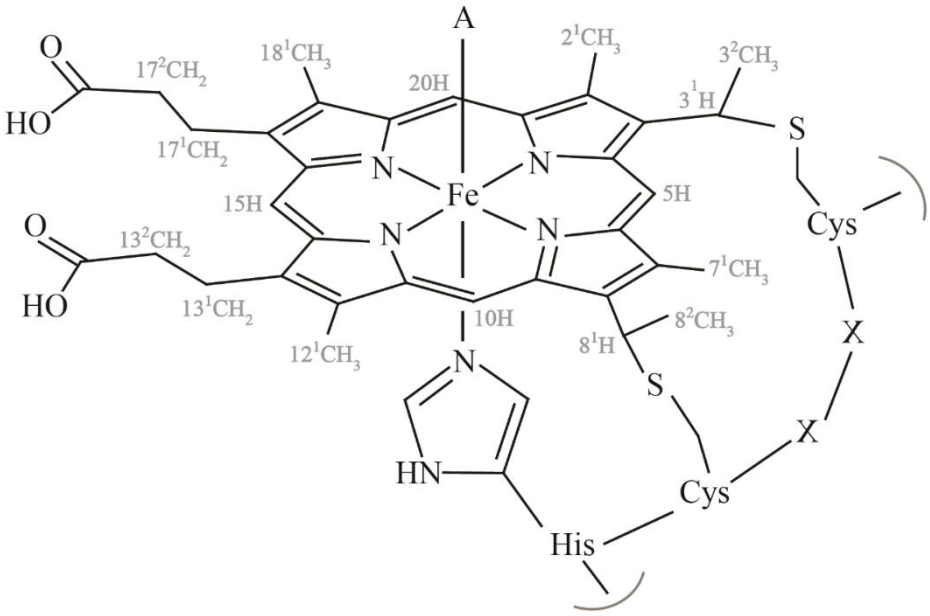

Figure 1.2 – Schematic representation of a *c*-type heme and its respective polypeptide binding motif (Cys-X-X-Cys-His). A represents the distal axial ligand. The heme substituents are labeled in grey according to the IUPAC-IUB nomenclature [34]. Image reproduced from [35].

The iron (0) is a transition metal with 26 electrons arranged in the following electron configuration: $1s^2 2s^2 2p^6 3s^2 3p^6 3d^6 4s^2$, also represented as $[Ar]3d^6 4s^2$. s, p and d represent the orbitals, the superscript numbers represent the electron occupancies, and the [Ar] is to emphasize the occupancy of the higher energy orbitals. Orbitals 3d and 4s are the ones with higher energy and determine the electronic properties and the chemical behavior of the iron. In *c*-type cytochromes iron exists in two oxidation states, the ferrous (reduced) and ferric (oxidized) states, that are represented as Fe(II): $[Ar]3d^6 4s^0$ and Fe(III): $[Ar]3d^5 4s^0$, respectively [33]. The main function of *c*-type cytochromes is to transfer electrons, by cycling between its two oxidation states.

The electronic properties and chemical characteristics of the iron are dependent on the electron distribution in its five 3d orbitals: two orbitals with higher energy (e_g) and three orbitals with lower energy (t_{2g}). Each of its 3d orbitals can be occupied up to two electrons. The energy separation between the higher and lower energy orbitals is influenced by the ligands which coordinate the iron at the heme [33].

The crystal field theory states that the bonding between the iron and the ligands is entirely electrostatic [36]. The electron distribution is dependent on the d-orbital splitting energy and on the pairing energy of electrons. In the case of a weak crystal field, the iron is in the high-spin state because the d-orbital splitting is smaller than the pairing energy and, consequently, the electrons remain mostly unpaired in the orbitals. This occurs when the heme iron bounds to an asparagine, lysine, tyrosine or a water molecule. In the case of a strong crystal field, the d-orbital splitting is

larger than the pairing energy, causing the electrons to enter the lower energy orbitals and pair to yield the low spin state. This occurs when the axial ligands are a methionine or a histidine [33].

Cytochrome *c* can be divided into four general classes, from I-IV. Class I are characterized by having the heme-attachment site near the N-terminus and the heme are axially coordinated by a histidine and a methionine. Class II cytochromes have the heme-attachment site closer to the C-terminus and include both high and low spin hemes. Class III includes the multiheme cytochromes axially coordinated by two histidine. Finally, Class IV includes cytochromes which have prosthetic groups other than the heme [37].

1.4 Extracellular electron transfer

The high number of *c*-type cytochromes that *G. sulfurreducens* can produce indicates unmistakably their importance in the electron transport and suggests flexibility and redundancy in the electron transfer networks [25] [38]. The genome of *G. sulfurreducens* encodes for 73 multiheme cytochromes, a much higher number than monoheme cytochromes. The main advantage of having a high content of multiheme cytochromes is to provide the cell with a high electron storage capacity. Furthermore, it allows electron transfer through large distances without various physiological partners and binding events. Typically, the heme groups of these cytochromes are arranged along the polypeptide chain, with no more than 16 Å distance between them, allowing a fast electron exchange [39] [40]. In contrast to monoheme cytochromes, they can receive or give various electrons simultaneously [41]. Due to the typical His-His coordination of the hemes in multiheme cytochromes, whereas in monoheme the His-Met coordination is more abundant, their redox potential are generally lower [42]. Additionally, they cover higher redox potential ranges due to the distinct heme redox potential values. Only a few monoheme cytochromes from *G. sulfurreducens* have been studied but their structural and functional characterization is also important for the fully understanding of the electron transfer chains.

The most common methodologies to identify the proteins involved in the different electron transfer pathways of *G. sulfurreducens* is through gene knockout studies and proteomic analysis under different cell's growth conditions. The current model for the extracellular electron transfer pathway of *G. sulfurreducens* is depicted in Figure 1.3.

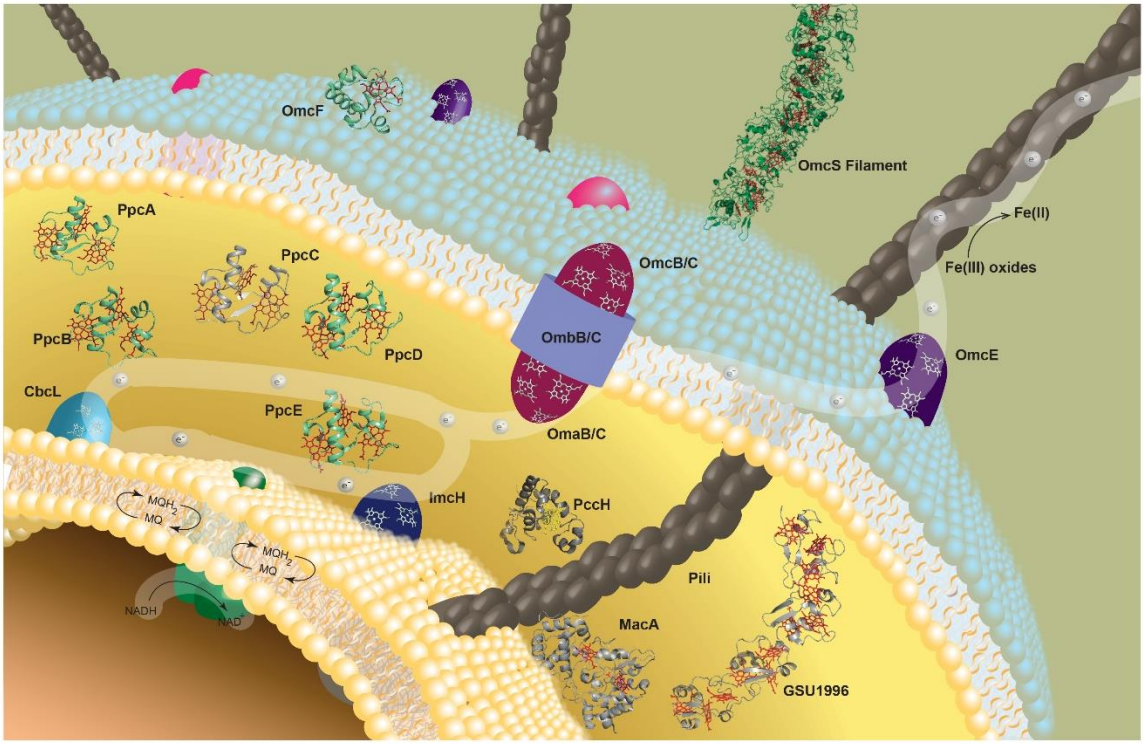

Figure 1.3 – Model for the extracellular electron transfer pathway of *G. sulfurreducens.* The flow of electrons is represented in white, passing from the menaquinol/menaquinone pool to either CbcL or ImcH, in the inner membrane. Then, the electrons pass to GSU1996 (PDB code 3OV0 [43]), MacA (PDB code 4AAL [44]), and the PpcA family in the periplasm [PpcA (PDB code 1OS6 [45]), PpcB (PDB code 3BXU [46]), PpcC (PDB code 3H33 [47]), PpcD (PDB code [47]) and PpcE (PDB code 3H34 [47]). Electrons are then transported through the porin-cytochrome trans-outer membrane complexes, OmaB-OmbB-OmcB or OmaC-OmbC-Omc, to the outer membrane cytochromes as OmcF (PDB code 3CU4 [48]), OmcE and OmcZ. The OmcS (PDB code 6EF8 [49]) filaments and Pili are also represented, which transfer electron through large distances. PccH (PDB 4RLR [50]) is also represented, cytochrome involved in electron transfer from electrodes.

In this model, electrons resultant from the oxidation of nutrients at *G. sulfurreducens* cytoplasm are transferred through a group of cytochromes towards terminal electron acceptors. The model postulates that the electrons from nicotinamide adenine dinucleotide (NADH) are transferred to a menaquinone/menaquinol (MQ/MQH_2) pool via an NADH dehydrogenase located at the inner membrane [35]. This dehydrogenase converts the NADH to its oxidized form (NAD^+) by the loss of electrons. Quinones are hydrophobic molecules that move freely along the membrane, and are able to receive or donate one or two electrons [51].

Initially it was thought that MacA (GSU0466) of *G. sulfurreducens*, a diheme inner membrane associated *c*-type cytochrome, important in the reduction of Fe(III) and U(VI) oxides, would be involved in the electron transport from the inner membrane to the periplasm [52] [53]. However, it was recently found that *G. sulfurreducens* uses at least two different pathways to transport electrons out of the inner membrane quinone pool before reducing acceptors beyond the outer membrane: the CbcL-dependent pathway operating with acceptors at or below redox potentials of -100 mV (*vs* the normal hydrogen electrode, NHE) and the ImcH-dependent pathway

operating above this value [54] [55]. CbcL (GSU0274) is constituted by a HydC/FdnI diheme cytochrome *b*, connected to a nine-heme cytochrome *c* [55]. ImcH (GSU3259) contains up to three transmembrane helices, a NapC/NirT homology region, and up to seven-heme cytochrome *c* [54]. The most likely role of MacA is to act as a peroxidase and it is capable of electrochemically mediate electron transfer to triheme periplasmatic cytochromes [56].

From CbcL or ImcH, electrons are transferred to a family of triheme *c*-type cytochromes composed of five members: PpcA (GSU0612), PpcB (GSU0364) 77%, PpcC (GSU0365) 62%, PpcD (GSU1024) 57% and PpcE (GSU1760) 65%. This family, that has an amino acid identity in the range of 57-77 %, is important in the reduction of Fe(III) and UV(VI) and are likely electron reservoirs [57]. This family, denominated as PpcA family, is one of the most conserved cytochromes among *Geobacter* species. In the case of *G. metallireducens*, the PpcA family is constituted by the following cytochromes: PpcA (Gmet2902) 80%, PpcB (Gmet3166) 72%, PpcC (Gmet3165) 79%, PpcE (Gmet1846) and PpcF (Gmet0335) 69%. The percentage of identity presented is between the cytochromes of *G. metallireducens* and their homologous in *G. sulfurreducens*. Since the degree of homology between the PpcD from *G. sulfurreducens* is very low in comparison with the other PpcA-family members of *G. metallireducens*, the fifth cytochrome was denominated as PpcF [58]. Due to their homology, it is thought that the family has the same function in both species.

At the periplasm is also located the twelve-heme *c*-type cytochrome GSU1996, which is composed by four similar triheme domains (A-D). This nanowire was proposed to be an electrically conductive element [43] [59].

The electrons pass from the cytoplasm to the cell's exterior through porin-cytochrome trans-outer membrane complexes that provide a heme conduit for continuous electron transfer across the outer membrane. These complexes are composed by three subunits: OmaB/OmaC are eight-heme cytochrome *c* localized in the periplasm; OmbB/OmbC are porin-like β-barrel membrane-integrated proteins; and OmcB/OmcC which are dodecaheme cytochrome *c* localized in the cell surface. It is proposed that OmbB/OmbC serve as a sheath through which OmaB/OmaC and OmcB/OmcC might be inserted [60]. These complexes have shown direct involvement in Fe(III) citrate and ferrihydrite reduction [61].

Finally, the electrons reach the outer membrane cytochromes localized at the cell exterior, as is the case of: OmcF (GSU2432), OmcE (GSU0618), OmcS (GSU2504) and OmcZ (GSU2076). OmcF is a monoheme cytochrome *c* involved in Fe(III) reduction and current production [48] [62]. OmcE is a tetraheme cytochrome *c* important in Fe(III) oxide reduction [63]. OmcS, a six-heme *c*-type outer membrane cytochrome with bis-histidine axial coordination, is involved in extracellular electron transfer to insoluble electron acceptors [49] [63] [64]. Additionally, it was discovered that OmcS, is able to polymerize and form electrically conductive filament. These nanowires are able to transport electrons to remote electron acceptors [49]. OmcZ

is an eight-heme cytochrome *c* involved in electron transfer current producing biofilms [65]. Most recently it was discovered that OmcZ forms oligomers, that also constitute nanowires with higher conductivity than the ones formed by OmcS [66] [67]. Furthermore, OmcZ was hypothesized to transiently bind to riboflavin, which shuttles electrons to extracellular substrates [68]. In addition to OmcS and OmcZ filaments, PilA (GSU1496) a non-cytochrome protein can form fibers, constituting electrically conductive Pili [69]. Both Pili and cytochrome OmcS are also involved in interspecies electron transfer, such as to *G. metallireducens* [70].

The previously described model proposes a possible flow of electrons from the cell interior to electrodes. Electron transfer can also occur in the reverse direction in *G. sulfurreducens* [71]. Until now, the only unequivocally known player in the electron transfer from electrodes is the periplasmic monoheme *c*-type cytochrome PccH (GSU3274). In fact, the absence of PccH inhibits the ability of *G. sulfurreducens* to accept electrons from electrodes [71]. Furthermore, *pccH* is the highest transcript gene when cells were grown using a graphite cathode as the only electron donor and fumarate [71].

Another monoheme *c*-type cytochrome proposed to be involved in the electron transfer from electrodes was designated as cytochrome GSU2515. Although its involvement in the process is yet to be proven, it is the second most expressed *c*-type cytochrome in current-consuming cells [71].

Cytochromes are not only involved in the electron transfer processes of *G. sulfurreducens*. In fact, *c*-type cytochromes such as GSU0582 and GSU0935 are involved in signaling responses, which are mechanisms that couple environmental stimuli to adaptive responses. GSU0582 and GSU0935 are the most studied sensors, they contain one *c*-type heme group and are part of the methyl accepting chemotaxis proteins [72] [73]. However, these bacteria encode for ten signal transduction proteins, mainly located in the periplasm and with at least one *c*-type heme [25] [74].

In this section it has been referred some of the proteins from *G. sulfurreducens* that have already been identified and characterized in more detail. However, there are still a considerable number of proteins whose function and structures are still yet to be elucidated. Not only is important to characterize functionally and structurally the already identified cytochromes, but also to pinpoint all the proteins involved in the electron flow, including their physiological partners. Only then the extracellular electron transfer can be fully understood and assist the selection of target proteins for improved electron transfer rates.

1.5 Structural and thermodynamic characterization of *G. sulfurreducens* cytochromes

Nuclear magnetic resonance (NMR) and X-ray crystallography are the most used techniques to determine the tertiary structure of biological molecules, inclusively for the *c*-type cytochromes. However, due to the intrinsic characteristics of these molecules, both techniques have their setbacks. Due to the presence of heme groups and the iron properties, the polypeptide chain signals are broadened and deviated from their typical position in the NMR spectrum, an effect that is aggravated in the oxidized state and for multiheme cytochromes. These characteristics complicate the assignment of the NMR signals and consequently the structural determination. Another setback of NMR structural determination is that proteins must be isotopically produced, a methodology that has been improved lately but is still a limiting step due to the low production yields. For these reasons, most of the cytochrome's structures deposited in the Protein Data Bank (PDB: http://www.rcsb.org/pdb/) were determined by X-ray crystallography, and the ones determined by NMR were mostly acquired in the reduced state. Nevertheless, the structure determined by X-ray crystallography represents the average over molecules arranged in a periodic crystal lattice, whereas with NMR spectroscopy the structure is the average over oriented molecules in solution, which conditions are more similar to the physiological environment of the biomolecules. Advantageously, the solution structure provides information about the internal motions and dynamics of the protein and allows determining interaction regions with possible physiological partners.

PpcA is the best studied cytochrome of *G. sulfurreducens*. The first cytochrome's structure of this bacteria was determined for PpcA, by X-ray crystallography in the oxidized state [45]. The first solution structure determined for a *G. sulfurreducens* cytochrome was also obtained for PpcA as well, but in the reduced state [75]. Finally the first and only NMR structure of a cytochrome from *G. sulfurreducens* in the oxidized state was also determined for PpcA [76].

The crystal structure was also determined for PpcB-E cytochromes, all in the oxidized state [46] [77]. The PpcA family c_7-type cytochromes have a similar structure, with a heme spatial arrangement structurally homologous to the thetraheme cytochromes c_3. However, PpcA family does not have the heme II and the corresponding polypeptide segment, hence the hemes are numbered I, III and IV [78]. All PpcA-family members are low spin with His-His axial coordination. Heme I is the highest exposed heme, whereas heme III is the lowest exposed one, and heme IV shows the largest positive electrostatic surface (except in the case of PpcE). The most conserved region between the family members is around heme IV, and the least conserved one around heme I [77]. The heme core structures are similar within the PpcA-family (see Figure 1.3), being heme I and IV somewhat parallel, and both perpendicular to heme III [45] [46] [75] [77].

The structure of GSU1996 was determined by X-ray crystallography in the oxidized state [43]. It is constituted by four domains, each containing three hemes with homology to the PpcA-family, with exception to the heme IV which is His-Met coordinated. MacA structure was also determined by X-ray crystallography in the reduced, oxidized and in intermediate stats [44]. It is constituted by two globular domains each with a *c*-type heme denominated high and low potential, due to their significant redox potential difference. These hemes are His-Met and His-His coordinated, respectively.

On the other hand, the structure of OmcS filaments was determined by cryo-electron microscopy. The OmcS hemes are distanced 3.5-6 Å from each other, with the hemes forming parallel-staked pairs. Each OmcS contacts only with one other unit on either side, and the various units are assembled through micrometer-long polymerization [49]. The structure of OmcZ filaments was also determined by cryo-electron microscopy. These filaments also form parallel-stacked hemes, as OmcS, but with a denser stacking. This was indicated to be the reason for the increased conductivity of OmcZ filaments. Furthermore, the structure of OmcZ is reach in β-sheet secondary structure, in contrast with the one of OmcS [67]. Both cytochromes have His-His coordinated hemes [49] [67].

The structure of OmcF was determined both by NMR (reduced state) [79] and X-ray crystallography (oxidized state) [80] [81], and resembles the structure of cytochrome c_6 from green algae *Monoraphidium braunii*. Its heme group is low-spin and has His-Met axial coordination.

Finally, the structure of PccH was determined in the oxidized state by X-ray crystallography. PccH is His-Met coordinated. The structure is unique among class I cytochromes, being constituted by two lobes with the heme sandwiched in between. Due to its structural characteristics, and taking in consideration the sequence phylogenetic analysis, it was proposed that PccH constitutes a new subclass within the class I cytochromes [50].

The thermodynamic characterization of monoheme cytochromes is theoretically simpler than multiheme, since only the reduced or the oxidized states exist in solution. Thus, the global redox potential of the protein corresponds to that of the heme group. In the case of multiheme cytochromes, the existence of various heme groups implies that various intermediate states of oxidation can exist in solution. Additionally, each heme has its own redox potential and the global potential describes only the overall redox macroscopic behavior, and is unlikely to correspond to those of the heme groups. The contribution of each heme to the overall redox potential, and their order of oxidation/reduction, can be determined by analyzing the microstates using NMR spectroscopy [82].

The redox potential can be determined by redox titrations, followed by visible spectroscopy, or by electrochemical techniques, namely cyclic voltammetry. The redox potential values of the *G. sulfurreducens* cytochromes studied until date span from -251 to +180 mV (pH

7 *vs* NHE) (Table 1.1). These corresponds to a large potential window, demonstrating the versatility of *G. sulfurreducens* cytochromes.

Table 1.1– Redox potential values (mV *vs* NHE) of *G. sulfurreducens c*-type cytochromes studied to date at pH 7. The respective references are indicated.

Cytochrome	Redox potential (mV)	Ref
OmcZ	-220	[65]
OmcS	-212	[83]
MacA	-188	[44]
PpcC	-143	[84]
PpcB	-137	[46]
PpcE	-134	[85]
PpcD	-132	[85]
GSU1996	-124	[84]
PpcA	-117	[46]
PccH	-24	[86]
OmcF	+180	[80]

1.6 Objectives and thesis outline

The main goal of this thesis is to contribute to the elucidation of the electron transfer mechanisms in *G. sulfurreducens*, and pave the way for future improvement of bioremediation and biotechnological applications. This work was focused on three monoheme *c*-type cytochromes: OmcF, PccH and GSU2515. Their heterologous production was optimized or developed, and their structural and functional characterization accomplished at different extend.

Following the general introduction is presented in this chapter, Chapter 2 focuses on the description of the fundaments of NMR and electrochemistry, the two main techniques used in this thesis. Chapter 3 focuses on the backbone and side-chain assignment of OmcF in the oxidized state, followed by the mapping of its interaction regions with PpcA using NMR chemical shift perturbation experiments. Chapter 4 presents a detailed thermodynamic and kinetic study of OmcF, which was further complemented by the site-directed mutagenesis design of OmcF

mutants, followed by the evaluation of their impact on the modulation of the redox potential of this cytochrome. Chapter 5 focuses on the backbone, side-chain and heme assignment of PccH in the oxidized state. Chapter 6 is dedicated to the functional characterization of GSU2515 and its possible involvement in the electron transfer pathway from electrodes. Chapter 7 describes some preliminary studies that can be explored in the future, within the scope of the presented thematic, and finally, Chapter 8 describes the general conclusions of the work.

1.7 References

[1] R. Kumar, L. Singh, Z. A. Wahid, and M. F. M. Din, "Exoelectrogens in microbial fuel cells toward bioelectricity generation: a review," *Int. J. Energy Res.*, vol. 39, no. 8, pp. 1048–1067, 2015.

[2] D. R. Lovley, "Dissimilatory Metal Reduction," *Annu. Rev. Microbiol.*, vol. 47, no. 1, pp. 263–290, 1993.

[3] B. Erable, N. M. Duţeanu, M. M. Ghangrekar, C. Dumas, and K. Scott, "Application of electro-active biofilms," *Biofouling*, vol. 26, no. 1, pp. 57–71, 2010.

[4] T. Zheng *et al.*, "Progress and prospects of bioelectrochemical systems: electron transfer and its applications in the microbial metabolism.," *Front. Bioeng. Biotechnol.*, vol. 8, p. 10, 2020.

[5] S. Ghosh Ray and M. M. Ghangrekar, "Enhancing organic matter removal, biopolymer recovery and electricity generation from distillery wastewater by combining fungal fermentation and microbial fuel cell," *Bioresour. Technol.*, vol. 176, pp. 8–14, 2015.

[6] B. E. Logan *et al.*, "Microbial fuel cells: methodology and technology," *Environ. Sci. Technol.*, vol. 40, no. 17, pp. 5181–5192, 2006.

[7] C. Santoro, C. Arbizzani, B. Erable, and I. Ieropoulos, "Microbial fuel cells: From fundamentals to applications. A review," *J. Power Sources*, vol. 356, pp. 225–244, 2017.

[8] K. Rabaey and W. Verstraete, "Microbial fuel cells: novel biotechnology for energy generation," *Trends Biotechnol.*, vol. 23, no. 6, pp. 291–298, 2005.

[9] D. R. Lovley, "Electromicrobiology," *Annu. Rev. Microbiol.*, vol. 66, no. 1, pp. 391–409, 2012.

[10] H. Ren, H. Tian, C. L. Gardner, T.-L. Ren, and J. Chae, "A miniaturized microbial fuel cell with three-dimensional graphene macroporous scaffold anode demonstrating a record power density of over 10000 Wm^{-3}," *Nanoscale*, vol. 8, no. 6, pp. 3539–3547, 2016.

[11] K. P. Nevin *et al.*, "Anode biofilm transcriptomics reveals outer surface components essential for high density current production in *Geobacter sulfurreducens* fuel cells," *PLoS One*, vol. 4, no. 5, p. e5628, 2009.

[12] K. Rabaey and R. A. Rozendal, "Microbial electrosynthesis — revisiting the electrical route for microbial production," *Nat. Rev. Microbiol.*, vol. 8, no. 10, pp. 706–716, 2010.

[13] M. AS, J. DA, and G. MM, "Architectural adaptations of Microbial Fuel Cells," *Appl. Microbiol. Biotechnol.*, vol. 102, no. 22, 2018.

[14] Y. H *et al.*, "Selection of a variant of *Geobacter sulfurreducens* with enhanced capacity for current production in microbial fuel cells," *Biosens. Bioelectron.*, vol. 24, no. 12, 2009.

[15] J. HM *et al.*, "Engineering of a synthetic electron conduit in living cells," *Proc. Natl. Acad.*

Sci. U. S. A., vol. 107, no. 45, 2010.

[16] K. Richter, M. Schicklberger, and J. Gescher, "Dissimilatory reduction of extracellular electron acceptors in anaerobic respiration.," *Appl. Environ. Microbiol.*, vol. 78, no. 4, pp. 913–21, 2012.

[17] D. Lovley, D. Holmes, and K. Nevin, "Dissimilatory Fe(III) and Mn(IV) reduction," *Acad. Press*, vol. 49, pp. 219–286, 2004.

[18] D. R. Lovley *et al.*, "*Geobacter*: the microbe electric's physiology, ecology, and practical applications.," in *Advances in microbial physiology*, vol. 59, 2011, pp. 1–100.

[19] J. R. Lloyd and D. R. Lovley, "Microbial detoxification of metals and radionuclides," *Curr. Opin. Biotechnol.*, vol. 12, no. 3, pp. 248–53, 2001.

[20] K. P. Nevin *et al.*, "Anode biofilm transcriptomics reveals outer surface components essential for high density current production in *Geobacter sulfurreducens* fuel cells," *PLoS One*, vol. 4, no. 5, p. e5628, 2009.

[21] Z. M. Summers, H. E. Fogarty, C. Leang, A. E. Franks, N. S. Malvankar, and D. R. Lovley, "Direct exchange of electrons within aggregates of an evolved syntrophic coculture of anaerobic bacteria," *Science*, vol. 330, pp. 1413–1415, 2010.

[22] D. R. Lovley and E. J. Phillips, "Organic matter mineralization with reduction of ferric iron in anaerobic sediments.," *Appl. Environ. Microbiol.*, vol. 51, no. 4, pp. 683–9, 1986.

[23] D. R. Lovley and E. J. Phillips, "Novel mode of microbial energy metabolism: organic carbon oxidation coupled to dissimilatory reduction of iron or manganese.," *Appl. Environ. Microbiol.*, vol. 54, no. 6, pp. 1472–80, 1988.

[24] F. Caccavo, D. J. Lonergan, D. R. Lovley, M. Davis, J. F. Stolz, and M. J. McInerney, "*Geobacter sulfurreducens* sp. nov., a hydrogen- and acetate-oxidizing dissimilatory metal-reducing microorganism.," *Appl. Environ. Microbiol.*, vol. 60, no. 10, pp. 3752–9, 1994.

[25] B. A. Methé *et al.*, "Genome of *Geobacter sulfurreducens*: metal reduction in subsurface environments.," *Science*, vol. 302, no. 5652, pp. 1967–1969, 2003.

[26] M. V Coppi, C. Leang, S. J. Sandler, and D. R. Lovley, "Development of a genetic system for *Geobacter sulfurreducens*.," *Appl. Environ. Microbiol.*, vol. 67, no. 7, pp. 3180–7, 2001.

[27] A. M. Speers and G. Reguera, "Electron donors supporting growth and electroactivity of *Geobacter sulfurreducens* anode biofilms," *Appl. Environ. Microbiol.*, vol. 78, no. 2, pp. 437–444, 2012.

[28] S. K. Chapman, S. Daff, and A. W. Munro, "Heme: The most versatile redox centre in biology?," Springer, Berlin, Heidelberg, 1997, pp. 39–70.

[29] S. E. J. Bowman and K. L. Bren, "The chemistry and biochemistry of heme *c*: functional bases for covalent attachment," *Nat. Prod. Rep.*, vol. 25, no. 6, p. 1118, 2008.

[30] I. Bertini, G. Cavallaro, and A. Rosato, "Cytochrome *c* : Occurrence and Functions," *Chem. Rev.*, vol. 106, no. 1, pp. 90–115, 2006.

[31] D. H. Gonzales and W. Neupert, "Biogenesis of mitochondrial *c*-type cytochromes," *J. Bioenerg. Biomembr.*, vol. 22, no. 6, pp. 753–68, 1990.

[32] M. Hansson and C. von Wachenfeldt, "Heme *b* (protoheme IX) is a precursor of heme *a* and heme *d* in *Bacillus subtilis*," *FEMS Microbiol. Lett.*, vol. 107, no. 1, pp. 121–125, 1993.

[33] G. R. Moore and G. W. Pettigrew, "Stereochemical and Physicochemical Properties of Hemes," in *Cytochromes c Evolutionary, Structural and Physicochemical Aspects*, Springer Berlin Heidelberg, Berlin, Heidelberg, 1990, pp. 1–25.

[34] G. P. Moss, "Nomenclature of tetrapyrroles (Recommendations 1986)," *Eur. J. Biochem.*, vol. 178, no. 2, pp. 277–328, 1988.

[35] C. A. Salgueiro and J. M. Dantas, "Multiheme Cytochromes," in *Multiheme Cytochromes*, Springer Berlin Heidelberg, Berlin, Heidelberg, 2016, pp. 1–39.

[36] J. H. van Vleck, "Theory of the variations in paramagnetic anisotropy among different salts of the iron group," *Phys. Rev.*, vol. 41, pp. 208–215, 1932.

[37] R. P. Ambler, "Sequence variability in bacterial cytochromes *c*," *Biochim. Biophys. Acta*, vol. 1058, no. 1, pp. 42–7, 1991.

[38] L. Morgado, A. P. Fernandes, J. M. Dantas, M. A. Silva, and C. A. Salgueiro, "On the road to improve the bioremediation and electricity-harvesting skills of *Geobacter sulfurreducens*: functional and structural characterization of multihaem cytochromes," *Biochem. Soc. Trans.*, vol. 40, no. 6, pp. 1295–1301, 2012.

[39] L. J. Smith, A. Kahraman, and J. M. Thornton, "Heme proteins-Diversity in structural characteristics, function, and folding," *Proteins Struct. Funct. Bioinforma.*, vol. 78, no. 10, pp. 2349–2368, 2010.

[40] M. Breuer, K. M. Rosso, J. Blumberger, and J. N. Butt, "Multi-haem cytochromes in *Shewanella oneidensis* MR-1: structures, functions and opportunities," *J. R. Soc. Interface*, vol. 12, no. 102, p. 20141117, 2015.

[41] A. V. Xavier, "Energy transduction coupling mechanisms in multiredox center proteins," *J. Inorg. Biochem.*, vol. 28, no. 2–3, pp. 239–243, 1986.

[42] G. W. Pettigrew and G. R. Moore, "Cytochromes *c*: biological aspects," in *Molecular Biology*, Springer Berlin Heidelberg, 1987, p. 282.

[43] P. R. Pokkuluri *et al.*, "Structure of a novel dodecaheme cytochrome *c* from *Geobacter sulfurreducens* reveals an extended 12nm protein with interacting hemes," *J. Struct. Biol.*, vol. 174, no. 1, pp. 223–233, 2011.

[44] J. Seidel *et al.*, "MacA is a second cytochrome *c* peroxidase of *Geobacter sulfurreducens*," *Biochemistry*, vol. 51, no. 13, pp. 2747–2756, 2012.

[45] P. R. Pokkuluri, Y. Y. Londer, N. E. C. Duke, W. C. Long, and M. Schiffer, "Family of cytochrome c_7-type proteins from *Geobacter sulfurreducens*: structure of one cytochrome c_7 at 1.45 Å resolution," *Biochemistry*, vol. 43, no. 4, pp. 849–859, 2004.

[46] L. Morgado *et al.*, "Structural insights into the modulation of the redox properties of two *Geobacter sulfurreducens* homologous triheme cytochromes," *Biochim. Biophys. Acta - Bioenerg.*, vol. 1777, no. 9, pp. 1157–1165, 2008.

[47] P. R. Pokkuluri *et al.*, "Structural characterization of a family of cytochromes c_7 involved in Fe(III) respiration by *Geobacter sulfurreducens*," *Biochim. Biophys. Acta - Bioenerg.*, vol. 1797, no. 2, pp. 222–232, 2010.

[48] B.-C. Kim, C. Leang, Y.-H. R. Ding, R. H. Glaven, M. V Coppi, and D. R. Lovley, "OmcF, a putative *c*-type monoheme outer membrane cytochrome required for the expression of other outer membrane cytochromes in *Geobacter sulfurreducens*.," *J. Bacteriol.*, vol. 187, no. 13, pp. 4505–4513, 2005.

[49] F. Wang *et al.*, "Structure of microbial nanowires reveals stacked hemes that transport electrons over micrometers," *Cell*, vol. 177, no. 2, pp. 361–369, 2019.

[50] J. M. Dantas, L. M. Campelo, N. E. C. Duke, C. A. Salgueiro, and P. R. Pokkuluri, "The structure of PccH from *Geobacter sulfurreducens* - a novel low reduction potential monoheme cytochrome essential for accepting electrons from an electrode," *FEBS J.*, vol. 282, no. 11, pp. 2215–2231, 2015.

[51] B. Alberts, A. Johnson, J. Lewis, M. Raff, K. Roberts, and P. Walter, "Electron-transport chains and their proton pumps," in *Molecular Biology of the Cell*, Garland Science, 2002.

[52] J. E. Butler, F. Kaufmann, M. V. Coppi, C. Nunez, and D. R. Lovley, "MacA, a diheme *c*-type cytochrome involved in Fe(III) reduction by *Geobacter sulfurreducens*," *J. Bacteriol.*, vol. 186, no. 12, pp. 4042–4045, 2004.

[53] B.-C. Kim and D. R. Lovley, "Investigation of direct vs. indirect involvement of the *c* -type cytochrome MacA in Fe(III) reduction by *Geobacter sulfurreducens*," *FEMS Microbiol. Lett.*, vol. 286, no. 1, pp. 39–44, 2008.

[54] C. E. Levar, C. H. Chan, M. G. Mehta-Kolte, and D. R. Bond, "An inner membrane cytochrome required only for reduction of high redox potential extracellular electron acceptors.," *MBio*, vol. 5, no. 6, p. e02034, 2014.

[55] L. Zacharoff, C. H. Chan, and D. R. Bond, "Reduction of low potential electron acceptors requires the CbcL inner membrane cytochrome of *Geobacter sulfurreducens*," *Bioelectrochemistry*, vol. 107, pp. 7–13, 2016.

[56] J. M. Dantas, A. Brausemann, O. Einsle, and C. A. Salgueiro, "NMR studies of the interaction between inner membrane-associated and periplasmic cytochromes from *Geobacter sulfurreducens*," *FEBS Lett.*, vol. 591, no. 12, pp. 1657–1666, 2017.

[57] J. R. Lloyd *et al.*, "Biochemical and genetic characterization of PpcA, a periplasmic *c*-type cytochrome in *Geobacter sulfurreducens*.," *Biochem. J.*, vol. 369, no. Pt 1, pp. 153–61, 2003.

[58] M. R. Ferreira, J. M. Dantas, and C. A. Salgueiro, "The triheme cytochrome PpcF from *Geobacter metallireducens* exhibits distinct redox properties," *FEBS Open Bio*, vol. 8, no. 12, pp. 1897–1910, 2018.

[59] M. N. Alves, A. P. Fernandes, C. A. Salgueiro, and C. M. Paquete, "Unraveling the electron transfer processes of a nanowire protein from *Geobacter sulfurreducens*," *Biochim. Biophys. Acta - Bioenerg.*, vol. 1857, no. 1, pp. 7–13, 2016.

[60] Y. Liu *et al.*, "A trans-outer membrane porin-cytochrome protein complex for extracellular electron transfer by *Geobacter sulfurreducens* PCA.," *Environ. Microbiol. Rep.*, vol. 6, no. 6, pp. 776–85, 2014.

[61] Y. Liu, J. K. Fredrickson, J. M. Zachara, and L. Shi, "Direct involvement of ombB, omaB, and omcB genes in extracellular reduction of Fe(III) by *Geobacter sulfurreducens* PCA," *Front. Microbiol.*, vol. 6, p. 1075, 2015.

[62] B.-C. Kim, B. L. Postier, R. J. DiDonato, S. K. Chaudhuri, K. P. Nevin, and D. R. Lovley, "Insights into genes involved in electricity generation in *Geobacter sulfurreducens* via whole genome microarray analysis of the OmcF-deficient mutant," *Bioelectrochemistry*, vol. 73, no. 1, pp. 70–75, 2008.

[63] T. Mehta, M. V Coppi, S. E. Childers, and D. R. Lovley, "Outer membrane *c*-type cytochromes required for Fe(III) and Mn(IV) oxide reduction in *Geobacter sulfurreducens*," *Appl. Environ. Microbiol.*, vol. 71, no. 12, pp. 8634–41, 2005.

[64] D. E. Holmes *et al.*, "Microarray and genetic analysis of electron transfer to electrodes in *Geobacter sulfurreducens*," *Environ. Microbiol.*, vol. 8, no. 10, pp. 1805–1815, 2006.

[65] K. Inoue *et al.*, "Purification and characterization of OmcZ, an outer-surface, octaheme *c*-type cytochrome essential for optimal current production by *Geobacter sulfurreducens*," *Appl. Environ. Microbiol.*, vol. 76, no. 12, pp. 3999–4007, 2010.

[66] T. A. Clarke and M. J. Edwards, "Uncovering nature's electronics," *Nat. Chem. Biol.*, vol. 16, pp. 1041–1042, 2020.

[67] S. E. Yalcin *et al.*, "Electric field stimulates production of highly conductive microbial OmcZ nanowires," *Nat. Chem. Biol.*, vol. 16, pp. 1136–1142, 2020.

[68] M. A. Thirumurthy and A. K. Jons, "*Geobacter* cytochrome OmcZs binds riboflavin: implications for extracellular electron transfer," *Nanotechnology*, vol. 31, no. 12, p. 124001, 2020.

[69] G. Reguera, K. P. Nevin, J. S. Nicoll, S. F. Covalla, T. L. Woodard, and D. R. Lovley, "Biofilm and nanowire production leads to increased current in *Geobacter sulfurreducens* fuel cells," *Appl. Environ. Microbiol.*, vol. 72, no. 11, pp. 7345–8, 2006.

[70] P. M. Shrestha, A.-E. Rotaru, Z. M. Summers, M. Shrestha, F. Liu, and D. R. Lovley, "Transcriptomic and genetic analysis of direct interspecies electron transfer," *Appl. Environ. Microbiol.*, vol. 79, no. 7, pp. 2397–2404, 2013.

[71] S. M. Strycharz *et al.*, "Gene expression and deletion analysis of mechanisms for electron transfer from electrodes to *Geobacter sulfurreducens*," *Bioelectrochemistry*, vol. 80, no. 2, pp. 142–150, 2011.

[72] M. A. Silva, T. G. Lucas, C. A. Salgueiro, and C. M. Gomes, "Protein folding modulates the swapped dimerization mechanism of methyl-accepting chemotaxis heme sensors," *PLoS One*, vol. 7, no. 9, p. e46328, 2012.

[73] M. A. Silva, R. C. Valente, P. R. Pokkuluri, D. L. Turner, C. A. Salgueiro, and T. Catarino, "Thermodynamic and kinetic characterization of two methyl-accepting chemotaxis heme sensors from *Geobacter sulfurreducens* reveals the structural origin of their functional difference," *Biochim. Biophys. Acta - Bioenerg.*, vol. 1837, no. 6, pp. 920–928, 2014.

[74] Y. Y. Londer, I. S. Dementieva, C. A. D'Ausilio, P. R. Pokkuluri, and M. Schiffer, "Characterization of a *c*-type heme-containing PAS sensor domain from *Geobacter sulfurreducens* representing a novel family of periplasmic sensors in *Geobacteraceae* and other bacteria," *FEMS Microbiol. Lett.*, vol. 258, no. 2, pp. 173–181, 2006.

[75] L. Morgado, V. B. Paixão, M. Schiffer, P. R. Pokkuluri, M. Bruix, and C. A. Salgueiro, "Revealing the structural origin of the redox-Bohr effect: the first solution structure of a cytochrome from *Geobacter sulfurreducens*," *Biochem. J.*, vol. 441, no. 1, pp. 179–187, 2012.

[76] L. Morgado, M. Bruix, P. R. Pokkuluri, C. A. Salgueiro, and D. L. Turner, "Redox- and pH-linked conformational changes in triheme cytochrome PpcA from *Geobacter sulfurreducens*," *Biochem. J.*, vol. 474, no. 2, pp. 231–246, 2017.

[77] P. R. Pokkuluri *et al.*, "Structural characterization of a family of cytochromes c_7 involved in Fe(III) respiration by *Geobacter sulfurreducens*," *Biochim. Biophys. Acta*, vol. 1797, no. 2, pp. 222–32, 2010.

[78] M. Pessanha *et al.*, "Redox characterization of *Geobacter sulfurreducens* cytochrome c_7: physiological relevance of the conserved residue F15 probed by site-specific mutagenesis.," *Biochemistry*, vol. 43, no. 30, pp. 9909–17, 2004.

[79] J. M. Dantas, M. A. Silva, D. Pantoja-Uceda, D. L. Turner, M. Bruix, and C. A. Salgueiro, "Solution structure and dynamics of the outer membrane cytochrome OmcF from *Geobacter sulfurreducens*," *Biochim. Biophys. Acta - Bioenerg.*, vol. 1858, no. 9, pp. 733–

741, 2017.

[80] P. R. Pokkuluri *et al.*, "Outer membrane cytochrome *c*, OmcF, from *Geobacter sulfurreducens*: High structural similarity to an algal cytochrome c_6," *Proteins Struct. Funct. Bioinforma.*, vol. 74, no. 1, pp. 266–270, 2009.

[81] P. Lukat, M. Hoffmann, and O. Einsle, "Crystal packing of the c_6-type cytochrome OmcF from *Geobacter sulfurreducens* is mediated by an N-terminal Strep-tag II," *Acta Crystallogr. Sect. D Biol. Crystallogr.*, vol. 64, no. 9, pp. 919–926, 2008.

[82] D. L. Turner, C. A. Salgueiro, T. Catarino, J. Legall, and A. V Xavier, "NMR studies of cooperativity in the tetrahaem cytochrome c_3 from *Desulfovibrio vulgaris*," *Eur. J. Biochem.*, vol. 241, no. 3, pp. 723–731, 1996.

[83] X. Qian *et al.*, "Biochemical characterization of purified OmcS, a *c*-type cytochrome required for insoluble Fe(III) reduction in *Geobacter sulfurreducens*," *Biochim. Biophys. Acta - Bioenerg.*, vol. 1807, no. 4, pp. 404–412, 2011.

[84] T. C. Santos, M. A. Silva, L. Morgado, J. M. Dantas, and C. A. Salgueiro, "Diving into the redox properties of *Geobacter sulfurreducens* cytochromes: a model for extracellular electron transfer," *Dalton Trans.*, vol. 44, no. 20, pp. 9335–44, 2015.

[85] L. Morgado, M. Bruix, M. Pessanha, Y. Y. Londer, and C. A. Salgueiro, "Thermodynamic characterization of a triheme cytochrome family from *Geobacter sulfurreducens* reveals mechanistic and functional diversity," *Biophys. J.*, vol. 99, no. 1, pp. 293–301, 2010.

[86] T. C. Santos, A. R. de Oliveira, J. M. Dantas, C. A. Salgueiro, and C. M. Cordas, "Thermodynamic and kinetic characterization of PccH, a key protein in microbial electrosynthesis processes in *Geobacter sulfurreducens*," *Biochim. Biophys. Acta - Bioenerg.*, vol. 1847, no. 10, pp. 1113–1118, 2015.

1. Introduction

2. Fundaments of Nuclear Magnetic Resonance and Electrochemistry

2.1 Fundaments of Nuclear Magnetic Resonance

Nuclear Magnetic Resonance (NMR) spectroscopy has been widely used in protein biochemistry, since it is a very transversal technique, providing information about the structure and dynamics of proteins. As most of the studies are performed in solution, they mimic the conditions that biomolecules experience in the cell. In this section, the NMR principles, the spectroscopic parameters, as well as the main NMR experiments used in protein biochemistry will be briefly described.

2.1.1 The basis of NMR

NMR is based on the magnetic properties of atomic nuclei and their ability to selectively absorb radiofrequency in the presence of an external magnetic field.

Nuclei have spin (*I*) because they rotate around the nucleus axis. The value of *I* depends on its number of protons and neutrons. When the atomic number and mass of a nuclei are equal, the quantum spin number is equal to 0, and consequently no NMR signal is detected. When one of these values is odd, the quantum spin number is different from 0 and the nuclei have magnetic properties. These are the NMR active nuclei, and the most used are the ones with $I = ½$, which include ^{1}H, ^{13}C, ^{15}N, ^{19}F and ^{31}P.

Because of its spin state, the nuclei have a magnetic moment (μ), which is perpendicular to the plane stablished by the charged particle's movement. These particles have such a rotating movement that generates nuclear magnetic dipoles. The magnetic moment depends on the spin number and on the gyromagnetic ratio (γ) (equation 2.1). γ is a constant value, characteristic of each nucleus, and corresponds to the frequency at which they precess around an applied external magnetic field (B_0).

$$\mu = I\gamma \tag{2.1}$$

Each *I* has $2I + 1$ possible values, meaning that for a nucleus with a $I = ½$ there are two possible magnetic quantum numbers (m_I): ½ and -½. In the absence of B_0, all nuclei of the same isotope have the same energy (degenerated state). In the presence of an external magnetic field (B_0), there is a splitting of nuclei spin energies levels, separated by an energy difference (ΔE). So, in the case of $I = ½$ nuclei, the sate $m_I = ½$ (α) becomes parallel to B_0, whereas the state $m_I = -½$ (β) becomes antiparallel.

The distribution of spin populations between the two energy states (α and β) is given by the Boltzmann equation (2.2), where *N* are the populations of the two energy states, k_B the Boltzmann constant and *T* the temperature.

$$\frac{N_\beta}{N_\alpha} = e^{-\Delta E/k_B T} \tag{2.2}$$

However, the nuclei do not align or oppose B_0, they rather create a movement of precession around the B_0 axis with an angular frequency (ω), that is dependent on the intrinsic characteristics

of the nucleus and B_0. This precession frequency is denominated as Larmor frequency (υ) and is given by the following equation (2.3).

$$\omega = \gamma B_0 = 2\pi\upsilon \quad (2.3)$$

The energy difference between the two levels (ΔE) is given by equation 2.4, where h is the Plank constant. Since γ is a property of the nuclei, the larger its value, the larger the separation between the levels of energy and therefore the better the sensitivity of the nuclei in NMR.

$$\Delta E = h\upsilon = h\gamma B_0 / 2\pi \quad (2.4)$$

The nuclear magnetic dipoles aligned with B_0 have the lowest energy state hence, according to the Boltzmann distribution, is the biggest population in equilibrium. However, at room temperature, the difference between the two populations is very small. Even so, this imbalance creates a net nuclear moment composed by the dipole moments of all the nuclei present. Magnetization (M) is this net nuclear magnetic moment and is represented by a parallel vector to B_0. The biggest the energy difference between the two populations (ΔE), the largest the length of the magnetization. When the energy applied is equal to ΔE, the transition between the two energy states occurs, M becomes oriented with B_0 and the absorption of energy by the nuclei is measured by NMR.

A pulse, which is a single variation of radiofrequency power, is used in NMR to excite the radiofrequency region of the nucleus. When a 90 º pulse (B_1) is applied along the x axis, with a frequency equal to ΔE, the spins that are aligned in the z axis (M) move to the xy plane. M recovers with time to its equilibrium position, which decay is detected in the form of a free induction decay (FID). FID means that the collected signal is "free" from the influence of B_1, is "induced" in the coil and "decays" back to equilibrium. In fact, a pulse sequence is applied in NMR experiments, rather than a single pulse. A series of pulses is applied between time delays during which the nuclear spins' magnetization evolves.

After excitation and absorption of energy, the systems return to equilibrium by restoration of the initial populations and phase randomization of the wave-functions of the nuclear spins. These are called relaxation mechanisms and occur by interaction of the spins with the surroundings (*lattice*). The longitudinal spin-lattice relaxation time (T_1) corresponds to the time for the exponential return of M to its initial orientation, and the system's population reverts to an uneven distribution. The transversal spin-lattice relaxation time (T_2) corresponds to the exponential time that takes the system to return to a random arrangement of phases. T_1 is responsible for the loss of signal intensity and T_2 for the broadening of the signals.

The signals obtained are converted by a Fourier transformation (FT), where the different spins contributions to the FID are separated by applying the FT to the time-dependent signal. This results in a typical NMR spectrum [1].

2.1.2 Spectroscopic parameters in NMR

Theoretically, all nuclei have the same Larmor frequency that is dependent on the B_0. However, the electron density surrounding each nucleus generates a local magnetic field (B_{local}). Consequently, each nucleus will have a slightly different Larmor frequency, difference that makes NMR such a powerful technique. So, the Larmor frequency is described as following (equation 2.5), where σ is the shielding constant which is positive or negative depending if the local field adds or subtracts from the applied field.

$$\omega = \gamma B_0 \, (1 - \sigma) \tag{2.5}$$

σ depends on various contributions: (i) the diamagnetic contribution describes the behavior of spherical distributed electronic clouds; (ii) the paramagnetic contribution is the alteration of the electron wave-functions by the presence of other nuclei, and its contribution is much larger than the diamagnetic; (iii) the contribution of paramagnetic compounds, such as metals, is caused by the presence of unpaired electrons that induce broadening of the NMR signals due to relaxation effects; (iv) chemical bonds, such as carbon-carbon triple bond, create a magnetic field giving rise to neighbor anisotropy contribution; (v) a ring-current effect contribution is created by the magnetic field of planar aromatic rings and heme groups; (vi) electric field contribution is caused by the presence of strong polar groups that create intramolecular fields, distorting the electron density of the rest of the molecule; (vii) the solvent contribution when the adequate buffer is not chosen for the NMR experiments.

The difference between the theoretical and experimental frequency is given by the chemical shifts (δ in ppm) (equation 2.6), where υ_0 is the standard's resonance frequency and υ the nucleus' specific resonance frequency.

$$\delta = \frac{\upsilon - \upsilon_0}{\upsilon_0} * 10^6 \tag{2.6}$$

If $\delta < 0$, the magnetic field experienced by the nuclei is weaker that the experienced by the standard. If $\delta > 0$ the nuclei experience stronger magnetic field than the standard compound. A signal reference standard is needed to quantify the resonance frequencies. The common standard for protons is ^{1}H resonance of tetramethylsilane (TMS), but 4,4-dimethyl-4-silapentane-1-sulfonic acid (DSS) and water are also used. In biomolecular studies, calibration with ^{13}C and ^{15}N is used [1], which considers the reference of ^{1}H [2]. Together with the chemical shift information, signal intensity gives information about the nucleus or group of nuclei that are responsible for a particular resonance.

Interactions that divide magnetically equivalent nuclei, into two or more populations, cause splitting of its respective peaks in the NMR spectra. In fact, each magnetic nucleus is influenced by its interaction with the other nuclei. The strength of this interaction is related to the coupling constant (^nJ), which is the scalar product of the magnetic moments of the interacting nuclei. *n*

relates to the number of covalent bonds, and the magnitude of the spin-spin coupling decreases with increasing number of intervening bonds. *J* is measured in Hz and is independent on B_0.

There is another class of coupling, dipolar coupling that gives rise to the Nuclear Overhauser effect (NOE). This occurs when two spins, that are not scalarly coupled, are spatially close enough to interrelate through dipole-dipole interactions. When a radiofrequency is irradiated at the resonance frequency of one of these spins, the intensity of the second one is modified, being this modification the NOE. This effect is crucial in obtaining structural information of the molecules [1].

2.1.3 NMR experiments

The most basic NMR experiment is a one-dimensional (1D) spectrum that covers the frequency range of the measured nuclei and presents signals which chemical shift, intensity, shape and multiplicity depend on the features of the molecule in study. 1D ^{1}H experiments are the most common. The design of the pulse sequence, for this type of experiments, consists of a pre-acquisition delay (d1) that allows the system's return to equilibrium between scans. Then, a 90º pulse of radiofrequency is applied which orientates *M* in the xy axis, away from the z axis where it was aligned with B_0. The decay of magnetization during time (t) is detected in the FID form. The pulse sequence can be applied indefinitely (Figure 2.1 A).

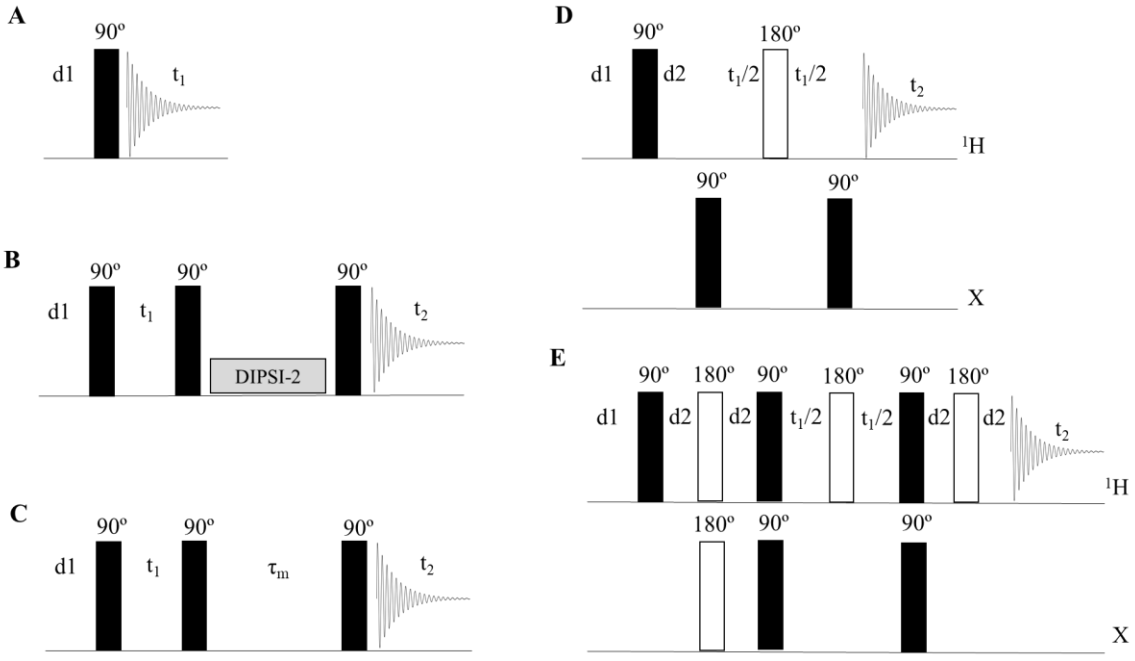

Figure 2.1 – 1D and 2D NMR experiments used in this Thesis. (A) 1D experiment, **(B)** 2D ^{1}H, ^{1}H TOCSY, **(C)** 2D ^{1}H, ^{1}H NOESY, **(D)** 2D ^{1}H, X HMQC and **(E)** 2D ^{1}H, X HSQC. Black and white rectangles represent 90º and 180º pulses, respectively. The FID represents the data acquisition periods. The time delay is represented as t_1 and t_2, and the mixing time as τ_m. Pre-acquisition delay is represented as d1, and d2 is optimized to be ½ *J* in the HMQC, and ¼ in HSQC. DIPSI-2 is a pulse sequence designed for isotropic mixing purposes in 2D ^{1}H,^{1}H TOCSY. Adapted from [1] [3].

In NMR, extra dimensions allow to distinguish peaks that are overlapped in the 1D spectrum and allow to identify connectivities. These experiments start with the preparation stage, which is the same as 1D experiments, including the d1 and the pulse. Secondly, in the evolution stage the incremental time (t_1) is implemented. This time has the particularity of incrementing, as the experiment progresses, and follows equation 2.7, where t is the starting evolution time, d is a fixed short delay and n is the number of FIDs.

$$t_1 = t + nd \tag{2.7}$$

The third stage of multidimensional experiments is mixing, where several pulses and fixed delays are included, modulating the magnetization to render information in the spectrum. The final step is the detection of the signal generated along the previous stages, by recording the FID during a fixed delay (t_2).

Multidimensional NMR experiments can be either homonuclear or heteronuclear, meaning same and different nuclei in the various dimensions, respectively. In homonuclear experiments, the same irradiation frequency is applied, and the spectral widths are equal in all dimensions. In heteronuclear experiments, tuning of the irradiation frequencies is needed and the spectral widths are different. The 2D experiments used in this thesis were ^{1}H, ^{1}H TOCSY, ^{1}H, ^{1}H NOESY, ^{1}H, X HMQC and ^{1}H, X HSQC. The principles of these experiments will be hereon explained.

2D ^{1}H, ^{1}H TOCSY (TOtal Correlation SpectroscopY) is a homonuclear experiment based on the *J* coupling of protons participating in a particular spin system [4]. The correlation is produced when a direct *J* coupling exists between nuclei and also between nuclei that are connected by a chain of coupling. A composite pulse sequence is applied in the mixing stage, which is composed by a train of hard pulses, and aims to transfer magnetization through scalar coupling. One of the most used isotropic mixing sequences is the decoupling in the presence of scalar interactions (DIPSI) (Figure 2.1 B). The magnetization is usually transferred up to six bonds, but it can be interrupted by small or null proton-proton coupling, and by the presence of hetero-atoms. This is the case of the CO-NH bond between consecutive amino acids, causing TOCSY experiments to only show connectivities within each amino acid of the sequence. In the case of aromatic amino acids, the aromatic ring is not scalar coupled with the rest of the side chain. The assignment of each spin system through 2D ^{1}H, ^{1}H TOCSY is based on the fact that each amino acid has a specific pattern of range frequencies. However, through only analyzing this spectrum, is not possible to determine the localization of each amino acid in the polypeptide chain.

2D ^{1}H, ^{1}H NOESY (Nuclear Overhauser Effect SpectroscopY) experiment relies on NOE. This experiment is very similar to 2D ^{1}H, ^{1}H TOCSY (Figure 2.1 C), but it shows cross-peaks between nuclei distanced no greater than 5-6 Å. In fact, the signal intensity is related to the distance (r^{-6}) between spins. NOESY is complementary to TOCSY, since it is possible to assign the specific amino acid to a position in the protein, considering the inter-residual connectivities observed.

2D ^{1}H, X HSQC (Heteronuclear Single Quantum Coherence) and ^{1}H, X HMQC (Heteronuclear Multiple Quantum Coherence) give information about single-bond correlations between a sensitive nucleus (^{1}H) and a heteronucleus (^{13}C or ^{15}N). In both experiments, the initial excitation and the detection is on the most sensitive nucleus, which permits to achieve highly sensitive gains. In HSQC, an initial pulse sequence generates single quantum coherence between ^{1}H and X, which magnetization evolves during t_1. Then, a second pulse sequence is applied to transfer the magnetization back to ^{1}H for detection (Figure 2.1 E). In HMQC, the pulse sequence generates hetereonuclear multiple quantum coherences that also evolve during t_1. The signal is detected in t_2 on the ^{1}H dimension with X decoupling (Figure 2.1 D). The main difference between the two experiments is than HMQC is affected by homonuclear proton *J* coupling during t_1, whereas HSQC is not. Plus, HSQC has higher resolution than HMQC. The 2D ^{1}H,^{15}N HSQC is one of the most transversal experiments in biomolecular NMR, giving both qualitative and quantitative information. It is considered to be the fingerprint of a protein [1].

3D experiments follow the same scheme as 2D, with the addition of a second evolution period and an additional mixing period between the first mixing period and the acquisition. The 3D experiments used in this thesis are hereon explained.

3D TOCSY are constituted by 2D ^{1}H,^{1}H TOCSY which peaks are dispersed in a third dimension. This can be the ^{15}N chemical shift of the NH groups (3D TOCSY-HSQC) or the ^{13}C chemical shifts of the side chains (3D HCCH-TOCSY). The 3D NOESY follows the same principle but it considers spatial interactions [1].

3D HNCA provides information about the connections between the NH group with the C_α of the respective amino acid ($C_{\alpha i}$, strong signal), and the preceding one ($C_{\alpha i-1}$, weak signal). The magnetization passes from the ^{1}HN to the ^{15}N, then to the $C_{\alpha i}$ and $C_{\alpha i-1}$ via *J* coupling, and back to ^{1}HN for detection (Figure 2.2 A) [1].

3D HN(CO)CA correlates NH group with the C_α of the preceding amino acid, through the CO group. Magnetization passes from the NH group to CO via *J* coupling however, the CO group in this experiment is not detected (Figure 2.2 B) [1].

3D HNCACB correlates the NH group with the $C_{\alpha i}$, $C_{\alpha i-1}$, $C_{\beta i}$ and $C_{\beta i-1}$. Magnetization is transferred from the H_α and H_β to their respective C_α and C_β (Figure 2.2 C). The 3D HN(CO)CACB correlates the NH group with the $C_{\alpha i-1}$ and $C_{\beta i-1}$. The magnetization is transferred from the H_α and H_β to their respective C_α and C_β, and then from C_α to C_β. The magnetization is transferred to CO and the HN for detection, but the CO group is not detected (Figure 2.2 D). These two experiments are not very sensitive, and are used to confirm signals attributed from the analysis of other spectra [1] [3].

3D HNCO experiment correlates the NH group to the CO of the preceding residue. Magnetization is transferred from the ^{1}HN to the ^{15}N and then to the preceding CO via *J* coupling, and finally back to ^{1}HN for detection. In this experiment, the CO is detected (Figure 2.2 E) [1].

In 3D HN(CA)CO the magnetization is transferred from NH group to the C_α, then to CO. The same occurs for the previous residue, thus two carbonyl groups are observed in the spectrum. Since coupling between N and $C_{\alpha i}$ is stronger than with $C_{\alpha i-1}$, the CO of the respective residue has a more intense peak, and the C_α are not detected (Figure 2.2 F) [1].

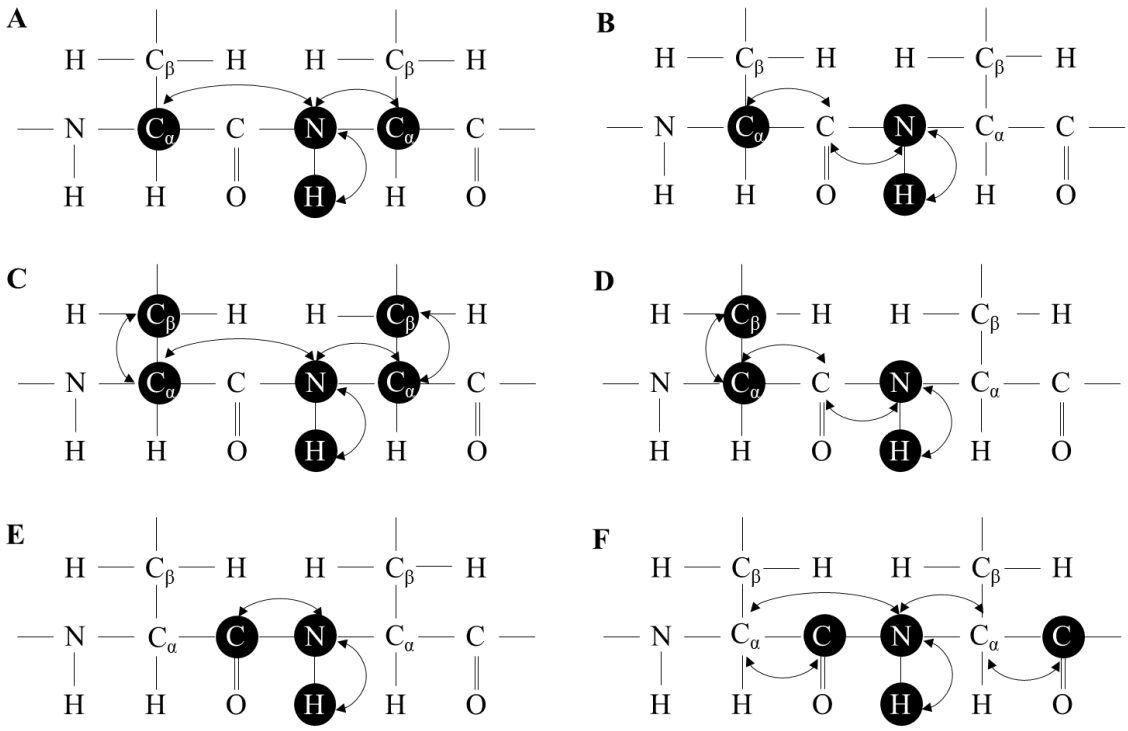

Figure 2.2 – 3D NMR experiments used in this Thesis. (A) corresponds to HNCA, **(B)** to HN(CO)CA, **(C)** to HNCACB, **(D)** to HN(CO)CACB, **(E)** to HNCO and **(F)** to HN(CA)CO. Black circles indicate the nuclei detected by the experiments. Arrows indicate the magnetization transfer. Adapted from [1] [3].

2.1.4 NMR assignment methodologies

The assignment of the polypeptide signals of a protein is a starting point for structural and functional studies. In cytochromes it is possible to assign the backbone, side-chains and heme substituents signals both in the reduced and oxidized states. The assignment strategies will be addressed, by using the previously mentioned NMR experiments.

Backbone assignment relies on the correlation between the 2D ^{1}H,^{15}N HSQC and sequential assignment using the 3D experiments: HNCA, HN(CO)CA, HNCO, HN(CA)CO, HNCACB and HN(CO)CACB. A NH signal is selected from the 2D ^{1}H, ^{15}N HSQC spectrum and then the $^{1}H_i$ and $^{15}N_i$ shifts are introduced in the 3D experiments, where pairs of C_α/C_β and CO are identified. Through the analysis of the different 3D experiments is possible to attribute the carbon shifts to the residue and its preceding one. The next residue can be found in a HN plane where $C_{\alpha i}$, $C_{\beta i}$ and CO_i are now $C_{\alpha i-1}$, $C_{\beta i-1}$ and CO_{i-1}. Alternatively, the H_{i-1} N_{i-1} plane can be found where $C_{\alpha i-1}$, $C_{\beta i-1}$ and CO_{i-1} are now $C_{\alpha i}$, $C_{\beta i}$ and CO_i. By repeating this sequential analysis is possible to attribute

the HN signals in the 2D ^{1}H,^{15}N HSQC spectrum and perform the backbone assignment of the protein (Figure 2.3).

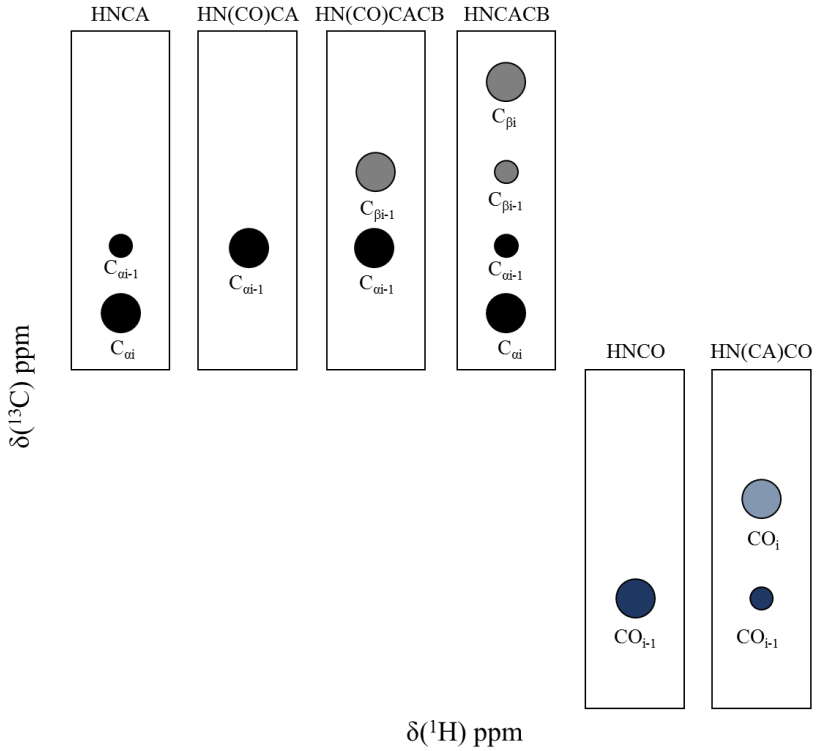

Figure 2.3 – Backbone assignment strategy using the 3D experiments: HNCA, HN(CO)CA, HN(CO)CACB, HNCACB, HNCO and HN(CA)CO. Scheme of the observable signals in ^{1}H and ^{13}C coordinates at a given ^{15}N chemical shift. The dimension of the circles is illustrative of the intensity of the peaks.

The chemical shifts of C_α and C_β are the starting points to identify the remaining aliphatic ^{1}H and ^{13}C signals in the 3D HCCH-TOCSY spectra, which are then confirmed in the 2D ^{1}H, ^{1}H TOCSY. The sequential assignment can be confirmed by analysis of the 2D ^{1}H, ^{1}H NOESY and 3D ^{1}H, ^{15}N NOESY-HSQC spectra. The ^{1}H and ^{13}C signals can further be independently confirmed by analysis of the 2D ^{1}H, ^{13}C HSQC [1].

For the backbone and side-chain assignment, the strategy for the oxidized and reduced states is the same. However, for the heme substituents' assignment it is necessary to implement different methodologies since the redox state significantly affects their chemical shifts.

In the diamagnetic reduced form, scalar connectivities between the thioether methine ($3^{1}H$ and $8^{1}H$) and thioether methyl ($3^{2}CH_3$ and $8^{2}CH_3$) are visible in the 2D ^{1}H, ^{1}H TOCSY. Thioether methyl groups are localized in the spectrum from -1 to 3 ppm, and thioether methines from 6 to 8 ppm. In the 2D ^{1}H, ^{1}H NOESY spectrum, spatial correlations are observed with the other heme substituents, which also have typical regions in spectrum: methyl groups from 3 to 5 ppm ($2^{1}CH_3$, $7^{1}CH_3$, $12^{1}CH_3$ and $18^{1}CH_3$), and meso protons from 8 to 10 ppm (5H, 10H, 15H and 20H). The connectivities observed both in the 2D ^{1}H, ^{1}H TOCSY and ^{1}H, ^{1}H NOESY spectra are depicted in Figure 2.4. The only ambiguous assignment is between 5H and 10H protons, since both stablish

connections with a thioether methine, thioether methyl and a heme methyl. This is overcome by observing the thioether connectivities with the 2^1CH_3 and 7^1CH_3 methyl substituents [5].

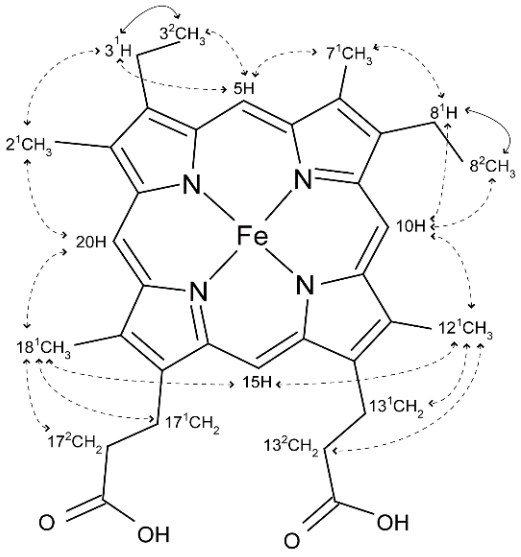

Figure 2.4 – Diagram of the heme *c*, showing the connectivities used to assign the heme substituent signals. Solid arrows illustrate the connectivities observed in the 2D ^1H, ^1H TOCSY (except for heme propionates), and dashed arrows to the NOE connectivities observed in the 2D ^1H, ^1H NOESY. Heme substituents are numbered according to the IUPAC-IUB nomenclature [6].

In the oxidized state, the hemes are paramagnetic causing the chemical shifts of their substituents to spread out along the spectra. The assignment strategy consists in the analysis of a 2D ^1H, ^{13}C HMQC, where methyl groups and propionates have typical ^1H, ^{13}C regions. Methyl groups are typically at higher ^1H and low ^{13}C frequencies, while α propionates (17^1CH_2 and 13^1CH_2) and β propionates (17^2CH_2 and 13^2CH_2) form pairs of resonances positioned at lower and higher ^{13}C frequencies, respectively. Furthermore, by superposition of 2D ^1H, ^{13}C HMQC acquired in isotopically labelled protein and with natural abundance, the rest of the heme substituents can be identified. The assignment of the propionates and the thioether groups can be done through analysis of the 2D ^1H, ^1H TOCSY spectrum. Furthermore, intraheme correlations between the propionates and thioether groups are observed with the closest methyl group, in the 2D ^1H, ^1H NOESY spectrum [7].

The assignment of the backbone, side-chain and heme substituents is of upmost importance to assist in the structural and functional characterization of cytochromes.

2.2 Fundaments of Electrochemistry

Electrochemical methods have been used in different biological/biochemical areas. In fact, bioelectrochemistry has been applied in the determination of the redox potential of proteins, including cytochromes, among other parameters such as kinetics of electron transfer and thermodynamic data. Electrochemistry has been used as a tool to understand the biochemistry (structure and function) of metalloproteins and to exploit its use in biosensors and bioelectronics [8].

In this section, some basic fundaments of electrochemistry will be explained, as well as the techniques and the setups used in this Thesis.

2.2.1 The basis of electrochemistry

Electrochemistry is based on the charge separation associated with charge transfer that occurs homogeneously in solution, and heterogeneously on electrode surfaces. Charge transfer half-reactions (reduction and oxidation) occur in opposite directions, assuring electroneutrality. The charge transfer is secured by conducting paths both in solution and externally.

Electron reactions occur in the interface between the electrode and solution, by charge transfer from or to the electrode. Electron transfer occurs when there is a correspondence between the energies of the electron orbitals in the donor and acceptor. For reduction to occur, there is a minimum energy that the electrons supplied by the electrode must have. In the case of oxidation, there is a maximum energy that the lowest unoccupied level of the electrode must have to receive electrons.

Electrode reactions are related to the standard potential (E^o) through the Nernst equation, where v_i are the stoichiometric numbers of each species in the electrode reaction, and n is the number of electrons involved (equation 2.8). R is the universal gas constant, T the temperature and F the Faraday constant. α_i is the chemical activity of the species, $\alpha_i = y_i c_i$ where y_i is the activity coefficient and c_i the concentration of species. Electrode reactions are, by convention, expressed as reductions, and E^o is measured in relation to the normal hydrogen electrode (NHE).

$$E = E^o - \frac{RT}{nF} \sum v_i \, ln \, a_i \tag{2.8}$$

The tendency for a reduction to occur is given by the following equation (2.9), where ΔG^o is the Gibbs free energy and n the number of transferred electrons. The more negative the value of E^o, the higher the tendency for the species to be reduced.

$$\Delta G^o = -nFE^o \tag{2.9}$$

The Nernst equation can be applied when the oxidized and the reduced species are at equilibrium at the electrode surface. This occurs when the kinetics of the electrode reaction (k_o) is much faster than the transport of species (k_d). By contrast, an irreversible reaction occurs with the opposite conditions. Quasi-reversible reactions intermediate between the two conditions.

Exchange current (I_o), another important parameter in electrochemistry, which is related to the electrode reactions rate and it is the intensity of anodic and cathodic current at equilibrium. It is equivalent to the standard rate constant (k_o). The current (I) is related to the rates of the electrode reactions, being lg (I) linear to the potential [9] [10].

2.2.2 Electrochemical setup

The electrochemical cell design varies with the specific needs of a given experiment. It contains at least two electrodes, being the working electrode always one of them, plus the reference electrode and/or the counter electrode. The current passes between the working and the counter electrodes, being the last one used to complete the electrical circuit. The difference in potential is measured between the reference and the working electrodes. The obtained potential is due to alterations recorded in the working electrode, since the potential of the reference electrode remains stable in a specific range of experimental conditions. The working and reference electrodes must be as close as possible to minimize the electrical noise. The potential is controlled externally by a potentiostat, or the current is controlled by a galvanostat.

Nowadays, the working electrode is usually solid, and it can have various forms. Its constitution depends on the electroactive species in analysis however, in bioelectrochemistry it is commonly constituted by carbon-based materials. Solid non-disposable working electrodes must be polished before use to ensure that they are free of physical defects, guaranteeing as much surface homogeneity as possible, and to remove possible deposited impurities. Solid electrodes can also be electrochemically cleaned. Reference electrodes provide a potential value to which other potentials can be referred to, and their potential must be stable to perturbations in the system. The most used reference electrodes are calomel and silver/silver chloride (Ag/AgCl). The standard hydrogen electrode is also of great importance, since it defines the normal electrode potential scale. In fact, by convention, this electrode has the potential of 0 V. Counter electrodes are usually made of platinum foil or gauze.

An electrochemical cell must be filled with a supporting electrolyte, which is the principal source of electrically conducting ionic species. It is mandatory to ensure that the electrolyte is inert in the potential range and conditions (including temperature) of the experiment. The electrolyte should also minimize the migration of electroactive ions and confine the interfacial potential difference. Buffers such as citrate, phosphate and acetate can be used. Additionally, the oxygen in the electrolyte and in the electrochemical cell must be removed if it interferes with the measurements. This is done because the presence of oxygen may contribute to the current measurement, since it is easily reduced at the usual potential ranges used in bioelectrochemistry. Besides, it can oxidize electrode surfaces. Degassing is ensured by addition of an inert gas, such as argon or nitrogen. Also, an anaerobic chamber can be used attaining the electrochemical measurements inside it [9] [10].

2.2.3 Voltammetry

Several electrochemical techniques can be used to determine the reduction potential of electroactive species, however potential sweep methods have been the most used ones. Voltammetry is based on the application of a continuous time-varying potential to the working electrode, *versus* a reference one, leading to redox reactions involving the electroactive species in solution. This technique has the advantages of being applicable to a wide range of potential windows and it is possible to obtain kinetic and thermodynamic parameters for the redox centers in study.

Cyclic voltammetry is the most used type of voltammetry in the study of biomolecules. In this method, at a chosen potential value (E_{max}), the sweep direction is inverted until it reaches E_{min}, and then switched again for a determined number of times. It is also important to establish the initial and final potential (E_i and E_f, respectively), the initial sweep direction and the scan rate (v). The peak current (I_p) is registered at the zone where the potential is applied and the electrode reactions occur, being dependent on the kinetics and transport by diffusion of the electroactive species. Anodic and cathodic peak currents are registered (I_{pa} and I_{pc}, respectively), as well as the anodic and cathodic peak potentials (E_{pa} and E_{pc}, respectively). I_p corresponds to the maximum registered current and the E_p to the potential value where that maximum current is observed.

Cyclic voltammetry can be used to determine if a system is reversible, by recording several voltammograms at different scan rates. In fact, the peak current and the square root of the scan rate must be linear ($I_p \propto v^{½}$). Furthermore, the ratio between the anodic and the cathodic peak currents must be close to 1 ($I_{pa} / I_{pc} \cong 1$). The peak current is given by the Randles-Sevcik equation (2.10), where n is the number of electrons transferred, A the electrode area, D the diffusion coefficient of the electroactive species, v the scan rate and C the concentration (C_0 is the concentration of the oxidized species).

$$I_p = (2.69 * 10^5) n^{3/2} A D_0^{1/2} v^{1/2} C_0 \quad (2.10)$$

In reversible systems, the potential (E_p) must also be independent of the scan rate (v), and the difference between the anodic and the cathodic potential (ΔE_p) must go by the equation 2.11 (at 25 ºC).

$$\Delta E_p = |E_{pa} - E_{pc}| = 2.2 \frac{RT}{nF} \quad (2.11)$$

In irreversible systems, the concentrations of reduced and oxidized species do not follow the Nernst equation. The linear sweep and the cyclic voltammetry have the same profile since the reverse peak does not appear upon changing the scan direction.

In quasi-reversible systems, the irreversibility increases with the extension of the scan rate, associated with a decrease in peak current and increase in separation between the anodic and the cathodic peaks. The peak current is not directly proportional to the square root of the scan rate,

and the difference between the anodic and the cathodic potential increases with the scan rate (Figure 2.5 A) [9] [10].

2.2.4 Thin layer electrochemical systems

When the quantity of analyte is not a problem it can be dissolved in the electrolyte solution. However, for the case of many biomolecular systems, the produced quantity is an issue. A technique denominated thin layer is applied in voltammetry, which consists in the entrapment of the electroactive species to a thin layer at the working electrode surface. In this system, the thickness is much less than the diffusion layer, causing the electrolysis to be rapid and about 100% of the electroactive species are converted.

In this system, the counter and reference electrodes are placed outside of the thin layer. The most common configuration is based on the use of membranes that compress the analyte towards the working electrode surface.

Reversible reactions in thin-layer regime have different characteristics than in normal cells. I_p is proportional to v, and no longer to $v^{½}$. Furthermore, there is no separation between the anodic and cathodic peak currents and the curve is symmetric around E_p. The ratio between the anodic and the cathodic peak currents it is still expected to be close to 1 (Figure 2.5 B) [9].

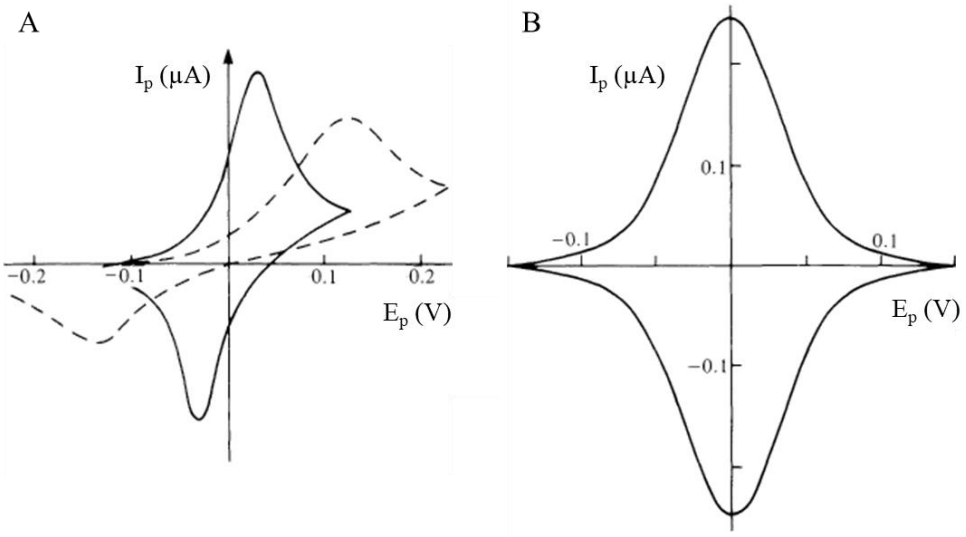

Figure 2.5 – Cyclic voltammograms. (A) corresponds to the effect of increasing irreversibility on the curve shape, from reversible (continuous line) to quasi-reversible (dashed line). **(B)** corresponds to a reversible system in a thin-layer regime. Figure adapted from [9].

The Laviron's mathematical approach can be applied in thin-layer systems [11], to determine kinetic parameters. Considering that the concentrations of reactant and product are uniform throughout the cell, equation 2.12 can be defined for the current.

$$I = nFAk_{sh}\left(c_o e^{\frac{-\alpha nF(E-E^O)}{RT}} - c_r e^{\frac{(1-\alpha)nF(E-E^O)}{RT}}\right) = -\frac{nFVdc_o}{dt} \quad (2.12)$$

Where I is the current, A the area of the electrode, V the volume of the thin cell, c_o and c_r the concentrations of the oxidized and reduced species respectively, c_t is their constant sum ($c_t = c_o + c_r$), and k_{sh} the heterogeneous rate constant (cm s^{-1}). n, α, F, R, T have their usual significance, regarding the Nernst equation. The parameter m is stablished according to equation 2.13.

$$m = \frac{RTk_{sh}}{Fnv} \tag{2.13}$$

When m tends to ∞, the system tends to reversibility and the cathodic and anodic peaks are symmetrical to the potential axis. On the contrary, when m tends to 0, the system tends to irreversibility.

The value of k_{sh} can be determined from the difference in potential between the anodic and cathodic peaks (ΔE_p) and for a known α value. When the value of ΔE_p is greater than $200/n$ (mV), α can be determined from the slop of the plot E_p *vs* log v, that is $-2.3RT/\alpha nF$ and $-2.3RT/(1-\alpha)nF$ for cathodic and anodic peaks, respectively. k_{sh} can be determined using equation 2.14 for the cathodic (v_c) and anodic (v_a) peaks.

$$k_{sh} = \frac{\alpha nFv_c}{RT} = \frac{1-\alpha nFv_a}{RT} \tag{2.14}$$

When the value of ΔE_p is smaller than $200/n$ (mV), the determination of α cannot be determined precisely, since a small error in the determination of E_{pa} and E_{pc} causes a large error in the activity coefficient (y). However, for α values close to 0.5 (between 0.3 and 0.7), k_{sh} can still be determined with relatively small error associated. By using the following theoretical graphic (Figure 2.6), that relates the value of $n\Delta E_p$ and 1/m, the value of k_{sh} can be determined using the previous equation (2.13) [11].

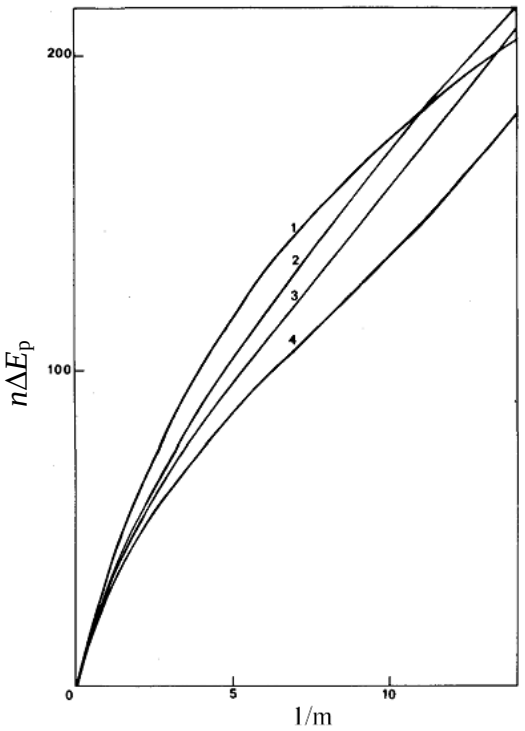

Figure 2.6 – Variation of $n\Delta E_p$ with 1/m. Curve 1 is respective to α = 0.5, curve 2 to α = 0.8, curve 3 to α = 0.85 and curve 4 to α = 0.9. Figure adapted from [11].

2.3 References

[1] S. Briefs and I. N. Biochemistry, *NMR for chemists and biologists*, vol. 51, no. 08. 2014.

[2] D. S. Wishart *et al.*, "^{1}H, ^{13}C and ^{15}N chemical shift referencing in biomolecular NMR.," *J. Biomol. NMR*, vol. 6, no. 2, pp. 135–140, 1995.

[3] J. Cavanagh, *Protein NMR spectroscopy : principles and practice*. Academic Press, 2007.

[4] L. Braunschweiler and R. . Ernst, "Coherence transfer by isotropic mixing: Application to proton correlation spectroscopy," *J. Magn. Reson.*, vol. 53, no. 3, pp. 521–528, 1983.

[5] D. L. Turner, C. A. Salgueiro, J. LeGall, and A. V. Xavier, "Structural studies of *Desulfovibrio vulgaris* ferrocytochrome c_3 by two-dimensional NMR," *Eur. J. Biochem.*, vol. 210, no. 3, pp. 931–936, 1992.

[6] G. P. Moss, "Nomenclature of tetrapyrroles (Recommendations 1986)," *Eur. J. Biochem.*, vol. 178, no. 2, pp. 277–328, 1988.

[7] L. Morgado, A. P. Fernandes, Y. Y. Londer, M. Bruix, and C. A. Salgueiro, "One simple step in the identification of the cofactors signals, one giant leap for the solution structure determination of multiheme proteins.," *Biochem. Biophys. Res. Commun.*, vol. 393, no. 3, pp. 466–70, 2010.

[8] G. Gilardi, A. Fantuzzi, and S. J. Sadeghi, "Engineering and design in the bioelectrochemistry of metalloproteins.," *Curr. Opin. Struct. Biol.*, vol. 11, no. 4, pp. 491–9, 2001.

[9] C. M. A. Brett and A. M. O. Brett, *Electrochemistry: Principles, Methods and Applications*. Oxford University Press, 1993.

[10] A. J. Bard and L. R. Faulkner, *Electrochemical methods : fundamentals and applications*, 2nd ed. John Wiley & Sons, 2001.

[11] E. Laviron, "General expression of the linear potential sweep voltammogram in the case of diffusionless electrochemical systems," *J. Electroanal. Chem. Interfacial Electrochem.*, vol. 101, no. 1, pp. 19–28, 1979.

3. Backbone and side-chain assignment of the cytochrome OmcF in the oxidized state

3.1 Introduction

OmcF is a small monohemic cytochrome from *G. sulfurreducens*, containing 104 amino acids, which includes a predicted lipid anchor formed by the first 19 residues, a molecular weight of approximately 11 kDa and a predicted isoelectric point of 7.8. OmcF has one low-spin *c*-type heme group with axial His-Met coordination and is predicted to be localized at the outer-membrane of the bacterium [1]. The structure of OmcF's soluble part (OmcFs, residues 20 to 104) was determined both in the oxidized and reduced states [1] [2].

Genetic studies carried out in OmcF-deficient strains have shown its involvement in the reduction of Fe(III) citrate, U(VI) and in the current production in MFC [3] [4]. These genetic studies were based in the growth of a OmcF-deficient strain, which caused the transcript levels of genes encoding for other outer membrane proteins (OmcB and OmcC) to be severely diminished. OmcB and OmcC have been pinpointed as direct participants in the electron transfer to Fe(III) citrate or to electrode surfaces in microbial fuel cells [5] [6]. OmcB and OmcC are *c*-type cytochromes with 12 heme-binding domains, are 79% identical in structure and 77% identical regarding the amino acid sequence. OmcB and OmcC are part of porin-cytochrome trans-outer membrane complexes, being the subunit localized at the cell exterior, and are involved in the electron transfer from the periplasm to the cell exterior [7]. Despite OmcB and OmcC being homologous proteins, OmcC is theorized to not have a key role in Fe(III) citrate reduction [8].

These results indicate that the presence of OmcF is necessary for the expression of OmcB and OmcC proteins. Kim and co-workers [3] also verified that a OmcB-deficient strain reduces Fe(III) citrate poorly, suggesting that the inability of the OmcF-deficient strain to reduce Fe(III) citrate is caused by the small level of expression of OmcB. These studies pinpointed OmcF as a crucial protein in these respiratory pathways. However, it is still unclear what is the role of this cytochrome in iron reduction and current production, despite being proved that the mechanisms involved are different. In both cases, OmcF appears to have a regulatory role in the transcription of genes that encode for proteins directly involved in Fe(III) reduction and current production in MFC [3] [4].

Although it is known that OmcF is an outer-membrane protein, it is still unclear the orientation of its soluble part, which could be either oriented towards the periplasm or to the extracellular space. A possible indication can be provided by the analysis of the biomolecular interaction with periplasmic proteins, such as PpcA (GSU0612). PpcA is the most studied cytochrome of *G. sulfurreducens* and is part of a periplasmatic protein family of five triheme cytochromes [9] [10]. Due to their location in the cell and the identified functions, it is proposed that this family of cytochromes is a reservoir of electrons, bridging the electron transfer from cytoplasm to the cell exterior [11] [12]. Genetic studies revealed that the deletion of *ppcA* affected

the reduction of Fe(III) and U(VI) [11] [13], and the gene was up-regulated when *G. sulfurreducens* cultures were grown in the presence of Fe(III) citrate and Fe(III) oxide [9].

The genetic studies suggested that PpcA and OmcF take part in the same electron transfer pathways, increasing the possibility of being physiological partners. If it is the case, the heme redox potential of PpcA (-117 mV at pH 7) [10] compared to that of OmcF (+180 mV at pH 7) [1] would favor the reduction of the latter.

In this chapter the backbone and side chain assignment of OmcFs is described in the oxidized state, in addition to that already obtained for the reduced state [14]. Furthermore, the heme substituents of OmcF have already been assigned for both redox states [2]. These assignments pave the way to probe the interaction regions between this protein and its putative redox partners. The backbone, side-chain and heme assignment of PpcA in both reduced [15] and oxidized [16] states have also been obtained. In this work, NMR chemical shift interaction studies between OmcF and PpcA were carried out in the oxidized state since analysis of protein-protein interactions are facilitated, due to easier manipulation of the samples, and due to the spectral distribution of the signals. Additionally, by conducting the studies in the oxidized state, it will represent a good base of comparison with other molecular interactions performed previously with PpcA [16]–[20].

3.2 Materials and Methods

3.2.1 Protein expression and purification

The protocols for the production and purification of OmcF and PpcA are similar, except for the plasmids used to transform *Escherichia coli* cells, and the buffers used in the purification processes, obviously due to the difference in pI between the two proteins.

E. coli cells BL21 (DE3), containing plasmid pEC86 which encodes for the expression of *c*-type cytochrome maturation proteins in aerobic conditions [21], were transformed with the vector pLBM4, in the case of OmcF, or pCK32, in the case of PpcA. pLBM4 plasmid contains the gene that encodes for the soluble part of OmcF [1] and it is based on pCKN5, a derived vector of pCK32 with a *NotI* site at the end of the leader peptide coding sequence, which avoids the addition of extra residues at the N-terminus [22]. pCK32, which contains the sequence for mature PpcA, is a pUC derivate that includes the lac promotor and a OmpA leader sequence [23] (Figure 3.1).

For the transformation of *E. coli* cells, the plasmid containing the gene that encodes for the protein of interest was added to the *E. coli* solution, and placed in ice for 30 min. Then the solution was put for 1 min at 42 ºC, followed by another minute in ice. 500 µL of 2x Yeast extract (2xYT) medium was added and the cells incubated at 37 ºC, at 200 rpm and for 1 h. 2xYT medium is

constituted by 20 g/L of yeast extract, 16 g/L of tryptone and 5g/L of NaCl. Cells were inoculated in 2xYT solid medium, containing 15 g/L agar and supplemented with 34 μg/mL chloramphenicol and 100 μg/mL ampicillin, overnight at 37 ºC.

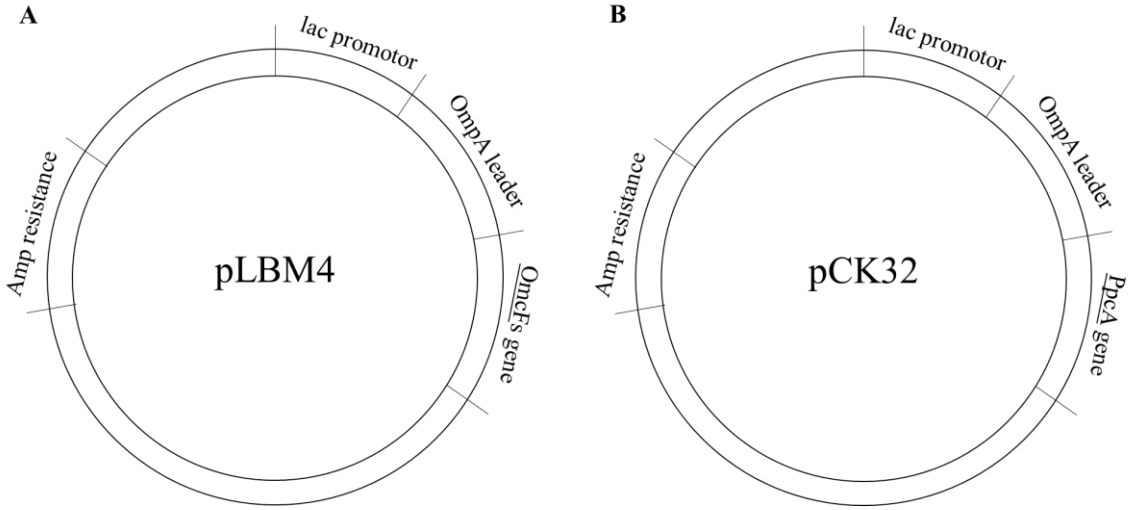

Figure 3.1 – pLBM4 and pCK32 vectors design, encoding for OmcF (A) and PpcA (B) proteins, respectively. Adapted from [22] [23].

3.2.2 Production of natural abundance proteins

After transformation, one colony was added to 50 mL of 2xYT liquid medium containing the same concentration of chloramphenicol and ampicillin. The culture was incubated overnight, at 30 ºC and at 200 rpm. After reaching an OD_{600nm} between 1.8 and 2.0, 10 mL of the culture was transferred to 1 L of 2xYT medium with the same antibiotics and incubated at 30 ºC and at 180 rpm, until the OD_{600nm} reached a value between 1.5 and 1.8. At this point, OmcF expression was induced using 20 μM isopropyl β-D-thiolgalactopyranoside (IPTG), and PpcA with 60 μM. The culture was incubated at 160 rpm and 30 ºC, for approximately 16 h.

3.2.3 Production of isotopic enriched proteins

The isotopic enrichment of the samples (^{15}N and ^{13}C) was carried out as previously described by Fernandes and co-workers [24]. According to this method, after transformation one colony was added to 5 mL of 2xYT liquid medium containing the same antibiotics as previously described. The culture was incubated overnight, 30 ºC and at 200 rpm. From the 5 mL culture, 1 mL was transferred to a 50 mL of 2xYT medium, supplemented with the same antibiotics, and inoculated at 30 ºC and at 200 rpm. After reaching an OD_{600nm} between 1.8 and 2.0, from the 50 mL culture 10 mL were transferred to a 1 L of 2xYT medium, supplemented with the same antibiotics, and inoculated at 30 ºC and at 180 rpm. When the OD_{600} reached a value between 1.5 and 1.8, cells were harvested by two centrifugations at 6400 *xg* for 20 min. The cell pellet was resuspended twice with 250 mL of a salt solution (110 mM KH_2PO_4, 240 mM Na_2HPO_4 and 43 mM NaCl). After a final centrifugation, the cell pellet was resuspended in 250 mL of minimal

medium M9, containing 22 mM KH_2PO_4, 48 mM Na_2HPO_4, 8.6 mM NaCl, 20 mg/L biotin, 2 mM $MgSO_4.7H_2O$, 0.1 mM $CaCl_2$, 5 μM $MnCl_2.4H_2O$, 10 μM $FeSO_4.7H_2O$, 20 mg/L vitamin B1, 1 mM of the heme precursor α-aminolevulinic acid, 2 g/L ^{13}C-Glucose as carbon source, 1 g/L $^{15}NH_4Cl$ as nitrogen source, and the same antibiotic concentrations as previously described. Cultures were inoculated for 1 h 30 min at 30 ºC and at 180 rpm. OmcF expression was induced by adding 200 μM of IPTG, and PpcA expression was induced by adding 600 μM of IPTG. Cells were grown overnight at 30 ºC and at 160 rpm.

3.2.4 Isolation of the periplasmic fraction and protein purification

Cells were then harvested at 6,400 *xg* for 20 min. The periplasmic fraction was isolated using a lysis buffer, containing 15 mg/mL of lysozyme, 0.2 g/mL of sucrose, 100 mM Tris-HCl pH 8.0 and 0.5 mM EDTA, in a ratio 30 mL per 1 L of cell culture. The periplasmic fraction was recovered by centrifugation at 1,4700 *xg* and at 4 ºC for 20 min. The supernatant constituted the periplasmic fraction, which was ultracentrifugated at 225,000 *xg* and at 4 ºC for 1 h. This fraction was then dialyzed twice, for 24 h, with the adequate buffer to perform the following purification steps, and then centrifuged at 8,000 *xg* for 30 min and at 4 ºC.

The resulting protein solution was loaded onto cation-exchange columns (2x5 mL Bio-Scale™ Mini UNOsphere S cartridges, Bio-Rad) pre-equilibrated with 20 mM sodium acetate pH 5 (OmcF) or 10 mM Tris-HCl pH 8.5 (PpcA). The fractions were eluted with a sodium chloride linear gradient: 0 to 200 mM for OmcF and 0 to 300 mM for PpcA. The fractions containing the protein of interest were pooled and concentrated with successive centrifugations at 5,000 *xg* for 10 min and at 4 ºC using Amicon™ Ultra-4 Centrifugal Filter Devices. The resulting samples was then loaded onto a XK 16/70 Superdex™ 75 prep grade column (GE Healthcare Life Sciences) pre-equilibrated with 20 mM sodium acetate pH 5 with 200 mM NaCl (OmcF) or 100 mM sodium phosphate pH 8 (PpcA). In all chromatographies, proteins were eluted at 1 mL/min. All chromatographies were performed using AKTA™ Prime Plus or AKTA™ Pure Chromatography Systems (GE Healthcare Life Sciences)

The protein purity was evaluated by Coomassie staining sodium dodecyl sulphate polyacrylamide gel electrophoresis (SDS-PAGE). The protein concentration was determined by visible spectroscopy, using an absorption molar coefficient of $23.8x10^{-3}$ $M^{-1}cm^{-1}$ for OmcF [25], and $97.5x10^{-3}$ $M^{-1}cm^{-1}$ for PpcA [26], and by using the absorbance of the cytochrome's α band in the reduced state. Experiments were performed in a UV-visible scanning spectrophotometer Evolution 201 (Thermo Scientific), at room temperature, in a 1 cm path length quartz cuvettes. Reduced samples were achieved by adding sodium dithionite.

3.2.5 NMR studies

3.2.5.1 Sample preparation

For NMR samples prepared in H_2O, after protein purification, the buffer was permuted by successive centrifugations, using Amicon™ Ultra-4 Centrifugal Filter Devices, at 5,000 *xg*, for 10 min and at 4 ºC. In the case of samples prepared in 100% D_2O, first the buffer from the purification was permuted to 20 mM NaCl, using Amicon™ filters as well. Then, the samples were frozen at -80 ºC and underwent several cycles of lyophilization and subsequently were solubilized in the respective buffer prepared in D_2O.

For the backbone assignment of OmcFs, all samples were prepared in 45 mM sodium phosphate (final ionic strength 100 mM) at pH 7. Complementary spectra were acquired for samples in the same buffer but at pH 5. All protein samples were prepared with 1 mM of final concentration and in 92% H_2O / 8% D_2O.

In the case of the pH-linked conformation experiments, the sample was prepared with 0.6 mM of concentration and in 92% H_2O / 8% D_2O 45 mM sodium phosphate (final ionic strength 100 mM) at pH 7, as well. The pH value was adjusted with increasing amounts of NaOD or DCl, and the pH values checked with a glass micro electrode.

In the case of protein-protein interaction studies, samples were prepared in 8 mM phosphate buffer, pH 7 and 20 mM final ionic strength. To observe the protein NH signals, samples were prepared in 92% H_2O / 8% D_2O, and to observe the heme substituents signals the samples were prepared in 100% D_2O. The titrated protein had the final concentration of 180 µM, and the titrant protein was prepared so that each addition was equimolar. After titration, the pH of the samples was measured.

3.2.5.2 NMR experiments

All NMR spectra were acquired in a Bruker Avance III 600 MHz spectrometer equipped with a triple-resonance cryoprobe. The ^{1}H chemical shifts were calibrated using the water signal as internal reference, and the ^{15}N, ^{13}C calibrated by indirect referencing [27]. Processing of data was done using TOPSPIN (Bruker Biospin, Karlsruhe, Germany) and data analysis with Sparky (TD Goddard and DG Kneller, Sparky 3, University of California, San Francisco, USA).

3.2.5.3 Backbone and side chain assignment

2D ^{1}H, ^{15}N HSQC spectrum shows the correlation between the amide proton (HN) and the nitrogen (N) for the backbone and side chains amide groups. It is considered to be the NMR "fingerprint" of the protein, since at least one signal of each amino acid is present in it, with the exception of the proline residues. Due to the very rapid exchange with the solvent, the N-terminal NH is also not observed in this spectrum. The amide signals of arginine, lysine, histidine and tryptophan side-chains can also be visible. Due to the data present is this spectrum, several

information can be obtained, including the protein folding, aggregation, stability and dynamic regions. Furthermore, chemical shift perturbations can be studied, due to the presence of other protein or ligand, variation in pH, ionic strength and temperature.

The backbone, side-chains and heme signals of OmcFs have already been assigned in the reduced state [14]. In this work, the same methodology was used to do the assignment in the oxidized state, as described in Chapter 2.

In order to assign the backbone and side chain signals of OmcFs, the following NMR experiments were recorded for the labelled protein at 25 ºC: 2D ^{1}H, ^{15}N HSQC and ^{1}H, ^{13}C HSQC; 3D HNCACB, HN(CO)CACB, HNCA and HN(CO)CA; 3D ^{1}H, ^{1}H, ^{15}N NOESY, HCC(H) TOCSY and HC(C)H TOCSY. To further assist the assignment, 2D experiments were recorded for the unlabeled protein: ^{1}H,^{1}H TOCSY (45 ms) and ^{1}H,^{1}H NOESY (80 ms).

A set of complementary NMR spectra, namely ^{1}H,^{15}N HSQC and 3D spectra (CBCANH; CBCA(CO)NH; HNCA; HN(CO)CA; ^{1}H,^{1}H,^{15}N NOESY) were also acquired at 30 ºC, in order to confirm dubious signals and further complete the assignment. The specifications of each NMR experiment recorded are described in Chapter 2.

3.2.5.4 pH-linked conformational changes in the oxidized state

A series of 2D ^{1}H,^{15}N HSQC experiments were recorded in the pH range of 5.3 to 9.2 to determine the effect of pH in the OmcF's backbone. All experiments were recorded at 25 ºC.

In order to calculate the pK_a values of the most affected NH signals, a modified Henderson-Hasselbach equation was used to fit the data, considering only one pK_a value (Equation 3.1). δ_{obs}, δ_A and δ_B correspond to the observed, protonated and deprotonated chemical shifts, respectively.

$$\delta_{obs} = \delta_A + (\delta_B - \delta_A)\frac{10^{pH-pKa}}{1+10^{pH-pKa}} \quad (3.1)$$

The pH titration data were analyzed according to the strategy of Schumann and co-workers [28], in which the weighted average chemical shift ($\Delta\delta_{comb}$) of each NH signal were calculated using Equation 3.2. $\Delta\delta$H and $\Delta\delta$N are the differences in ^{1}H and ^{15}N chemical shifts, respectively. $\Delta\delta$H and $\Delta\delta$N are the chemical shift change in ppm in ^{1}H and ^{15}N, respectively. $w_i = |\gamma^{15}_N|/|\gamma^{1}_H|$ is a weighting factor that accounts for the differences in nuclei sensitivity, which in this case is 0.102.

$$\Delta\delta_{comb} = \sqrt{\Delta\delta^2 H + (w_i \Delta\delta N)^2} \quad (3.2)$$

3.2.5.5 Protein-protein interaction between OmcF and PpcA

The heme signals of both OmcF [2] and PpcA [29] have already been assigned in the oxidized state, as well as the NH backbone signals of PpcA [16]. The heme signals of OmcF were assigned in 45 mM sodium phosphate buffer, with a final ionic strength of 100 mM at pH 7 [2].

The heme signals of PpcA were assigned in 80 mM sodium phosphate buffer, with a final ionic strength of 250 mM at pH 7 [29]. The NH backbone signals of PpcA were assigned in 45 mM sodium phosphate buffer, with a final ionic strength of 100 mM at pH 7 [16]. The NMR signals for both cytochromes were re-assigned in the present work for 20 mM ionic strength.

The chemical shift perturbation on the heme signals were analyzed for each protein by recording 1D ^{1}H following the addition of each protein. The titrations ranged from 1:0 to 1:5, by adding increasing equimolar amounts of OmcF to a 180 μM sample of PpcA, and vice-versa. For the analysis of the chemical shift perturbation on the backbone signals, 2D ^{1}H, ^{15}N HSQC were recorded at 1:0 and 1:5 of each protein ratio. The pH value chosen for the NMR experiments (pH 7) was in accordance with the physiological pH of *G. sulfurreducens*. All experiments were recorded at 25 ºC.

2D ^{1}H, ^{15}N HSQC data was analyzed by the strategy of Schumann and co-worker [28], in which the weighted average chemical shift ($\Delta\delta_{comb}$) of each NH signal was calculated in accordance to Equation 3.2. In order to determine the most affected signals, a cut-off value was determined with the standard deviation to zero value (σ_0^{corr}), in accordance with Equation 3.3. N corresponds to the number of $\Delta\delta_{comb}$ values determined. The σ_0 was determined from all $\Delta\delta_{comb}$ values, and those exceeding three times the value of σ_0 were removed. A σ_0^{corr} was obtained for the remaining $\Delta\delta_{comb}$ values. This process was repeated until no $\Delta\delta_{comb}$ value was larger than the σ_0^{corr}, being this the cut-off value.

$$\sigma_0^{corr} = \sqrt{\frac{1}{N}\Sigma(\Delta\delta_{comb} - 0)^2} \quad (3.3)$$

3.3 Results and discussion

3.3.1 Assignment of the NMR signals

The assignment of the backbone signals of OmcF in the oxidized state was carried out by analyzing 2D (^{1}H,^{15}N-HSQC; ^{1}H,^{1}H TOCSY; ^{1}H,^{1}H NOESY) and the 3D (CBCANH; CBCA(CO)NH; HNCA; HN(CO)CA; ^{1}H,^{1}H,^{15}N NOESY; HCC(H) TOCSY; HC(C)H TOCSY) NMR spectra, using the strategy described previously in Chapter 2 [30]. However, a set of NH signals could not be identified and correspond to the region between the residues 41 and 52. These results may indicate that this region of the protein is more dynamic and possibly these signals are in slow to intermediate exchange rate between more than one conformation. The same was observed for the OmcF in the reduced state though for an adjacent region (residues between 52 and 58) [2].

As an attempt to assign the missing signals, NMR experiments were done a pH 5 and at 30 ºC. In fact, the temperature increase causes the decrease of the peaks' linewidths due to the more rapid tumbling of the protein in solution, and also measure the exchange rate regime between multiple conformations in particular regions of the protein. Furthermore, at lower pH

levels, the protons of amino acids exchange more slowly with the solvent and thus favoring their observation. With this strategy, it was possible to identify additional signals, even though the following NH signals remained unassigned: Gln[41], Asn[44], Thr[45], His[47], Glu[49], Lys[50], Thr[51] and Leu[52]. His[47] is a protonable amino acid which is positioned close to the propionate D of the heme group, being strongly affected by the paramagnetic effect of the unpaired electron. The paramagnetic effect in His[47] and its presence in the dynamic region of OmcF, may explain why its NH peak is not observed. The two first amino acids of OmcFs (Ser[20] and Gly[21]) and the last one (Phe[103]) were also unassigned.

The assignment percentage obtained was the following: ^{15}N (88%), ^{1}HN (86%), $^{13}C_{\alpha}$ (87%) and $^{13}C_{\beta}$ (76%). The assignment of OmcFs in the oxidized state is depicted in Figure 3.2 and reported in the Appendix section (Table A.1).

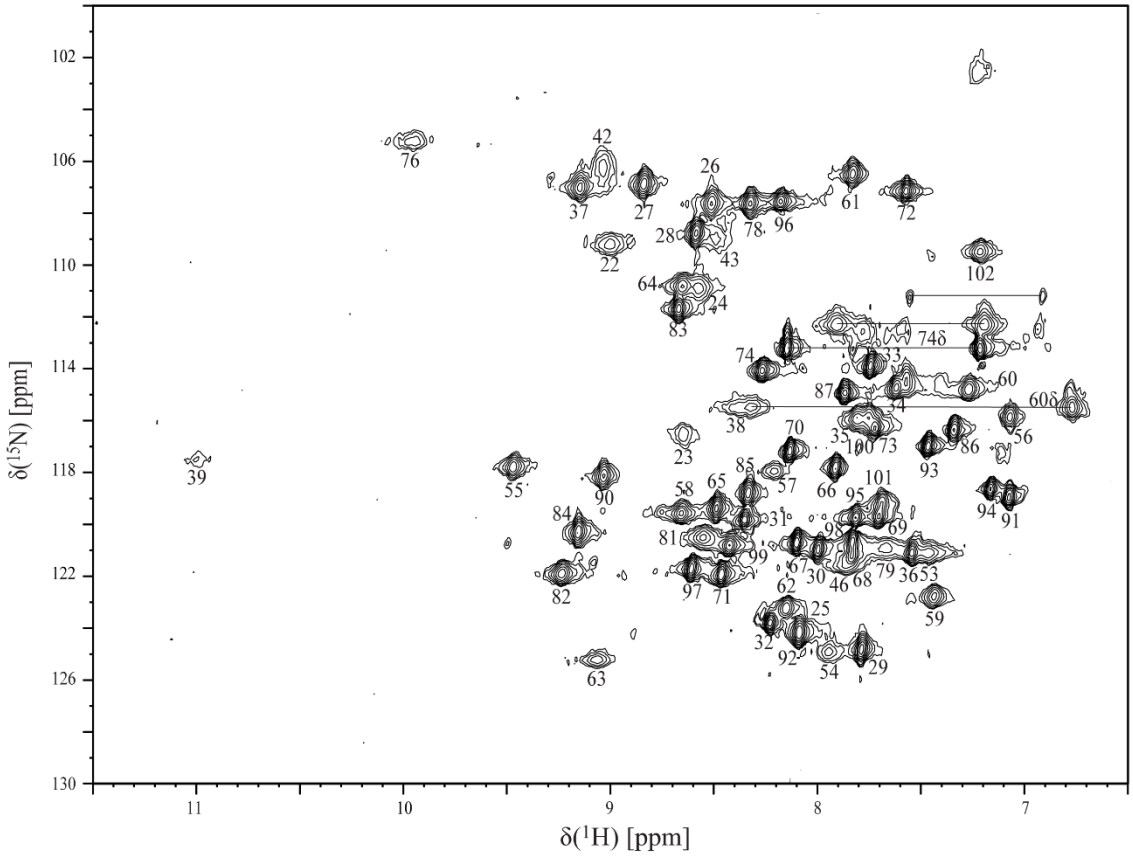

Figure 3.2 – 2D ^{1}H, ^{15}N HSQC spectra of labelled OmcFs in the fully oxidized state. Sample with concentration of 1 mM, prepared in 45 mM sodium phosphate buffer pH 7, final ionic strength of 100 mM, 25 ºC, 600 MHz. Labels correspond to the ^{1}H-^{15}N connectivities for backbone and side-chain groups (Nδ of Asn[60] and Asn[74]). Horizontal black lines correspond to the side-chain groups of asparagine and glutamine residues.

3.3.2 Secondary structure prediction

The solution secondary structure of OmcF was predicted by using the assignment of the protein's backbone signals and TALOS+ software [31]. The data obtained indicates that α-helices are dominant, as it was observed in the crystal structure of the protein [1] (*cf.* panels A and B in Figure 3.3). There is a good agreement between the solution and the X-ray data [1]. Only two small exceptions were observed between residues 39 to 43 and residues 84 to 86. Furthermore, in the segment between residues 39 and 43 is located the heme binding motif residues (Cys[35]-Ala[36]-Gly[37]-Cys[38]-His[40]) which are strongly affected by the heme paramagnetic effect and might affect the prediction.

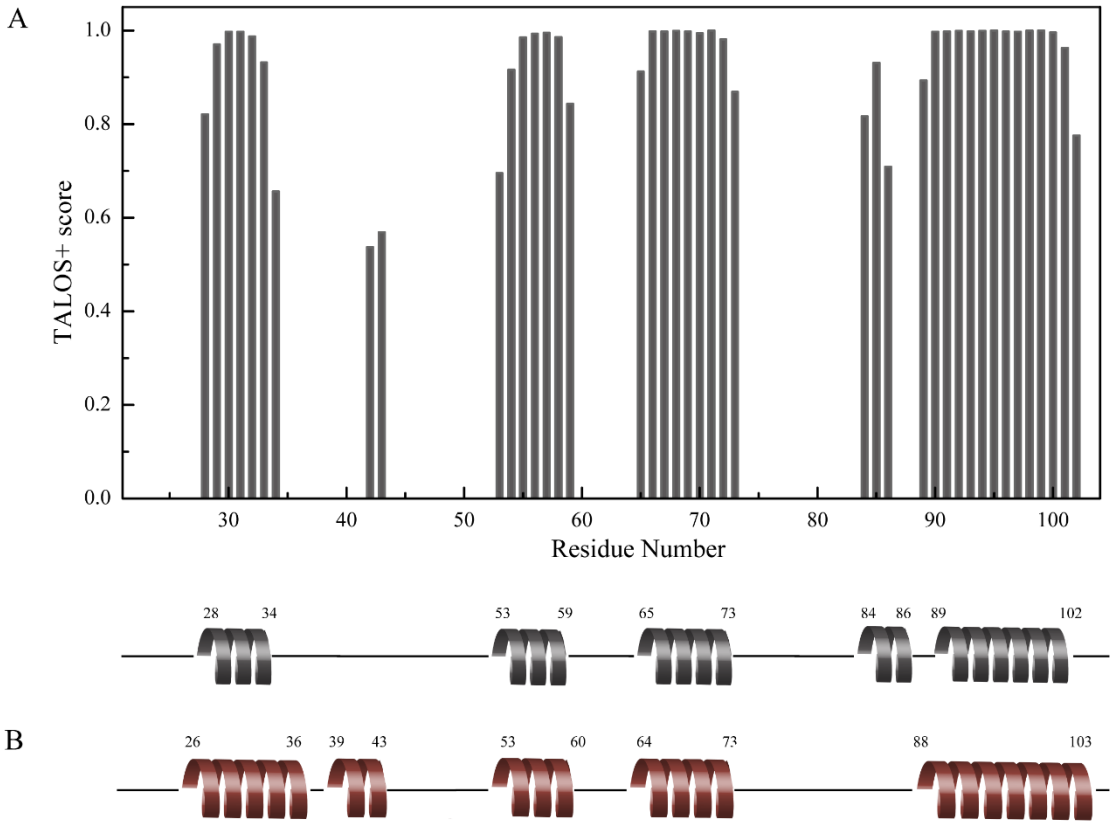

Figure 3.3 - Secondary structural elements of OmcFs. (A) Secondary structure elements predicted by TALOS+ [31]. The residues represented by the gray bars are predicted to be located in α-helical secondary structural elements. The author has chosen to not consider α-helixes with less than three amino acids. **(B)** Comparison of secondary structural elements from the TALOS+ prediction (this work) and those obtained from the X-ray crystal structure (PDB code: 3CU4 [1]). The residue numbers are shown on top of each secondary structural element.

3.3.3 pH-linked conformational changes

The pH titration of the OmcF backbone NH signals is indicated in Figure 3.4. The most affected signals, with a $\Delta\delta_{comb}$ higher than 0.5, are Thr[33], His[34], Gly[42], Arg[54], Glu[58] and Ala[81] (Figure 3.4 A). The mentioned residues are located in two distinct regions: one constituted by Thr[33], His[34] and Ala[81], the second by Gly[42], Arg[54] and Glu[58] (Figure 3.4 C). The same was observed

for the reduced state, but one of the regions was constituted by different amino acids [2]. In fact, residues Thr[33] and His[34] are in the N-terminal α-helix of OmcF and also show the largest chemical shift differences in the reduced state. His[47] and Glu[49], which show high chemical shift variation in the reduced state, their respective NH signals were unassigned in the oxidized state.

All backbone signals with the largest chemical shift deviation have pK_a values within the pH range of 6 to 8 (Figure 3.4 B). These results may be indicative of the proximity of these amino acids to the redox-Bohr center of OmcF, being its protonation/deprotonation responsible for their chemical shifts. This correlates with the modulation of the redox potential by the pH (redox-Bohr) effect observed in the heme range, as it will be discussed in Chapter 4.

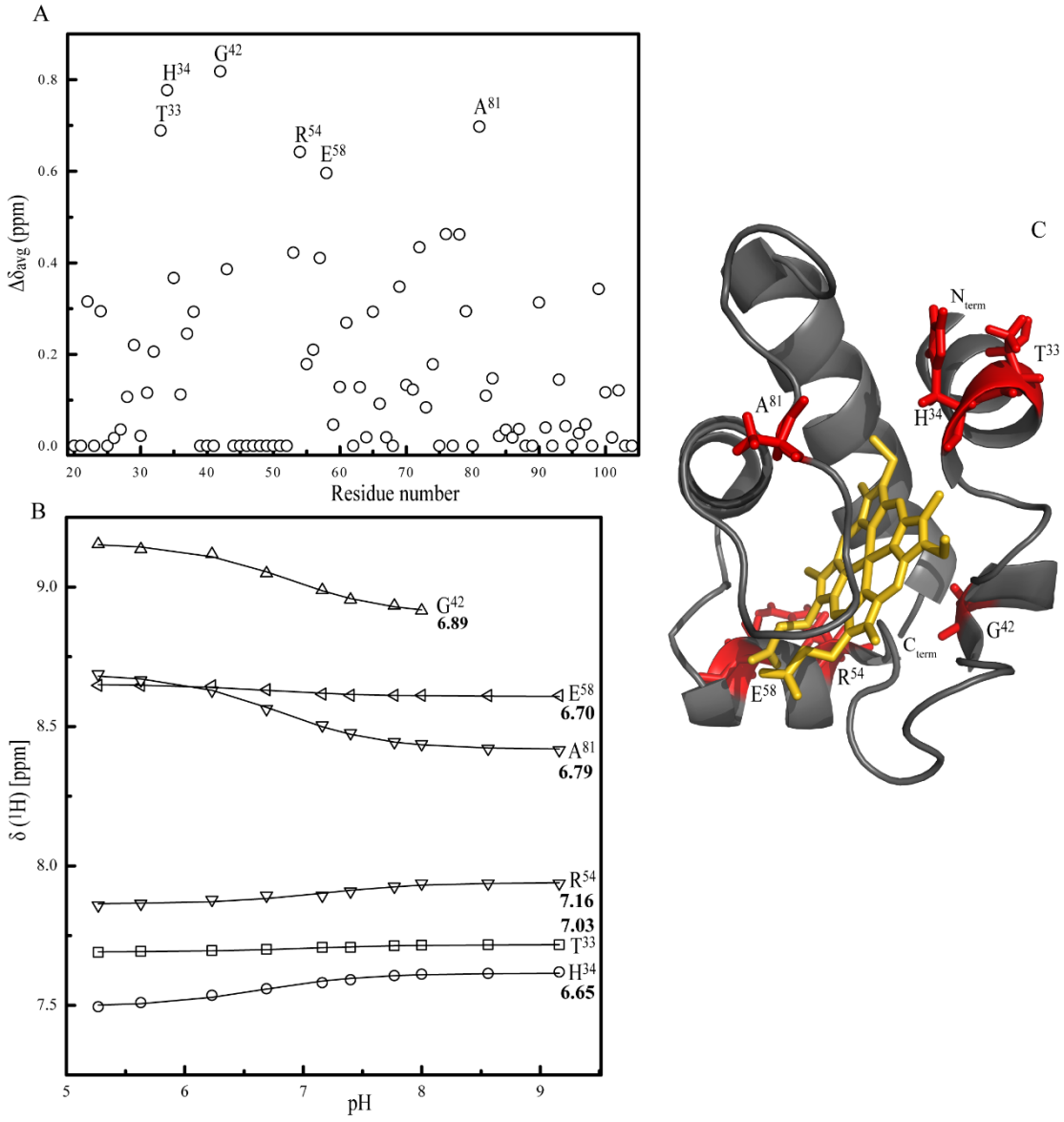

Figure 3.4- pH-linked conformational changes of OmcF, in the oxidized state. (A) Average chemical shift differences ($\Delta\delta_{avg}$) between pH 4.6 and 9.3. **(B)** pH titration data of the most affected OmcF amide H signals, with the respective calculated pK_a values in bold. **(C)** Mapping of the residues showing large pH-dependent shifts (red) on the OmcF X-ray structure (PDB code: 3CU4 [1]). The OmcF backbone and the heme group is colored gray and yellow, respectively. The N- and C-termini are labelled. Figure was produced using PyMOL (The PyMOL Molecular Graphics System, Version 1.3 Schrödinger, LLC).

3.3.4 Molecular interactions between OmcF and PpcA

The assignment of OmcFs signals obtained for the oxidized sate was further explored to analyze the interaction between OmcF and PpcA. Despite the existence of the assignments for both proteins in the reduced forms, working with the oxidized proteins has some advantages, including easier manipulation of the sample. In the oxidized state it is not necessary to add exogenous compounds, as it was the case of OmcF, that could interfere with the interaction between the proteins. Another advantage is, due to the paramagnetic effect of the unpaired electron of the heme, the amino acid and heme signals are more spread out along the spectrum, causing fewer peak overlaps and allowing a better analysis of the chemical shift of the signals.

The biomolecular interactions between OmcF and PpcA were investigated by NMR chemical shift perturbation experiments. Particularly for the heme methyl substituents, the signals in the oxidized state are more spread out along the spectra and are located in less crowded regions, being ideal for this type of experiments. In fact, the methyl signals of both proteins are in distinct spectral regions, with the exception for the heme methyl $2^{1}CH_3$ of OmcF and $18^{1}CH_3^{III}$ of PpcA, both located in a crowded region of the spectrum. Consequently, the molecular interactions between the two cytochromes was monitored by probing the chemical shift perturbation of their methyl signals with the addition of increasing amounts of OmcF to a PpcA sample, and vice-versa. The 1D ^{1}H NMR spectra of both titrations are indicated in Figure 3.5. In Figure 3.6 is depicted the ^{1}H chemical shift changes analysis of the heme methyl groups upon addition of the other cytochrome.

The heme methyl groups that showed the highest chemical shift variations are $12^{1}CH_3$ of the heme IV of PpcA, and the $7^{1}CH_3$ of OmcF. Due to broadness, the latter signal was not possible to monitor for ratios above 1:1. The heme methyl $7^{1}CH_3^{I}$ and $7^{1}CH_3^{IV}$ overlap in the 1D NMR spectra and for this reason the same chemical shift variation (from 0.01 to 0.05 ppm) was considered. The binding curves of the methyl groups of each cytochrome are depicted in the Appendix section (Figure A.1). As mentioned above, the chemical shift variation of the heme methyl $2^{1}CH_3$ methyl from OmcF and $18^{1}CH_3^{III}$ of PpcA were not monitored. These two methyl groups share the same heme face and thus it is unlikely they are more affected than their neighbors. In the future, chemical shift perturbation experiments followed by 2D ^{1}H, ^{13}C HMQC NMR spectra can be explored to confirm this hypothesis.

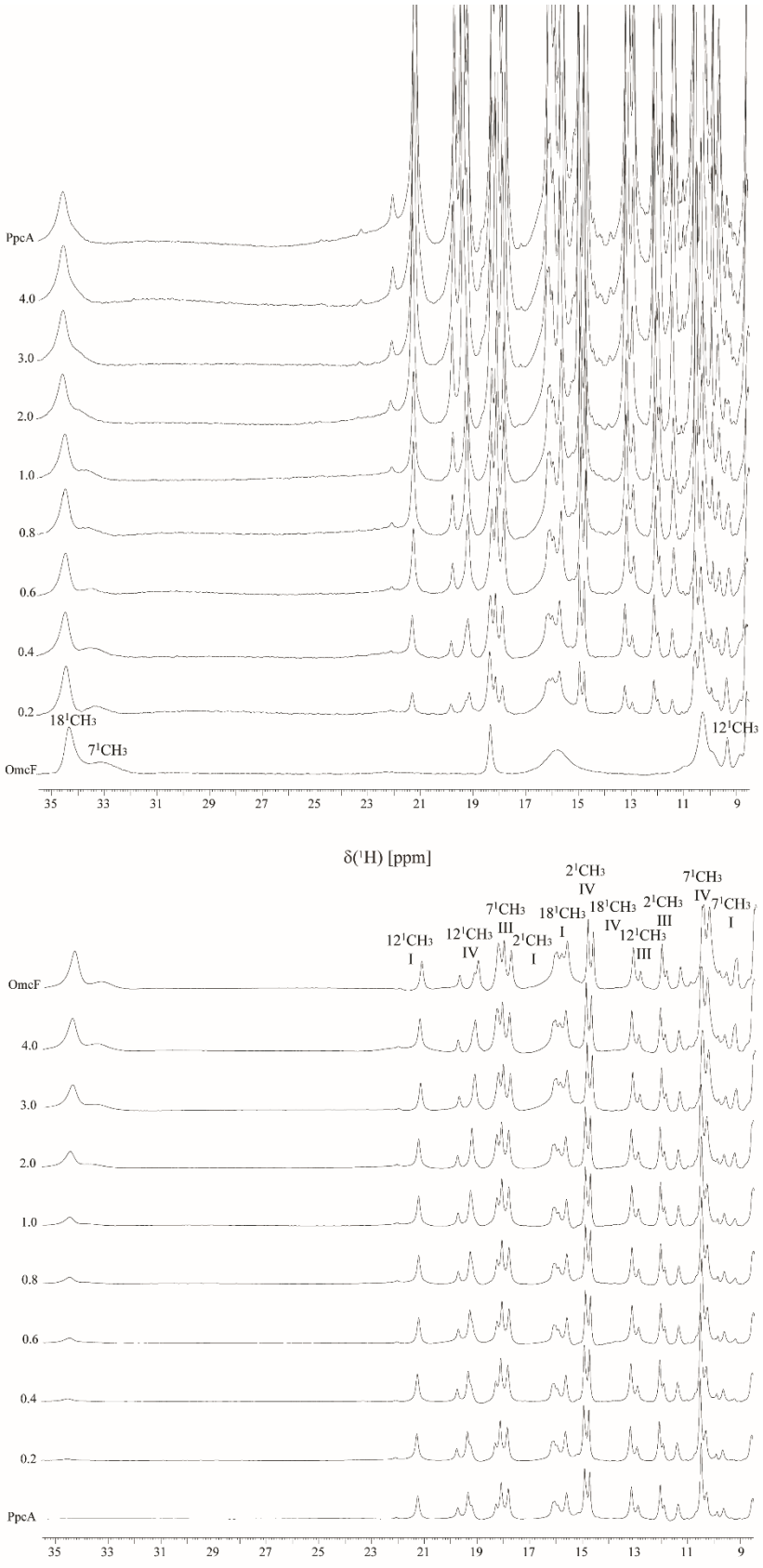

Figure 3.5 – Expansion of the low-field region of the 1D ^{1}H NMR spectra, in the oxidized state (25 ºC and pH 7), of OmcF in the presence of increasing amounts of PpcA (top figure) and vice-versa (bottom figure). The molar ratio between the two proteins is indicated on the left side of the spectra. The heme methyl signals of each protein are indicated, according to the IUPAC-IUB nomenclature [32].

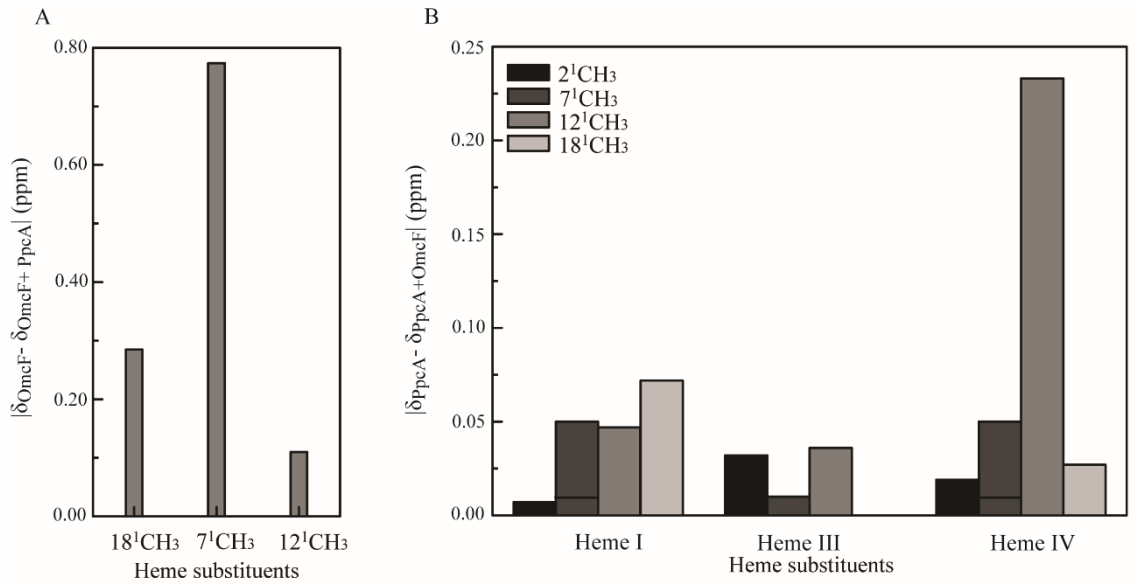

Figure 3.6 - ^{1}H chemical shift changes of the heme methyl groups of OmcF (A) and PpcA (B) upon addition of the other cytochrome. Comparison of the heme ^{1}H chemical shifts observed in the 1D ^{1}H NMR spectra of OmcF (δ_{OmcF}) and those of PpcA (δ_{PpcA}) in the relation 1:5, except of the heme methyl $7^{1}CH_3$ of OmcF, which is not possible to assign. In the case of PpcA, the heme methyl groups $7^{1}CH_3^{I}$ and $7^{1}CH_3^{IV}$ are undistinguishable in the 1D NMR spectra. For this reason, the same chemical shift variation is represented for both signals. The heme substituents are numbered according to the IUPAC-IUB nomenclature [32].

In the present study, the analysis of the NMR chemical shift perturbation measurements of PpcA and OmcF was further extended to the NH backbone signals. The chemical shift perturbations on the backbone NH signals of both cytochromes were monitored by 2D ^{1}H, ^{15}N HSQC experiments (Figure 3.7). The NH signals showing highest chemical shift perturbation in OmcF are Gly^{22} and Cys^{38} (Figure 3.8 A). For PpcA, the most affected signals are from Ala^{8}, Phe^{15}, Lys^{18}, Gly^{40} and Ala^{46} (Figure 3.8 B). These amino acids were selected through the calculated cut-off for each experiment: 0.014 ppm for OmcF + PpcA experiment, and 0.028 ppm for PpcA + OmcF experiment.

In the case of OmcF, from the amino acids which present the biggest chemical shift deviation, Gly^{22} is located at the N terminal, which is prone to mobility. Furthermore, Cys^{38} is covalently attached to the heme and placed in the vicinity of $7^{1}CH_3$, which was also the most affected methyl. It is unclear if there are more amino acids that have chemical shift perturbations with the addition of PpcA, since there is a region of OmcF which was not assigned in the oxidized state. Since this region (41-52) is adjacent to Cys^{38}, it is likely some of its amino acids take also part in the interaction between these two cytochromes. In order to confirm this hypothesis, an interaction study should be done in the reduced state, since the NH signals of the amino acids 41 to 52 from OmcF are assigned in this redox state.

Thus, and despite a few affected residues are not in the same regions and might result from slightly conformational changes, it is clear that the most affected residues and heme

substitutes are located in the region of heme IV in PpcA and on the top right corner of the heme in OmcF. These results are in accordance with previous interaction studies involving PpcA in the oxidized state [16]–[20]. In fact, all these studies pinpointed the region of heme IV as the interaction site, with chemical shift changes with the same order of magnitude as the ones obtained in the present study.

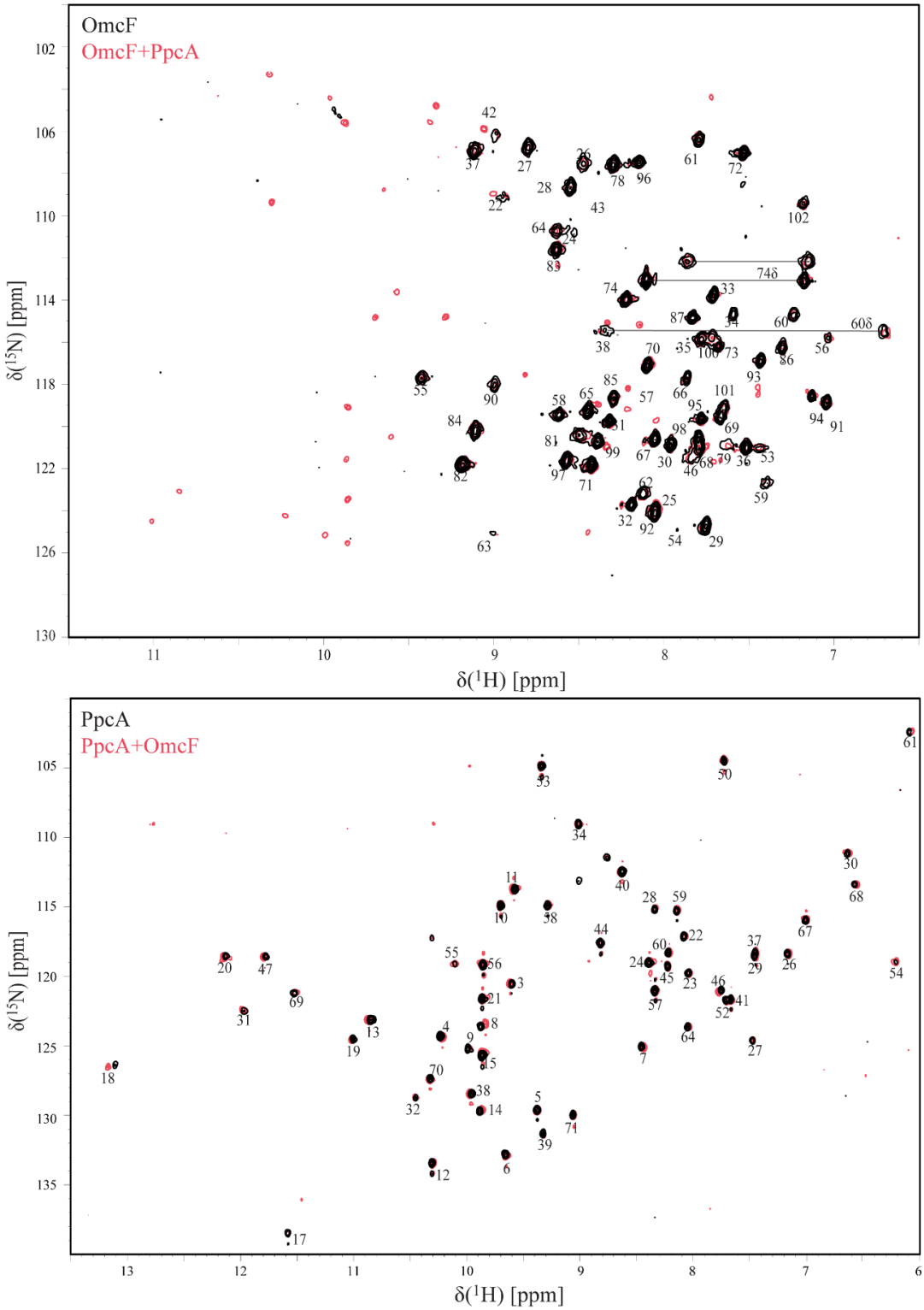

Figure 3.7– Overlay of the 2D ^{1}H, ^{15}N HSQC spectra of ^{15}N-labelled OmcF in the presence of PpcA (top figure) and vice-versa (bottom figure), in a 1:5 ratio (25 ºC, pH 7). The signals correspondent to

the reference spectrum are contoured in black, and in the presence of the titrated protein in red. The NH assignment of OmcF and PpcA is indicated with numbered labels.

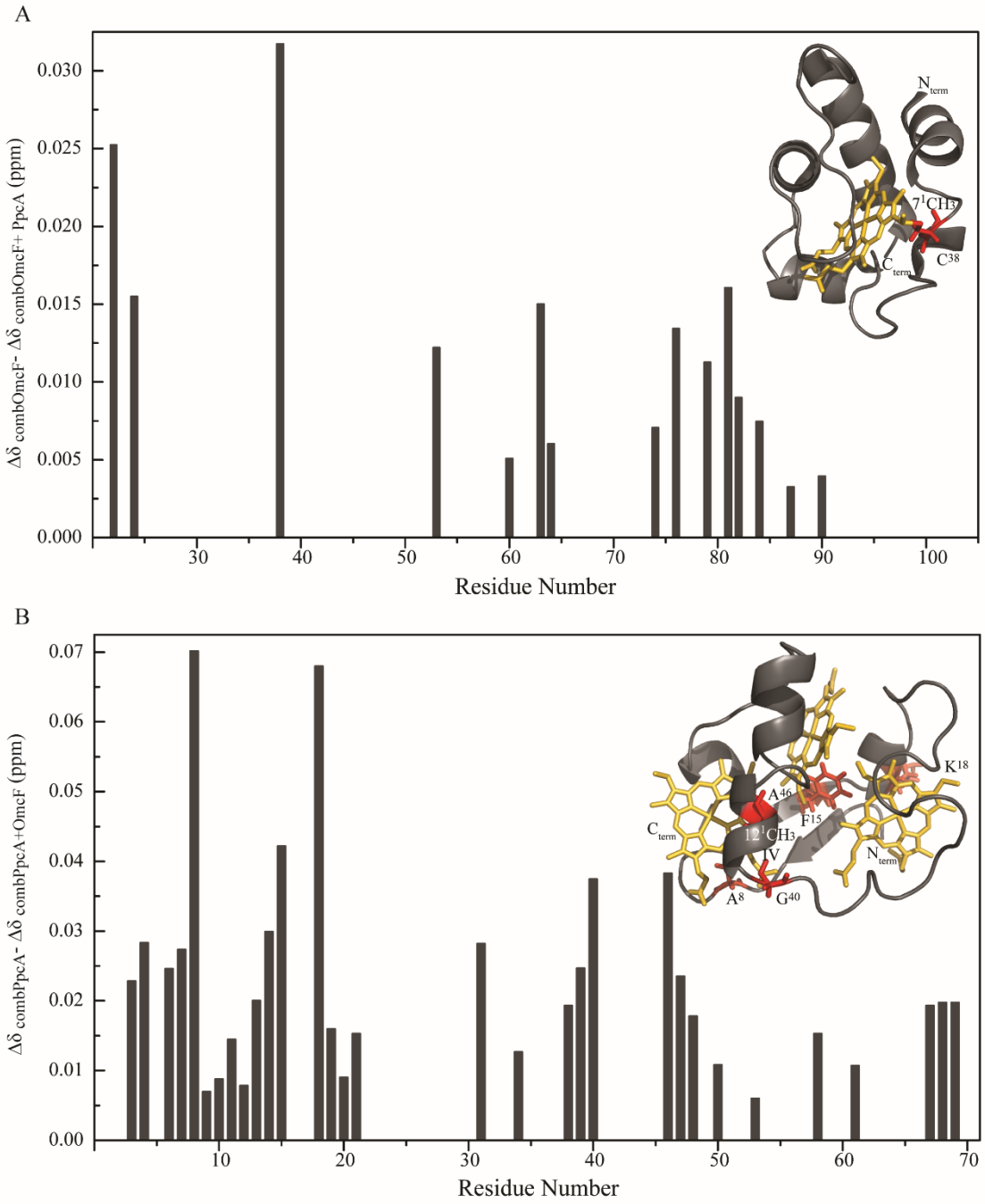

Figure 3.8 - Effects on the polypeptide in the NMR signals of OmcF (A) and PpcA (B) upon addition of the other cytochrome. Comparison between the combined ^{1}H and ^{15}N chemical shifts observed in the 2D ^{1}H, ^{15}N HSQC NMR spectra of OmcF ($\Delta\delta_{combOmcF}$) and those of PpcA ($\Delta\delta_{combPpcA}$). In both panels is represented the structure of the correspondent protein with the amino acids which NH signals showed the biggest chemical shift deviation: OmcF, PDB code: 3CU4 [1]; PpcA PDB code: 2MZ9 [33]. In the structure is also highlighted the heme methyl groups that showed the biggest chemical shift deviation: $12^{1}CH_{3}^{IV}$ of PpcA, and the $7^{1}CH_{3}$ of OmcF. The heme substituents are numbered according to the IUPAC-IUB nomenclature [32]. Figures of the structures were produced using PyMOL (The PyMOL Molecular Graphics System, Version 1.3 Schrödinger, LLC). The polypeptide chain and the heme group of both proteins are colored gray and yellow, respectively. The N- and C-termini are labelled. Residues with the biggest chemical shift deviation are labelled and colored red. Gly^{22} is not represented in the structure of OmcF because there is no predicted 3D structure for this amino acid in the oxidized state.

3.4Conclusions

The assigned NH groups from the backbone and side-chain residues of OmcF constitutes the so-called protein NMR fingerprints, and was used to predict the secondary structure elements of OmcF in solution and to probe pH-linked conformational changes in the oxidized state. It was also explored to map the molecular interactions between OmcF and PpcA. The results obtained show that the secondary structural elements are conserved in solution.

A polypeptide segment of OmcF (from amino acid 41 to 52) was identified to be a more dynamic region in the oxidized state, which may be indicative of its involvement in interaction with other molecules. To confirm this hypothesis, a study of the OmcF dynamic properties in the oxidized state would be necessary, as the one preformed for the reduced state [2]. Furthermore, the analysis of the chemical shift variation of the NH backbone signals allowed mapping the pH-linked conformation changes due to protonation/deprotonation events of the redox-Bohr center. In fact, His^{47} has been hypothesized to be the redox-Bohr center of OmcF, being the pK_a of its side-chain well framed within the one of the protein [2]. It was not possible to determine the pH-linked conformations of His^{47} in the oxidized state since this amino acid is part of the dynamic region of OmcF.

Finally, the NMR fingerprint was explored to probe the interactions between the cytochromes OmcF and PpcA. The chemical shift perturbations were not significant but the affected signals suggest that OmcF interacts with PpcA in the region close to its heme group and residue 38, which is close to the dynamic region in the oxidized state, and with residues surrounding heme IV in PpcA.

3.5 References

[1] P. R. Pokkuluri *et al.*, "Outer membrane cytochrome *c*, OmcF, from *Geobacter sulfurreducens*: High structural similarity to an algal cytochrome c_6," *Proteins Struct. Funct. Bioinforma.*, vol. 74, no. 1, pp. 266–270, 2009.

[2] J. M. Dantas, M. A. Silva, D. Pantoja-Uceda, D. L. Turner, M. Bruix, and C. A. Salgueiro, "Solution structure and dynamics of the outer membrane cytochrome OmcF from *Geobacter sulfurreducens*," *Biochim. Biophys. Acta - Bioenerg.*, vol. 1858, no. 9, pp. 733–741, 2017.

[3] B.-C. Kim, C. Leang, Y.-H. R. Ding, R. H. Glaven, M. V Coppi, and D. R. Lovley, "OmcF, a putative *c*-type monoheme outer membrane cytochrome required for the expression of other outer membrane cytochromes in *Geobacter sulfurreducens*.," *J. Bacteriol.*, vol. 187, no. 13, pp. 4505–4513, 2005.

[4] B.-C. Kim, B. L. Postier, R. J. DiDonato, S. K. Chaudhuri, K. P. Nevin, and D. R. Lovley, "Insights into genes involved in electricity generation in *Geobacter sulfurreducens* via whole genome microarray analysis of the OmcF-deficient mutant," *Bioelectrochemistry*, vol. 73, no. 1, pp. 70–75, 2008.

[5] T. Mehta, M. V Coppi, S. E. Childers, and D. R. Lovley, "Outer membrane *c*-type cytochromes required for Fe(III) and Mn(IV) oxide reduction in *Geobacter*

sulfurreducens," *Appl. Environ. Microbiol.*, vol. 71, no. 12, pp. 8634–41, 2005.

[6] D. E. Holmes *et al.*, "Microarray and genetic analysis of electron transfer to electrodes in *Geobacter sulfurreducens*," *Environ. Microbiol.*, vol. 8, no. 10, pp. 1805–1815, 2006.

[7] Y. Liu *et al.*, "A trans-outer membrane porin-cytochrome protein complex for extracellular electron transfer by *Geobacter sulfurreducens* PCA.," *Environ. Microbiol. Rep.*, vol. 6, no. 6, pp. 776–85, 2014.

[8] C. Leang, M. V Coppi, and D. R. Lovley, "OmcB, a *c*-type polyheme cytochrome, involved in Fe(III) reduction in *Geobacter sulfurreducens*," *J. Bacteriol.*, vol. 185, no. 7, pp. 2096–2103, 2003.

[9] Y.-H. R. Ding *et al.*, "Proteome of *Geobacter sulfurreducens* grown with Fe(III) oxide or Fe(III) citrate as the electron acceptor," *Biochim. Biophys. Acta - Proteins Proteomics*, vol. 1784, no. 12, pp. 1935–1941, 2008.

[10] L. Morgado, M. Bruix, M. Pessanha, Y. Y. Londer, and C. A. Salgueiro, "Thermodynamic characterization of a triheme cytochrome family from *Geobacter sulfurreducens* reveals mechanistic and functional diversity," *Biophys. J.*, vol. 99, no. 1, pp. 293–301, 2010.

[11] J. R. Lloyd *et al.*, "Biochemical and genetic characterization of PpcA, a periplasmic *c*-type cytochrome in *Geobacter sulfurreducens*.," *Biochem. J.*, vol. 369, no. Pt 1, pp. 153–61, 2003.

[12] Y.-H. R. Ding *et al.*, "The proteome of dissimilatory metal-reducing microorganism *Geobacter sulfurreducens* under various growth conditions," *Biochim. Biophys. Acta - Proteins Proteomics*, vol. 1764, no. 7, pp. 1198–1206, 2006.

[13] E. S. Shelobolina *et al.*, "Importance of *c*-type cytochromes for U(VI) reduction by *Geobacter sulfurreducens*," *BMC Microbiol.*, vol. 7, p. 16, 2007.

[14] J. M. Dantas, M. Silva e Sousa, C. A. Salgueiro, and M. Bruix, "Backbone, side chain and heme resonance assignments of cytochrome OmcF from *Geobacter sulfurreducens*," *Biomol. NMR Assign.*, vol. 9, no. 2, pp. 365–368, 2015.

[15] L. Morgado, V. B. Paixão, C. A. Salgueiro, and M. Bruix, "Backbone, side chain and heme resonance assignments of the triheme cytochrome PpcA from *Geobacter sulfurreducens*.," *Biomol. NMR Assign.*, vol. 5, no. 1, pp. 113–6, 2011.

[16] J. M. Dantas, L. Morgado, T. Catarino, O. Kokhan, P. Raj Pokkuluri, and C. A. Salgueiro, "Evidence for interaction between the triheme cytochrome PpcA from *Geobacter sulfurreducens* and anthrahydroquinone-2,6-disulfonate, an analog of the redox active components of humic substances," *Biochim. Biophys. Acta - Bioenerg.*, vol. 1837, no. 6, pp. 750–760, 2014.

[17] A. P. Fernandes, T. C. Nunes, C. M. Paquete, and C. A. Salgueiro, "Interaction studies between periplasmic cytochromes provide insights into extracellular electron transfer pathways of *Geobacter sulfurreducens*," *Biochem. J.*, vol. 474, no. 5, pp. 797–808, 2017.

[18] M. R. Ferreira, J. M. Dantas, and C. A. Salgueiro, "Molecular interactions between *Geobacter sulfurreducens* triheme cytochromes and the electron acceptor Fe(III) citrate studied by NMR.," *Dalton Trans.*, vol. 46, no. 7, pp. 2350–2359, 2017.

[19] J. M. Dantas, A. Brausemann, O. Einsle, and C. A. Salgueiro, "NMR studies of the interaction between inner membrane-associated and periplasmic cytochromes from *Geobacter sulfurreducens*," *FEBS Lett.*, vol. 591, no. 12, pp. 1657–1666, 2017.

[20] M. R. Ferreira and C. A. Salgueiro, "Biomolecular interaction studies between cytochrome PpcA from *Geobacter sulfurreducens* and the electron acceptor Ferric Nitrilotriacetate

(Fe-NTA)," *Front. Microbiol.*, vol. 9, p. 2741, 2018.

[21] E. Arslan, H. Schulz, R. Zufferey, P. Kunzler, and L. Thony-Meyer, "Overproduction of the *Bradyrhizobium japonicum c*-type cytochrome subunits of the cbb_3 oxidase in *Escherichia coli*," *Biochem. Biophys. Res. Commun.*, vol. 251, no. 3, pp. 744–747, 1998.

[22] Y. Y. Londer, P. R. Pokkuluri, V. Orshonsky, L. Orshonsky, and M. Schiffer, "Heterologous expression of dodecaheme 'nanowire' cytochromes *c* from *Geobacter sulfurreducens*," *Protein Expr. Purif.*, vol. 47, no. 1, pp. 241–248, 2006.

[23] Y. Y. Londer, P. R. Pokkuluri, D. M. Tiede, and M. Schiffer, "Production and preliminary characterization of a recombinant triheme cytochrome c_7 from *Geobacter sulfurreducens* in *Escherichia coli*," *Biochim. Biophys. Acta*, vol. 1554, no. 3, pp. 202–11, 2002.

[24] A. P. Fernandes, I. Couto, L. Morgado, Y. Y. Londer, and C. A. Salgueiro, "Isotopic labeling of *c*-type multiheme cytochromes overexpressed in *E. coli*," *Protein Expr. Purif.*, vol. 59, no. 1, pp. 182–188, 2008.

[25] P. Lukat, M. Hoffmann, and O. Einsle, "Crystal packing of the c_6-type cytochrome OmcF from *Geobacter sulfurreducens* is mediated by an N-terminal Strep-tag II," *Acta Crystallogr. Sect. D Biol. Crystallogr.*, vol. 64, no. 9, pp. 919–926, 2008.

[26] S. Seeliger, R. Cord-Ruwisch, and B. Schink, "A periplasmic and extracellular *c*-type cytochrome of *Geobacter sulfurreducens* acts as a ferric iron reductase and as an electron carrier to other acceptors or to partner bacteria.," *J. Bacteriol.*, vol. 180, no. 14, pp. 3686–91, 1998.

[27] D. S. Wishart *et al.*, "^{1}H, ^{13}C and ^{15}N chemical shift referencing in biomolecular NMR," *J. Biomol. NMR*, vol. 6, no. 2, pp. 135–140, 1995.

[28] F. H. Schumann, H. Riepl, T. Maurer, W. Gronwald, K.-P. Neidig, and H. R. Kalbitzer, "Combined chemical shift changes and amino acid specific chemical shift mapping of protein–protein interactions," *J. Biomol. NMR*, vol. 39, no. 4, pp. 275–289, 2007.

[29] L. Morgado, I. H. Saraiva, R. O. Louro, and C. A. Salgueiro, "Orientation of the axial ligands and magnetic properties of the hemes in the triheme ferricytochrome PpcA from *G. sulfurreducens* determined by paramagnetic NMR," *FEBS Lett.*, vol. 584, no. 15, pp. 3442–3445, 2010.

[30] C. A. Salgueiro, D. L. Turner, and A. V Xavier, "Use of paramagnetic NMR probes for structural analysis in cytochrome c_3 from *Desulfovibrio vulgaris*," *Eur. J. Biochem.*, vol. 244, no. 3, pp. 721–734, 1997.

[31] Y. Shen, F. Delaglio, G. Cornilescu, and A. Bax, "TALOS+: a hybrid method for predicting protein backbone torsion angles from NMR chemical shifts," *J. Biomol. NMR*, vol. 44, no. 4, pp. 213–223, 2009.

[32] G. P. Moss, "Nomenclature of tetrapyrroles (Recommendations 1986)," *Eur. J. Biochem.*, vol. 178, no. 2, pp. 277–328, 1988.

[33] L. Morgado, M. Bruix, P. R. Pokkuluri, C. A. Salgueiro, and D. L. Turner, "Redox- and pH-linked conformational changes in triheme cytochrome PpcA from *Geobacter sulfurreducens*," *Biochem. J.*, vol. 474, no. 2, pp. 231–246, 2017.

3. Backbone and side-chain assignment of the cytochrome OmcF in the oxidized state

4. Thermodynamic and kinetic properties of OmcF [1]

[1]Partially reproduced from the following articles, in accordance with the Editors' Copyright Policy. Liliana R. Teixeira, Joana M. Dantas, Carlos A. Salgueiro, Cristina M. Cordas (2018) "Thermodynamic and kinetic properties of the outer membrane cytochrome OmcF, a key protein for extracellular electron transfer in *Geobacter sulfurreducens"*, Biochimica et Biophysica Acta (BBA) – Bioenergetics 1859 (10), 1132-1137 (doi: 10.1016/j.bbabio.2018.07.007); and from Liliana R. Teixeira, Marta P. Fonseca, Cristina M. Cordas, Norma E. C. Duke, P. Raj Pokkuluri, Carlos A. Salgueiro (2020) "Modulation of the redox potential and electron/proton transfer mechanisms in the outer membrane cytochrome OmcF from *Geobacter sulfurreducens*", Frontiers in Microbiology 10, 2941 (doi: 10.3389/fmicb.2019.02941).

4.1 Introduction

The structure of OmcF resembles that of cytochromes c_6 from photosynthetic algae and cyanobacteria, particularly the ones from *Scenedesmus obliquus* [1] and *Monoraphidium braunii* [2]. Although the amino acid sequence of OmcF shows a higher homology with cytochrome c_6 of *S. obliquus*, its structure and the geometry of the axial methionine is much similar to the one of from *M. braunii* (Figure 4.1) [3]. However, at pH 7 the redox potential value of OmcF (+180 mV *vs* NHE) [3] is considerably smaller compared to that obtained for cytochrome c_6 from photosynthetic algae and cyanobacteria (around +350 mV *vs* NHE) [4]. Furthermore, OmcF cytochrome displays a slightly negative surface, including the heme group vicinity and is a more basic protein (pI 7.8). Another important difference between OmcF and cytochrome c_6 from *M. braunii* is the modulation of the reduction potential values in the pH physiological range. Indeed, a difference was observed for OmcF (+140 mV *vs* NHE, at pH 8) [3] whereas no variation was observed for the redox potential of cytochrome c_6 from *M. braunii* in the pH range 7 to 8 (+358 mV *vs* NHE) [5]. The observed pH dependence of the redox potential at pH 7 and 8 for OmcF (redox Bohr-effect) indicates that the protein is able to couple electron and proton transfer in the physiological pH of *G. sulfurreducens*.

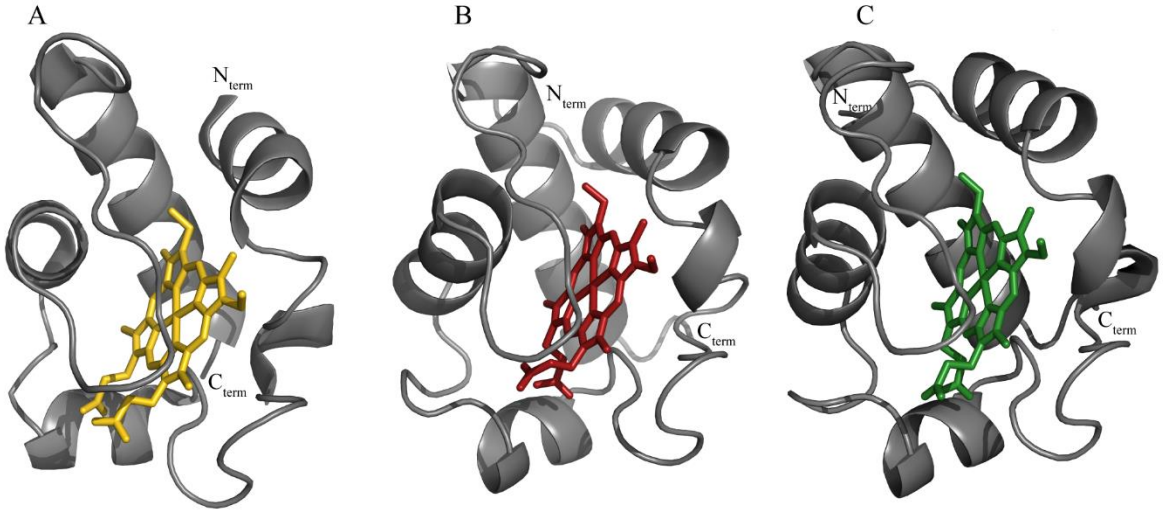

Figure 4.1 – Comparison between the structure of OmcF (PDB code: 3CU4 [3]) of *G. sulfurreducens* (A), of cytochromes c_6 (PDB code: 1CED [2]) of *M. braunii* (B) and of *S. obliquus* (C) (PDB code: 1C6O [1]). All structures are represented in the oxidized state. The OmcF and cytochromes c_6 polypeptide chain are colored gray. The heme of OmcF, c_6 from *M. braunii* and c_6 from *S. obliquus* are colored yellow, red and green respectively. The N- and C-termini are labelled. Figure was produced using PyMOL (The PyMOL Molecular Graphics System, Version 1.3 Schrödinger, LLC).

The crystal and the solution structures of the soluble part of OmcF were determined in the oxidized and reduced states, respectively [3] [6]. The comparison between the oxidized and reduced structures of OmcF showed that they are generally similar [6]. However, redox-linked conformational changes were identified in some polypeptide segments, particularly Ala^{53}-Ile^{62}, Asn^{74}-Gly^{78}, Glu^{84}-Ala^{90} and the C-terminus (residues Val^{100}-Pro^{104}). In addition, the study of the

pH-dependence of the OmcF backbone and side-chain NH NMR signals allowed the identification of important pH-linked conformational changes [6]. In the reduced state, the most affected signals were residues Thr^{33}, His^{34}, His^{47}, Glu^{49}, Leu^{52} and Gly^{76}, whereas in the oxidized state were the residues Thr^{33}, His^{34}, Gly^{42}, Arg^{54}, Glu^{58} and Ala^{81}.

Given the relevance of the outer-membrane cytochromes in the *G. sulfurreducens* extracellular electron transfer pathways, it is important to investigate the kinetics and thermodynamics properties of the electron transfer components that ultimately regulate the cellular redox balance. Furthermore, the identification of the redox-Bohr center of OmcF is important to elucidate the functional mechanism of this cytochrome and to contribute to the understanding of the extracellular electron transfer processes in *G. sulfurreducens*. The protonatable site of the imidazole ring of histidine 47 (His^{47}) has been hypothesized as the redox-Bohr center based: (i) on the typical pK_a value for a histidine side chain and (ii) on its location near the heme in the structure of OmcF (Figure 4.2) [6]. However, there are other protonable amino acids in the vicinity of the heme, which include lysine 50 and asparagine 60, and additionally the protonable propionates of the heme, that are also suitable to be the redox-Bohr center of the cytochrome.

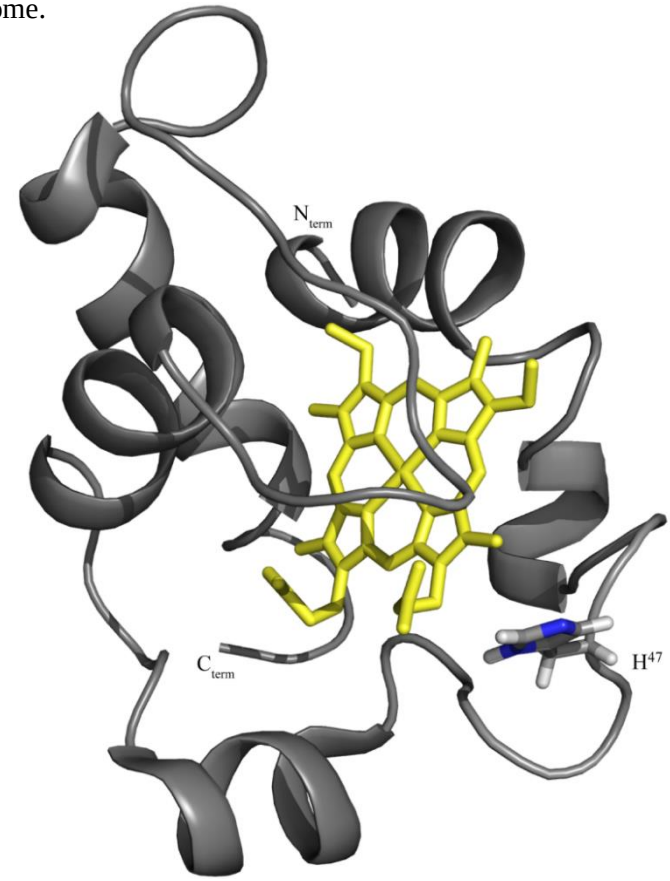

Figure 4.2 - OmcF's lowest-energy solution structure, determined by NMR in the reduced state (PDB code: 5MCS [6]**), highlighting the location of residue His^{47}.** The OmcF polypeptide chain and the heme group are colored gray and yellow, respectively. The N- and C-termini, as well as side chain and H$^{\alpha}$ proton of His^{47} are labelled. Figure was produced using PyMOL (The PyMOL Molecular Graphics System, Version 1.3 Schrödinger, LLC).

This chapter describes a detailed electrochemical study of OmcF from *G. sulfurreducens* using cyclic voltammetry in a thin layer regime. The thermodynamic and kinetic data, as well as the pH modulation of the reduction potential of OmcF are rationalized in structural terms. In addition, site-directed mutagenesis studies were carried out to identify the redox-Bohr center. For each mutant, the impact on the protein's redox potential and redox-Bohr effect were evaluated through cyclic voltammetry. NMR spectroscopy was also used to confirm that the overall fold is not affected in the mutated proteins. For one of the mutants it was possible to obtain a crystal structure, which will be also discussed.

4.2 Materials and methods

4.2.1 Site-directed mutagenesis

Targeted amino acids of OmcF were substituted to study the influence of the mutations in the protein's redox potential. The mutations were performed by using the NZYMutagenesis kit (NZYTech) and the pLBM4 vector (encoding for the soluble part of OmcF formed by residues 20 to 104) as template [3]. The necessary oligonucleotides were designed by the QuikChange Primer Design program (Agilent Technologies), and are indicated in Table 4.1. All primers were synthesized by Invitrogen and the mutations were confirmed by DNA sequencing (STAB VIDA).

Table 4.1 - Primers used to clone the OmcF's mutants. The temperatures (T) of melting for each primer were calculated using the T_m calculator thermo scientific web tool (https://www.thermofisher.com/).

Plasmid	Oligonucleotides	T of melting (ºC)
OmcFH47I	5'-agggtcttttccgggatgacggtgttgcctcc-3' 5'-ggaggcaacaccgtcatcccggaaaagaccct-3'	78
OmcFH47F	5'-agggtcttttccgggaagacggtgttgcctcc-3' 5'-ggaggcaacaccgtcttcccggaaaagaccct-3'	78
OmcFG76K	5'-ggccggcatgcccggcttcgggttgcggatgta-3' 5'-tacatccgcaacccgaagccgggcatgccggcc-3'	79
OmcFK50H	5'-cgcgccagggtatgttccgggtggacggt-3' 5'-accgtccacccggaacataccctggcgcg-3'	78
OmcFK50Q	5'-cgccagggtctgttccgggtggacg-3' 5'-cgtccacccggaacagaccctggcg-3'	78
OmcFK50E	5'-cgccagggtctcttccgggtggacg-3' 5'-cgtccacccggaagagaccctggcg-3'	78
OmcFN60F	5'-gtccggatgccgaaggcctcccgccg-3' 5'-cggcgggaggccttcggcatccggac-3'	79
OmcFY71E	5'-ccgggttgcggatctcggccgccacgtcc-3' 5'-ggacgtggcggccgagatccgcaacccgg-3'	81

4.2.2 Production and purification of OmcF and its mutants

OmcF production and purification followed the procedure described in the previous chapter (Chapter 3). For the production and purification of labelled and unlabeled OmcF's mutants, the protocols applied were the same as for the wild-type protein, since the mutations did not affect significantly the molecular weight or the pI value of the protein.

4.2.3 Electrochemical studies

Assays were performed with a CHI 440b potentiostat, using a three electrodes' configuration in a single compartment electrochemical cell, inside a Faraday cage. The working electrode was a pyrolytic graphite disk with 3 mm diameter, the counter electrode was a platinum wire, and the reference electrode was a saturated silver/silver chloride, with a potential of +197 mV (*vs* NHE at 25 ºC). The working electrode was polished with two different grades of alumina (1 and 0.3 µm), subjected to a Millipore water ultra-sound bath for 2 min, and washed thoroughly with Millipore water. After the electrode was dried, 3 µL of neomycin sulphate (2 mM) and 5 µL of the OmcF protein solution (255 µM) were pipetted on top of the electrode. Neomycin sulphate was added to enhance the positive charge in the electrode surface, improving the proteins' interaction, since OmcF surface is mainly negative including in the heme group vicinity (Figure 4.3). The solution added was let to evaporate (solvent casting technique), at room temperature, until it reached approximately half of the initial volume. The protein was then entrapped using a cellulose membrane (spectra/Pro) with a 6 to 8 kDa cut-off and fitted with two O-rings, as described previously [7] [8]. This was done so that the protein solution formed a uniform thin layer on the electrode surface. The electrode was immersed into the supporting electrolyte solution. Before starting the electrochemical assays, the electrolyte was degassed for a minimum 30 min by using a continuous flow of argon. All assays were performed in an anaerobic environment, with a positive pressure of argon maintained in the electrochemical cell headspace.

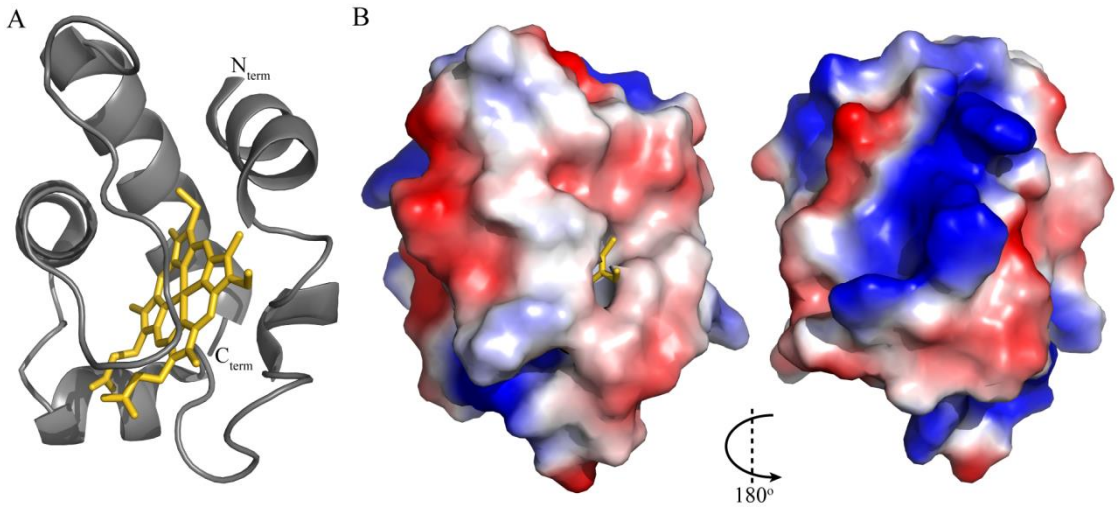

Figure 4.3 - X-ray crystal structure of cytochrome OmcF from *G. sulfurreducens* in the oxidized state (PDB code: 3CU4 [3]). (A) Ribbon diagram. The peptide chain and the heme are color-coded gray and

yellow, respectively. The N- and C-termini are labelled. **(B)** Surface electrostatic potential. Red indicates negative and blue indicates positive potential. The left and right panels are related by a 180° rotation. The protein orientation is the same in panel A and left panel B. Figure was produced using PyMOL (The PyMOL Molecular Graphics System, Version 2.0 Schrödinger, LLC).

The electrolyte used for the independent assays at pH 6, 7 and 8 was 32 mM NaPi with NaCl (100 mM final ionic strength), both for OmcF wild-type and its mutants. The electrolyte used for both pH and temperature dependence assays was a mixture of buffers, including tris(hydroxymethyl)aminomethane (Tris), citric acid and dibasic sodium phosphate, with NaCl (100 mM final ionic strength) (Table 4.2). The range used for the pH dependence assays was between 2.5 and 9.0.

Table 4.2 – Electrolyte composition at different pH values, for electrochemical pH and temperature studies. Solutions calculations were set to a final volume of 200 mL.

pH	Solutions						
	0.1 M $C_6H_8O_7$ (mL)	0.2 M Na_2HPO_4 (mL)	0.02 M Tris pH9 (mL)	37% HCl (mL)	*Solution pH 2.6 (mL)	NaCl (g)	H_2O (mL)
***2.6**	89.2	10.8	-	-		-	100.0
2.5	89.2	10.8	1.0	-	-	1.064	99.0
2.9	79.6	20.4	1.0	-	-	0.966	99.0
3.3	71.8	28.2	1.0	-	-	0.877	99.0
4.0	61.4	38.6	1.0	-	-	0.685	99.0
4.4	55.6	44.4	1.0	-	-	0.600	99.0
5.1	48.6	51.4	1.0	-	-	0.448	99.0
5.5	44.4	55.6	1.0	-	-	0.363	99.0
6.3	35.8	64.2	1.0	-	-	0.068	99.0
7.1	13.0	87.2	1.0	0.3	-	-	98.5
7.6	-	-	182.0	-	18.0	0.432	-
8.1	-	-	187.0	-	13.0	0.653	-
8.5	-	-	192.0	-	8.0	0.849	-
9.0	-	-	200.0	-	-	0.969	-

Both kinetics and pH dependence experiments were performed at room temperature (25 ºC). The temperature dependence assays were performed at pH 5.1, 7.1 and 8.5 in the temperature range of 5 to 40 ºC.

For each experiment, after the cell reached thermic equilibrium, cyclic voltammograms were recorded at different scan rates from 2.5 to 100 mVs^{-1}. At least three independent replicates were performed for each assay. From the midpoint redox potential obtained for each scan rate using the second cycle (using $E^{0\prime} = 0.5(E_{pa}+E_{pc})$) the average and standard deviation values were calculated. Controls were performed applying the same methodology but in the absence of

protein. The obtained redox potential values were corrected for the NHE reference scale (Equation 4.1), considering the experimental temperature dependence of the reference electrode [7] [8] [9].

$$E^{0'}(\mathrm{mV}) = 197 - 1.01\mathrm{x}\ (\mathrm{T} - 25^{0}\mathrm{C}) \quad (4.1)$$

4.2.4 NMR studies

NMR spectra were acquired on a Bruker Avance 600 MHz spectrometer with a triple-resonance cryoprobe at 25 ºC. To assist the assignment of the backbone and side chain NH signals in each mutant, ^{15}N-labeled samples were prepared in 45 mM sodium phosphate (pH 7) with 100 mM final ionic strength in 92% H_2O / 8% D_2O. Natural abundance samples of the mutants were prepared in the same buffer to assist the assignment of the heme substituent signals. OmcF wild-type samples were also prepared in the same buffer (pH 6.1 and 9.4) in D_2O (99.9 %) to study the pH dependence of the heme substituents' signals.

For the preparation of samples in D_2O (99.9 %), they were concentrated and the buffer permuted to 20 mM NaCl using Amicon™ Ultra-a centrifugal filter device. Samples were frozen at -80 ºC and underwent two cycles of lyophilization, being then solubilized with the previously mentioned buffer prepared in D_2O.

Reduction of the proteins was achieved by adding an equimolar solution of sodium dithionite, after degassing the samples with a continuous flow of argon. First, a concentrated solution of sodium dithionite was prepared to access its reduction activity by UV-visible spectroscopy, considering the absorbance at 314 nm. Taking into consideration this determined value, and that sodium dithionite gives two electrons but OmcF only has one heme group, one calculated the equimolar amount of the reductant needed for the concentrated sample of protein.

The fully reduction of the samples was confirmed by 1D ^{1}H NMR. 2D ^{1}H, ^{15}N HSQC spectra were acquired for ^{15}N-labeled samples, whereas 2D ^{1}H, ^{1}H TOCSY (60 ms) and 2D ^{1}H, ^{1}H NOESY (80 ms) were acquired for natural abundance samples.

The water signal was used to calibrate the ^{1}H chemical shifts. ^{15}N chemical shifts, were calibrated using indirect referencing [9]. The data were processed using TOPSPIN (Bruker Biospin, Karlsruhe, Germany) and analyzed with Sparky (TD Goddard and DG Kneller, Sparky 3, University of California, San Francisco, United States of America).

4.3 Results and discussion

4.3.1 Electrochemical studies

The thin-layer technique used, requires the immobilization of the protein in a pyrolytic graphite electrode surface, by entrapment on a cellulose membrane, and was successfully used before in other systems [10] [11]. It has the advantages of requiring small amounts of protein per assay (typically in the µL range), easy electrode preparation, relatively inexpensive and simple

preparation methodology [11]. This experimental setup was firstly tested for cytochrome OmcF samples at pH 7 and 8, for which values were previously obtained by redox potentiometric titrations [3]. Therefore, cyclic voltammograms were obtained separately for each pH using scan rates between 2.5 and 100 mVs^{-1}. As an example, typical voltammograms obtained for pH 7 are indicated in Figure 4.4. At the scan rate range 2.5 to 20 mVs^{-1}, the signals show a quasi-reversible electrochemical behavior, in agreement with the thin-layer regime (see inset in Figure 4.4). Thus, the redox potential values were determined using only the linear area of the plot peak current *versus* the scan rate. The quasi reversible electrochemical behavior was verified through the usual criteria for the thin layer regime, namely: the ratio of the cathodic (I_{pc}) and anodic (I_{pa}) peak current intensities are approximately 1; the I_{pc} and I_{pa} are linearly proportional to the scan rate, and the separation between the cathodic (E_{pc}) and anodic (E_{pa}) peak potential (ΔE_p) increases with the applied scan rate. The estimated thin layer thickness was in average 2.5 μm [10 - 13].

As illustrated in Figure 4.4, well-defined redox pairs are visible, which were assigned to the OmcF heme group. The same behavior was observed at pH 6 and 8, though the signals were slightly broader. This might indicate that the protein is more robust at physiological pH for *G. sulfurreducens* growth (pH 7) [14]. The redox potential values obtained at pH 6, 7 and 8 were +214.5 ± 3.9 mV, +179.3 ± 2.0 mV and +136.3 ± 2.2 mV (*vs* NHE), respectively. These results are in agreement with values determined by potentiometric redox titrations by Pokkuluri and co-workers [3] *vs* NHE: + 180 ± 5 mV (pH 7) and +127 ± 5 mV (pH 8).

The heterogeneous charge transfer rate constant (k_{sh}) was also determined at pH 7 for cytochrome OmcF using the Laviron's formulation and assuming a charge transfer coefficient of 0.5 [15]. At this pH, and at scan rate 10 mV s^{-1}, a k_{sh} value of 0.16 ± 0.01 cm s^{-1} was obtained. This value is higher compared to the one determined for *G. sulfurreducens* monoheme cytochrome PccH (0.09 ± 0.02) [11] and most *c*-type cytochromes [16] [17], indicating a high electron transfer efficiency for OmcF.

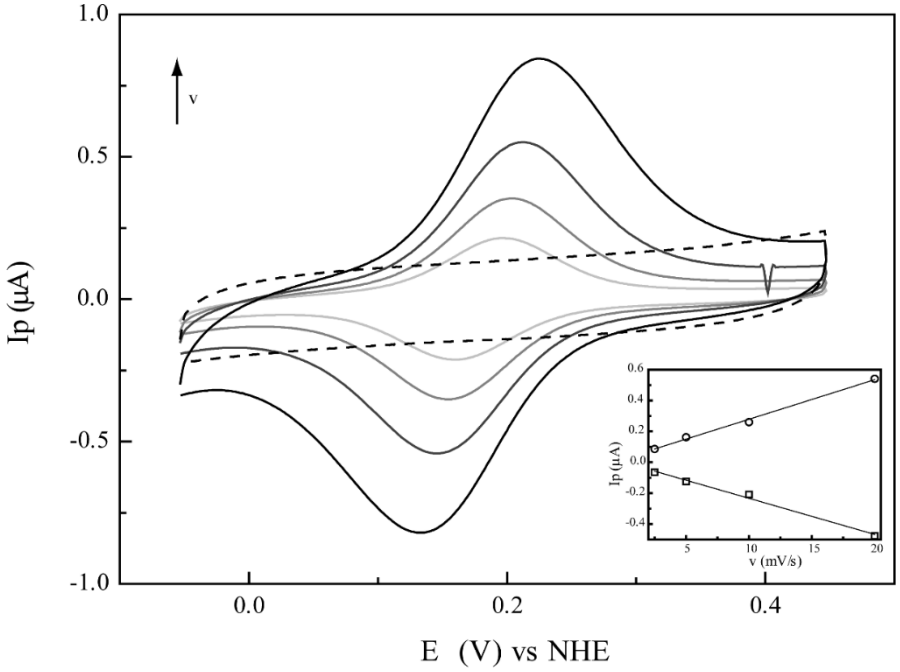

Figure 4.4 - Cyclic voltammograms of cytochrome OmcF at scan rates (ν) from 2.5 to 20 mV s^{-1} (pH 7). The dashed line represents the control at 20 mV s^{-1}. The control was prepared in the same experimental conditions in the absence of the protein. **Inset:** peak current as a function of the scan rate. Anodic and cathodic peak currents are represented by squares and circles, respectively.

4.3.2 Redox-Bohr effect

The redox potential values of cytochromes can be modulated by the solution pH, a property that is functionally relevant if observed in the physiological range. This modulation is designated redox-Bohr effect, in analogy with the Bohr-effect in the hemoglobin [18], and illustrates the stabilization of the reduced *versus* the oxidized state by the pH.

The observed pH dependence of the redox potential at pH 6, 7 and 8 indicates that the protein is able to thermodynamically couple electron and proton transfer in the *G. sulfurreducens* physiological pH range for growth. Therefore, in order to characterize in detail the redox properties of the redox-Bohr center, the studies were extended to the pH range of 2.5 to 9.0. The redox potential was measured at three different scan rates (5, 10 and 20 mVs^{-1}). After the acquisition of the voltammograms for each pH, the measurement was repeated at pH 7 to check for protein hysteresis and to validate each assay. With the exception of pH 2.5 and 2.9, the voltammograms were reproducible and, therefore the observed variations reflect the influence of the pH on the redox-Bohr center properties. Consequently, the values obtained at pH 2.5 and 2.9 were not considered for the global analysis of the pH effect on the redox potentials. For the other pH values, the voltammogram signals show a quasi-reversible electrochemical behavior. The results obtained for each pH, at 5 mVs^{-1} scan rate, are depicted in Figure 4.5.

The analysis of Figure 4.5 clearly shows that OmcF displays a considerable redox-Bohr effect in the physiological pH range. The redox potential increasing with the pH decreasing can

be explained on an electrostatic basis since the progressive protonation of an acid/base group(s), in the vicinity of the heme, is expected to increase its affinity for electrons and stabilize the oxidized form of the protein. In order to access the properties of the protonatable group(s) in the vicinity of the OmcF heme, the pH dependence of the redox potential was fitted considering one acid/base group model (Equation 4.2) yielding the following pK_a values for the oxidized and reduced states: pK_{ox} = 6.73 ± 0.02, pK_{red} = 7.55 ± 0.02. In this case, the results obtained are also explained on an electrostatic basis, as the extra electron in the heme iron stabilizes the protonated form of the redox-Bohr center, favoring the increase of its pK_a value.

$$E^{0\prime} = E^{0} - 0.0592 \times log\left(\frac{K_{ox}+[H^+]}{K_{red}+[H^+]}\right) \quad (4.2)$$

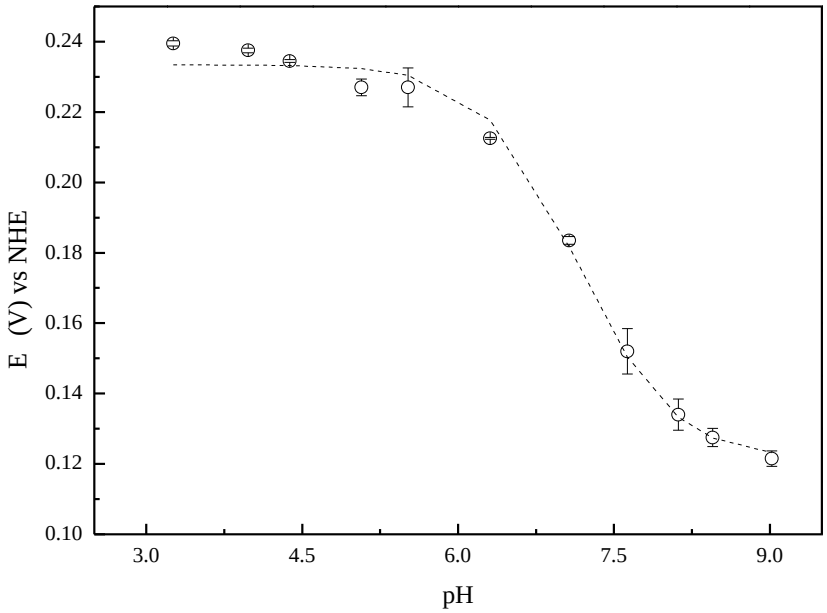

Figure 4.5 - pH dependence of the redox potential of cytochrome OmcF determined by cyclic voltammetry at the membrane pyrolytic graphite electrode (scan rate 5 mV s^{-1}) in a mix buffer Tris/citrate/phosphate with NaCl (100 mM final ionic strength). The line represents the data fit considering one protonable center. The error bars represent the standard deviation of five independent assays.

4.3.2 Thermodynamics parameters of cytochrome OmcF

The thermodynamic properties of the cytochrome OmcF redox transition were also accessed by cyclic voltammetry experiments by monitoring the dependence of the redox potential with the temperature. The study was carried out in the temperature range 5 to 40 ºC, at pH 5.1, 7.1 and 8.5 (Figure 4.6).

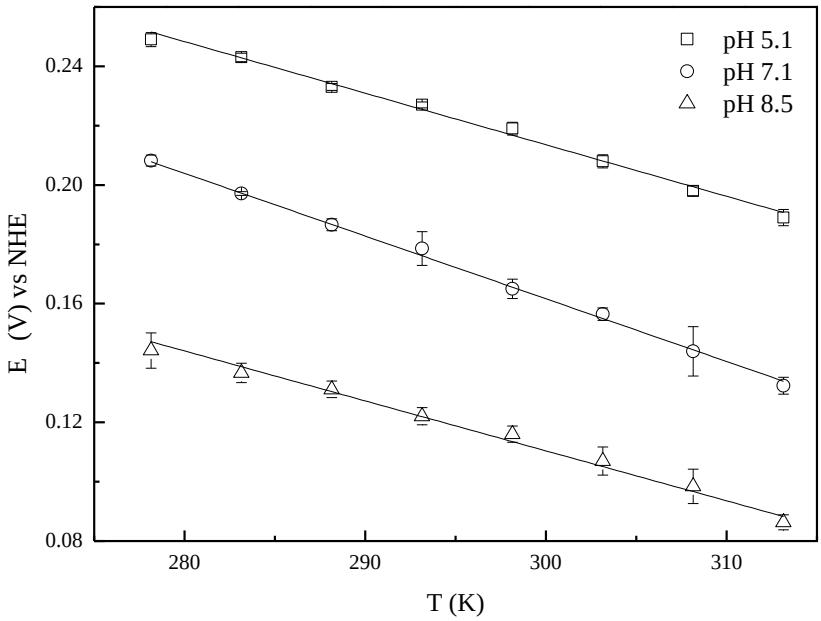

Figure 4.6 - Temperature dependence of the redox potential of cytochrome OmcF determined by cyclic voltammetry. The voltammograms were obtained at 10 mVs^{-1} scan rate for pH 5.1, 7.1 and 8.5 in a mix buffer Tris/citrate/phosphate with NaCl (100 mM final ionic strength). The error bars are the standard variation of five independent assays. The lines represent the linear fitting of the obtained results.

The data obtained allowed to estimate the enthalpy ($\Delta H^{\circ\prime}_{rc}$), entropy ($\Delta S^{\circ\prime}_{rc}$) and the Gibbs free energy ($\Delta G^{\circ\prime}_{rc}$) variations associated with the redox transition at each pH value (Table 4.3), using the following set of equations (4.3, 4.4 and 4.5). The variation of the Gibbs free energy values was calculated from $E^{0\prime}$ values determined at 25 ºC.

$$\Delta S^{0\prime}_{rc} = nF\, dE^{0\prime}/dT \tag{4.3}$$

$$\Delta H^{0\prime}_{rc} = -nF[E^{0\prime} - T(dE^{0\prime}/dT)] \tag{4.4}$$

$$\Delta G^{0\prime}_{rc} = -nF\Delta E^{0\prime}_{rc} \tag{4.5}$$

Table 4.3- Effect of the pH on the thermodynamic parameters of cytochrome OmcF. $\Delta S^{0\prime}_{rc}$ and $\Delta H^{0\prime}_{rc}$ associated with the redox transition at the redox center were determined from the redox potential dependence with temperature, and $\Delta G^{\circ\prime}_{rc}$ calculated from $E^{0\prime}$ values determined at 25 ºC.

pH	$\Delta S^{0\prime}_{rc}$ (J mol^{-1} K^{-1})	$\Delta H^{0\prime}_{rc}$ (kJ mol^{-1})	$\Delta G^{0\prime}_{rc}$ (kJ mol^{-1})
5.1	-164.1 ± 5.6	-70.3 ± 0.1	5.8 ± 2.0
7.1	-204.0 ± 4.5	-76.8 ± 1.3	4.5 ± 2.5
8.5	-146.1 ± 3.9	-54.5 ± 0.1	5.6 ± 1.9

The values obtained indicated that the thermodynamic parameters are not significantly affected by the pH. Even at higher pH (8.5), for which one could expect some pronounced

conformation changes due to the ionization of propionate groups, the data attained does not point to significant changes induced by higher alkalinity and are comparable with data obtained for other *c*-type monoheme cytochromes [11] [19] [20]. Therefore, in the case of OmcF, the protein structure shields the propionate groups, hindering significant conformational changes due to pH variations. In our case, the slight increase of the enthalpy variation at pH 8.5 may reflect a small degree of destabilization due to the ionization. The more negative charge, resulting from deprotonation may influence the hydrophobic center resulting in the small increment of the entropy at this pH value [21]. Overall, the negative values of the enthalpy variation suggests that the iron center is stabilized upon reduction, in agreement with the described behavior of beef heart cytochrome *c* [22] and other cytochromes or metalloproteins, as a result of the heme Fe(II)–axial ligands π-back bonding interactions [11] [23] [24]. As described in the literature, the observed values for entropy variation associated with the redox process can result from a combination of several factors, namely electronic, vibrational and solvent interactions [25]. These entropy values suggest some degree of solvent reorganization energies and, as so, differences in the structure in the proximity of the heme center between the oxidized and reduced forms of the OmcF. Also, the values compared to other *c*-type monoheme cytochromes, such as cytochrome PccH from *G. sulfurreducens* [11], beef heart cytochrome *c* [22], *Rhodopseudomonas palustris* cytochrome c_2 [26] or horse heart cytochrome *c* [19] are probably associated with the degree of solvent exposure associated with the redox process, as has been referred in the literature both for inorganic and biological systems [7] [22] [25] [27]. In fact, differences were observed between the reduced and oxidized structures of OmcF in the polypeptide region containing the residues Ala^{53}-Ile^{62}, Asn^{74}-Gly^{78}, Glu^{84}-Ala^{90} and Val^{100}-Pro^{104} [6], which confirm the existence of redox-linked conformational changes in this protein.

Finally, the redox free energy change ΔG^{0}' is the result of different contributions from the enthalpic and entropic factors, and the small positive values obtained for the Gibbs free energy must result from these compensation effects between both contributions.

4.3.3 Functional insights for OmcF

The thermodynamic properties and particularly the relatively high redox potential observed for OmcF suggest that the protein is more stable in the reduced state compared to the periplasmic triheme cytochromes from *G. sulfurreducens* (Figure 4.7). In fact, the much smaller and negative values observed for the periplasmic triheme cytochromes clearly favor the reduction of OmcF.

The available data in the literature for other *G. sulfurreducens* cytochromes participating in extracellular electron transfer shows that there is an overlap between their redox-active potential ranges to assure a smooth electron flow from the cytoplasmic oxidation of nutrients to terminal electron acceptors at the cell. Moreover, the potential windows of the cytochromes are well framed within several electrochemical studies carried out on *Geobacter* biofilms, which

detected a typical Nernstian response around -150 mV (*vs* NHE) [28] [29] [30]. The data obtained suggest that an eventual electron transfer from periplasmatic cytochromes to OmcF is highly thermodynamically favorable.

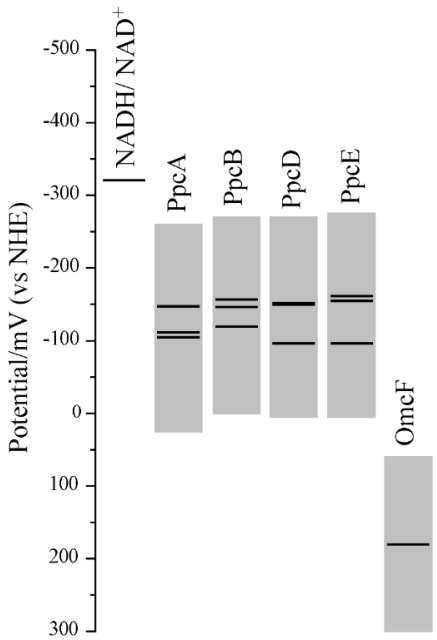

Figure 4.7 - Comparison of the redox-active windows obtained for periplasmic cytochromes and OmcF from *G. sulfurreducens* at pH 7. Horizontal black lines correspond to the reduction potential of the hemes *vs* NHE: OmcF (+179 mV); PpcA (-147, -104, -111 mV, for hemes I, III and IV, respectively); PpcB (-146, -156, -119 mV); PpcD (-150, -96, -151 mV) and PpcE (-154, -161, -96 mV) [31]. For the sake of completeness, the reduction potential value for $NADH/NAD^+$ (-320 mV) is also included.

4.3.4 Structural map of the redox-Bohr center of OmcF

In order to identify the candidates responsible for the observed redox-Bohr effect, the OmcF structures in the reduced and oxidized states were investigated [3] [6]. The structure of this *c*-type cytochrome shows that the side chains of three putative candidates (Cys^{35}, Cys^{38} and His^{39}) are part of the heme group binding motif and bind to the redox co-factor. In addition to these residues, the protein contains several additional protonatable groups: the N- and C-termini, two heme propionic acids at positions 13 (P_{13}) and 17 (P_{17}), six arginine, two aspartic acid, five glutamic acid, two non-axial histidine, two lysine and two tyrosine residues. The amino acids which are the best candidates for the redox-Bohr center are His^{47}, Lys^{50} and Asn^{60}, due to their proximity to the heme group. His^{47} side chain is close to the propionate 13 (P_{13}) and the typical pK_a values of this amino acid [6] are framed within the ones observed for OmcF (pK_{ox} = 6.73, pK_{red} = 7.55). Moreover, the position of His^{47} in cytochrome c_6 of *M. braunii* is occupied by a non protonable amino acid, which might explain the inexistence of redox-Bohr effect. On the other hand, Lys^{50} is located between the propionic acid group of the heme, forming a hydrogen bond with the propionate 17 (P_{17}). Finally, Asn^{60} blocks the solvent access to the heme. The mentioned amino acids were selected to construct OmcF mutants. His^{47} was replaced by isoleucine (OmcFH47I), which is the corresponding amino acid in cytochrome c_6 of *M. braunii* (Ile^{27}), and

by a phenylalanine (OmcFH47F) to study the loss of an ionisable proton. Lys^{50} was substituted by a histidine (OmcFK50H), which is the correspondent amino acid in the cytochrome c_6 (His^{30}). The same amino acid was replaced by a glutamic acid (OmcFK50E) and, in another mutant, by a glutamine (OmcFK50Q) to study the effect of charge. Asn^{60} was replaced by phenylalanine (OmcFN60F), which is the correspondent amino acid in cytochrome c_6 (Phe^{40}).

Furthermore, in this work we try to understand the origin for the different redox potential values calculated for OmcF and cytochrome c_6 from *M. braunii* has a much higher redox potential. In order to do so, Tyr^{71} and Gly^{76} were pinpointed as putative crucial amino acids for the increase of the redox potential. Tyr^{71} interacts with the two propionates through a water molecule, forming hydrogen bridges. The mutant constructed for this amino acid was OmcFY51E, where the glutamic acid was introduced to study the effect of the proton loss. Gly^{76} is strategically placed between the two propionates and substituting it with a protanable amino acid such as lysine (OmcFG76K), which is the corresponding amino acid in the c_6 from *M. braunii* (Lys^{58}), might increase the redox potential.

4.3.5 OmcF mutants' production and purification

OmcF mutants were produced and purified following the same methodology as for the wild-type protein. The protein yields obtained for each mutant for natural abundance and ^{15}N-labeled proteins are reported in Table 4.4. Only the mutants OmcFH47I and OmcFH47F were produced in minimal medium for reasons which will be explained further in this chapter.

Table 4.4 - Expression yields of OmcF and its mutants for natural abundance and ^{15}N-labeling proteins.

Protein	Yield for natural abundance (mg/L)	Yield for ^{15}N-labeling (mg/L)
OmcF	18.0	2.1
OmcFH47I	15.4	1.2
OmcFH47F	17.4	0.7
OmcFK50H	10.4	-
OmcFK50E	18.2	-
OmcFK50Q	14.0	-
OmcFN60F	13.8	-
OmcFY51E	0.1	-
OmcFG76K	8.7	-

In sum, all mutants had similar yields, comparing with the wild-type protein, except for OmcFY51E, which had a considerable low yield. The UV-visible spectra of all mutants showed similar features compared to the native protein. As example, the absorption peaks for OmcF in the oxidized and reduced states are presented in Table 4.5, together with the data correspondent to the mutants OmcFH47I and OmcFH47F.

Table 4.5 - Absorption peaks in the visible region of the electronic spectra of OmcF and mutants OmcFH47I and OmcFH47F.

Protein	**Peaks in the electronic absorption spectra**			
	Soret	β	α	Other
OmcF				
Oxidized	411			528; 562
Reduced	417	522	552	
OmcFH47I				
Oxidized	411			528; 563
Reduced	417	523	553	
OmcFH47F				
Oxidized	411			528; 563
Reduced	417	523	552	

4.3.6 Effect of the mutations on the redox-Bohr center properties

As proved by Pokkuluri and co-workers [3], and by the electochemical studies described previously in this chapter, the redox potential of OmcF is strongly modulated in the pH range 6 to 8, the physiological range for the *G. sulfurreducens* growth. The redox potential values of the OmcF mutants were measured by cyclic voltammetry. For proper comparison, measurements for the mutant proteins were carried out in the same experimental conditions as for the wild-type protein. The cyclic voltammograms were recorded in the potential window between 0 and 350 mV, with scan rates between 2.5 and 100 mVs^{-1}. For mutants which showed well-defined redox pairs, a quasi-reversible electrochemical behavior was observed between the scan rates 2.5 to 20 mVs^{-1}, as it was also the case for the wild-type cytochrome. The redox potential values of the mutants were determined by the average of the anodic and cathodic peak potentials (at the point of maximum current intensity), as for the wild-type protein, and are indicated in Table 4.6 at pH 6, 7 and 8.

Table 4.6 - Redox potential values (vs NHE) for OmcF and its mutants determined by cyclic voltammetry at pH 6, 7 and 8. The respective standard errors are indicated.

	E^0 (mV *vs* NHE)		
	pH 6	pH 7	pH 8
OmcF	214.5 ± 3.9	179.3 ± 2.0	136.3 ± 2.2
OmcFH47I	179.8 ± 2.6	153.0 ± 1.8	125.0 ± 4.5
OmcFH47F	178.0 ± 1.6	147.5 ± 3.9	120.3 ± 3.5
OmcFK50H	-	144.5 ± 1.8	69.3 ± 16.6
OmcFK50E	-	136.0 ± 1.4	53.2 ± 37.5
OmcFK50Q	-	163.5 ± 3.5	116.3 ± 6.0
OmcFN60F	-	165.0 ± 1.5	117.5 ± 3.5
OmcFY51E	-	186.0 ± 2.9	-
OmcFG76K	-	142.5 ± 3.9	123.3 ± 2.4

For all OmcF mutants, well-defined redox pairs were visible at pH 7, being assigned to the OmcF heme group. At pH 8, only the following mutants showed a similar behavior: OmcFH47I, OmcFH47F, OmcFK50Q, OmcFN60F and OmcFG76K. It was possible to determine the redox potential of the mutants OmcFK50H and OmcFK50E at pH 8, but with a very high standard deviation associated. For the mutant OmcFY51E was impossible to obtain the redox potential at pH 8, although the redox potential of OmcFY51E is higher at pH 7 than the wild-type protein. OmcFG76K mutant showed smaller redox potential values, both at pH 7 and 8 compared to the wild-type. These results indicate that neither the mutations lead to an approximation of the redox potential of OmcF and the cytochrome c_6 from *M. braunii*.

For OmcFH47I and OmcFH47F mutants, the redox potential values were lower than the values found for the wild-type cytochrome, both at pH 7 and 8, being the studies extended to pH 6. This indicates that the oxidized form in the mutants is more stabilized as expected for a replacement of the positively charged side chain of His^{47} by the uncharged side chain in the mutants. As observed for the wild-type cytochrome, the redox potential values of the His^{47} mutants were also pH-dependent. However, the difference between the redox potential values of the His^{47} mutants and those of the wild-type decreases with the increase in pH, which indicates that the replacements have a smaller impact on the redox properties of the heme group at higher pH. Overall, the data obtained suggested that the redox-Bohr center is protonated at pH 6 and deprotonated at pH 8. This is also in agreement with the pK_a values previously determined for the redox-Bohr center ($pK_{ox} = 6.7$; $pK_{red} = 7.6$) and explains the higher impact of the substitutions at

pH 6. The additional positive charge in the redox-Bohr center at pH 6 stabilizes the reduced state (higher redox potential values) whereas the loss of the positive charge at higher pH facilitates the oxidation of the heme and stabilizes the oxidized state (lower redox potential values). This is also reflected on the differences observed for the redox potential values of the mutants compared to the wild-type cytochrome at pH 6 (34.7 and 36.5 mV for OmcFH47I and OmcFH47F, respectively) and 8 (11.3 and 16.0 mV for OmcFH47I and OmcFH47F, respectively). In fact, in the wild-type at pH 6 the side chain of His^{47} is protonated and positively charged, whereas at pH 8 the side chain of His^{47} is deprotonated and uncharged. In the His^{47} mutants, the replacements do not introduce any charge variation in the vicinity of the heme group at both pH values.

The voltammograms for the His^{47} mutants, at pH 7, are depicted in Figure 4.8. From the analysis of Table 4.6 it is also clear that the pH dependence of the redox potential values is only smaller in the OmcFH47I and OmcFH47F mutants, compared to the wild-type cytochrome. These results confirm unequivocally the involvement of His^{47} in the pH modulation of the redox potential of OmcF. However, the fact that the redox-Bohr effect was not completely abolished by the replacement of His^{47} by non- protonatable residues, suggested that additional acid group(s) might be involved in the global redox-Bohr effect. However, based on the results obtained for the other mutants (Table 4.6) none of the other mutants are suitable candidates.

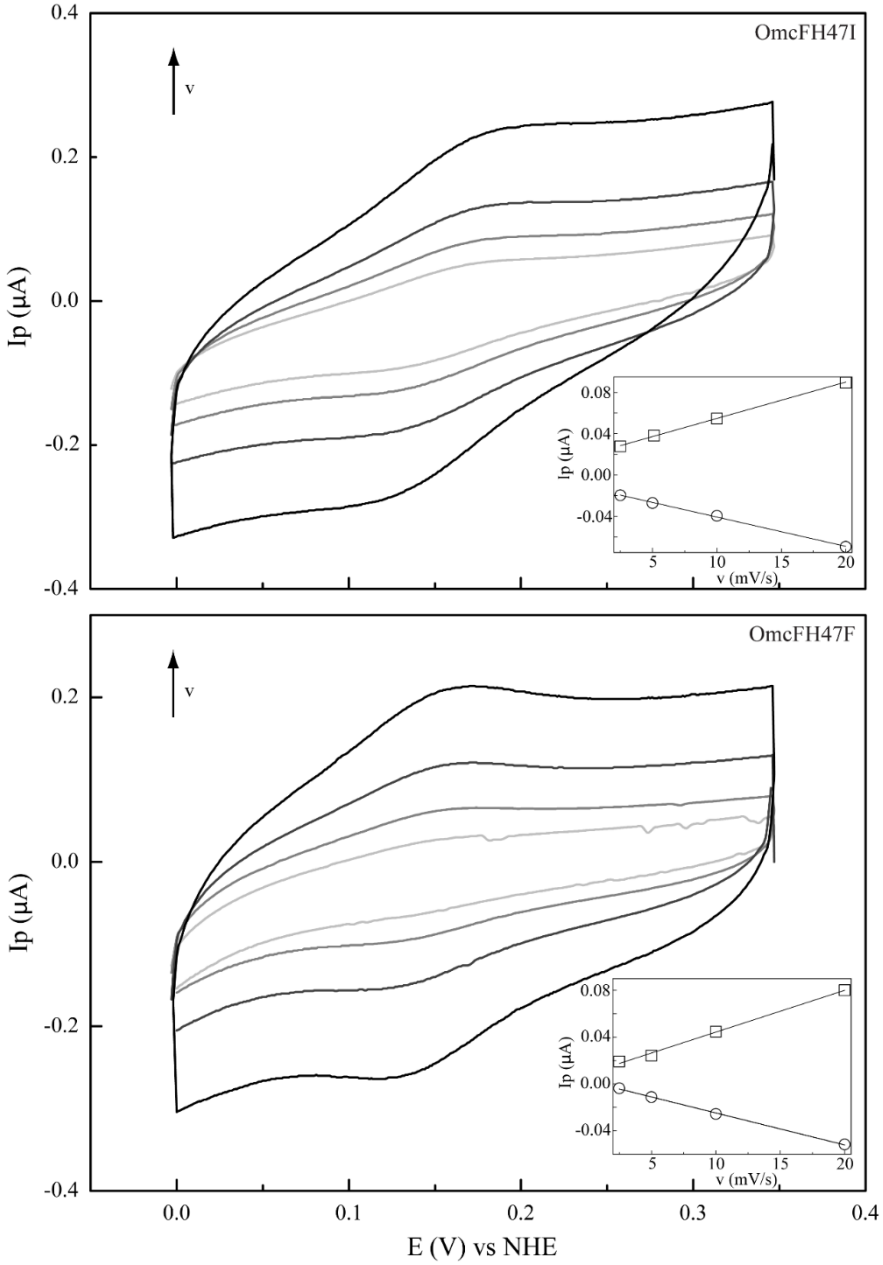

Figure 4.8 - Cyclic voltammograms of mutants OmcFH47I (top) and OmcFH47F (bottom) at scan rates (*ν*) from 2.5 to 20 mV s^{-1} (pH 7). Inset: peak current as a function of the scan rate. Anodic and cathodic peak currents are represented by squares and circles, respectively.

4.3.7 Impact of the mutations in His^{47}, on the global fold of the protein

The NMR chemical shifts of the nuclei are very sensitive to changes in their chemical environment and, consequently, can be explored to fingerprint the overall structure of the proteins in solution. Thus, the impact of the mutations on the protein conformation was evaluated by 2D ^{1}H, ^{15}N HSQC NMR experiments. The mutants OmcFH47I and OmcFH47F were analyzed by NMR spectroscopy, since His^{47} was the only amino acid identified to be involved in the pH modulation of the redox potential of OmcF. All experiments were performed in the reduced state, since the NH signal of His^{47} was not assigned in the oxidized state (Chapter 3). This analysis was

performed to evaluate if the alteration of the proteins' redox potential is caused by major rearrangement(s) in the proteins' structures.

The backbone and side chain NH signals of each mutant were assigned (Figure 4.9) using the same methodology described for the wild-type protein [32]. ^{15}N-labelled OmcFH47I and OmcFH47F were produced for 2D ^{1}H, ^{15}N HSQC NMR spectra, and natural abundance mutants for 2D ^{1}H, ^{1}H TOCSY and 2D ^{1}H, ^{1}H NOESY spectra. The assignments of OmcFH47F and OmcFH47I are reported in the Appendix section (Table A.2 and A.3, respectively). The comparison of the spectra obtained for the wild-type and the mutants showed a similar dispersion of signals, indicating that the overall fold is maintained (Figure 4.9).

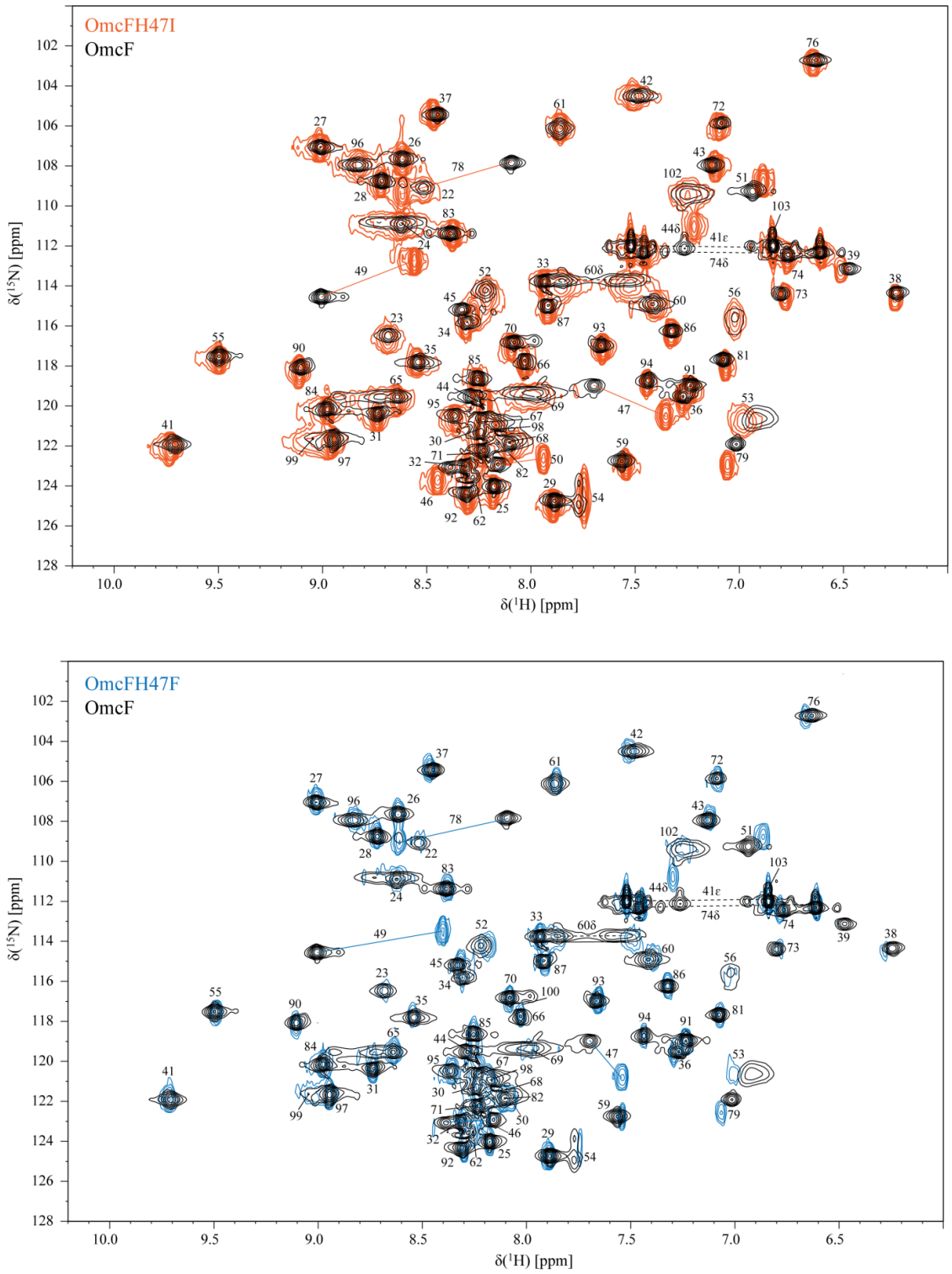

Figure 4.9 - 2D ^{1}H, ^{15}N HSQC NMR spectra of OmcF (black contours), OmcFH47I (orange contours) and OmcFH47F (blue contours) in the reduced state (25 ºC, pH 7). The most affected signals are connected by a straight line in each spectrum. Dashed lines correspond to side chains of amino acids.

The differences between the combined ^{1}H and ^{15}N chemical shifts observed in the mutants and wild-type 2D ^{1}H, ^{15}N HSQC NMR spectra (Figure 4.10 A) were calculated using equation 3.2 (Chapter 3). The analysis of the ^{1}H and ^{15}N combined chemical shift variation showed that the

residues located in the polypeptide segment Val^{46}-Lys^{50} and Gly^{78} were the most affected (Figure 4.10 A). The polypeptide segment Val^{46}-Lys^{50} includes the mutated residue (Ile^{47} and Phe^{47} for OmcFH47I and OmcFH47, respectively) and a proline residue (Pro^{48}). This residue does not possess the NH proton due to its cyclic nature and for this reason no chemical shift variation was observed. On the other hand, Gly^{78} is closely located to Val^{46}, whose side chain, together with the imidazole ring of His^{47}, form a pocket around the heme methyl 12^{1}CH$_3$ (see inset in Figure 4.10 A). Thus, the replacement of His^{47} residue introduced only small rearrangements at the vicinity of the mutation site, without affecting the global fold of the protein. The similar magnitude observed for the chemical shift variations in both mutants also suggested that the local rearrangements are similar.

Following the analysis of the impact of the mutated residues in the backbone and side chain NH signal, their impact was further evaluated regarding the heme substituent ^{1}H NMR signals. The heme substituent signals were assigned using 2D ^{1}H, ^{1}H TOCSY and 2D ^{1}H, ^{1}H NOESY NMR spectra, as described for the wild-type protein [32]. The assignment of these signals and their comparison with those obtained for the wild-type protein are indicated in Table 4.7 and Figure 4.10 B, respectively. In both mutants, the most affected signal is the heme methyl 12^{1}CH$_3$, which is the closest to the mutated residue (*cf.* insets in Figure 4.10 A and B). The other affected heme signals, although to a smaller extent, correspond to propionate protons (13CH$_2$ groups), the meso proton 10H and the thioether proton 8^{1}H, which are allocated to the heme face containing the methyl 12^{1}CH$_3$ (see inset in Figure 4.10 B). Therefore, the heme proton signals showing the largest chemical shift variations are in the vicinity of the most affected residues, namely the polypeptide segment Val^{46}-Lys^{50} and Gly^{78} (*cf.* insets in Figure 4.10 A and B), which further confirmed that the small conformational changes caused by the amino acid replacements are restricted to the neighboring regions of the mutated residue.

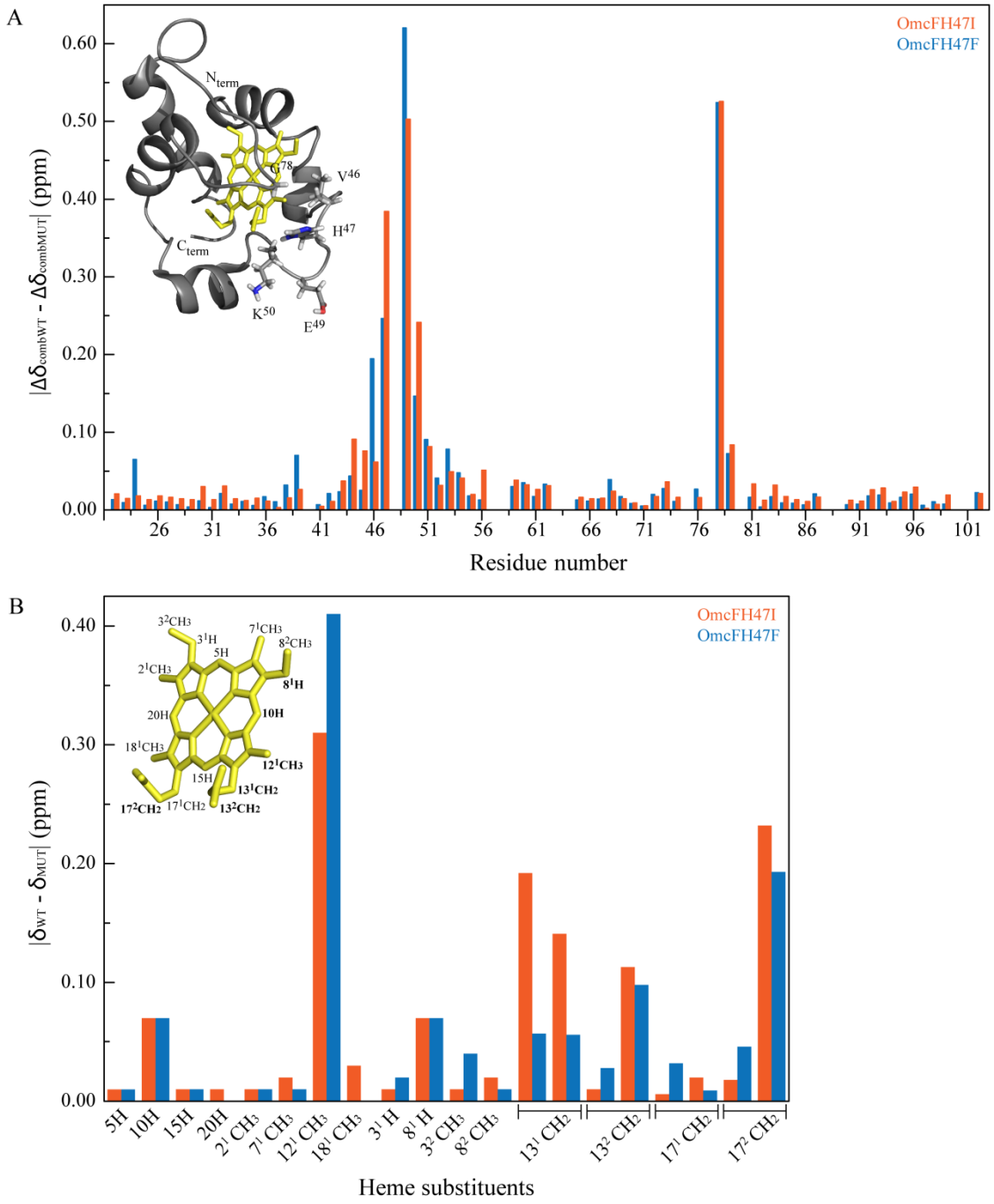

Figure 4.10 - Effects on the polypeptide and heme substituent's NMR signals caused by the replacement of His[47] by isoleucine or phenylalanine. (A) Comparison between the combined ^1H and ^{15}N chemical shifts observed in the 2D ^1H, ^{15}N HSQC NMR spectra of OmcF mutants ($\Delta\delta_{comb}MUT$) and those of OmcF ($\Delta\delta_{comb}WT$). The color code of the NMR spectra indicated in Figure 4.9 was used for each mutant: OmcFH47I (orange bars) and OmcFH47F (blue bars). The most affected residues are shown in the solution structure of cytochrome OmcF in the inset. The N- and C-termini are labelled. **(B)** Comparison of the heme ^1H chemical shifts observed in the 2D ^1H, ^1H NOESY NMR spectra of OmcF mutants (δ_{MUT}) and those of wild-type OmcF (δ_{WT}). The heme substituents are numbered according to the IUPAC-IUB nomenclature [34] and the most affected heme substituent signals are highlighted in bold in the heme diagram. In both panels the structural data correspond to OmcF's lowest-energy solution structure (PDB code: 5MCS [6]), produced with PyMOL (The PyMOL Molecular Graphics System, Version 1.3 Schrödinger, LLC).

Table 4.7- Proton chemical shifts of the heme substituents of OmcF mutants in the reduced state (25 ºC and pH 7). The chemical shifts of OmcF were previously determined [32] and are listed for comparison. The heme substituents are numbered according to the IUPAC-IUB nomenclature [34].

Heme substituent	Chemical shift (ppm)		
	OmcF	OmcFH47I	OmcFH47F
5H	10.10	10.09	10.09
10H	9.42	9.49	9.49
15H	9.59	9.58	9.60
20H	9.33	9.32	9.33
2^1CH_3	3.64	3.63	3.65
7^1CH_3	4.08	4.06	4.09
12^1CH_3	3.20	3.51	3.61
18^1CH_3	3.03	3.00	3.03
3^1H	5.48	5.49	5.50
8^1H	6.20	6.27	6.25
3^2CH_3	1.14	1.15	1.18
8^2CH_3	2.51	2.49	2.52
13^1CH_2	4.15	4.34	4.21
	4.45	4.30	4.39
13^2CH_2	2.88	2.87	2.91
	3.24	3.13	3.15
17^1CH_2	2.69	2.70	2.73
	4.11	4.09	4.11
17^2CH_2	2.02	2.00	1.97
	3.12	2.89	2.93

4.3.8 Structural probe of the redox-Bohr center in OmcF

In addition to the His^{47}, the heme propionates, 13 (P_{13}) and 17 (P_{17}), are the best additional candidates for the redox-Bohr effect. It was evaluated the pH dependence of the heme substituent signals of OmcF wild-type in the reduced state. The assignment of the entire set of the heme substituents in the oxidized state is more complex compared to the reduced state due to the paramagnetic effect of the heme unpaired electron [35]. This often impairs the full assignment of the heme signals in the oxidized state, which is in fact the case for OmcF. Because the assignment of the heme substituent signals of OmcF was fully obtained for the reduced state at pH 7 [32] this state was selected to evaluate the pH dependence of the heme substituent NMR signals. Considering the pK_a value of the redox-Bohr center in the reduced state ($pK_{red} = 7.6$), the pH values of 6.1 and 9.4 were selected to ensure a proper comparison of the heme substituent chemical shifts when the redox-Bohr center is fully protonated and deprotonated, respectively.

The assignment of the heme substituent signals at pH 6.1 and 9.4 was carried out using the same strategy as previously described at pH 7 (Chapter 2) [32] and are listed in Table 4.8. The variation of the heme substituent's chemical shifts at pH 6.1 and 9.4 is indicated in Figure 4.11 and shows that the heme propionate groups and methyl 12^1CH_3 are the most affected ones. However, the pH dependence of the heme propionates is quite distinct. Indeed, while the four protons of P_{17} were clearly affected by the pH, only one proton from P_{13} heme was affected. Such behavior, together with the fact that the heme methyl 18^1CH_3 is essentially pH independent, suggests that P_{13} is the best additional candidate for contribution to the redox-Bohr effect.

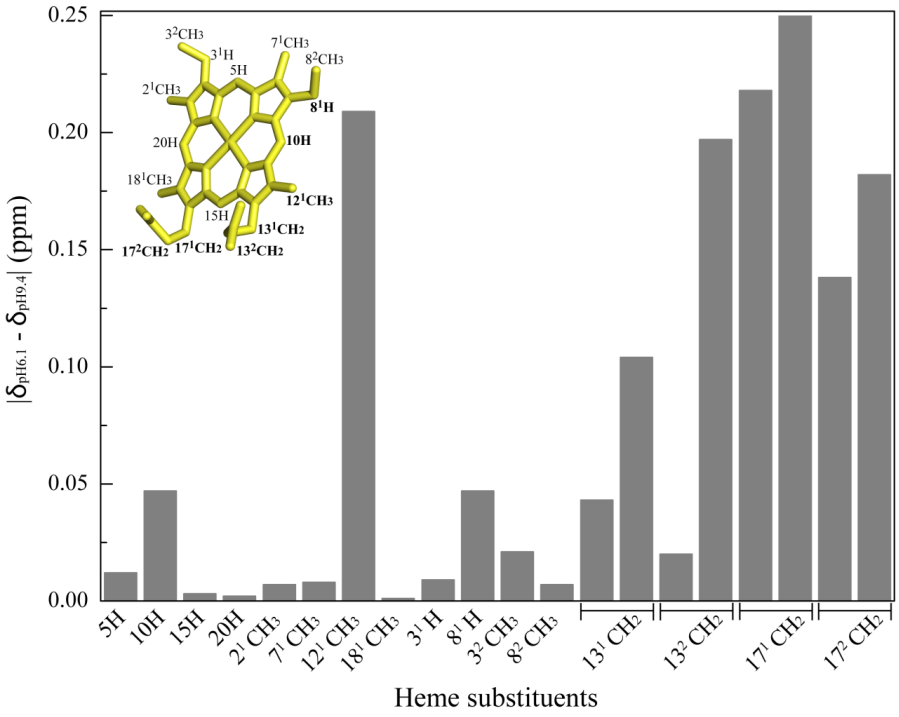

Figure 4.11 - Variation of OmcF's heme substituent's proton chemical shifts at pH 6.1 ($\delta_{pH6.1}$) and 9.4 ($\delta_{pH9.4}$). The heme substituents are numbered according to the IUPAC-IUB nomenclature [34] and the most affected heme substituent signals are highlighted in bold in the heme diagram. The heme group in the inset was taken from OmcF's lowest-energy solution structure (PDB code: 5MCS [6]) and was produced with PyMOL (The PyMOL Molecular Graphics System, Version 1.3 Schrödinger, LLC). The heme substituents are numbered according to the IUPAC-IUB nomenclature [34].

Table 4.8 - Proton chemical shifts of the heme substituents of OmcF in the reduced state at pH 6.1 and 9.4 (25 ºC). The heme substituents are numbered according to the IUPAC-IUB nomenclature [34].

Heme substituent	Chemical shift (ppm)	
	pH	
	6.1	9.4
5H	10.11	10.12
10H	9.42	9.46
15H	9.60	9.60
20H	9.35	9.35
2^1CH_3	3.65	3.65
7^1CH_3	4.08	4.09
12^1CH_3	3.14	3.35
18^1CH_3	3.04	3.04
3^1H	5.49	5.50
8^1H	6.19	6.23
3^2CH_3	1.15	1.17
8^2CH_3	2.50	2.51
13^1CH_2	4.15	4.19
	4.48	4.37
13^2CH_2	2.90	2.88
	3.31	3.11
17^1CH_2	2.64	2.86
	4.17	3.92
17^2CH_2	1.97	1.84
	3.08	3.26

In summary, the electrochemical studies carried out on OmcFH47I and OmcFH47F mutants and the pH dependence of the heme substituent NMR signals indicated that the two main contributors for the redox-Bohr effect in OmcF are the side chain of His^{47} and the heme propionate group P_{13}. The deprotonation/protonation of the histidine side chain explains the large chemical shift variation on heme methyl 12^1CH_3 that extends also to heme protons 10H and 8^1H, while the deprotonation/protonation of P_{13} is responsible for the significant variations observed for the chemical shift of the P_{17} protons.

4.3.9 Crystal Structure of OmcFH47I

The crystal structure of OmcFH47I mutant (PDB code: 6U97) was determined in the oxidized state by the collaborative group from the Argonne National Laboratory, Argonne, Illinois, USA. Crystallization and structure determination details are described in [37]. The

samples used had concentrations of 20 mg/mL and it was only possible to obtain crystals for the OmcFH47I mutant with the conditions previously reported for OmcF [3]. It was not possible to obtain crystals for the OmcFH47F mutant.

The OmcFH47I mutant crystallized in the same space group as the wild-type OmcF but with a slight difference in the unit cell dimensions resulting in a 1% decrease of volume in the mutant. The overall structure of the OmcFH47I mutant in the oxidized state is very close to that of the wild-type with an overall rmsd of 0.4 Å for all C_α atoms (residues 23 – 104). A C_α carbon trace of the overlap of the OmcFH47I mutant structure on the wild-type OmcF is shown in Figure 4.12. The electron density for the side chain of Ile^{47} clearly showed two conformations, refined at occupancies of 0.7 and 0.3. The two conformations of the isoleucine side chain differed primarily in the location of the CD1 methyl group. Deviations higher than the overall rmsd (ranging from 0.6 – 0.8 Å) were observed near the mutation site from residues 47 to 50, and from residue 76 to 78, which are in line with the analysis of the ^{1}H and ^{15}N combined NMR chemical shift variation (Figure 4.10 A). Deviations ranging from 1.0 to 1.3 Å were also seen in residues 84 to 86, which are distant from the heme, caused by different interactions across the crystal interface.

The replacement of the polar histidine residue by non-polar isoleucine did not cause any significant changes in the interactions of the heme with the protein, which was the same conclusion as for the NMR spectroscopic analysis. The isoleucine side chain(s) forms van der Waals contact(s) with the heme atoms. The propionate 13 (P_{13}), which is the closest to the mutation site, forms water mediated hydrogen bonds with Tyr^{71} and the other propionate in both wild-type and mutant structures. It also hydrogen bonds with other water molecules. Although this propionate can hydrogen bond with the side chain of His^{47} in the wild-type OmcF structure, this was not observed. On the other hand, the propionate 17 (P_{17}) forms a salt bridge with Lys^{50} (NZ) with one of its carboxyl oxygen atoms and hydrogen bonds with Asn^{60} (ND2) with the other oxygen atom. These interactions involving the P_{17} carboxyl oxygen atoms are observed in both native and OmcFH47I mutant structures. The interactions formed by the heme propionates are shown in Figure 4.13.

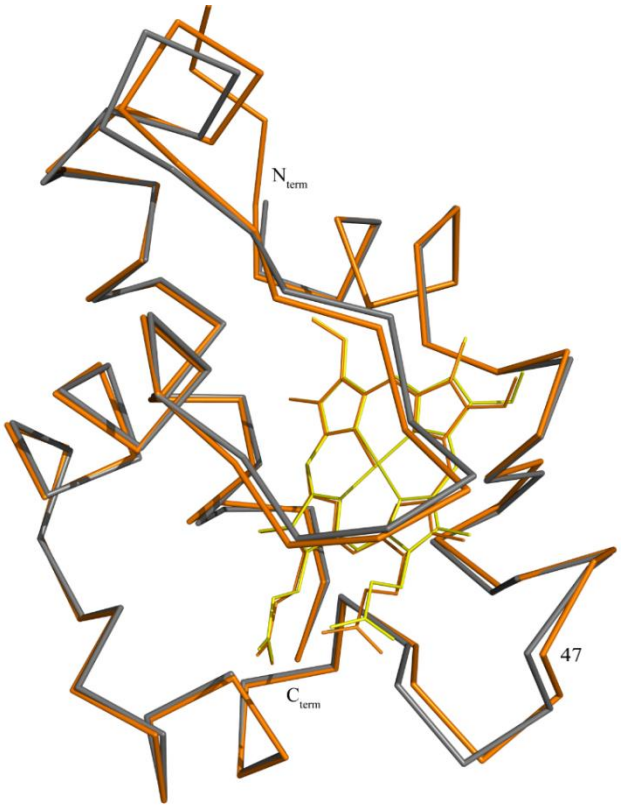

Figure 4.12 - OmcFH47I mutant (orange) (PDB code: 6U97) overlaid on the native OmcF (gray) (PDB code: 3CU4 [3]). The heme of the OmcFH4I mutant and native OmcF is colored orange and yellow, respectively. The two structures were overlapped using the C_α atoms of residues 26 – 104. The N- and C-termini are labelled, as well as the residue 47. Figure was produced using PyMOL (The PyMOL Molecular Graphics System, Version 1.3 Schrödinger, LLC).

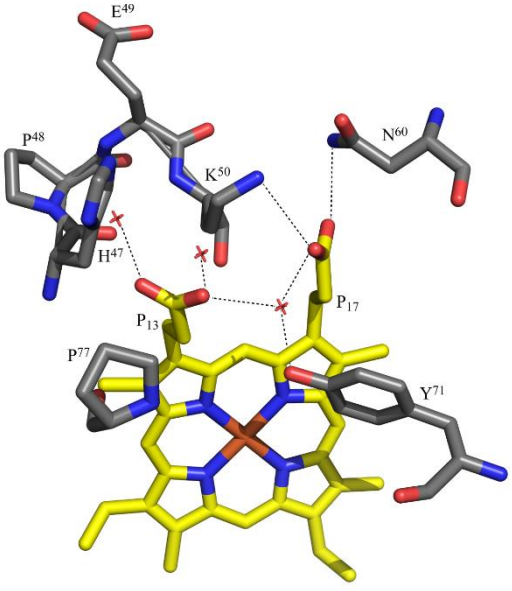

Figure 4.13 - Polar interactions involving the heme propionates of native OmcF (PDB code: 3CU4 [3]). Polar interactions are depicted as dashed lines. The residues His^{47}, Pro^{48}, Glu^{49}, Lys^{50}, Asn^{60} and Tyr^{71} are highlighted. The heme group is colored in yellow, with the iron atom colored in dark red. Blue and red colored atoms are nitrogen and oxygen, respectively, being gray representative of the rest of the amino acid chain. Red crosses represent water molecules. The propionates are labelled according to IUPAC-IUB nomenclature [34]. Figure was produced using PyMOL (The PyMOL Molecular Graphics System, Version 1.3 Schrödinger, LLC).

4.3.10 Heme propionate P_{13} and His^{47} are the redox-Bohr centers in OmcF

The observed hydrogen bond network established by the heme propionate groups, verified by X-ray crystallography, further supports the conclusion that P_{13} contributes to the global redox-Bohr effect in OmcF. In fact, it is common that the heme propionic acids ionize with pK_a values in the region 5 to 6 [36], and have been suggested as the groups responsible for the redox-Bohr effect in several monoheme cytochromes [12] [36] [40] [41]. In the oxidized crystal structures of wild-type OmcF (PDB code: 3CU4 [3]) and in the OmcFH47I mutant (present work, PDB code: 6U97), one of the carboxyl atoms of the heme propionate P_{17} forms a salt bridge with NZ of Lys^{50} and the other carboxyl oxygen atom hydrogen bonds with ND2 of Asn^{60}. Thus, this propionate is poised to be a hydrogen bond acceptor with both its carboxyl oxygen atoms, which stabilizes its deprotonated form. The stabilization offered by salt bridge with Lys^{50} and another hydrogen bond with Asn^{60} contributes to lower the pK_a of this propionate group (P_{17}) compared to that of propionate group P_{13}. The propionate P_{13} on the other hand does not form any interactions with the protein in the crystal structures. It is somewhat more exposed to solvent and only interacts with water molecules located in the crystal. This propionate is close to the side chain of His^{47} in the wild-type OmcF structure but does not form a hydrogen bond with it. In the solution structure of reduced OmcF (PDB code: 5MCS [6]), the family of 20 structures determined shows a propensity for propionate P_{13} to hydrogen bond with ND1 of His^{47} with one of its carboxyl oxygen atoms and the other carboxyl oxygen atom is within hydrogen bonding distance to main chain oxygen atom of Pro^{77}. The latter interaction will be unfavorable if this propionate is not in the protonated (neutral) form. The interaction between propionate P_{13} and the main chain oxygen of Pro^{77} is not seen in the crystal structure due to the intermolecular interactions with a neighboring molecule in the crystal. Alternatively, the difference could be related to redox conformational changes between the two structures, namely, crystal (oxidized) and solution (reduced). Therefore, we propose that the propionate P_{13} has a pK_a in the physiological range and, together with His^{47}, the two acid-base groups contribute to extend the range of the overall redox-Bohr effect in OmcF. Upon removal of His^{47} in the OmcFH47I mutants, the magnitude of the redox-Bohr effect observed is approximately 30% less than the wild-type cytochrome (54.8 and 57.7 mV for OmcFH47I and OmcFH47F, respectively, compared to 78.2 mV in OmcF).

4.4 Conclusions

The outer-membrane associated cytochrome OmcF from *G. sulfurreducens* has an important role in the extracellular electron transfer process in this bacterium and was electrochemically characterized in detail for the first time. The redox potential of OmcF and the heterogeneous charge electron transfer rate constant were determined. The pH dependence of the potential was described by a protonation event in the vicinity of the heme, and the pK_a values of

the redox-Bohr center were determined. Overall, the thermodynamic parameters ($\Delta H^{\circ'}_{rc}$, $\Delta S^{\circ'}_{rc}$ and $\Delta G^{\circ'}_{rc}$) suggested minor redox-linked conformational changes in the vicinity of the heme group, which are in line with the structural data obtained for the reduced and oxidized states. The redox potential determined for OmcF suggests that cells evolved to guarantee a down-hill electron transfer from the periplasm to the outer-membrane associated cytochrome OmcF.

The cytochrome OmcF showed an important pH modulation of the heme reduction potential (redox-Bohr effect) in the physiological range for *G. sulfurreducens* cellular growth. The spatial localization of His^{47} and the properties of its side chain suggested it as a good candidate for the redox-Bohr center of OmcF. This hypothesis was addressed in the present work by replacing His^{47} with the non-protonatable residues isoleucine and phenylalanine. The global fold of the mutants was assessed by NMR and the comparison of the polypeptide and heme signals showed that both the mutants were properly folded and that only local conformational changes were observed in the vicinity of the mutated residue regions. The crystal structure of OmcFH47I mutant determined at a high resolution also showed that the mutation did not affect the overall structure. Electrochemical cyclic voltammetry studies carried out for OmcFH47I and OmcFH47F, within the physiological pH range of *G. sulfurreducens*, showed that the redox potential values and the redox-Bohr effect were smaller compared to the wild-type cytochrome. This unequivocally confirmed the role of His^{47} in the pH modulation of the OmcF heme redox potential and electron/proton transfer mechanisms. However, the redox-Bohr effect was not fully abolished in the mutants (approximately 30% less in the mutants) suggesting the existence of another redox-Bohr center in OmcF, which was attributed to the heme propionate P_{13}. Therefore, these two acid-base groups with pK_a value in the physiological range (heme propionate P_{13} and His^{47}) contribute to the overall observed redox-Bohr effect. Given the cellular location of OmcF at the outer membrane, the existence of two independent acid-base centers that contribute to redox-Bohr effect may permit the protein to be functionally active in a wider pH range, in response to environment changes.

This study sheds light on how the cytochromes can extend the modulation of the redox potential within the physiological pH range not only through the interactions of their heme propionate groups with the neighboring protein atoms but also by utilizing strategic placement of additional protonatable residues near the heme. Delineation of such an intricate heme-protein interaction network is vital to a clearer understanding of the extracellular electron transfer processes mediated by these bacteria and the central role played by the multitude of cytochromes encoded within their genomes.

4.5 References

[1] J. Schnackenberg, M. E. Than, K. Mann, G. Wiegand, R. Huber, and W. Reuter, "Amino acid sequence, crystallization and structure determination of reduced and oxidized cytochrome c_6 from the green alga *Scenedesmus obliquus*," *J. Mol. Biol.*, vol. 290, no. 5, pp. 1019–1030, 1999.

[2] L. Banci, I. Bertini, M. A. De la Rosa, D. Koulougliotis, J. A. Navarro, and O. Walter, "Solution structure of oxidized cytochrome c_6 from the green alga *Monoraphidium braunii*," *Biochemistry*, vol. 37, no. 14, pp. 4831–4843, 1998.

[3] P. R. Pokkuluri et al., "Outer membrane cytochrome *c*, OmcF, from *Geobacter sulfurreducens*: High structural similarity to an algal cytochrome c_6," *Proteins Struct. Funct. Bioinforma.*, vol. 74, no. 1, pp. 266–270, 2009.

[4] J. A. R. Worrall et al., "Modulation of heme redox potential in the cytochrome c_6 family," *J. Am. Chem. Soc.*, vol. 129, no. 30, pp. 9468–75, 2007.

[5] A. P. Campos et al., "Cytochrome c_6 from *Monoraphidium braunii*. A cytochrome with an unusual heme axial coordination," *Eur. J. Biochem.*, vol. 216, no. 1, pp. 329–341, 1993.

[6] J. M. Dantas, M. A. Silva, D. Pantoja-Uceda, D. L. Turner, M. Bruix, and C. A. Salgueiro, "Solution structure and dynamics of the outer membrane cytochrome OmcF from *Geobacter sulfurreducens*," *Biochim. Biophys. Acta - Bioenerg.*, vol. 1858, no. 9, pp. 733–741, 2017.

[7] A. Lindgren, T. Larsson, T. Ruzgas, and L. Gorton, "Direct electron transfer between the heme of cellobiose dehydrogenase and thiol modified gold electrodes," *J. Electroanal. Chem.*, vol. 494, no. 2, pp. 105–113, 2000.

[8] H. Shkil, K. Dmytruk, O. Smutok, M. Gonchar, and A. Sibirny, "Bioelectrochemical detection of L-lactate respiration using genetically modified *Hansenula polymorpha* yeast cells overexpressing flavocytochrome b_2," *Bioelectrochemistry*, vol. 76, no. 1–2, pp. 175–179, 2009.

[9] D. S. Wishart et al., "^{1}H, ^{13}C and ^{15}N chemical shift referencing in biomolecular NMR," *J. Biomol. NMR*, vol. 6, no. 2, pp. 135–140, 1995.

[10] M. Correia dos Santos et al., "Electrochemical studies on small electron transfer proteins using membrane electrodes," *J. Electroanal. Chem.*, vol. 541, pp. 153–162, 2003.

[11] T. C. Santos, A. R. de Oliveira, J. M. Dantas, C. A. Salgueiro, and C. M. Cordas, "Thermodynamic and kinetic characterization of PccH, a key protein in microbial electrosynthesis processes in *Geobacter sulfurreducens*," *Biochim. Biophys. Acta - Bioenerg.*, vol. 1847, no. 10, pp. 1113–1118, 2015.

[12] A. J. Bard and L. R. Faulkner, *Electrochemical methods : fundamentals and applications*, 2nd ed. John Wiley & Sons, 2001.

[13] C. M. A. Brett and A. M. O. Brett, *Electrochemistry : Principles, Methods and Applications.* Oxford University Press, 1993.

[14] L. Morgado, M. Bruix, M. Pessanha, Y. Y. Londer, and C. A. Salgueiro, "Thermodynamic characterization of a triheme cytochrome family from *Geobacter sulfurreducens* reveals mechanistic and functional diversity," *Biophys. J.*, vol. 99, no. 1, pp. 293–301, 2010.

[15] E. Laviron, "General expression of the linear potential sweep voltammogram in the case of diffusionless electrochemical systems," *J. Electroanal. Chem. Interfacial Electrochem.*, vol. 101, no. 1, pp. 19–28, 1979.

[16] G. Sivashankar, Sivakolundu, and P. A. Mabrouk, "Cytochrome *c* structure and redox runction in mixed solvents are determined by the dielectric constant," *J. Am. Chem. Soc.*, vol. 122, no. 7, pp. 1513–1521, 2000.

[17] J.-H. Yoon, K.-S. Lee, J. Yang, M.-S. Won, and Y.-B. Shim, "Electron transfer kinetics and morphology of cytochrome *c* at the biomimetic phospholipid layers," *J. Electroanal. Chem.*, vol. 644, no. 1, pp. 36–43, 2010.

[18] M. F. Perutz, "Mechanisms of cooperativity and allosteric regulation in proteins," *Q. Rev. Biophys.*, vol. 22, no. 2, pp. 139–237, 1989.

[19] I. Taniguchi, T. Funatsu, M. Iseki, H. Yamaguchi, and K. Yasukouchi, "The temperature dependence of the redox potential of horse heart cytochrome *c* at a bis(4-pyridiyl)disulfide-modified gold electrode in sodium chloride solutions," *J. Electroanal. Chem. Interfacial Electrochem.*, vol. 193, no. 1–2, pp. 295–302, 1985.

[20] G. R. Moore, "Control of redox properties of cytochrome *c* by special electrostatic interactions," *FEBS Lett.*, vol. 161, no. 2, pp. 171–175, 1983.

[21] S. Mikami, H. Tai, and Y. Yamamoto, "Effect of the redox-dependent ionization state of the heme propionic acid side chain on the entropic contribution to the redox potential of *Pseudomonas aeruginosa* cytochrome c_{551}," *Biochemistry*, vol. 48, no. 33, pp. 8062–8069, 2009.

[22] G. Battistuzzi, M. Borsari, M. Sola, and F. Francia, "Redox thermodynamics of the native and alkaline forms of eukaryotic and bacterial class I cytochromes *c*," *Biochemistry*, vol. 36, no. 51, pp. 16247–16258, 1997.

[23] V. T. Taniguchi, N. Sailasuta—scott, F. C. Anson, and H. B. Gray, "Thermodynamics of metalloprotein electron transfer reaction," *Chem*, vol. 52, no. 10, pp. 2275–2281, 1980.

[24] G. Battistuzzi et al., "Redox reactivity of the heme Fe^{3+}/Fe^{2+} couple in native myoglobins and mutants with peroxidase-like activity," *JBIC J. Biol. Inorg. Chem.*, vol. 12, no. 7, pp. 951–958, 2007.

[25] P. Bertrand, O. Mbarki, M. Asso, L. Blanchard, F. Guerlesquin, and M. Tegoni, "Control of the redox potential in *c*-type cytochromes: importance of the entropic contribution," *Biochemistry*, vol. 34, no. 35, pp. 11071–11079, 1995.

[26] G. Battistuzzi, M. Borsari, L. Loschi, and M. Sola, “Redox thermodynamics, acid-base equilibria and salt-induced effects for the cucumber basic protein. General implications for blue-copper proteins,” *JBIC J. Biol. Inorg. Chem.*, vol. 2, no. 3, pp. 350–359, 1997.

[27] Y. Liu, L. C. Seefeldt, and V. D. Parker, “Entropies of redox reactions between proteins and mediators: the temperature dependence of reversible electrode potentials in aqueous buffers,” *Anal. Biochem.*, vol. 250, no. 2, pp. 196–202, 1997.

[28] E. Marsili, J. B. Rollefson, D. B. Baron, R. M. Hozalski, and D. R. Bond, “Microbial biofilm voltammetry: direct electrochemical characterization of catalytic electrode-attached biofilms,” *Appl. Environ. Microbiol.*, vol. 74, no. 23, pp. 7329–7337, 2008.

[29] S. Srikanth, E. Marsili, M. C. Flickinger, and D. R. Bond, “Electrochemical characterization of *Geobacter sulfurreducens* cells immobilized on graphite paper electrodes,” *Biotechnol. Bioeng.*, vol. 99, no. 5, pp. 1065–1073, 2008.

[30] Y. Liu, H. Kim, R. R. Franklin, and D. R. Bond, “Linking spectral and electrochemical analysis to monitor *c*-type cytochrome redox status in living *Geobacter sulfurreducens* biofilms,” *ChemPhysChem*, vol. 12, no. 12, pp. 2235–2241, 2011.

[31] T. C. Santos, M. A. Silva, L. Morgado, J. M. Dantas, and C. A. Salgueiro, “Diving into the redox properties of *Geobacter sulfurreducens* cytochromes: a model for extracellular electron transfer,” *Dalton Trans.*, vol. 44, no. 20, pp. 9335–44, 2015.

[32] J. M. Dantas, M. Silva e Sousa, C. A. Salgueiro, and M. Bruix, “Backbone, side chain and heme resonance assignments of cytochrome OmcF from *Geobacter sulfurreducens*,” *Biomol. NMR Assign.*, vol. 9, no. 2, pp. 365–368, 2015.

[33] F. H. Schumann, H. Riepl, T. Maurer, W. Gronwald, K.-P. Neidig, and H. R. Kalbitzer, “Combined chemical shift changes and amino acid specific chemical shift mapping of protein–protein interactions,” *J. Biomol. NMR*, vol. 39, no. 4, pp. 275–289, 2007.

[34] G. P. Moss, “Nomenclature of tetrapyrroles (Recommendations 1986),” *Eur. J. Biochem.*, vol. 178, no. 2, pp. 277–328, 1988.

[35] C. A. Salgueiro, D. L. Turner, and A. V Xavier, “Use of paramagnetic NMR probes for structural analysis in cytochrome c_3 from *Desulfovibrio vulgaris*,” *Eur. J. Biochem.*, vol. 244, no. 3, pp. 721–734, 1997.

[36] G. R. Moore, G. W. Pettigrew, R. C. Pitt, and R. J. P. Williams, “pH dependence of the redox potential of *Pseudomonas aeruginosa* cytochrome *c*-551,” *Biochim. Biophys. Acta - Bioenerg.*, vol. 590, no. 2, pp. 261–271, 1980.

[37] L. R. Teixeira, C. M. Cordas, M. P. Fonseca, N. E. C. Duke, P. R. Pokkuluri, and C. A. Salgueiro, “Modulation of the redox potential and electron/proton transfer mechanisms in the outer membrane cytochrome OmcF from *Geobacter sulfurreducens*,” *Front. Microbiol.*, vol. 10, p. 2941, 2020.

5. Backbone, side-chain and heme assignment of cytochrome PccH in the oxidized state[1]

[1]Partially reproduced from Liliana R. Teixeira, Pilar C. Portela, Leonor Morgado, David Pantoja-Uceda, Marta Bruix, Carlos A. Salgueiro (2019) Backbone assignment of cytochrome PccH, a crucial protein for microbial electrosynthesis in *Geobacter sulfurreducens*, Biomolecular NMR Assignments 13 (2), 321-326 (doi: 10.1007/s12104-019-09899-6), in accordance with the Editors' Copyright Policy.

5.1 Introduction

Microbial electrosynthesis is an increasingly interesting technology for the production of hydrogen and value-added chemicals [1] [2]. The understanding of the pathways responsible for the electron transfer from electrodes to terminal acceptors is therefore crucial to optimize electroactive microorganisms and to improve their practical applications.

The periplasmic cytochrome PccH, encoded by gene *gsu3274*, is the most expressed cytochrome in electron-uptake biofilms of *G. sulfurreducens*, far more abundant than genes encoding for proteins known to be essential for electron delivery (OmcZ and PilA) [1] [3]. Also, PccH deficient *G. sulfurreducens* strains were unable to uptake electrons from the electrode. Overall, these results unequivocally showed that not only PccH is a crucial protein for the microbial electrosynthesis pathways, but also that the electron-uptake and electron-deliver processes have distinct mechanisms [3].

The mature PccH is a monoheme *c*-type cytochrome with 129 amino acids, 15 kDa molecular weight, isoelectric point 7.83 and it is predicted to be located at the periplasm. The heme group is axially coordinated by one histidine and one methionine residues being low spin, both in the reduced (S=0) and oxidized (S=1/2) states [4]. The oxidized structure of the protein was determined by X-ray crystallography and showed that PccH has a unique fold compared to other *c*-type cytochromes from class I [5] (Figure 5.1). In fact, the heme group in cytochrome PccH is sandwiched between two lobes and is more solvent exposed compared to other monoheme cytochromes, contributing to the relatively low reduction potential value of the cytochrome. The unique structure of PccH and the fact that in a phylogenetic analysis it forms a separate group with its most homologous protein sequences, suggest that this cytochrome forms a new subclass of class I monoheme *c*-type cytochromes [5].

The redox potential of the cytochrome was measured by redox titrations and voltammetry: -24 ± 5 mV and -35 ± 5 mV (*vs* NHE) at pH 7 and pH 8, respectively [4] The redox-Bohr center was attributed to the heme propionates, since their pK_a values are well framed within the ones of PccH [6].

Despite the available structural and biophysical data for cytochrome PccH, there is no information regarding its redox partners and hence on the electron transfer mechanism for current-consuming *G. sulfurreducens* biofilms. Taking into consideration the potential values of PccH at the physiological pH of the bacteria, this cytochrome is thermodynamically suitable to bridge electron transfer from biocathodes, as graphite (-293 mV *vs* NHE) to electron acceptors, such as fumarate (30 mV *vs* NHE). Naturally, more proteins are involved in this process, namely membrane associated ones.

In this Chapter the assignment of the heme and backbone NMR signals of cytochrome PccH in the oxidized state is presented, which constitutes the foundation both to map the

interaction regions between possible physiological partners and, thus to elucidate the electron transfer mechanism from electrodes toward *G. sulfurreducens* cells.

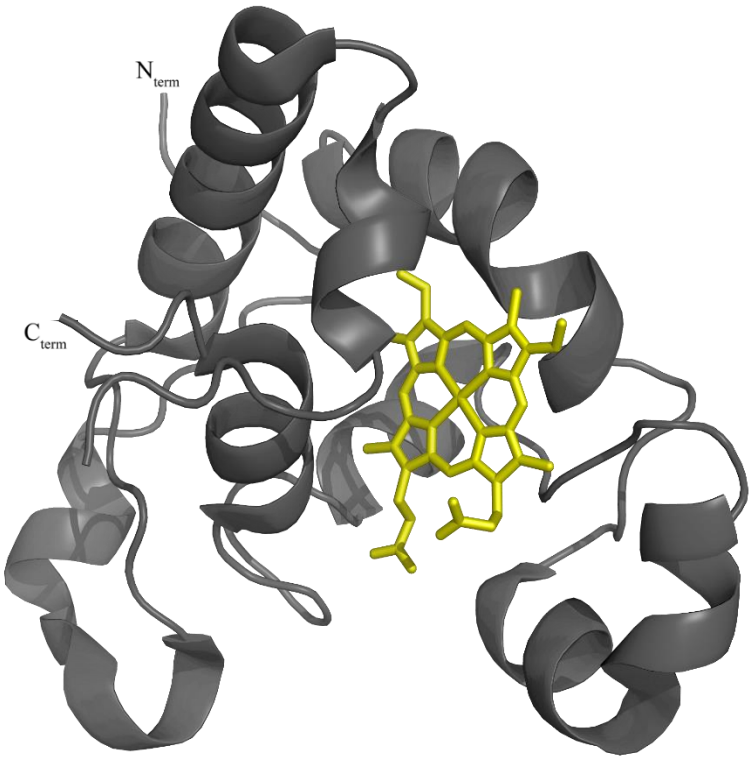

Figure 5.1 – Crystal structure of cytochrome PccH (PDB code: 4RLR [5]**).** The PccH polypeptide chain and the heme group are colored gray and yellow, respectively. The N- and C-termini are labeled. Figure was produced using PyMOL (The PyMOL Molecular Graphics System, Version 1.3 Schrödinger, LLC).

5.2 Materials and methods

5.2.1 Production of natural abundance and isotopic enriched protein

E. coli BL21 (DE3) cells containing the plasmids pEC86 and pCS3274 were used to produce both unlabeled and isotopically labeled (^{13}C and ^{15}N) PccH. The pEC86 plasmid encodes for cytochrome *c* maturation gene cluster [7], whereas the pCS3274 encodes for cytochrome PccH [4]. pCS3274 is a pVA203 derivate [8], which in its turn is derived from pCK32 vector by having a *NotI* site introduced at the end of the peptide coding sequence. This allows for cloning without adding extra residues at the N-terminus [9].

The production of unlabeled protein followed the procedure previously described in Chapter 3. In short, cells were grown in 2xYT supplemented with chloramphenicol (34 µg/mL) and ampicillin (100 µg/mL), at 30 ºC. When the OD_{600nm} of the culture reached a value between 0.7 and 0.8, protein production was induced by adding 100 µM of IPTG. Cells were harvested after 16–18 h of incubation [4].

In previous works, we were able to isotopically label *c*-type multiheme and monohemic cytochromes using the methodology reported by Fernandes and co-workers [10] as explained in Chapter 3. Following this procedure, *E. coli* cells were firstly grown in 50 mL of 2xYT medium and, after reaching an OD_{600nm} value between 1.8 and 2.0, the culture was transferred to 1 L of 2xYT. When the OD_{600nm} reached a value between 1.5 and 1.8, cells were transferred to M9 medium, supplemented with 1 g/L of $^{15}NH_4Cl$, 2 g/L of $^{13}C_6$-D-glucose and 1 mM of the heme precursor α-aminolevulinic acid. After 1 h 30 min at 30 ºC, protein production was induced by adding 100 µM of IPTG. However, in the case of cytochrome PccH, it was not possible to obtain sufficient amounts of labeled protein with this method. A possible explanation for the low levels of expression is the relatively high concentration of glucose (2 g/L) in the M9 medium, which might inhibit the cellular uptake of IPTG. In order to confirm this hypothesis, the previous method was repeated with the following alteration: supplementation of the M9 medium with 5 mL/L of glycerol and 0.5 g/L of $^{12}C_6$-D-glucose [11], instead of 2 g/L of $^{13}C_6$-D-glucose. Using this methodology, it was possible to express and label the protein however, only in ^{15}N, and not in ^{13}C.

In order to produce the necessary amounts of the ^{13}C and ^{15}N labeled protein, a new methodology was used. In this case, after transformation and colony peaking, the cells were first grown for approximately 9 h in 5 mL of 2xYT medium at 30 ºC and 200 rpm. 1 mL of culture was then transferred to 50 mL of minimal medium M9 (supplemented with $^{15}NH_4Cl$, $^{13}C_6$-D-glucose and α-aminolevulinic acid) and incubated for approximately 14 h at 30 ºC and at 200 rpm. 50 mL of culture were transferred to 1 L of M9 medium (supplemented as previously described) and incubated at 30 ºC and at 180 rpm, until the OD_{600nm} reached a value between 0.7 and 0.8. Protein expression was induced by adding 100 µM of IPTG, and the culture was incubated for approximately 16 h at 30 ºC and at 160 rpm. All media were supplemented with the same antibiotic concentrations, as previously described.

5.2.2 Isolation and purification of cytochrome PccH

To isolate the periplasmatic fraction containing the targeted protein, both labeled and unlabeled, cells were firstly centrifuged at 6400 ×*g* for 20 min and then lysed using a buffer containing 100 mM Tris–HCl at pH 8, 0.5 mM EDTA, 20% sucrose and 0.5 mg/mL of lysozyme. The periplasmatic fraction was recovered by centrifugation and followed by an ultracentrifugation, as previously described [4]. The supernatant was dialyzed with 10 mM Tris–HCl pH 8 and loaded onto cation-exchange columns (2×5 mL BioScale™ Mini UNOsphere S cartridges, Bio-Rad) pre-equilibrated with the same buffer. The fractions were collected using a sodium chloride gradient between 0 and 300 mM. The samples containing the protein were loaded onto a XK 16/70 Superdex™ 75 prep grade column (GE Healthcare Life Sciences) pre-equilibrated with 100 mM sodium phosphate buffer pH 8. Both chromatographies were

performed at a glow-rate of 1 mL/min. Protein purity was assessed by SDS-PAGE stained with BlueSafe (NZYTech). Protein concentration was determined by UV–visible spectroscopy, at room temperature in a 1 cm path length quartz cuvettes, using the extinction coefficient of 32.5 mM^{-1} cm^{-1} [4].

5.2.3 NMR samples preparation and experiments

NMR samples with 0.6 mM of ^{15}N and ^{13}C labeled PccH were prepared in 92 % H_2O / 8 % D_2O, containing 32 mM of sodium phosphate buffer (final ionic strength 100 mM) at pH 7.5. Samples of unlabeled protein were prepared with a concentration of 1 mM of cytochrome, in the same conditions as previously described.

All the NMR experiments were carried out at 25 ºC on a Bruker Avance 800 MHz spectrometer equipped with a *z*-gradient cryoprobe. For assignment of the protein's backbone and side chain NMR signals, the following spectra were acquired for the labeled protein: 2D ^{1}H, ^{15}N HSQC; 2D ^{1}H, ^{13}C HSQC; 3D HNCA; 3D HN(CO)CA; 3D HN(CA)CO; 3D HNCO; 3D CBCA(CO)NH; 3D HCC(H) TOCSY and 3D HC(C)H TOCSY. To assist and further confirm the assignment obtained from the above mentioned spectra, carbon edited 2D ^{1}H, ^{15}N HSQC experiments were also recorded accordingly to the methodology described by Pantoja-Uceda and co-workers [12] [13]. In these NMR spectra, the signal of the cross-peaks changes from one spectrum to another according to the amino acid type of the residue preceding the observable backbone NH and of its own residue in the protein sequence, providing independent starting points to the assignment of the protein signals.

2D ^{1}H, ^{13}C HSQC; 2D ^{1}H, ^{1}H TOCSY (45 ms) and 2D ^{1}H, ^{1}H NOESY (80 ms) were acquired for the unlabeled protein, in order to assign the heme substituents' signals. Due to the ring-current effect and the paramagnetic contribution, caused by the presence of unpaired electron, the NMR signals in the oxidized state are broader and more spread along the spectra. For these reasons, the chemical shifts of the heme substituents in the oxidized state are very different from the ones observed in the reduced state. To assist the assignment, the spectrum 2D ^{1}H, ^{13}C HSQC is of much importance, because typical ^{1}H, ^{13}C regions can be identified. 2D ^{1}H, ^{1}H TOCSY is also useful to identify the intraheme correlations with the propionates and the 2D ^{1}H, ^{1}H NOESY allows identifying cross-peaks between propionates and the closest heme group.

The ^{1}H chemical shifts were calibrated using the water signal as internal reference, whereas the ^{13}C and ^{15}N shifts were calibrated by indirect referencing [14]. The data was processed using TOPSPIN (Bruker Biospin, Karlsruhe, Germany) and analyzed with Sparky (TD Goddard and DG Kneller, Sparky 3, University of California, San Francisco, USA).

5.3 Results and discussion

5.3.1 Production and purification of PccH

For natural abundance protein production, the same methodology was used as previously described [4]. However, small differences in the methodology were implemented. The OD_{600nm} at which protein production is induced was 0.7 rather than 1.5. Additionally, the aeration of the cultures was increased, by growing less volume in the flasks. These alterations lead to a substantial increase in protein production, from 4.7 to 30.6 mg/L of culture.

Initially, the labeled PccH cytochrome was produced according to the method developed by Fernandes and co-workers [10]. However, the production yield was 0.6 mg/L, much smaller compared to the yield of the natural abundance protein (30.6 mg/L) and clearly insufficient for the proposed studies.

The hypothesis that the glucose in the M9 medium might inhibit the IPTG uptake by the cells was confirmed by its replacement by glycerol. In this case, the yields increased approximately 3 times. Therefore, the low levels of protein expression were related to the presence of glucose in the M9 medium, which was inhibiting the uptake of IPTG by the cells. In fact, glycerol is a carbon source, but not a simple sugar as glucose, favoring IPTG uptake by the cells and concomitant protein expression. However, with this method was only possible to label the protein in ^{15}N, and not in ^{13}C.

A method based on the work of Marley and co-workers (2001) [15] was implemented. This method implied the use of M9 as described before [10], but the ^{15}N and ^{13}C sources were only added to the culture 4 h after the addition of IPTG. According to the authors, this strategy would permit the uptake of IPTG by the cell before the labeled isotopes. Although the production yield increased (3.2 mg/L), the protein was only approximately 10% labeled, a value estimated from the analysis of 1D ^{1}H NMR spectra. These results indicated that the protein production was induced before the uptake of the isotopes.

For these reasons, a new method was developed, where the cells were grown in M9. In this case, the production yield obtained was 2.5 mg/L, however lower than the one obtained for the previous method, the protein was approximately 100% labeled both in ^{15}N and ^{13}C. This turned out to be the most effective method which allowed to conduit the proposed NMR studies.

5.3.2 Assignment and data deposition

The effective and directional electron transfer along respiratory chains relies on the precise establishment of interacting redox networks between physiological partners. In case of monoheme cytochromes, as it is the case of PccH, the electron donor and acceptor must interact nearby the heme group to warrant an effective electron transfer within the redox complex. Thus, to proper map the interacting docking regions within a redox complex established with PccH, in addition

to the protein's backbone NMR signals, it is also necessary to assign the heme substituent NMR signals. The assignment of these signals was obtained by the combined use of 2D ^{1}H, ^{13}C HSQC, 2D ^{1}H, ^{1}H TOCSY and 2D ^{1}H, ^{1}H NOESY NMR spectra following the methodology previously described (Chapter 2) [16].

The combined information of the 2D ^{1}H,^{15}N HSQC and the 3D spectra allowed the almost complete assignment of the protein's backbone: ^{15}N (98%), ^{1}HN (98%), $^{13}C_{\alpha}$ (99%), $^{1}H_{\alpha}$ (92%), $^{13}C_{\beta}$ (98%), $^{1}H_{\beta}$ (81%) and ^{13}CO (96%). Regarding the side chain assignment, the following results were obtained: $^{13}C_{\gamma}$ (85%), $^{1}H_{\gamma}$ (66%), $^{13}C_{\delta}$ (81%), $^{1}H_{\ddot{o}}$ (67%), $^{13}C_{\varepsilon}$ (92%) and $^{1}H_{\varepsilon}$ (50%). The chemical shifts were deposited in BioMageResBank (http://www.bmrm.wisc.edu) under BMRB accession number 27869, and is reported in the Appendix section (Table A.4). The 2D ^{1}H, ^{15}N HSQC obtained for cytochrome PccH is depicted in Figure 5.2.

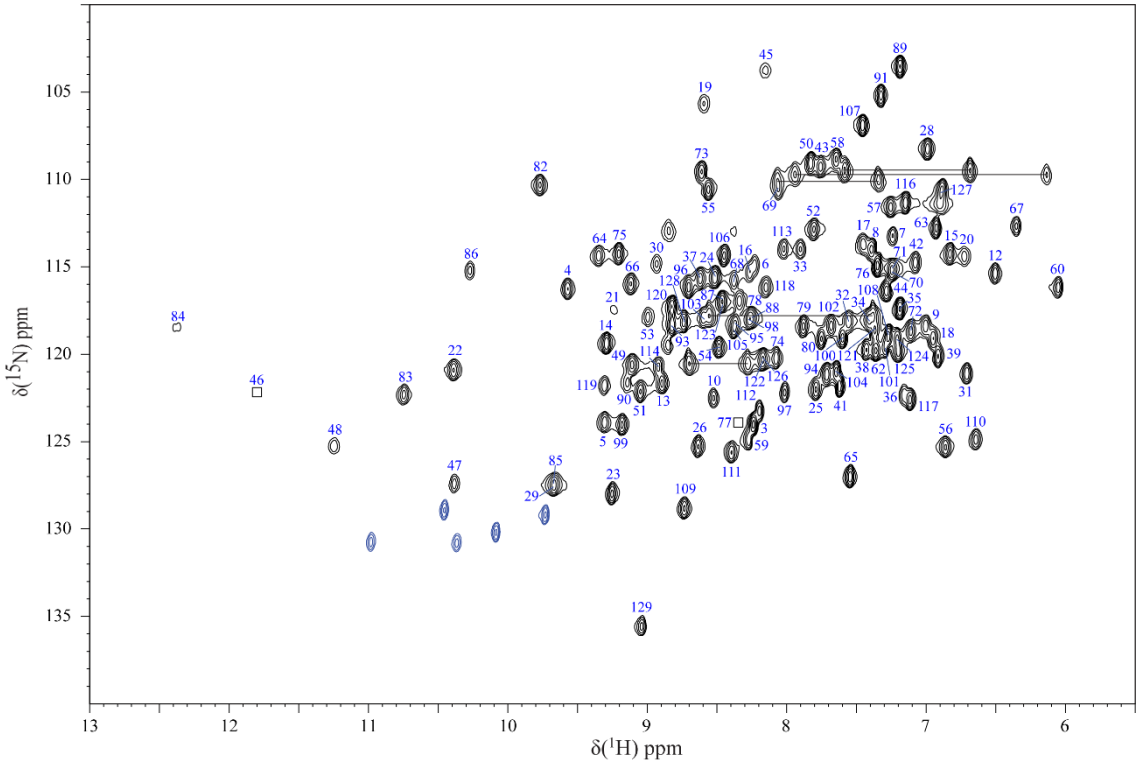

Figure 5.2 - 2D ^{1}H, ^{15}N HSQC spectra of PccH in the fully oxidized state (25 ºC, pH 7.5, and 100 mM ionic strength). Blue labels represent ^{1}H-^{15}N backbone connectivity. Horizontal black lines correspond to the side-chain groups of asparagine and glutamine residues. Signals in blue correspond to the side-chain $NH_{\varepsilon 1}$ signal from tryptophan residues. The empty box corresponds to the position of weak NH signals only visible at lower contour levels.

Compared to non-heme proteins, the heme ring-current shifts, caused by the aromatic porphyrin rings, as well as the paramagnetic effects due to the presence of the heme iron unpaired electron, are responsible for significant differences observed in the chemical shifts of the same nuclei in non-heme proteins [17]. This is more notorious for the heme axial ligands (His^{21} and Met^{84}) and cysteine residues in the heme binding motif (Cys^{17} and Cys^{20}). In addition to the

residues that are directly bound to the heme group, nuclei from neighboring residues also showed important changes in their chemical shifts. This is the case of residues Arg[47], Met[48], Tyr[57], Arg[69], Leu[70] and Asn[83] (Table 5.1).

Table 5.1 – Absolute value of the difference between the assigned and the reference chemical shifts retrieved from [17]. N.A defines amino acids for which it was not possible to assign a chemical shift.

Residue	Nuclei				
	^{13}CO	$^{13}C_{\alpha}$	$^{13}C_{\beta}$	^{1}HN	^{15}N
Cys[17]	1.3	3.1	6.3	0.98	5.0
Cys[20]	0.9	0.4	6.2	1.70	4.3
His[21]	3.6	8.2	N.A	0.82	0.8
Arg[47]	1.6	4.5	0.3	2.15	6.9
Met[48]	1.7	1.6	6.9	2.97	5.5
Tyr[57]	1.6	0.0	1.3	0.86	8.8
Arg[69]	1.5	0.5	0.7	0.17	10.0
Leu[70]	3.4	1.1	0.7	0.92	6.8
Asn[83]	6.3	4.5	1.3	2.40	3.6
Met[84]	2.3	5.3	N.A	4.10	1.2

5.3.3 Secondary structure prediction

The assigned protein's backbone signals was then used to predict its secondary structure in solution using the TALOS+ software [18]. The data obtained indicates that the dominant secondary structural elements are α-helices. The prediction closely matches that of the crystal structure of the protein [5] (*cf.* panels A and B in Figure 5.3). The only exception corresponds to the polypeptide segment between residues 18 and 21 (Figure 5.3 B). However, this is not unexpected since this polypeptide segment contains the heme binding motif residues (Cys[17]-Ala[18]-Gly[19]-Cys[20]-His[21]). The heme binding residues in this motif (Cys[17], Cys[20] and His[21]) are strongly affected by the heme environment and for this reason the secondary structural elements in this region cannot be accurately predicted. It is also important to note that in the X-ray crystal structure the polypeptide segment between the residues 75 and 77 was not visible in the electron density map [5]. In the present work, TALOS+ predicts a random coil between residues 69 and 81, on one hand, complementing the X-ray observations and, on the other, elucidating the most likely secondary structure element of residues 75 to 77 (Figure 5.3).

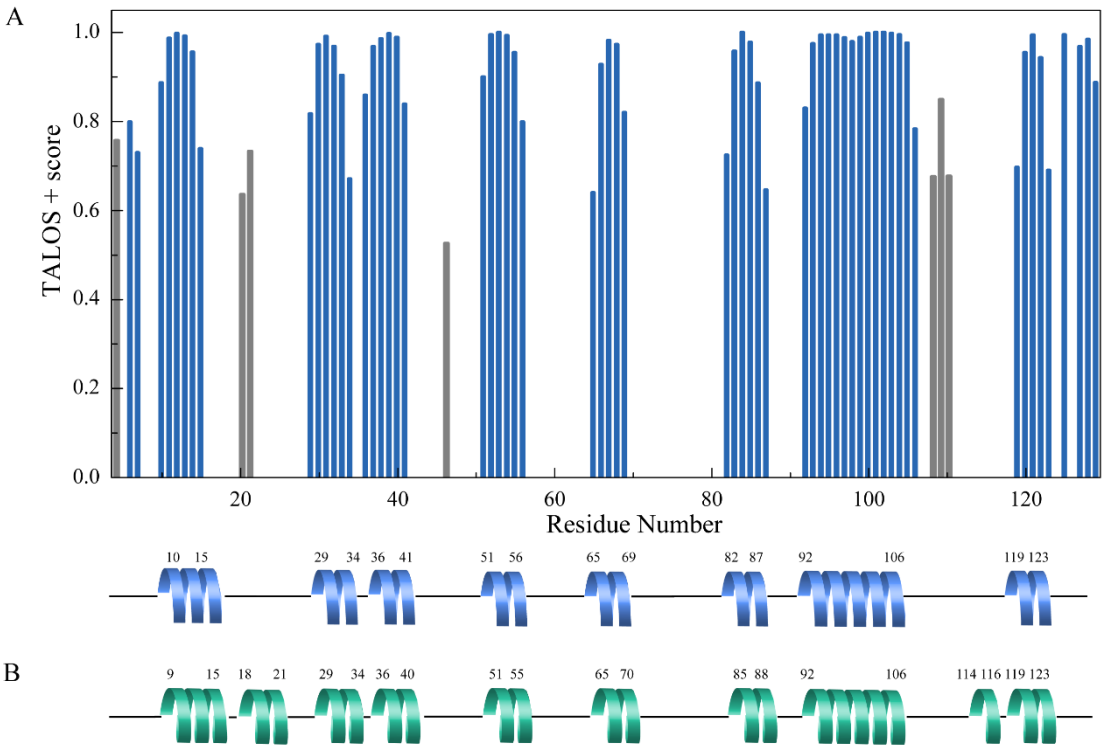

Figure 5.3 - Secondary structural elements of PccH. (A) Secondary structure elements predicted by TALOS+ [14]. The residues represented by the blue bars are predicted to be located in α-helical secondary structural elements and the residues represented by gray bars correspond to predicted β-sheet secondary structural elements. The author has chosen to not consider the β-sheet predictions since they do not encompass sufficient amino acids to actually form secondary structure. **(B)** Comparison of secondary structural elements from the TALOS+ prediction (this work) and those obtained from the X-ray crystal structure (PDB code: 4RLR [5]). The residue numbers are shown on top of each secondary structural element.

5.4 Conclusions

Overall, the results obtained in the present work constitute important foundations to investigate and structurally map the interactions between PccH and physiological partners. Furthermore, this study confirms the secondary structure determined previously by X-ray crystallography [5].

Previous studies demonstrated that PccH does not interact with PpcD [5], which is another cytochrome that has a higher expression in *G. sulfurreducens* growing on electrodes [3]. One possible partner for PccH is the cytochrome encoded by gene *gsu2515*, which also presented higher transcription levels in current consuming cells [3]. This may be indicative that *gsu2515* also takes part on the electron transfer from electrodes, and a potential physiological partner of PccH, which is until now the only known cytochrome involved in this process. NMR-based biomolecular interaction studies between PccH, the most overexpressed cytochrome in electron-uptake biofilms of *G. sulfurreducens*, and its redox partners might contribute to the understanding of the extracellular electron transfer mechanism in microbial electrosynthesis.

5.5 References

[1] K. P. Nevin *et al.*, "Anode biofilm transcriptomics reveals outer surface components essential for high density current production in *Geobacter sulfurreducens* fuel cells," *PLoS One*, vol. 4, no. 5, p. e5628, 2009.

[2] K. Rabaey and R. A. Rozendal, "Microbial electrosynthesis — revisiting the electrical route for microbial production," *Nat. Rev. Microbiol.*, vol. 8, no. 10, pp. 706–716, 2010.

[3] S. M. Strycharz *et al.*, "Gene expression and deletion analysis of mechanisms for electron transfer from electrodes to *Geobacter sulfurreducens*," *Bioelectrochemistry*, vol. 80, no. 2, pp. 142–150, 2011.

[4] J. M. Dantas, D. M. Tomaz, L. Morgado, and C. A. Salgueiro, "Functional characterization of PccH, a key cytochrome for electron transfer from electrodes to the bacterium *Geobacter sulfurreducens*," *FEBS Lett.*, vol. 587, no. 16, pp. 2662–2668, 2013.

[5] J. M. Dantas, L. M. Campelo, N. E. C. Duke, C. A. Salgueiro, and P. R. Pokkuluri, "The structure of PccH from *Geobacter sulfurreducens* - a novel low reduction potential monoheme cytochrome essential for accepting electrons from an electrode," *FEBS J.*, vol. 282, no. 11, pp. 2215–2231, 2015.

[6] T. C. Santos, A. R. de Oliveira, J. M. Dantas, C. A. Salgueiro, and C. M. Cordas, "Thermodynamic and kinetic characterization of PccH, a key protein in microbial electrosynthesis processes in *Geobacter sulfurreducens*," *Biochim. Biophys. Acta - Bioenerg.*, vol. 1847, no. 10, pp. 1113–1118, 2015.

[7] E. Arslan, H. Schulz, R. Zufferey, P. Kunzler, and L. Thony-Meyer, "Overproduction of the *Bradyrhizobium japonicum c*-type cytochrome subunits of the cbb_3 oxidase in *Escherichia coli*," *Biochem. Biophys. Res. Commun.*, vol. 251, no. 3, pp. 744–747, 1998, doi: 10.1006/bbrc.1998.9549.

[8] P. R. Pokkuluri *et al.*, "Structural characterization of a family of cytochromes c_7 involved in Fe(III) respiration by *Geobacter sulfurreducens*," *Biochim. Biophys. Acta - Bioenerg.*, vol. 1797, no. 2, pp. 222–232, 2010.

[9] Y. Y. Londer, P. R. Pokkuluri, V. Orshonsky, L. Orshonsky, and M. Schiffer, "Heterologous expression of dodecaheme 'nanowire' cytochromes *c* from *Geobacter sulfurreducens*," *Protein Expr. Purif.*, vol. 47, no. 1, pp. 241–248, 2006.

[10] A. P. Fernandes, I. Couto, L. Morgado, Y. Y. Londer, and C. A. Salgueiro, "Isotopic labeling of *c*-type multiheme cytochromes overexpressed in *E. coli*," *Protein Expr. Purif.*, vol. 59, no. 1, pp. 182–188, 2008.

[11] F. W. Studier, "Protein production by auto-induction in high-density shaking cultures," *Protein Expr. Purif.*, vol. 41, no. 1, pp. 207–234, 2005.

[12] D. Pantoja-Uceda and J. Santoro, "Amino acid type identification in NMR spectra of

proteins via β- and γ-carbon edited experiments," *J. Magn. Reson.*, vol. 195, no. 2, pp. 187–195, 2008.

[13] D. Pantoja-Uceda and J. Santoro, "New amino acid residue type identification experiments valid for protonated and deuterated proteins," *J. Biomol. NMR*, vol. 54, no. 2, pp. 145–153, 2012.

[14] D. S. Wishart *et al.*, "^{1}H, ^{13}C and ^{15}N chemical shift referencing in biomolecular NMR," *J. Biomol. NMR*, vol. 6, no. 2, pp. 135–140, 1995.

[15] J. Marley, M. Lu, and C. Bracken, "A method for efficient isotopic labeling of recombinant proteins," *J. Biomol. NMR*, vol. 20, no. 1, pp. 71–75, 2001.

[16] C. A. Salgueiro, D. L. Turner, and A. V Xavier, "Use of paramagnetic NMR probes for structural analysis in cytochrome c_3 from *Desulfovibrio vulgaris*," *Eur. J. Biochem.*, vol. 244, no. 3, pp. 721–734, 1997.

[17] D. S. Wishart, C. G. Bigam, A. Holm, R. S. Hodges, and B. D. Sykes, "^{1}H, ^{13}C and ^{15}N random coil NMR chemical shifts of the common amino acids. I. Investigations of nearest-neighbor effects," *J. Biomol. NMR*, vol. 5, no. 1, pp. 67–81, 1995.

[18] Y. Shen, F. Delaglio, G. Cornilescu, and A. Bax, "TALOS+: a hybrid method for predicting protein backbone torsion angles from NMR chemical shifts," *J. Biomol. NMR*, vol. 44, no. 4, pp. 213–223, 2009.

5. Backbone, side-chain and heme assignment of cytochrome PccH in the oxidized state

6. Characterization of cytochrome GSU2515

6.1 Introduction

Little is known about the cytochrome encoded by the gene annotated in the Kyoto Encyclopedia of Genes and Genomes (KEGG) as *gsu2515*. It is a mono-hemic *c*-type cytochrome with 141 amino acids, containing one heme-binding Cys-X-X-Cys-His sequence (Cys^{93}-Ala^{94}-Gly^{95}-Cys^{96}-His^{97}), and a signal-peptide including the first 31 amino acids (Figure 6.1). The cytochrome has a molecular mass of 12 kDa, an isoelectric point of 7.02 (values determined by ExPASy tool), and it is predicted to be localized at the periplasm.

```
          10        20        30        40        50        60
MAKRIQTVTRGHITAAAALVIGVLAAFTADANTGRTADGSVPRTPAIIATPGERTIQADPAYPLP

      70        80        90       100       110       120
QPAERKSRTEARRSGPIDGATLYYTGNCAGCHGTMANMKGTTAEMIRFAIDNNVGGMGFHVN

  130       140
LTPEELHSIADALK
```

Figure 6.1 - Amino acid sequence of the cytochrome GSU2515. The signal peptide is indicated in gray and the *c*-type heme binding motif (CXXCH) is underlined.

Genetic studies showed that the gene encoding for cytochrome GSU2515 is expressed under Fe(III) reducing conditions, together with other yet to be studied cytochromes, annotated in the KEGG genome data base entry as GSU0105 and GSU0701 [1]. The cytochrome GSU2515 is not expressed in cultures grown on fumarate, elucidating its relevance in the Fe(III) reduction pathway [1]. On the other hand, this protein is the second most expressed *c*-type cytochrome in current-consuming cells, after PccH [2].

The biochemical characterization of the cytochrome GSU2515 will be presented in this chapter. The protein was heterologously expressed in *E. coli* cells and characterized through circular dichroism, UV-visible and NMR spectroscopic techniques. The protein stability was accessed, as well as the determination of secondary structure elements, the heme-spin state and the redox potential functional range. Biomolecular interactions between the cytochrome and PccH were also evaluated by NMR chemical shift perturbation experiments.

6.2 Material and methods

6.2.1 Cloning of cytochrome GSU2515

Genomic DNA of *G. sulfurreducens* was kindly provided by Prof. D.R. Lovely (University of Massachusetts, Amherst). Gene sequence information (Gene ID: 2685673) was obtained from KEGG web site. As mentioned above, cytochrome GSU2515 has 141 amino acids, from which the first 31 are predicted to be the signal peptide. For this reason, the *gsu2515* gene was cloned excluding the signal peptide.

Cloning was performed by the restriction free technique, using the plasmid pVA203 as template. This plasmid is a derivative of pkIVLen004, which contains the *lac* promotor and the OmpA leader sequence [3] [4]. Firstly, a PCR amplification was done in order to extract the gene of interest from the *G. sulfurreducens* genome. The primers used were: 5'-gctaccgttgcggccgccaatacgggccggaccgcc-3' and 5'-agcttgtcgacggagctcgaatttatttgagggcgtcggcaatg-3'. The oligonucleotides were designed using the rf-cloning program (www.rf-cloning.org) and synthesized by Invitrogen. The reaction mixture was constituted by the reaction buffer (10 µL), dNTP's mix (1 µL of 10 U/µL), double-stranded DNA template (0.5 µL), forward and reverse primers (1 µL of 50 µM), Phusion® high-fidelity DNA polymerase (Thermo Scientific) (0.5 µL of 2 U/ µL) and MilliQ water up to 50 µL. The PCR was divided into three segments: denaturation was at 98 ºC for 7 min; the annealing was at 65 ºC for 1 min; and finally, the extension was at 72 ºC for 20 sec/ kb of plasmid. Thirty-five cycles were performed. The PCR product was then purified using the NZYGelpure kit (Nzytech).

These procedures were followed by a second PCR amplification, where the hybridization of the gene onto the vector was performed. The plasmid pVA203 was used as template, in a 20:1 insert:plasmid ratio. The solution contained the reaction buffer as well (4 µL), dNTP's mix (0.4 µL of 10 U/µL), Phusion® high-fidelity DNA polymerase (0.5 µL of 2 U/ µL) and MilliQ water up to 20 µL. The PCR was divided into three segments: denaturation was at 98 ºC for 7 sec; annealing at 69 ºC for 20 sec; and the extension was at 72 ºC for 20 sec/ kb of plasmid. Thirty cycles were performed.

The PCR product was then treated with *DpnI*, by adding the enzyme (1 U/ µg of DNA) and let it incubate for 1 h at 37 ºC. The enzyme was inactivated by incubating the reaction at 80 ºC for 20 min.

In order to obtain the desired vector containing the gene of interest, competent *E. coli* cells (DH5α) were transformed. The transformation protocol was the same as described previously (Chapter 3), but in this case by using Luria-Bertani (LB) medium. LB medium is constituted by 5 g/L of yeast extract, 10 g/L of tryptone and 10 g/L of NaCl. After transformation, cells were inoculated in LB solid medium, containing 15 g/L of agar and ampicillin (100 µg/mL). Colonies were selected from the plates to perform a colony PCR, with the following reaction composition: reaction buffer (2 µL), dNTP's mix (0.4 µL of 10 U/µL), forward and reverse primers (0.2 µL of 50 µM), Taq DNA polymerase (VWR) (0.2 µL of 5 U/ µL) and MilliQ water until the final volume of 20 µL. The PCR was divided into three segments: denaturation was at 95 ºC for 30 sec; the annealing was at 55 ºC for 30 sec; and finally, the extension was at 72 ºC for 45 sec. Thirty-five cycles were performed. The size of PCR products was confirmed by using an agarose gel (1.5%), DNA quantification and purity were determined using NanoDrop, and the DNA was sequenced by STAB VIDA.

6.2.2 Expression tests

All the *E. coli* strains containing the plasmid pEC86 available in the laboratory were used for expression tests: BL21 (DE3), Tuner, SF110, JM109, C43 and JCB7123. In each case, after transformation of the cells with the vector containing *gsu2515*, one colony was transferred to 5 mL of 2xYT medium, supplemented with 34 μg/mL chloramphenicol and 100 μg/mL ampicillin. Cultures were grown overnight, at 30 ºC and at 200 rpm, until reaching an OD_{600nm} of 1.8-2.0. 1% of volume was transferred to a 50 mL of 2xYT medium and cultures inoculated at 30 ºC and at 180 rpm until the OD_{600nm} reached a value between 0.7-0.8, and 1.5-1.8. Protein production was induced with IPTG, at different concentrations, at both OD_{600nm} values to infer which one was optimal for protein production. Protein production was monitored by withdrawing aliquots and analyzing them by SDS-PAGE.

6.2.3 Expression and purification of the cytochrome

The cytochrome was produced by heterologous expression in *E. coli* JCB7123, which was the selected strain from the expression tests, containing the plasmid pEC86 and the constructed vector containing the *gsu2515* gene. Cells were grown in 2xYT medium, supplemented with chloramphenicol and ampicillin, to an OD_{600nm} value of 0.7, followed by the protein expression induction with 100 μM of IPTG. The cultures were incubated overnight at 30 ºC and then harvested by centrifugation (6400 *xg* for 20 min). The disruption of the cells was obtained by resuspending the pellet with a buffer containing 100 mM Tris-HCl (pH 8), 0.5 mM EDTA and 20% sucrose, followed by two freeze–thaw cycles (-80 ºC for a minimum of 3 h). After this procedure, 0.5 mg/mL of lysozyme were added, together with a small amount of DNase, 0.17 mg/mL of phenylmethylsulphonyl fluoride and 0.32 mg/mL of benzamidine. Phenylmethylsulphonyl fluoride and benzamidine are proteases inhibitors and were added to prevent protein degradation. The periplasmatic fraction was obtained by a centrifugation step at 14,700 *xg* for 20 min followed by an ultracentrifugation step at 225,000 *xg* for 1 h.

6.2.4 Protein purification

The solution buffers and techniques used for protein purification were selected taking into consideration the pI (7.02) and molecular weight (12 kDa) of the cytochrome.

Firstly, the protein was dialyzed against 20 mM sodium acetate pH 5. Protein purification started by a cation-exchange chromatography step using a 2×5 mL BioScale™ Mini UNOsphere S cartridges (Bio-Rad), equilibrated with 20 mM sodium acetate pH 5.0. The fractions containing the protein of interest were selected through analysis of SDS-PAGE, stained with BlueSafe (NZYTech), and dialyzed against 10 mM Tris-HCl pH 8.5. The solution was then loaded into an anion-exchange column (2×5 mL HiTrap Q HP, GE Healthcare Life Sciences), equilibrated with 10 mM Tris-HCl pH 8.5. In the cation-exchange chromatography the protein was eluted with a 0-

200 mM NaCl gradient, and in the second chromatography with 0-300 mM NaCl, both at a flow rate of 1 mL/min.

Fractions containing the protein of interest were concentrated and buffer exchanged to 100 mM sodium phosphate buffer (pH 8) using Amicon™ Ultra centrifugal filter device. The samples were then loaded onto a XK 16/70 Superdex™ 75 prep grade column (GE Healthcare Life Sciences) pre-equilibrated with the same buffer. The cytochrome was eluted with a flow-rate of 0.5 mL/min. Protein purity was evaluated by SDS-PAGE stained with BlueSafe (NZYTech).

6.2.5 UV-visible analysis, quantification and molar extinction coefficient

Experiments were performed in a UV-visible scanning spectrophotometer Evolution 201 (Thermo Scientific), at room temperature, in a 1 cm path length quartz cuvettes. Firstly, an oxidized spectrum was acquired, and then a reduced one, by adding sodium dithionite. UV-visible spectra were recorded in a range of 350-700 nm. The molar extinction coefficient value of cytochrome GSU2515 was determined by the Lowry method, using horse-heart cytochrome *c* as standard [5]. The protein concentration was determined by using the absorbance of the cytochrome's α band (551 nm) in the reduced state, using the molar extinction coefficient obtained.

6.2.6 Redox titrations followed by visible spectroscopy

Redox titrations were performed inside an anaerobic glove box (MBraun, Garching, Germany) at 25 ºC, with oxygen levels kept under 1 ppm with argon circulation. Samples with final concentration 60 µM were prepared in 45 mM sodium phosphate (100 mM final ionic strength) at pH 7.

A solution of mediators was added to the cytochrome, with a final concentration of 1.5 µM [6] and covering a potential range from +280 to -440 mV, in relation to NHE, to assist the electron transfer between the electrode and the protein redox center. The following mediators were used: potassium ferricyanide (+430 mV), p-benzoquinone (+280 mV), tetramethyl-1,4-phenylenediamine (+260 mV), 1,2-naphtoquinone-4-sulphonic acid (+215 mV), 1,2-napthoquinone (+143 mV), trimethylhydroquinone (+115 mV), phenazine methosulfate (+80 mV), phenazine ethosulfate (+55 mV), gallocyanine (+21 mV), methylene blue (+11 mV), indigo tetrasulfonate (-30 mV), indigo trisulfonate (-70 mV), indigo disulfonate (-120 mV), 2-hydroxy-1,4-naphtoquinone (-145 mV), antraquinone-2,6-disulfonate (-185 mV), antraquinone-2-sulfonate (-225 mV), safranine 0 (-280 mV), neutral red (-325 mV), benzyl viologen (-345 mV), diquat (-350 mV) and methyl viologen (-440 mV).

The redox titrations were performed in the reduced direction, by adding successive amounts of sodium dithionite, and in the oxidative direction, by adding potassium ferricyanide. The electrode used was a Pt/Ag/AgCl, calibrated with quinhydrone saturated solutions at pH 4 and 7.

The potential was measured after each addition of reductant or oxidant agent, and when stable a correspondent visible spectrum was recorded, using an Evolution 300 (Thermo Scientific) spectrophotometer.

Two replicates were performed. By integrating the area of the α-peak (551 nm) above the line connecting the flanking isosbestic point (544 and 559 nm) in the reduced fraction, it was possible to subtract the optical contribution of the redox mediators [7]. Each measured potential value was then corrected to the NHE reference (+207 mV at 25 ºC) and the data was fitted by using the Nernst equation (equation 2.8, Chapter 2), considering one-electron transfer.

6.2.7 Circular dichroism spectroscopy

Circular dichroism (CD) experiments were performed on a Chirascan qCD spectropolarimeter (Applied Photophysics, BioLab) with a thermostatic cell support using a 0.2 mm path-length cell quartz. CD spectra were acquired for 1 mg/mL of cytochrome on 45 mM sodium phosphate buffer with NaCl (100 mM final ionic strength) at pH 6.

Circular dichroism spectra were the average of three scans obtained by collecting data at 3 sec/nm from 190 to 260 nm. After recording a CD spectrum at 25 °C, the thermal unfolding was monitored by a linear temperature increase from 5 to 95 °C, at 0.4 sec/nm and 1 °C/min. The ellipticity variation was recorded at 222 nm. The CD spectra were recorded after cooling back the sample to 25 °C. All spectra and signals were corrected for the buffer contribution. The melting temperature of the protein was obtained through a sigmoid fitting of the data.

6.2.8 NMR studies

For the assignment of the heme substituents of cytochrome GSU2515, all samples were prepared in 45 mM sodium phosphate (100 mM final ionic strength), in D_2O (99.9%) at pH 6, with a final concentration of 1 mM. Cytochrome GSU2515 samples were pulled down, concentrated and the buffer exchanged to 20 mM NaCl using Amicon™ Ultra centrifugal filter device. Samples were then frozen at -80 ºC and underwent two cycles of lyophilization, being then solubilized with the above mentioned buffer. Reduced samples were prepared by firstly degassing them with a continuous flow of argon and secondly by the addition of an equimolar solution of sodium dithionite.

All NMR spectra were acquired in a Bruker Avance III 600 MHz spectrometer equipped with a triple-resonance cryoprobe at 25 ºC. The ^{1}H chemical shifts were calibrated using the water signal as internal reference, and the ^{13}C calibrated by indirect referencing [8]. Processing of data was done using TOPSPIN (Bruker Biospin, Karlsruhe, Germany) and data analysis with Sparky (TD Goddard and DG Kneller, Sparky 3, University of California, San Francisco, United States of America).

The following set of experiments were acquired both in the oxidized and reduced states for cytochrome GSU2515: 1D ^{1}H; 2D ^{1}H, ^{1}H TOCSY (60 ms) and ^{1}H, ^{1}H NOESY (80 ms). For the oxidized sample a 2D ^{1}H, ^{13}C HMQC was also acquired.

For the protein-protein interaction studies, cytochrome GSU2515 and PccH samples were prepared in 8 mM sodium phosphate (25 mM final ionic strength), in D_2O (99.9%), at pH 7 in the oxidized state. PccH was produced at natural abundance, as described in the Chapter 5. The chemical shift perturbations of the heme signals were analyzed for each protein by recording successive 1D ^{1}H after each protein addition. The titrations ranged for 1:0 to 1:4, by adding increasing equimolar amounts of cytochrome GSU2515 to a 180 µM sample of PccH, and vice-versa.

The chemical shift variation of the heme methyl signals of cytochrome GSU2515 and PccH, upon addition of the other cytochrome, was used to determine the dissociation constant (K_d). K_d was determined by using a nonlinear least-square fit of the chemical shift data ($\Delta\delta$), considering one-site binding model and by correcting for the dilution effect. The value was determined by using Equations 6.1 to 6.3, in which $\Delta\delta_{bind}$ is the chemical shift change, $\Delta\delta_{max}$ is the maximum chemical shift change, and R is the molar ratio. [titrated] and [titrant] are the concentrations of both cytochromes, and the under script 0 is indicative of the stock concentrations of each cytochrome.

$$\Delta\delta_{bind} = \frac{1}{2}\Delta\delta_{max}(A - \sqrt{A^2 - 4R}) \quad (6.1)$$

$$A = 1 + R + \frac{K_d[titrated]_0 R + [titrant]_0}{[titrated]_0[titrant]_0} \quad (6.2)$$

$$R = \frac{[titrant]}{[titrated]} \rightarrow \infty \quad (6.3)$$

6.3 Results and discussion

6.3.1 Analysis of the cytochrome GSU2515 amino acid sequence

The amino acid sequence was analyzed using the basic local alignment search tool (BLAST-NCBI) to search for sequences with high homology. The highest scores were obtained for *c*-type cytochromes from *Geobacter* bacteria: *G. pickeringii* (58%) and *G. metallireducens* (56%). To our best knowledge, there is no biochemical information regarding the mentioned proteins. The alignment of these sequences was preformed using Clustal Omega tool (EMBL-EBI) and it is represented in Figure 6.2.

.

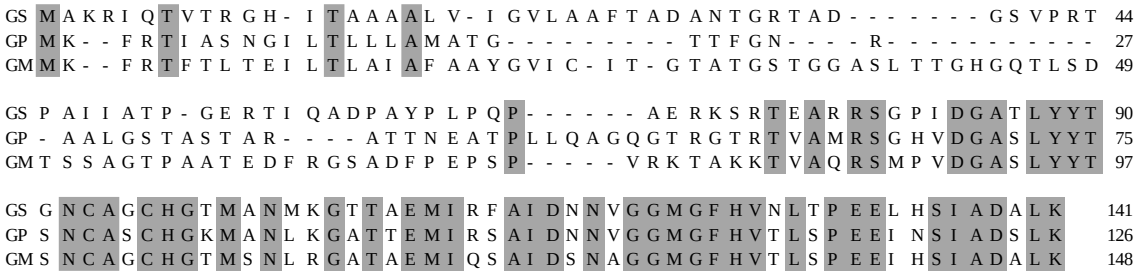

Figure 6.2 – Alignment of GSU2515 amino acid sequence, from *G. sulfurreducens* (GS) with putative *c*-type cytochrome from other species of *Geobacter*: *G. pickeringii* (GP) and *G. metaliireducens* (GM). The conserved residues are highlighted in gray. The numbers on the right represent the amino acid number of each sequence.

6.3.2 Production and purification of cytochrome GSU2515

Expression tests indicated that *E. coli* strain JCB7123 originates the highest protein yield. However, it was not possible to recover the periplasmatic fraction through the traditionally enzymatic lysis, being necessary to apply the freeze-thawing technique.

Due to the high variety of proteins obtained from the cell lysis, before the molecular exclusion chromatography step, two ionic chromatographic steps were necessary. The calculated isoelectric point for cytochrome GSU2515 is 7.02, being the first purification step a cation exchange chromatography at pH 5.0, followed by an anionic exchange chromatography at pH 8.5. On the first chromatography, fractions containing the desired protein were eluted from 20 to 80 % of NaCl (200 mM). On the second chromatography, the protein was eluted from 40 to 50 % of NaCl (300 mM). During the molecular exclusion chromatography, the protein was eluted at approximately 70 mL of the elution buffer. The elution profile obtained for the three chromatographic steps are depicted in Figure 6.3. After all the chromatography steps, one single band was obtained in SDS-PAGE, at approximately 12 kDa (Figure 6.3 D).

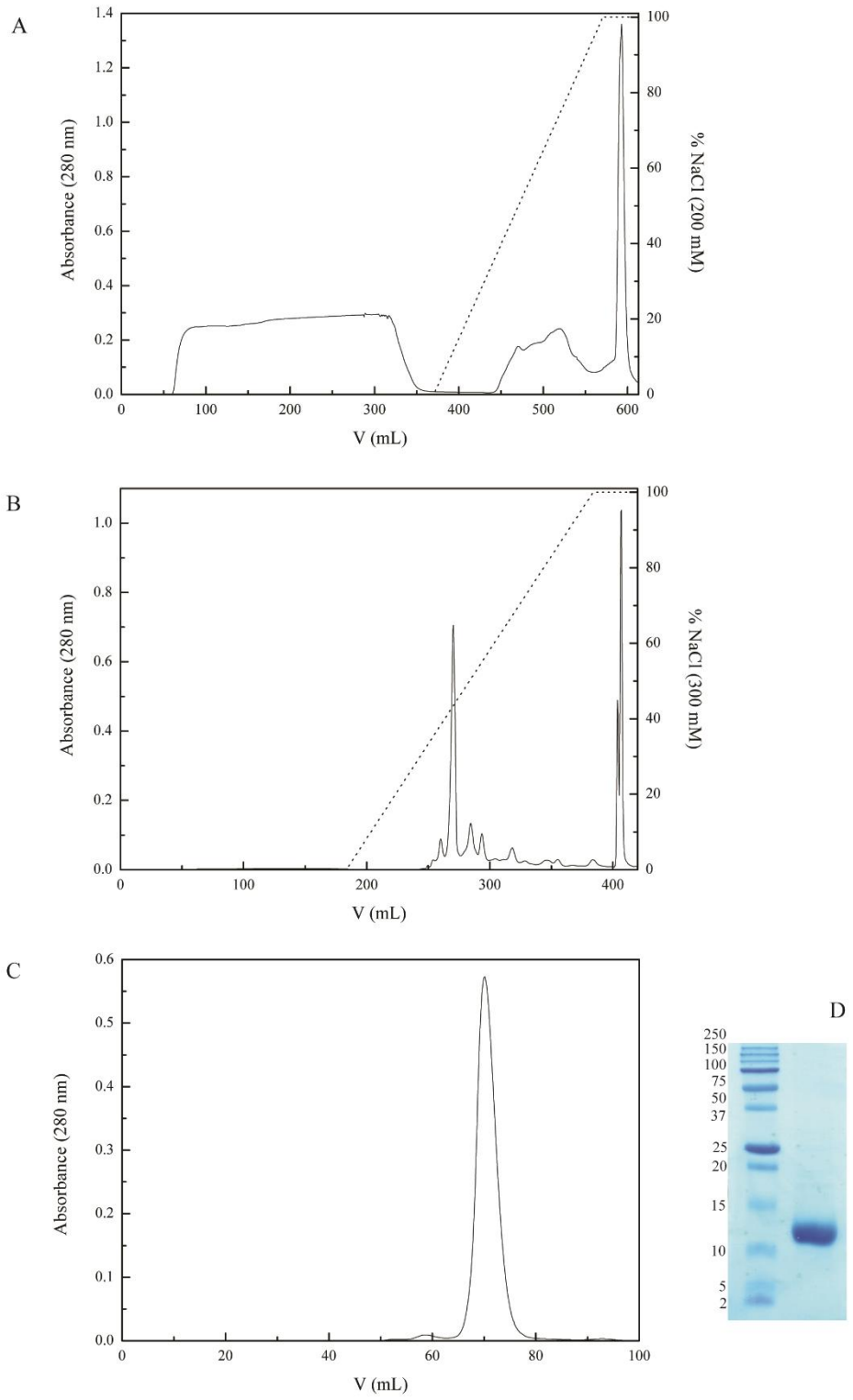

Figure 6.3 - Purification of cytochrome GSU2515. (A) Elution profile for the cation exchange chromatography with 20 mM sodium acetate pH 5, eluted at a flow-rate of 1 mL/min. **(B)** Elution profile for the anion exchange chromatography with 10 mM Tris-HCl pH 8.5, eluted at a flow-rate of 1 mL/min. In (A) and (B), the primary axis reports the variation of absorbance at 280 nm (solid line), and the secondary axis represents the NaCl gradient profile (dashed line). **(C)** Elution profile for the molecular exclusion chromatography, equilibrated with 100 mM sodium phosphate buffer, pH 8 at a flow-rate of 1 mL/min. **(D)** SDS-PAGE analysis of the pure cytochrome stained with BlueSafe (NZYTech). The first line corresponds to the molecular weight markers (Precision Plus ProteinTM, BioRad) and the numbers on the left refer to their molecular weight (kDa).

During the protein manipulation process, it was realized that it is considerably unstable. In fact, one noticed that storing the protein at 4 ºC causes its degradation. In fact, after being stored for two weeks at 4 ºC, the SDS-PAGE gel of the sample showed an additional band at approximately 6 kDa (Figure 6.4 A), This was further confirmed by molecular exclusion chromatography where two peaks were obtained (Figure 6.4 B), a different elution pattern than previously (Figure 6.3 C). Consequently, in order to prevent protein degradation, purified cytochrome GSU2515 was stored further on at -20 ºC in various aliquots.

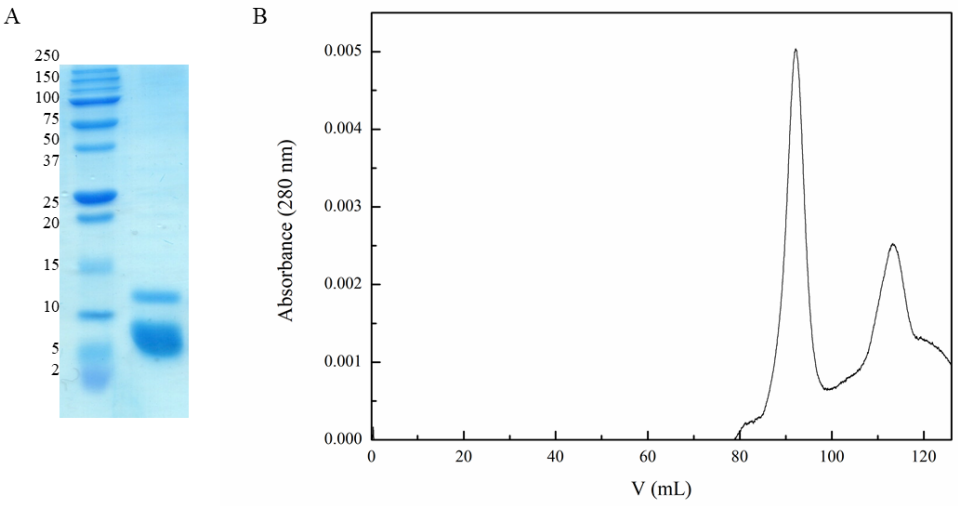

Figure 6.4 – Probing the cytochrome GSU2515 degradation. (A) SDS-PAGE analysis of the cytochrome stained with BlueSafe (NZYTech). The first line corresponds to the molecular weight markers (Precision Plus ProteinTM, BioRad) and the numbers on the left refer to their molecular weight (kDa). **(B)** Elution profile for the molecular exclusion chromatography, equilibrated with 100 mM sodium phosphate buffer pH 8, eluted at a flow-rate of 1 mL/min.

The molecular mass of cytochrome GSU2515 was confirmed by MALDI-TOF mass spectrometry. This data was obtained by the Mass Spectrometry Unit (UniMS), ITQB/iBET, Oeiras, Portugal.

6.3.3 UV-visible analysis, quantification and molar extinction coefficient

Using UV-visible spectroscopy it was possible to probe the heme spin-state of the cytochrome. In the oxidized state, the spectrum has a maximum of 407, 532 and 587 nm. In the reduced state, the Soret band is at 417 nm, the β-band at 522 nm and the α-band at 551 nm (Figure 6.5). These features are typical of a low-spin hexacoordinated heme. No band is observed at 695 nm in the oxidized form, even with a very high concentrated sample, which would have been an indicative of a methionine axial coordination. However, its absence does not exclude this possibility [9]. The calculated molar extinction coefficient of the cytochrome, using the α-band in the reduced state and the Lowry method, was 23.4 mM^{-1} cm^{-1}. Using the molar extinction coefficient it was possible to obtain the expression yield of the cytochrome: 7.3 mg/L.

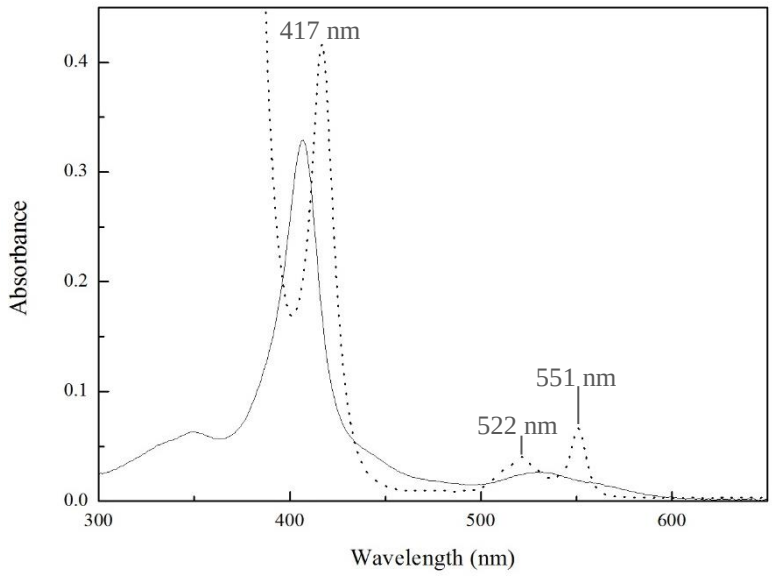

Figure 6.5 – UV-visible spectral features of cytochrome GSU2515. The solid line corresponds to the oxidized state and the dashed line to the reduced state. The absorbance values of the bands correspondent to the reduced state are represented in the figure.

6.3.4 Determination of the redox potential

Redox titrations at pH 7 were performed for cytochrome GSU2515 (Figure 6.6). Since no hysteresis is observed, the reductive and oxidative curves are superimposable, one can conclude that the redox process is fully reversible. At pH 7, the reduction potential of cytochrome GSU2515 (-112.8 ± 2.4 mV *vs* NHE) is considerably lower compared to the one of its putative physiological partner PccH (-24 mV *vs* NHE, at pH 7) [10] [11]. The lower redox potential value favors the oxidized form of the cytochrome and permits it to be redox active in the typical negative working potential ranges of *G. sulfurreducens* (approximately -150 mV *vs* NHE, at pH 7) [12].

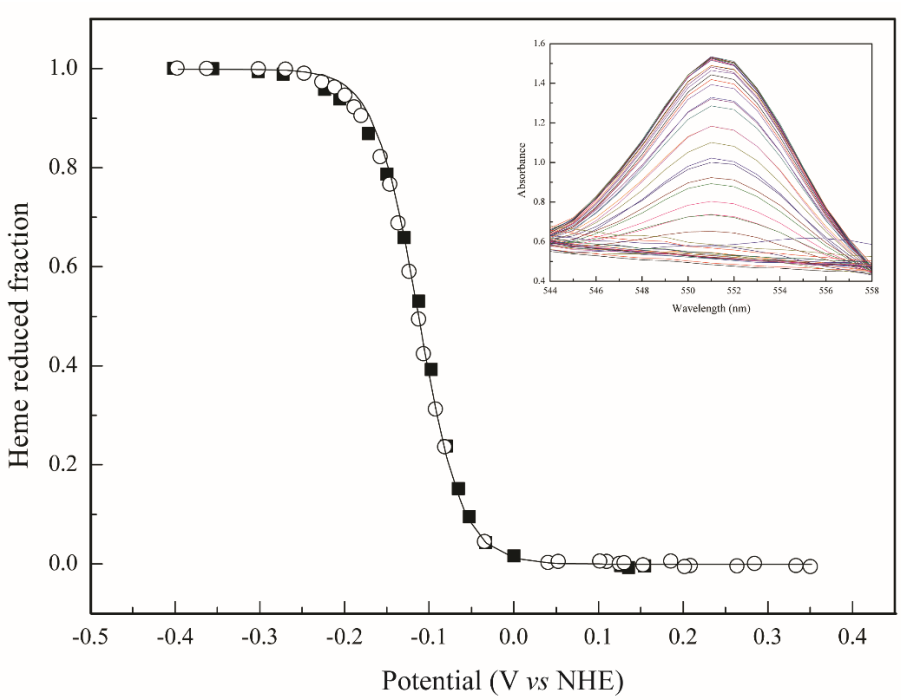

Figure 6.6 – Redox titration of cytochrome GSU2515 at pH 7, followed by visible spectroscopy. The circles and the squares represent the data points in the reductive and oxidative state, respectively. The continuous line represents the fit to the Nernst curve for one-electron reduction with -112.8 ± 2.4 mV. **Inset:** α-band region of the visible spectra acquired through the redox titration.

6.3.5 Circular dichroism studies

CD spectroscopy was used to probe the secondary structure of the cytochrome GSU2515. The spectrum of the native protein is typical of a folded protein with high α-helix content, which is characterized by intense negative bands at 208 nm and 222 nm (Figure 6.7 A). The thermal stability of the protein was accessed by a temperature-induced unfolding, followed by far-UV CD spectroscopy at 25 ºC. After the temperature ramp, the signals became slightly weaker, however the CD spectrum is essentially equivalent to the initial one (Figure 6.7 A). This leads to the conclusion that the protein structure is very stable upon temperature variation, which is also corroborated by the relatively high value of the midpoint thermal unfolding (T_m) calculated from the fitting of the data (Figure 6.7 B): 65.6 ± 2.1 ºC.

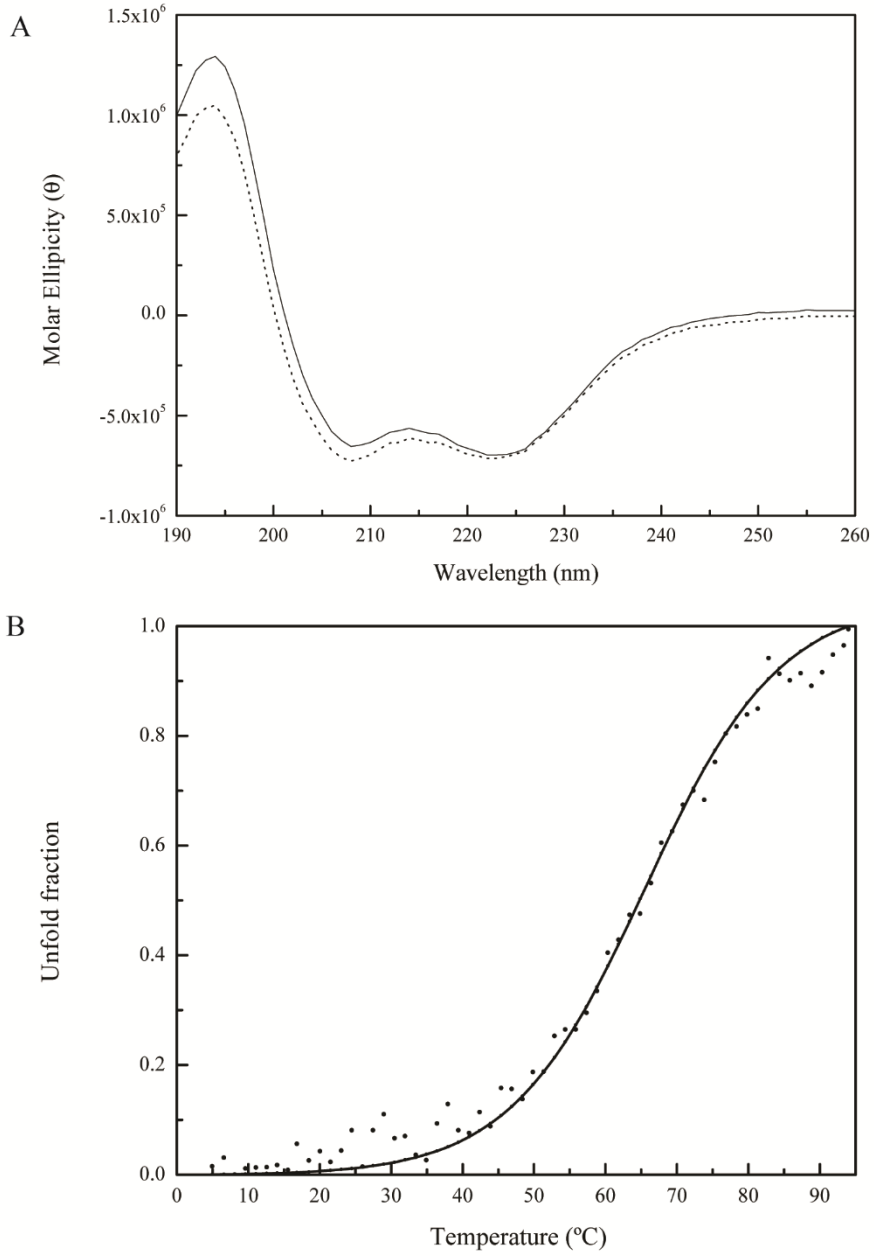

Figure 6.7 – Spectroscopic characterization of cytochrome GSU2515 by circular dichroism. (A) Far UV-CD spectra of cytochrome GSU2515 at 25 °C as purified (solid line) and after the temperature ramp, also at 25 ºC (dashed line). **(B)** Thermal unfolding of cytochrome GSU2515, whereas the solid line corresponds to the sigmoid fitting of the data (dots), from which the melting temperature was determined.

6.3.6 NMR spectroscopic characterization of cytochrome GSU2515

6.3.6.1 Assignment of the heme substituents

By using NMR spectroscopy, it was possible to confirm that the heme group of cytochrome GSU2515 is low-spin. In fact, the protein signals in the 1D ^{1}H NMR spectra in the oxidized state cover a spectral width between -20 and 35 ppm, whereas in the reduced form they cover a region of -5 to 10 ppm (Figure 6.8). These spectral ranges are typical of a low-spin heme rather than those of high-spin cytochromes whose signals are broader and cover wider regions [13]. In sum,

from the NMR spectra is possible to conclude the cytochrome is paramagnetic in the oxidized state (S=1/2) and diamagnetic (S=0) in the reduced state.

In the oxidized state, two of the heme methyl groups (18^1CH_3 and 7^1CH_3, 33.2 and 22.1 ppm, respectively) are localized more downfield than the other two (12^1CH_3 and 2^1CH_3, 10.2 and 6.8 ppm, respectively). These chemical shift pattern is somewhat similar to those of horse cytochrome *c*: 34.6 ppm for 18^1CH_3, 31.8 ppm for 7^1CH_3, 10.1 ppm for 12^1CH_3, and 7.1 ppm for 2^1CH_3 [15]. This chemical shift pattern is a consequence of the asymmetry in the distribution of the delocalized unpaired electron on the molecular orbitals of the heme porphyrin. In fact, the heme methyl pairs $18^1CH_3/7^1CH_3$ and $12^1CH_3/2^1CH_3$ are attached to diametrically opposed pyrrole rings of the porphyrin [15].

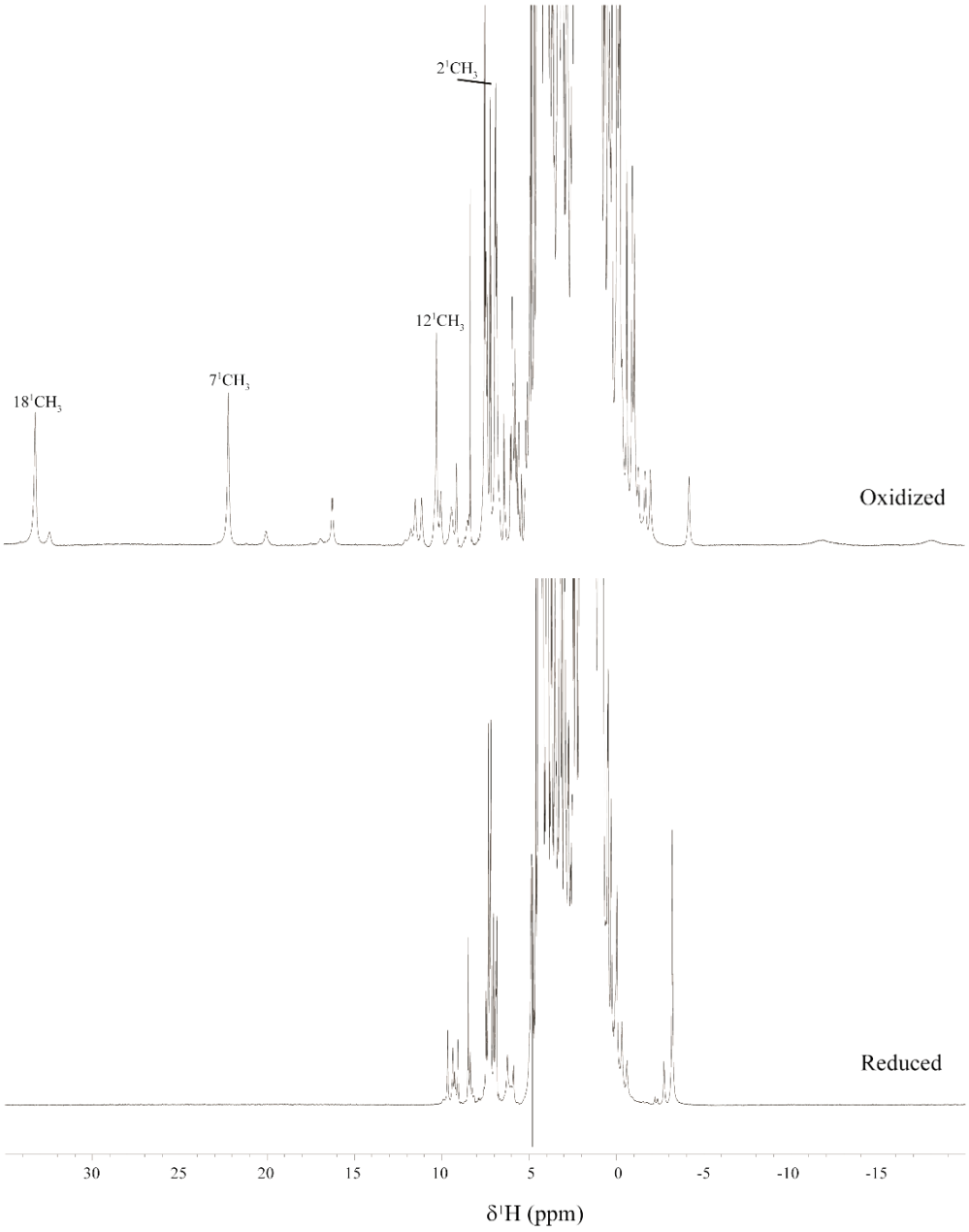

Figure 6.8 - 1D ^{1}H NMR spectra of the oxidized (upper) reduced and (lower) cytochrome GSU2515 obtained at 25 ºC and pH 6. The signals of the heme methyl groups in the oxidized spectra are labelled in the oxidized spectrum, according to the IUPAC-IUB nomenclature [14].

NMR spectroscopy was also explored to assign the heme substituents signals. The assignment strategy on the oxidized state consisted in the analysis of a 2D ^{1}H, ^{13}C HMQC, where methyl groups and propionates have typical ^{1}H, ^{13}C regions (Figure 6.9). Then, through analysis of 2D ^{1}H, ^{1}H TOCSY and 2D ^{1}H, ^{1}H NOESY, it was possible to identify the intraheme correlations between the propionates and the closest methyl group. On the other hand, the strategy used for the reduced state firstly consisted in the analysis of the 2D ^{1}H, ^{1}H TOCSY, where scalar connectivities are observed between a thioether methine and a thioether methyl group, which constitutes the initial step of the assignment. Then the other intraheme constituents were identified in the 2D ^{1}H, ^{1}H NOESY. In this spectrum typical regions are identified for the heme substituents (Chapter 2).

Overall, it was possible to assign the heme methyl and the propionate groups in the oxidized state, and all the heme substituents in the reduced state except for the propionates (Table 6.1). In the oxidized state was not possible to identify one of the propionates groups, probably due to their overlapping with other protein signals.

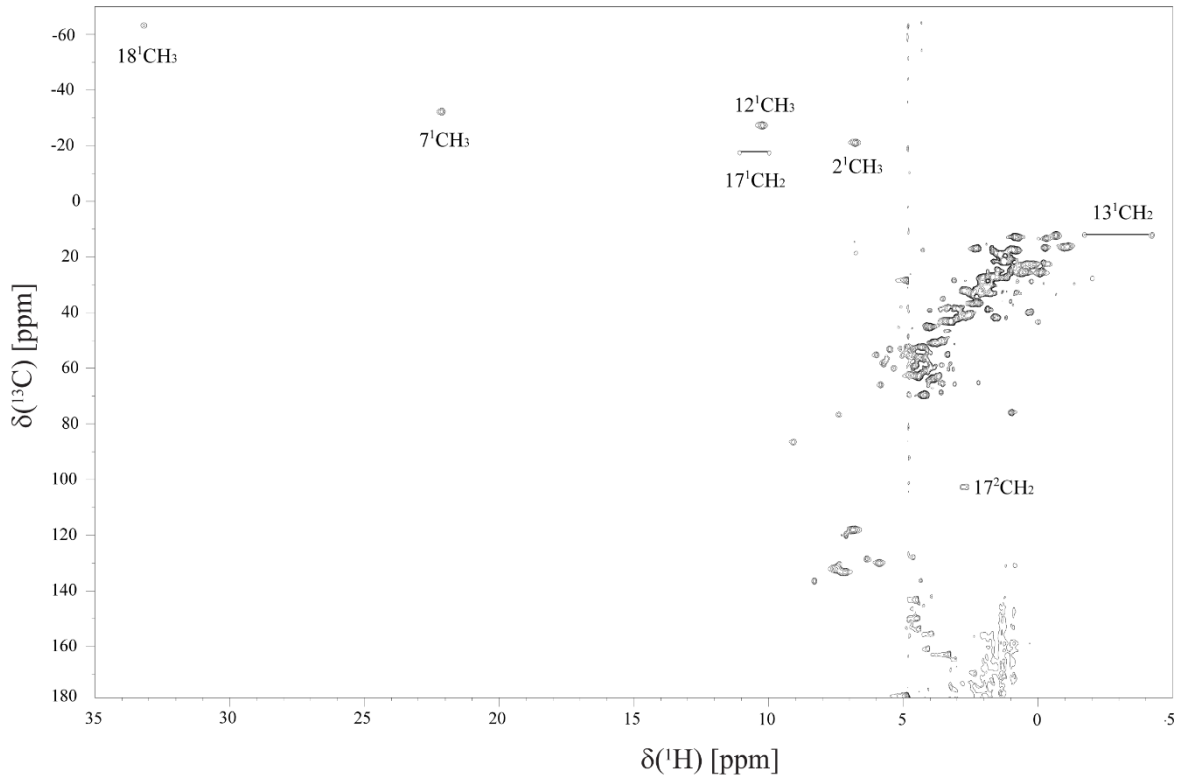

Figure 6.9 – 2D ^{1}H, ^{13}C HMQC NMR spectrum of cytochrome GSU2515 in the oxidized state (25 ºC and pH 6). Labels represent the heme substituents identified, the methyl groups and the propionates, according to the IUPAC-IUB nomenclature [14]. The peaks of the protons connected with the same carbon atoms are connected by a straight black line.

Table 6.1 – Heme substituent assignment in the reduced and oxidized states (25 ºC and pH 6). The heme substituents are identified according to the IUPAC-IUB nomenclature [14].

Heme substituent	Reduced	Oxidized	
	^{1}H (ppm)		^{13}C (ppm)
5H	9.26		
10H	9.36		
20H	9.07		
15H	9.66		
3^{1}H	5.90		
$3^{2}CH_3$	2.04		
8^{1}H	6.25	0.96	76.08
$8^{2}CH_3$	1.96	2.28	-33.15
$2^{1}CH_3$	3.53	6.78	-20.90
$7^{1}CH_3$	3.51	22.14	-32.07
$12^{1}CH_3$	3.44	10.23	-27.13
$18^{1}CH_3$	3.28	33.20	-63.01
$13^{1}CH_2$		-1.72	12.29
		-4.23	
$13^{2}CH_2$		-	-
		-	
$17^{1}CH_2$		11.07	-17.22
		9.98	
$17^{2}CH_2$		2.80	102.86
		2.65	

6.3.6.2 Protein-protein interaction studies between cytochrome GSU2515 and PccH

As previously mentioned, cytochrome GSU2515 and PccH are the most expressed *c*-type cytochromes in current-consuming cells [2]. Since it has already been proven that PccH is crucial for this process and is, until date, the only identified cytochrome to play part in the electron transfer from electrodes, it would be interesting to evaluate if cytochrome GSU2515 is its physiological partner.

The molecular interactions between cytochrome GSU2515 and PccH were investigated using NMR chemical shift perturbations. Particular focus was placed in the signals of the heme methyl substituents, whose signals in the oxidized state are more spread out along the spectra and located in less crowded regions, being ideal to probe the chemical shift variations. In fact, the methyl signals of both proteins are in distinct spectral regions, with the exception for $2^{1}CH_3$ of cytochrome GSU2515 which is located at a crowded area of the spectrum. Consequently, the molecular interactions between the two cytochromes was monitored by probing the chemical shift

perturbation of their methyl signals with the addition of increasing amounts of cytochrome GSU2515 to a PccH sample, and vice-versa (Figure 6.10).

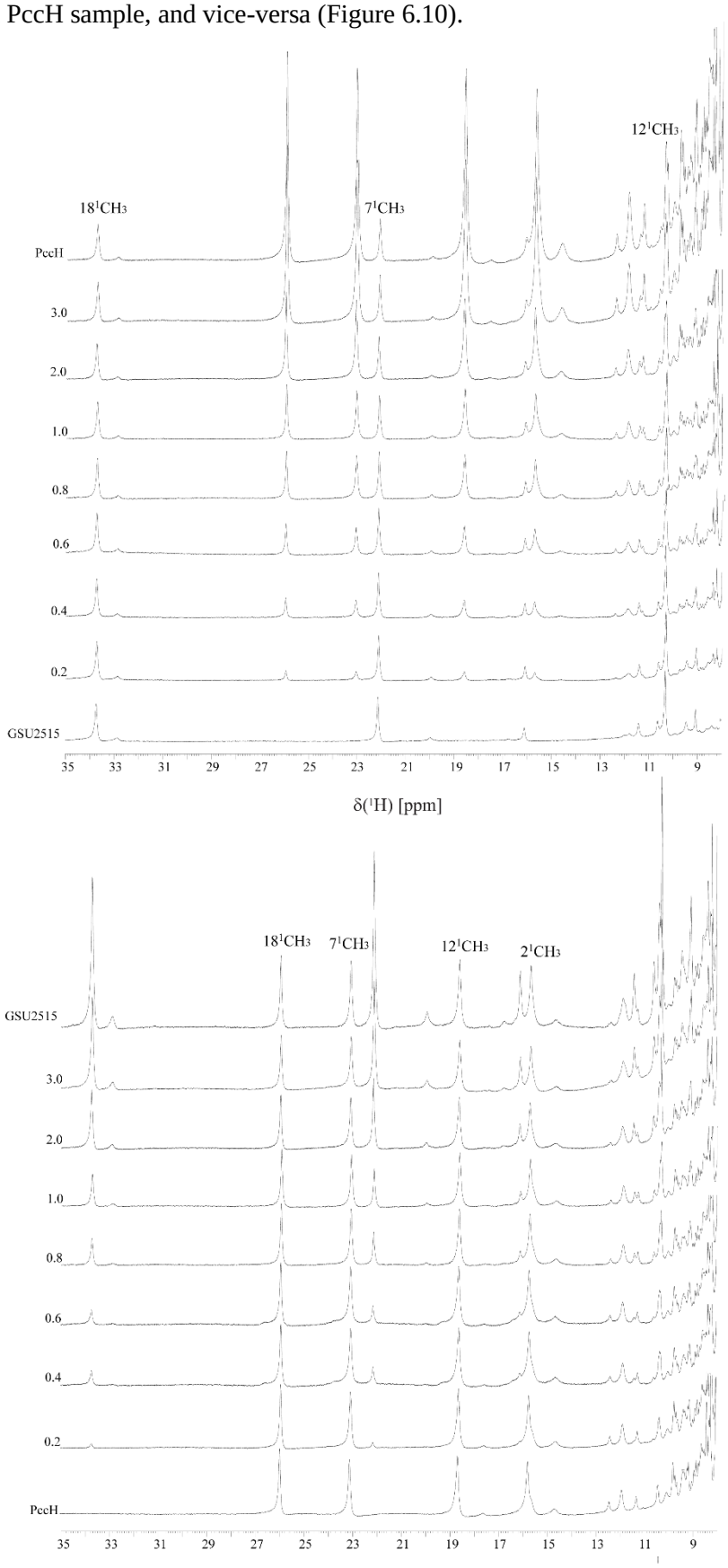

Figure 6.10 – Expansion of the low-field region of the 1D ^{1}H NMR spectra, in the oxidized state (25 ºC and pH 7), of cytochrome GSU2515 in the presence of increasing amounts of PccH (top figure)

and vice-versa (bottom figure). The molar ratio between the two proteins is indicated on the left side of the spectra. The heme methyl signals of each protein are indicated, according to the IUPAC-IUB nomenclature [14], with the exception of 2^1CH_3 of cytochrome GSU2515 which is located at a crowded area of the spectrum (6.78 ppm).

The most affected methyl groups are 2^1CH_3 for PccH and 18^1CH_3 for cytochrome GSU2515. The results suggest that there is interaction between the two cytochromes (Figure 6.11) and it was possible to determine the K_d value from the fitting of the titration curve of the most affected methyl, the 2^1CH_3 of PccH cytochrome (Figure 6.11 C). The determined K_d value is in the micromolar range (325 μM), which suggests the formation of a low affinity complex, as expected for redox partners and compatible with the transient interactions in electron transfer complexes [16] [17]. The binding curves of the other methyl groups of PccH and of cytochrome GSU2515 are depicted in the Appendix section (Figure A.2).

To also evaluate the effect of the presence of PccH on the 2^1CH_3 methyl of cytochrome GSU2515 at 6.78 ppm, 2D ^1H, ^{13}C HMQC NMR spectra should be recorded in the absence and in the presence of PccH. In this spectrum the carbon/proton connectivities are found in a very typical region, and therefore can be easily identified. This study can be further extended to the chemical shift perturbation measurements of the PccH backbone NH signals, which assignment is already available. Such study could conceivably identify the protein region interacting with cytochrome GSU2515.

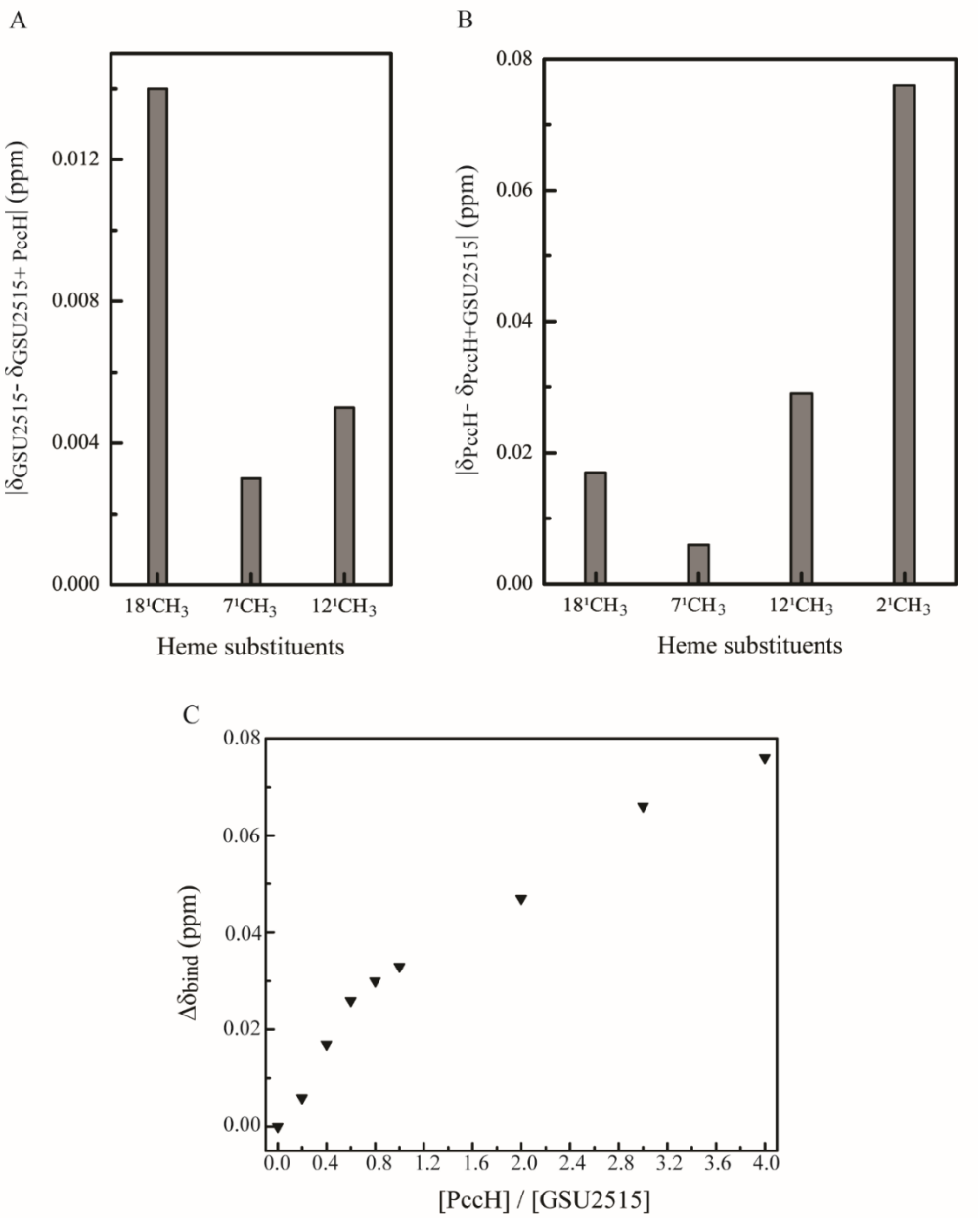

Figure 6.11 - ^{1}H chemical shift changes of the heme methyl groups of cytochrome GSU2515 (A) and PccH (B) upon addition of the other cytochrome. Comparison of the heme ^{1}H chemical shifts observed in the 1D ^{1}H NMR spectra of cytochrome GSU2515 ($\delta_{GSU2515}$) and those of PccH (δ_{PccH}) in the ratio 1:4. The heme substituents are numbered according to the IUPAC-IUB nomenclature [14]. **(C)** Binding curve of the methyl $2^{1}CH_3$ of PccH, in the presence of the cytochrome GSU2515 at different concentrations. Comparison of the ^{1}H chemical shifts of the heme methyl observed in the 1D ^{1}H NMR spectra of PccH (δ_{PccH}) upon addition of cytochrome GSU2515 ($\delta_{GSU2515}$). A K_d value was calculated from the binding curve.

6.3.7 Functional insights of cytochrome GSU2515

According to the interaction results between PccH and cytochrome GSU2515, there is evidence that they might be physiological partners, being both involved in the acceptance of electrons from electrode pathway. Being cytochrome GSU2515 predicted to be localized at the periplasm, it would be likely involved in the downstream electron transport events in the periplasm, together with PccH.

Since *pccH* and *gsu2515* genes showed the highest transcript abundance when *G. sulfurreducens* cells use graphite cathode as the sole electron donor to reduce fumarate to succinate [2] and considering their redox potential values, one can schematize a possible electron transfer pathway involving these two cytochromes (Figure 6.12). The available data suggest that cytochrome GSU2515 (-122.8 mV *vs* NHE) could function as electron donor to PccH (-24 mV *vs* NHE) [10] [11]. However, other electron transfer components involved in the electron transfer from electrode to fumarate (+30 mV *vs* NHE), that are probably located at the outer- and inner-membrane, need to be identified. One possible electron transfer component in this pathway is the triheme cytochrome PpcD, a high expressed cytochrome in *G. sulfurreducens* cells growing on an electrode [2]. Previous studies have shown that this cytochrome does not interact with PccH [18], however it is still a candidate to interact with cytochrome GSU2515.

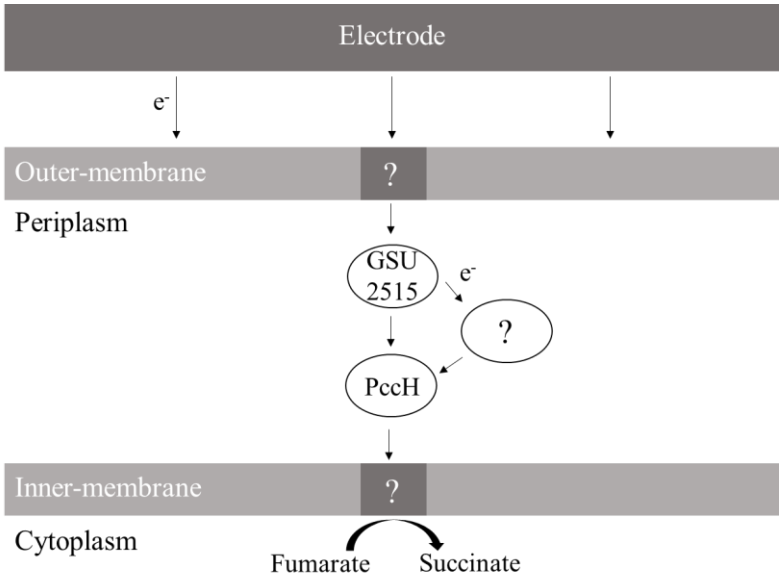

Figure 6.12 – Schematic representation of a possible electron transfer pathway that involve cytochrome GSU2515 and PccH in *G. sulfurreducens* grown using graphite cathode as a sole electron donor and fumarate as terminal electron acceptor. The arrows indicate possible electron flow from/to still unknown redox partners of cytochrome GSU2515 and PccH.

6.4 Conclusions

This Chapter describes the first biochemical study for the mono-hemic *c*-type cytochrome GSU2515 from *G. sulfurreducens*. The secondary structure of the protein is dominated by α-helixes and the heme group is low-spin in both reduced and oxidized states. The redox potential was determined at pH 7 (-112.8 mV *vs* NHE), which is well framed in the working potential ranges of *G. sulfurreducens* (approximately -150 mV *vs* NHE). It was also possible to obtain preliminary indications that cytochrome GSU2515 takes part on the electron transfer process from electrodes to cells, together with PccH.

Although there is strong evidence that cytochrome GSU2515 takes part in the electron transfer from electrons to cells, it is still not clear its role in the process, and further studies are necessary to determine the precise role of this cytochrome in *G. sulfurreducens*.

6.5 References

[1] Y.-H. R. Ding *et al.*, "The proteome of dissimilatory metal-reducing microorganism *Geobacter sulfurreducens* under various growth conditions," *Biochim. Biophys. Acta - Proteins Proteomics*, vol. 1764, no. 7, pp. 1198–1206, 2006.

[2] S. M. Strycharz *et al.*, "Gene expression and deletion analysis of mechanisms for electron transfer from electrodes to *Geobacter sulfurreducens*," *Bioelectrochemistry*, vol. 80, no. 2, pp. 142–150, 2011.

[3] P. R. Pokkuluri *et al.*, "Structure of a novel c_7-type three-heme cytochrome domain from a multidomain cytochrome *c* polymer.," *Protein Sci.*, vol. 13, no. 6, pp. 1684–92, 2004.

[4] P. R. Pokkuluri *et al.*, "Structural characterization of a family of cytochromes c_7 involved in Fe(III) respiration by *Geobacter sulfurreducens*," *Biochim. Biophys. Acta - Bioenerg.*, vol. 1797, no. 2, pp. 222–232, 2010.

[5] O. H. Lowry, N. J. Rosebrough, A. L. Farr, and R. J. Randal, "Protein measurement with the Folin phenol reagent," *J. Biol. Chem.*, vol. 193, no. 1, pp. 265–75, 1951.

[6] P. L. Dutton, "Redox potentiometry: determination of midpoint potentials of oxidation-reduction components of biological electron-transfer systems," *Methods Enzymol.*, vol. 54, pp. 411–35, 1978.

[7] L. Morgado *et al.*, "Structural insights into the modulation of the redox properties of two *Geobacter sulfurreducens* homologous triheme cytochromes," *Biochim. Biophys. Acta - Bioenerg.*, vol. 1777, no. 9, pp. 1157–1165, 2008.

[8] D. S. Wishart *et al.*, "^{1}H, ^{13}C and ^{15}N chemical shift referencing in biomolecular NMR," *J. Biomol. NMR*, vol. 6, no. 2, pp. 135–140, 1995.

[9] G. R. Moore and G. W. Pettigrew, *Cytochromes c: Evolutionary, structural and physicochemical aspects*. Springer Berlin Heidelberg, 1990.

[10] J. M. Dantas, D. M. Tomaz, L. Morgado, and C. A. Salgueiro, "Functional characterization of PccH, a key cytochrome for electron transfer from electrodes to the bacterium *Geobacter sulfurreducens*," *FEBS Lett.*, vol. 587, no. 16, pp. 2662–2668, 2013.

[11] T. C. Santos, A. R. de Oliveira, J. M. Dantas, C. A. Salgueiro, and C. M. Cordas, "Thermodynamic and kinetic characterization of PccH, a key protein in microbial electrosynthesis processes in *Geobacter sulfurreducens*," *Biochim. Biophys. Acta - Bioenerg.*, vol. 1847, no. 10, pp. 1113–1118, 2015.

[12] Y. Liu, H. Kim, R. R. Franklin, and D. R. Bond, "Linking spectral and electrochemical

analysis to monitor *c*-type cytochrome redox status in living *Geobacter sulfurreducens* biofilms," *ChemPhysChem*, vol. 12, no. 12, pp. 2235–2241, 2011.

[13] I. Bertini and C. Luchinat, *NMR of paramagnetic molecules in biological systems*. Benjamin/Cummings Pub. Co, 1986.

[14] G. P. Moss, "Nomenclature of tetrapyrroles (Recommendations 1986)," *Eur. J. Biochem.*, vol. 178, no. 2, pp. 277–328, 1988.

[15] D. L. Turner, "Evaluation of ^{13}C and ^{1}H Fermi contact shifts in horse cytochrome *c*. The origin of the anti-Curie effect," *Eur. J. Biochem.*, vol. 211, no. 3, pp. 563–568, 1993.

[16] J. R. Perkins, I. Diboun, B. H. Dessailly, J. G. Lees, and C. Orengo, "Transient protein-protein interactions: structural, functional, and network properties," *Structure*, vol. 18, no. 10, pp. 1233–1243, 2010.

[17] Q. Bashir, S. Scanu, and M. Ubbink, "Dynamics in electron transfer protein complexes," *FEBS J.*, vol. 278, no. 9, pp. 1391–1400, 2011.

[18] J. M. Dantas, L. M. Campelo, N. E. C. Duke, C. A. Salgueiro, and P. R. Pokkuluri, "The structure of PccH from *Geobacter sulfurreducens* - a novel low reduction potential monoheme cytochrome essential for accepting electrons from an electrode," *FEBS J.*, vol. 282, no. 11, pp. 2215–2231, 2015.

7. Future Research Perspectives

This Chapter summarizes some of the work that was initiated under the scope of the Thesis. The work is still in a preliminary stage but also paves the way for future research on the topic.

7.1 Interaction studies with OmcF and its putative redox partners

To better understand the functional relevance of OmcF it is important to identify its physiological partners. However, the most likely candidates, the cytochromes OmcB and OmcC located at the outer membrane [1], were not yet successfully produced. The extracellular electron acceptor Fe(III) citrate is also as a good candidate to be a physiological partner of OmcF, since an OmcF-deficient strain showed considerably lower reduction levels of Fe(III) citrate [1]. In all cases, the experiments will follow the strategy described in Chapter 3 for the interaction studies between OmcF and PpcA. However, in the case of Fe(III) citrate, the paramagnetic nature of this compound will broad the signals of the interacting residues and thus, interactions will be mapped by the broadening of the signals instead of their chemical shift perturbation. In fact, Ferreira and co-workers [2] verified that upon the addition of Fe(III) citrate to cytochromes PpcA, PpcB and PpcE, certain NH signals show a decrease in the peak data height and increase in line broadening. These studies will elucidate if OmcF has only a regulatory role in the expression of OmcB and OmcC, or if it can interact directly with Fe(III) citrate.

7.2 Assignment of PccH in the reduced state

The assignment of the backbone, side-chain and heme of PccH in the reduced state is the natural next step to assist the determination of the NMR structure of the cytochrome in solution. The structure of PccH in the oxidized state has already been determined [3], however by obtaining it in the reduced state by NMR will allow to acquire structural insights into the functional mechanisms of the cytochrome. Furthermore, it can be used to study the dynamic properties of the polypeptide chain and to identify redox-linked conformational changes.

7.3 Production of labeled cytochrome GSU2515

In other to assign the backbone of GSU2515, one tried to produce ^{15}N and ^{13}C labelled protein. However, this was not possible since the expression yields were very low, both using the traditional method [4] and the one developed for PccH production (Chapter 5). To overcome this difficulty, one should determine the reason why the production yields are so low and hence develop a method of production taking this issue into consideration. Only with this information will be possible to assign the backbone of this cytochrome. Furthermore, it will be helpful to understand if PccH and GSU2515 are physiological partners, by also monitoring the chemical shift perturbations on the NH signals of the 2D ^{1}H, ^{15}N HSQC NMR spectra.

7.4 Identification of the sixth axial ligand of cytochrome GSU2515

Mutated forms of the cytochrome GSU2515 were designed by using the NZYMutagenesis kit (Nzytech) and pkIVLen004 as vector template (containing the gene of interest). This was done to identify the sixth heme axial ligand. In order to evaluate if this ligand is a methionine, the candidate amino acids (Met^{100}, Met^{103}, Met^{110} and Met^{122}) were substituted by an alanine, being hereafter named GSU2515M100A, GSU2515M103A, GSU2515M110A and GSU2515M122A. The primers used are indicated in Table 7.1. After the cloning protocol and the site-mutagenesis, the PCR product was digested with D*pnI*. In order to obtain the desired vector, containing the gene of interest, competent *E. coli* cells (DH5α) were transformed. DNA sizes were confirmed by using an agarose gel (1.5%), and DNA quantification and purity was accessed by using Nanodrop. All oligonucleotides were designed with QuikChange Primer Design program (Agilent Technologies) and synthesized by Invitrogen. Mutations were confirmed by DNA sequencing (STAB VIDA).

Table 7.1 - Primers used to clone the gene encoding for methionine mutants of cytochrome GSU2515. The temperatures (T) of melting for each primer were calculated using the T_m calculator thermo scientific web tool (https://www.thermofisher.com/).

Plasmid	Oligonucleotides	T of melting (ºC)
GSU2515M100A	5'-cccttcatgttcgccgcggtgccgtggcaacc-3' 5'-ggttgccacggcaccgcggcgaacatgaaggg-3'	89
GSU2515M103A	5'-gccgtggttcccttcgcgttcgccatggtgcc-3' 5'-ggcaccatggcgaacgcgaagggaaccacggc-3'	89
GSU2515M110A	5'-atggcgaagcggatcgcttccgccgtggttcc-3' 5'-ggaaccacggcggaagcgatccgcttcgccat-3'	87
GSU2515M122A	5'-gttcacgtgaaagcccgcgccgcccacgttgttg-3' 5'-caacaacgtgggcggcgcgggctttcacgtgaac-3'	88

The vectors containing the desired mutation were designed but it was not possible to produce and biochemically study these mutants in the scope of this thesis. Given the case that the axial ligand is one of the methionines selected to be mutated, a three-proton intensity peak at approximately 3 ppm would be absent of the mutant's 1D ^{1}H spectrum in the reduced state. If the second axial ligand is a histidine, it would only be possible to be identified by the backbone assignment of cytochrome GSU2515 or by the inspection of typical signals in 2D ^{1}H, ^{13}C HMSQC NMR spectra of additional mutants. Alternatively, by determining the protein structure by X-ray crystallography it would be possible to unequivocally identify the second heme axial ligand.

7.5 Determination of the redox-Bohr center of cytochrome GSU2515

To determine if the redox potential of GSU2515 is pH dependent, one should perform more UV-visible spectroscopy experiments at various pH values, including at pH 6 and 8, to identify if this cytochrome has redox-Bohr effect in the physiological pH of *G. sulfurreducens*. This information would be an important functional clue for this cytochrome, by determining if it can couple proton to electron transfer in this pH values, and if it can be involved in energy-conserving mechanisms.

7.6 Cloning of OmaB cytochrome

OmaB is an octaheme cytochrome *c* protein that is part of a trans-outer membrane protein complex that is proposed to ensure electron transfer from the periplasm to the cell exterior. This complex is constituted by three subunits: OmcB which is a dodecaheme cytochrome *c* located at the cell's exterior, OmbB that is an outer-membrane integral β-barrel protein, and finally OmaB that is located at the periplasm [5].

Genomic DNA of *G. sulfurreducens* was kindly provided by Prof. D.R. Lovely (University of Massachusetts, Amherst). Gene sequence information was obtained from KEGG web site, being the Gene ID: AAR36110. OmaB has 231 amino acids, from which the first 23 are predicted to be the signal peptide (Figure 7.1). For this reason, the *omaB* gene was cloned excluding the signal peptide and its cleavage site. OmaB is predicted to have 27 kDa molecular weight.

```
          10        20        30        40        50        60
MKKWFIALLLLTVSAFTVQMALADKMSHKEYATTPIGECNACHKGEGIAPNHDADWVRGHRV

          70        80        90       100       110       120
VASRAGKNCADCHVQQFCLDCHQGGGIEADLSTRTFMRDYVPKSHRSNFLSIHPTKALDNPQT

         130       140       150       160       170       180
CTRCHDQSYCNECHARFPKGSLRIKSHLMLGPNGQKYSFGLGEHAIEARRNLQSCQTCHPEGDV

190       200       210       220       230
CIQCHSSGKTSPHPRNWNSIKNNYKDRAGSRVCTKCHLPGTY
```

Figure 7.1 - Amino acid sequence of the periplasmic domain of cytochrome OmaB. The signal peptide is indicated in gray and the c-type heme binding motifs (CXXCH) are underlined.

The construction of the OmaB vector was performed by Gibson Assembly. With this technique, two pairs of primers were designed (Table 7.2): one for amplifying the gene *omaB* from the genomic DNA, which will incorporate homology regions between the gene and the plasmid; and another pair for the amplification of the vector. The homology regions correspond to the plasmid sequence where one wants to introduce the *omaB* gene. All oligonucleotides were designed with QuikChange Primer Design program (Agilent Technologies) and synthesized by Invitrogen. Mutations were confirmed by DNA sequencing (STAB VIDA). The vector used was pET22b(+), a commercial plasmid adequate for protein expression in the periplasm.

Table 7.2 - Primers used to clone the gene omaB into the pet22b(+) vector. The temperatures (T) of melting for each primer were calculated from thermo scientific web tool (https://www.thermofisher.com/). The homology regions between the two sets of primers are highlighted in bold.

	Oligonucleotides	**T of melting (ºC)**
omaB	5'- cagccggcgatggcc**gtccagatggcactg**-3' 5'- cgggctttgttagcagccgg**ttagtacgtaccaggaaggtg**-3'	89
pET22b(+)	5'- ccggctgctaacaaagcccgaaagg-3' 5'- ggccatcgccggctgggc -3'	80

Two high fidelity polymerase chain reactions were performed, one for the plasmid and another for the gene amplifications. The PCR reaction mixture constitutions and conditions are the same as presented in Chapter 6 (Materials and Methods section) for cloning of *gsu2515*, by using the Phusion® high-fidelity DNA polymerase (New England BioLabs).

Both plasmid (5403 bp) and gene (680 bp) had the desired sizes, which was confirmed by an agarose gel (1.5%). After these two PCR cycles and the products purified, they were mixed with the Gibson Master Mix Assembly (10 µL) for 1 h at 50 ºC. The amount of gene and plasmid used were calculated using the following equation:

$$pmols = (weight\ in\ ng) * 1.000/(base\ pairs * 650\ daltons) \quad (7.1)$$

The constructed vector was transformed in *E. coli* DH5α competent cells and plated in LB medium supplemented with 100 µg/mL of ampicillin. After transformation, some colonies were selected from the plates to perform a colony PCR (protocol described in Chapter 6). The correct insertion of the gene into the *omaB*-pET22b+ expression vector was confirmed by DNA sequencing (STAB VIDA).

Expression tests were performed with OmaB, by trying to heterologously produce it with various strains of *E. coli* (see expression tests section in Chapter 6), at various temperatures (25 and 30 ºC), and with different IPTG concentrations. However, OmaB was not successfully produced yet, perhaps due to its high heme content. At the moment, a better recombinant system is being developed.

7.7 Production of OmcE cytochrome

OmcE is a tetraheme *c*-type cytochrome predicted to be located at the outer-membrane, it has 232 amino acids, its signal peptide is constituted by the first 23 amino acids, and it is expected to have 30 kDa molecular weight. OmcE, together with OmcS, is hypothesized to be involved in the electron transfer to Fe(III) oxides since, when the *omcE* gene is deleted, *G. sulfurreducens* could no longer reduce Fe(III) oxide, but could still reduce soluble electron acceptors as Fe(III) citrate [6].

omcE gene has already been cloned, using restriction enzymes, and its production was attempted during the course of the thesis. BL21 (DE3) cells successfully grew OmcE, however it is still unfeasible to solubilize the cytochrome. Various techniques were used to isolate the protein, including enzymatic lysis with lysozyme, mechanical lysis with the use of french-press and freeze-thaw cycles, and all were unsuccessful. At the moment, the use of detergents to solubilize the cytochrome is being explored.

7.8 References

[1] B.-C. Kim, C. Leang, Y.-H. R. Ding, R. H. Glaven, M. V Coppi, and D. R. Lovley, "OmcF, a putative *c*-type monoheme outer membrane cytochrome required for the expression of other outer membrane cytochromes in *Geobacter sulfurreducens.*," *J. Bacteriol.*, vol. 187, no. 13, pp. 4505–4513, 2005.

[2] M. R. Ferreira, J. M. Dantas, and C. A. Salgueiro, "Molecular interactions between *Geobacter sulfurreducens* triheme cytochromes and the electron acceptor Fe(III) citrate studied by NMR," *Dalt. Trans.*, vol. 46, 2017.

[3] J. M. Dantas, L. M. Campelo, N. E. C. Duke, C. A. Salgueiro, and P. R. Pokkuluri, "The structure of PccH from *Geobacter sulfurreducens* - a novel low reduction potential monoheme cytochrome essential for accepting electrons from an electrode," *FEBS J.*, vol. 282, no. 11, pp. 2215–2231, 2015.

[4] A. P. Fernandes, I. Couto, L. Morgado, Y. Y. Londer, and C. A. Salgueiro, "Isotopic labeling of *c*-type multiheme cytochromes overexpressed in *E. coli*," *Protein Expr. Purif.*, vol. 59, no. 1, pp. 182–188, 2008.

[5] Y. Liu *et al.*, "A trans-outer membrane porin-cytochrome protein complex for extracellular electron transfer by *Geobacter sulfurreducens* PCA.," *Environ. Microbiol. Rep.*, vol. 6, no. 6, pp. 776–85, 2014.

[6] T. Mehta, M. V Coppi, S. E. Childers, and D. R. Lovley, "Outer membrane *c*-type cytochromes required for Fe(III) and Mn(IV) oxide reduction in *Geobacter sulfurreducens*," *Appl. Environ. Microbiol.*, vol. 71, no. 12, pp. 8634–41, 2005.

8. Conclusions

The aim of the work developed during this thesis was to contribute to the understanding of the electrons transfer pathways in *G. sulfurreducens.* Particular focus was made to biochemical and thermodynamic characterization of some monoheme cytochromes involved in electron transfer mechanisms, both from and towards extracellular acceptors.

The monoheme *c*-type cytochrome OmcF is essential for the extracellular electron transfer pathways involved in the reduction of iron and uranium oxy-hydroxides, as well as on electricity production in microbial fuel cells. In this thesis, the backbone and side-chain and heme signals of OmcF were assignment in oxidized state. Although this information has already been obtained for the reduced state, these results pave the way to determine possible physiological partners and ligands of OmcF. Perturbation experiments were explored to evaluate possible molecular interaction regions between OmcF and PpcA, a three-heme periplasmatic *c*-type cytochrome which is the most abundant periplasmic protein of *G. sulfurreducens*. The results obtained suggested that OmcF interacts with the triheme cytochrome in the vicinity of heme IV. The redox potential of PpcA is much lower compared to that of OmcF, indicating a favorable thermodynamic reduction of OmcF.

A detailed electrochemical characterization of OmcF was performed for the first time, using cyclic voltammetry, allowing to attain kinetics and thermodynamic data of the cytochrome. The heterogeneous electron transfer rate constant was determined at pH 7, indicating that the protein displays high electron transfer efficiency compared to other monoheme cytochromes. The pH dependence of the redox potential indicates that OmcF has an important redox-Bohr effect in the physiological pH range for *G. sulfurreducens* growth. The enthalpy, entropy and Gibbs free energy associated with the redox transaction were calculated, pointing the reduced form of the cytochrome as the most favorable. The data obtained indicates that *G. sulfurreducens* cells evolved to warrant a down-hill electron transfer from the periplasm to the outer-membrane associated cytochrome OmcF.

The redox-Bohr center of OmcF was suggested to be the protonatable site at the imidazole ring of His^{47} since it is localized in the vicinity of the heme propionate P_{13}. This hypothesis was tested by replacing the His^{47} with the non-protonatable residues isoleucine and phenylalanine. Both mutants were ^{15}N-labeled, and their overall fold confirmed to be the same as the wild-type by the analysis of 2D ^{1}H, ^{15}N HSQC NMR spectra. The pH dependence of the redox potential of the mutants was measured by cyclic voltammetry. Compared to the wild-type protein, the redox-Bohr effect of the mutants was smaller, but not fully abolished, confirming the role of His^{47} in the pH modulation of OmcF's redox potential. A study of pH effect on the NMR chemical shifts of the heme substituents suggested that the heme propionate P_{13} is the main redox-Bohr center in OmcF, and that the side chain of His^{47} supplies an additional acid-base center that extends the range of the overall redox-Bohr effect in OmcF.

The cytochrome PccH is the most expressed cytochrome when electrons are supplied to *G. sulfurreducens* biofilms. Studies have shown that the electron transfer toward *G. sulfurreducens* cells was completely inhibited by the deletion of the gene encoding for cytochrome PccH. Hence, this protein has a crucial role in microbial electrosynthesis mechanisms, which are currently unknown. In this work, the backbone, side-chain and heme signals of PccH were assignment in oxidized state. The data obtained paves the way to identify and structurally map the molecular interaction regions between the cytochrome PccH and its physiological redox partners. Furthermore, it was possible to predict the secondary structure using the NMR data obtained, which turned out to be complementary and in agreement with the previously determined structure by X-ray crystallography in the oxidized state.

A putative physiological redox partner of PccH is the cytochrome GSU2515, a still poorly understood monoheme that is localized at the periplasm and it is the second most expressed *c*-type cytochrome in current-consuming cells. A detailed biochemical and structural characterization of cytochrome GSU2515 was performed, being its secondary structure predicted to be mainly constituted by α-helixes. Its heme signals were assigned both in the reduced and oxidized states, being the heme group low-spin in both reduction states. Furthermore, molecular interaction studies between GSU2515 and PccH were performed recurring to 1D ^{1}H NMR spectra, giving an indication that these two cytochromes are physiological partners. Taking into consideration the redox potential of GSU2515, determined through redox titrations at pH 7, this cytochrome is thermodynamically capable of bridging the electron transfer between externals biocathodes and PccH, cytochrome which has a higher redox potential.

The studies developed for these three monoheme *c*-type cytochromes, OmcF, PccH and GSU2515, constitute important developments for the current understanding of the electron transfer mechanisms of *G. sulfurreducens*. Hopefully, they will constitute important stepping-stones for the optimization of the biotechnological and bioremediation technologies in which these bacteria are involved.

A. Appendix

A.1 NMR backbone and side-chain assignment of OmcF in the oxidized state

Table A.1 – Backbone and side-chain assignment of OmcF from *G. sulfurreducens* in the oxidized state. Samples prepared in 45 mM NaPi, 100 mM final ionic strength, 25 ºC.

Residue Number	Residue Type	Atom	Chemical Shift (ppm)
21	GLY	C_α	46.28
22	GLY	C_α	45.17
		HN	8.96
		N	109.10
		NH	8.96
23	SER	C_α	58.76
		C_β	63.97
		H_α	4.43
		$H_{\beta2}$	3.86
		$H_{\beta3}$	3.92
		HN	8.61
		N	116.50
24	GLY	C_α	45.15
		HN	8.53
		N	110.95
		NH	8.53
25	ALA	C_α	52.32
		C_β	19.57
		H_α	4.26
		HN	8.05
		N	124.01
		Q_β	1.27
26	GLY	C_α	44.43
		$H_{\alpha1}$	4.14
		$H_{\alpha2}$	4.17
		HN	8.47
		N	107.60
27	GLY	C_α	47.64
		$H_{\alpha1}$	3.70
		$H_{\alpha2}$	3.27
		HN	8.80
		N	106.97
28	GLY	C_α	46.66
		$H_{\alpha1}$	3.29
		HN	8.55
		N	108.70
29	GLU	C_α	59.39
		C_β	29.08
		C_γ	36.75
		H_α	4.02
		$H_{\gamma2}$	2.22
		HN	7.75
		N	124.73
30	LEU	C_α	57.60
		C_β	42.70
		H_α	3.83
		$H_{\beta2}$	1.69
		$Q_{\delta1}$	0.88
		HN	7.96
		N	120.96
31	PHE	C_α	61.98
		C_β	40.28
		H_α	3.26
		$H_{\beta2}$	2.72
		$H_{\beta3}$	2.38
		HN	8.31
		N	119.62
32	ALA	C_α	55.17
		C_β	17.85
		H_α	4.19
		HN	8.19
		N	123.79
		Q_β	1.58
33	THR	C_α	66.25
		C_β	69.57
		C_γ	20.17
		H_α	3.72
		H_β	3.60
		HN	7.71
		N	113.53
		$Q_{\gamma2}$	0.37
34	HIS	C_α	58.19
		C_β	33.51
		H_α	4.42
		$H_{\beta2}$	1.95
		$H_{\beta3}$	2.07
		HN	7.59
		N	114.70
35	CYS	C_α	53.85
		C_β	35.97
		$H_{\beta2}$	0.25
		$H_{\beta3}$	0.30
		HN	7.77
		N	115.81
36	ALA	C_α	55.70
		C_β	20.09
		HN	7.50
		N	121.01
		Q_β	2.04
37	GLY	C_α	47.44
		$H_{\alpha1}$	4.28
		$H_{\alpha2}$	4.33
		HN	9.11
		N	107.00
38	CYS	C_α	57.22
		H_α	6.89

		HN	8.35			N	117.73
		N	115.50	58	GLU	C_α	60.34
39	HIS	HN	10.95			C_β	28.85
		N	117.41			C_γ	38.18
42	GLY	C_α	45.44			H_α	3.62
		HN	8.99			$H_{\beta2}$	2.01
		N	106.14			$H_{\beta3}$	1.94
43	GLY	C_α	45.16			$H_{\gamma2}$	2.77
		HN	8.45			$H_{\gamma3}$	2.17
		N	109.00			HN	8.62
45	THR	C_α	63.34			N	119.41
46	VAL	C_α	63.48	59	ALA	C_α	54.61
		C_β	33.05			C_β	17.78
		HN	7.83			HN	7.40
		N	121.47			N	122.61
52	LEU	C_α	54.34	60	ASN	C_α	52.43
53	ALA	C_α	52.88			C_β	39.41
		C_β	19.49			H_α	4.99
		H_α	4.22			$H_{\beta2}$	3.09
		HN	7.42			$H_{\beta3}$	2.66
		N	121.10			HN	7.23
		Q_β	1.52			$HN_{\delta1}$	6.73
54	ARG	C_α	61.10			$HN_{\delta2}$	8.28
		C_β	30.70			N	114.70
		C_δ	43.64			N_δ	115.44
		C_γ	26.99	61	GLY	C_α	45.99
		H_α	3.61			HN	7.79
		$H_{\beta2}$	1.90			N	106.41
		$H_{\beta3}$	1.98	62	ILE	C_α	60.00
		$H_{\delta2}$	3.23			C_β	36.69
		$H_{\gamma2}$	1.40			$C_{\delta1}$	14.65
		$H_{\gamma3}$	1.56			$C_{\gamma1}$	26.97
		HN	7.90			$C_{\gamma2}$	19.13
		N	124.82			H_α	4.13
55	ALA	C_α	55.32			H_β	1.73
		C_β	18.22			$H_{\gamma12}$	1.41
		H_α	4.05			$H_{\gamma13}$	1.00
		HN	9.43			HN	8.12
		N	117.79			N	123.12
		Q_β	1.41			$Q_{\delta1}$	0.71
56	ARG	C_α	57.52			$Q_{\gamma2}$	0.52
		C_β	29.23	63	ARG	C_α	57.99
		C_δ	42.63			C_β	33.35
		H_α	4.11			C_δ	43.08
		$H_{\beta2}$	1.85			C_γ	28.77
		$H_{\beta3}$	1.88			H_α	4.45
		$H_{\delta2}$	3.22			$H_{\beta2}$	1.96
		HN	7.03			$H_{\beta3}$	1.86
		N	115.71			$H_{\delta2}$	3.23
57	ARG	C_α	59.70			$H_{\gamma2}$	1.41
		C_β	28.66			$H_{\gamma3}$	1.49
		C_δ	43.23			HN	9.03
		H_α	4.05			N	125.19
		HN	8.17	64	THR	C_α	59.56

		C_β	73.01			H_α	4.33
		C_γ	21.48			HN	8.10
		H_α	4.68			N	117.01
		H_β	4.72			Q_β	1.69
		HN	8.61	71	TYR	C_α	62.79
		N	110.80			C_β	39.63
		$Q_{\gamma2}$	1.24			$H_{\beta2}$	3.32
65	VAL	C_α	67.19			$H_{\beta3}$	3.73
		C_β	32.04			HN	8.42
		$C_{\gamma1}$	21.75			N	121.72
		$C_{\gamma2}$	22.79	72	ILE	C_α	65.45
		H_α	3.12			C_β	37.30
		H_β	1.97			$C_{\delta1}$	13.21
		HN	8.45			$C_{\gamma1}$	24.88
		N	119.38			$C_{\gamma2}$	16.49
		$Q_{\gamma1}$	0.91			H_α	5.43
		$Q_{\gamma2}$	0.94			H_β	1.76
66	ARG	C_α	59.50			$H_{\gamma12}$	1.31
		C_β	29.51			$H_{\gamma13}$	1.40
		C_δ	43.26			HN	7.53
		C_γ	28.32			N	107.10
		H_α	3.79			$Q_{\delta1}$	-0.10
		$H_{\beta2}$	1.78			$Q_{\gamma2}$	-0.66
		$H_{\beta3}$	1.82	73	ARG	C_α	56.70
		$H_{\delta2}$	3.19			C_β	31.13
		$H_{\gamma2}$	1.62			C_δ	43.52
		$H_{\gamma3}$	1.76			C_γ	26.98
		HN	7.88			$H_{\delta2}$	3.37
		N	117.71			$H_{\delta3}$	3.63
67	ASP	C_α	57.44			$H_{\gamma2}$	2.19
		C_β	41.07			HN	7.68
		H_α	4.57			N	116.12
		$H_{\beta2}$	3.16	74	ASN	C_α	52.58
		$H_{\beta3}$	2.86			C_β	39.93
		HN	8.04			H_α	5.88
		N	120.79			$H_{\beta2}$	3.17
68	VAL	C_α	66.96			$H_{\beta3}$	3.22
		C_β	30.87			HN	8.23
		$C_{\gamma1}$	20.91			$HN_{\delta1}$	7.17
		$C_{\gamma2}$	21.87			$HN_{\delta2}$	8.11
		H_α	3.12			N	114.00
		H_β	1.90			N_δ	113.19
		HN	7.80	75	PRO	C_α	66.17
		N	121.18	76	GLY	C_α	45.38
		$Q_{\gamma1}$	-0.05			H_α	4.38
		$Q_{\gamma2}$	0.51			HN	9.91
69	ALA	C_α	55.17			N	105.18
		C_β	18.18	77	PRO	C_α	63.51
		H_α	3.46			C_β	31.76
		HN	7.67			C_δ	49.70
		N	119.60			C_γ	27.64
		Q_β	1.21			H_α	4.33
70	ALA	C_α	54.40			$H_{\beta2}$	1.63
		C_β	18.78			$H_{\beta3}$	2.17

		$H_{\delta 2}$	3.74			$H_{\beta 2}$	2.05
		$H_{\gamma 2}$	1.96			$H_{\beta 3}$	2.02
		$H_{\gamma 3}$	1.88			$H_{\gamma 2}$	2.44
78	GLY	C_{α}	44.29			$H_{\gamma 3}$	2.59
		$H_{\alpha 1}$	2.94			HN	7.30
		$H_{\alpha 2}$	2.71			N	116.30
		HN	8.29	87	ILE	C_{α}	57.82
		N	107.60			C_{β}	39.64
79	MET	C_{α}	63.92			$C_{\delta 1}$	12.64
		HN	7.63			$C_{\gamma 1}$	26.39
		N	120.83			$C_{\gamma 2}$	17.31
80	PRO	C_{α}	63.26			H_{α}	4.35
		C_{β}	32.26			H_{β}	1.18
		C_{δ}	50.77			$H_{\gamma 12}$	0.77
		C_{γ}	27.50			$H_{\gamma 13}$	0.29
		H_{α}	4.45			HN	7.83
		$H_{\delta 2}$	3.78			N	114.90
		$H_{\delta 3}$	3.74			$Q_{\delta 1}$	-0.62
81	ALA	C_{α}	52.16			$Q_{\gamma 2}$	0.28
		C_{β}	20.38	88	PRO	C_{α}	62.39
		H_{α}	5.68			C_{β}	30.96
		HN	8.51			C_{δ}	51.08
		N	120.32			C_{γ}	27.69
		Q_{β}	1.98			$H_{\beta 2}$	2.59
82	PHE	C_{α}	56.90			$H_{\beta 3}$	1.91
		C_{β}	39.55			$H_{\delta 2}$	3.87
		H_{α}	4.68			$H_{\delta 3}$	3.46
		$H_{\beta 2}$	2.59			$H_{\gamma 2}$	2.04
		$H_{\beta 3}$	2.10	89	PRO	C_{α}	66.90
		HN	9.19			C_{β}	32.16
		N	121.90			C_{δ}	50.55
83	GLY	C_{α}	44.77			C_{γ}	27.67
		$H_{\alpha 1}$	4.06			H_{α}	3.94
		$H_{\alpha 2}$	4.47			$H_{\beta 2}$	2.00
		HN	8.63			$H_{\beta 3}$	2.44
		N	111.61			$H_{\delta 2}$	3.87
84	GLU	C_{α}	59.27			$H_{\delta 3}$	3.68
		C_{β}	29.47			$H_{\gamma 2}$	2.28
		C_{γ}	37.41			$H_{\gamma 3}$	2.00
		H_{α}	3.95	90	ALA	C_{α}	55.40
		$H_{\beta 2}$	2.00			C_{β}	18.35
		$H_{\gamma 2}$	2.40			H_{α}	4.03
		HN	9.12			HN	9.00
		N	120.29			N	118.10
85	ALA	C_{α}	53.88			Q_{β}	1.36
		C_{β}	18.09	91	ASP	C_{α}	56.29
		H_{α}	4.18			C_{β}	40.75
		HN	8.30			H_{α}	4.25
		N	118.89			$H_{\beta 2}$	2.31
		Q_{β}	1.41			$H_{\beta 3}$	2.51
86	MET	C_{α}	57.15			HN	7.04
		C_{β}	34.28			N	118.90
		C_{γ}	31.77	92	ALA	C_{α}	55.22
		H_{α}	4.33			C_{β}	17.62

		H_{α}	3.31			H_{α}	3.78
		HN	8.05			$H_{\beta 2}$	2.39
		N	124.30			HN	8.57
		Q_{β}	1.16			N	121.52
93	LEU	C_{α}	57.94	98	TYR	C_{α}	62.13
		C_{β}	41.17			C_{β}	38.19
		$C_{\delta 1}$	25.03			H_{α}	3.91
		$C_{\delta 2}$	22.99			$H_{\beta 2}$	2.71
		C_{γ}	26.65			$H_{\beta 3}$	2.80
		H_{α}	3.75			HN	7.80
		$H_{\beta 2}$	1.48			N	120.69
		$H_{\beta 3}$	1.69	99	VAL	C_{α}	65.88
		H_{γ}	1.61			C_{β}	31.42
		HN	7.43			$C_{\gamma 1}$	20.98
		N	116.91			$C_{\gamma 2}$	23.83
		$Q_{\delta 1}$	0.82			H_{α}	3.18
		$Q_{\delta 2}$	0.73			H_{β}	1.85
94	LYS	C_{α}	59.92			$H_{\gamma 1}$	0.54
		C_{β}	32.72			HN	8.39
		C_{δ}	30.02			N	120.79
		C_{ε}	42.53			$Q_{\gamma 1}$	0.52
		C_{γ}	25.46			$Q_{\gamma 2}$	0.41
		H_{α}	3.96	100	VAL	C_{α}	65.39
		$H_{\beta 2}$	1.46			C_{β}	31.32
		$H_{\beta 3}$	1.86			$C_{\gamma 1}$	20.85
		$H_{\delta 2}$	1.56			$C_{\gamma 2}$	21.98
		$H_{\delta 3}$	1.71			H_{α}	3.48
		$H_{\varepsilon 2}$	2.90			H_{β}	1.87
		$H_{\varepsilon 3}$	2.85			$H_{\gamma 2}$	0.73
		$H_{\gamma 2}$	1.43			HN	7.71
		$H_{\gamma 3}$	1.68			N	115.90
		HN	7.13			$Q_{\gamma 1}$	0.79
		N	118.69			$Q_{\gamma 2}$	0.74
95	ILE	C_{α}	65.75			C_{α}	65.36
		C_{β}	37.48			HN	7.72
		$C_{\delta 1}$	14.04			N	115.90
		$C_{\gamma 1}$	30.33	101	ALA	C_{α}	54.07
		Cγ2	18.06			C_{β}	19.44
		H_{α}	3.23			H_{α}	4.05
		H_{β}	1.32			HN	7.65
		$H_{\gamma 12}$	0.25			N	119.38
		$H_{\gamma 13}$	1.55			Q_{β}	1.23
		HN	7.78	102	SER	C_{α}	60.68
		N	119.43			C_{β}	62.71
		$Q_{\delta 1}$	0.00			H_{α}	3.86
		$Q_{\gamma 2}$	-0.14			$H_{\beta 2}$	2.47
96	GLY	C_{α}	48.07			HN	7.18
		$H_{\alpha 1}$	3.53			N	109.40
		$H_{\alpha 2}$	3.11	104	PRO	C_{α}	65.31
		HN	8.14			C_{δ}	52.34
		N	107.68			H_{α}	5.52
97	GLU	C_{α}	59.32				
		C_{β}	29.51				
		C_{γ}	36.42				

A.2 NMR H and NH assignment of OmcFH47F in the reduced state

Table A.2 – H and NH assignment of OmcFH47F mutant in the reduced state. Samples prepared in 45 mM NaPi pH 7, 100 mM final ionic strength, 25 ºC.

Residue Number	Residue Type	Atom	Chemical Shift (ppm)
21	GLY	$H_{\alpha1}$	4.05
		$H_{\alpha2}$	3.94
		HN	8.78
22	GLY	$H_{\alpha1}$	4.06
		HN	8.51
		N	109.15
23	SER	H_{α}	4.52
		$H_{\beta2}$	3.97
		HN	8.66
		N	116.63
24	GLY	$H_{\alpha1}$	4.07
		$H_{\alpha2}$	3.96
		HN	8.61
		N	110.95
25	ALA	H_{α}	4.37
		HN	8.18
		N	124.16
		Q_{β}	1.40
26	GLY	$H_{\alpha1}$	4.39
		$H_{\alpha2}$	4.04
		HN	8.61
		N	107.78
27	GLY	$H_{\alpha1}$	3.99
		$H_{\alpha2}$	3.61
		HN	9.00
		N	107.19
28	GLY	$H_{\alpha1}$	3.37
		$H_{\alpha2}$	2.19
		HN	8.72
		N	108.93
29	GLU	H_{α}	4.13
		$H_{\beta2}$	2.08
		$H_{\beta3}$	2.19
		$H_{\gamma2}$	2.31
		HN	7.89
		N	124.87
30	LEU	$H_{\beta2}$	2.17
		$H_{\beta3}$	1.48
		H_{γ}	1.12
		HN	8.23
		N	121.40
		$Q_{\delta1}$	0.98
31	PHE	H_{α}	4.24
		$H_{\beta2}$	2.94
		$H_{\delta1}$	7.33
		$H_{\varepsilon1}$	6.71
		HN	8.73
		HZ	6.84
		N	120.51
32	ALA	H_{α}	4.12
		HN	8.30
		N	123.09
		Q_{β}	1.58
33	THR	H_{α}	3.98
		H_{β}	3.92
		HN	7.91
		N	113.94
		$Q_{\gamma2}$	0.65
34	HIS	H_{α}	5.19
		$H_{\beta2}$	3.42
		$H_{\beta3}$	3.51
		$H_{\delta2}$	7.08
		$H_{\varepsilon1}$	7.90
		HN	8.31
		N	115.85
35	CYS	H_{α}	5.66
		$H_{\beta2}$	0.92
		$H_{\beta3}$	2.07
		HN	8.54
		N	117.89
36	ALA	H_{α}	3.13
		HN	7.29
		N	119.73
		Q_{β}	1.48
37	GLY	$H_{\alpha1}$	3.78
		$H_{\alpha2}$	3.67
		HN	8.46
		N	105.62
38	CYS	H_{α}	4.58
		$H_{\beta2}$	0.65
		$H_{\beta3}$	1.75

		HN	6.28			HZ	5.26
39	HIS	H_{α}	3.51			N	120.91
		$H_{\beta 2}$	1.00			H_{α}	4.61
		$H_{\beta 3}$	1.27	48	PRO	$H_{\beta 2}$	2.32
		$H_{\delta 1}$	8.97			$H_{\delta 2}$	3.79
		$H_{\delta 2}$	0.50			$H_{\delta 3}$	3.54
		HN	6.54			$H_{\gamma 2}$	2.03
		N	113.42			$H_{\gamma 3}$	1.89
40	PRO	H_{α}	4.19			HN	8.40
		$H_{\beta 2}$	1.99	49	GLU	N	113.67
		$H_{\beta 3}$	1.78			H_{α}	4.65
		$H_{\delta 2}$	2.69	50	LYS	HN	8.06
		$H_{\gamma 3}$	1.66			N	121.99
41	GLN	H_{α}	3.83			H_{α}	3.44
		$H_{\beta 2}$	2.27	51	THR	H_{β}	4.65
		$H_{\beta 3}$	1.98			$H_{\gamma 2}$	1.35
		$H_{\varepsilon 21}$	7.52			HN	6.88
		$H_{\varepsilon 22}$	6.84			N	108.97
		$H_{\gamma 2}$	2.32			$Q_{\gamma 2}$	1.08
		$H_{\gamma 3}$	2.29			H_{α}	3.95
		HN	9.71	52	LEU	$H_{\beta 2}$	0.82
		N	122.00			$H_{\beta 3}$	0.83
42	GLY	$H_{\alpha 1}$	2.38			H_{γ}	0.03
		$H_{\alpha 2}$	1.77			HN	8.18
		HN	7.50			N	114.36
		N	104.74			$Q_{\delta 1}$	-0.47
43	GLY	$H_{\alpha 1}$	3.69			$Q_{\delta 2}$	-1.08
		$H_{\alpha 2}$	3.25			H_{α}	4.01
		HN	7.11	53	ALA	HN	6.99
		N	108.00			N	120.75
44	ASN	H_{α}	3.97			Q_{β}	1.35
		$H_{\beta 2}$	2.48			$H_{\beta 2}$	1.99
		HN	8.25	54	ARG	$H_{\beta 3}$	1.90
		N	119.81			$H_{\delta 2}$	3.25
45	THR	HN	8.31			H_{ε}	7.58
		N	115.35			$H_{\gamma 2}$	1.44
46	VAL	H_{α}	4.10			HN	7.74
		H_{β}	2.56			N	124.28
		HN	8.19			H_{α}	4.09
		N	123.09	55	ALA	HN	9.49
		$Q_{\gamma 1}$	1.44			N	117.67
		$Q_{\gamma 2}$	1.20			Q_{β}	1.42
47	PHE	H_{α}	5.27			H_{α}	4.23
		$H_{\beta 2}$	3.18	56	ARG	$H_{\beta 2}$	1.90
		$H_{\beta 3}$	3.66			$H_{\beta 3}$	1.73
		HN	7.54			$H_{\delta 2}$	3.34

		$H_{\delta 3}$	3.32			$H_{\beta 3}$	1.69
		HN	7.03			$H_{\delta 2}$	3.24
		N	115.98			$H_{\gamma 2}$	1.85
		H_{α}	4.20			HN	8.02
57	ARG	H_{α}	4.21			N	117.84
58	GLU	$H_{\beta 2}$	2.04	67	ASP	H_{α}	4.57
		$H_{\beta 3}$	1.99			$H_{\beta 2}$	2.89
		$H_{\gamma 2}$	2.25			$H_{\beta 3}$	3.31
		$H_{\gamma 3}$	2.30			HN	8.23
		HN	8.40			N	120.89
		H_{α}	4.29	68	VAL	H_{α}	3.71
59	ALA	HN	7.54			H_{β}	2.55
		N	122.90			HN	8.11
		Q_{β}	1.64			N	121.81
		H_{α}	5.11			$Q_{\gamma 1}$	1.53
60	ASN	$H_{\beta 2}$	3.27			$Q_{\gamma 2}$	1.19
		$H_{\beta 3}$	2.88	69	ALA	H_{α}	3.91
		HN	7.38			HN	7.99
		N	114.96			N	119.53
		$H_{\alpha 1}$	4.29			Q_{β}	1.42
61	GLY	$H_{\alpha 2}$	3.76	70	ALA	H_{α}	4.14
		HN	7.85			HN	8.08
		N	106.20			N	117.01
		H_{α}	4.18			Q_{β}	1.51
62	ILE	H_{β}	1.91	71	TYR	H_{α}	3.71
		$H_{\gamma 12}$	0.91			$H_{\beta 2}$	3.34
		$H_{\gamma 13}$	1.47			$H_{\beta 3}$	2.92
		HN	8.25			HN	8.23
		N	123.69			N	122.33
		$Q_{\delta 1}$	0.74	72	ILE	H_{α}	2.61
		$Q_{\gamma 2}$	0.89			H_{β}	1.53
		$H_{\beta 3}$	1.90			HN	7.08
63	ARG	H_{ε}	7.43			N	106.11
		$H_{\gamma 2}$	1.48			$Q_{\delta 1}$	0.70
		$H_{\gamma 3}$	1.60			$Q_{\gamma 2}$	0.83
		H_{α}	4.83	73	ARG	H_{α}	3.89
64	THR	H_{β}	4.10			$H_{\beta 2}$	1.84
		$Q_{\gamma 2}$	1.31			$H_{\beta 3}$	1.79
		H_{α}	3.45			$H_{\delta 2}$	3.31
65	VAL	H_{β}	2.13			$H_{\delta 3}$	3.09
		HN	8.63			HN	6.78
		N	119.64			N	114.43
		$Q_{\gamma 1}$	1.12	74	ASN	H_{α}	4.48
		$Q_{\gamma 2}$	1.14			$H_{\beta 2}$	2.41
		H_{α}	3.93			$H_{\beta 3}$	2.27
66	ARG	$H_{\beta 2}$	1.85			$H_{\delta 21}$	7.45

		$H_{\delta 22}$	6.60	83	GLY	$H_{\alpha 1}$	4.15
		HN	6.78			$H_{\alpha 2}$	3.83
		N	112.63			HN	8.38
75	PRO	H_{α}	2.81			N	111.51
		$H_{\beta 2}$	0.07	84	GLU	H_{α}	3.94
		$H_{\beta 3}$	-0.29			HN	8.97
		$H_{\delta 2}$	2.64			N	120.29
		$H_{\delta 3}$	2.50	85	ALA	H_{α}	4.19
		$H_{\gamma 2}$	0.33			HN	8.25
		$H_{\gamma 3}$	0.50			N	118.83
76	GLY	$H_{\alpha 1}$	3.99			Q_{β}	1.38
		$H_{\alpha 2}$	3.67	86	MET	H_{α}	4.44
		HN	6.66			$H_{\beta 2}$	2.14
		N	103.00			$H_{\beta 3}$	2.13
77	PRO	H_{α}	4.06			$H_{\gamma 2}$	2.54
		$H_{\beta 2}$	2.22			$H_{\gamma 3}$	2.67
		$H_{\beta 3}$	2.03			HN	7.32
		$H_{\delta 3}$	3.54			N	116.36
78	GLY	$H_{\alpha 1}$	4.30	87	ILE	H_{α}	4.58
		$H_{\alpha 2}$	3.77			H_{β}	1.43
		HN	8.61			$H_{\gamma 12}$	1.15
		N	109.19			$H_{\gamma 13}$	0.70
79	MET	H_{α}	3.84			HN	7.91
		$H_{\beta 2}$	-0.53			N	115.07
		$H_{\beta 3}$	-2.88			$Q_{\delta 1}$	0.11
		$H_{\gamma 2}$	-1.23			$Q_{\gamma 2}$	0.72
		$H_{\gamma 3}$	-3.28	88	PRO	H_{α}	5.06
		HN	7.06			$H_{\beta 2}$	2.68
		N	122.63			$H_{\beta 3}$	2.01
80	PRO	H_{α}	3.67			$H_{\delta 2}$	4.07
		$H_{\beta 2}$	1.69			$H_{\delta 3}$	3.60
		$H_{\delta 2}$	3.59			$H_{\gamma 2}$	2.14
		$H_{\gamma 2}$	1.89			$H_{\gamma 3}$	2.06
		$H_{\gamma 3}$	1.73	89	PRO	H_{α}	4.05
81	ALA	H_{α}	3.41			$H_{\beta 2}$	2.48
		HN	7.07			$H_{\delta 2}$	3.97
		N	117.83			$H_{\delta 3}$	3.72
		Q_{β}	0.85	90	ALA	H_{α}	4.17
82	PHE	H_{α}	4.37			HN	9.10
		$H_{\beta 2}$	2.43			N	118.25
		$H_{\beta 3}$	2.23			Q_{β}	1.47
		$H_{\delta 1}$	6.78	91	ASP	H_{α}	4.52
		$H_{\varepsilon 1}$	7.10			$H_{\beta 2}$	2.64
		HN	8.11			$H_{\beta 3}$	2.76
		HZ	8.26			HN	7.23
		N	121.97			N	119.17

92	ALA	H_{α}	3.88
		HN	8.30
		N	124.50
		Q_{β}	1.45
93	LEU	H_{α}	4.05
		$H_{\beta 2}$	1.80
		$H_{\beta 3}$	1.74
		H_{γ}	1.70
		HN	7.65
		N	117.11
		$Q_{\delta 1}$	0.94
		$Q_{\delta 2}$	0.88
94	LYS	H_{α}	4.23
		$H_{\beta 2}$	2.18
		$H_{\delta 2}$	1.74
		$H_{\varepsilon 2}$	3.06
		$H_{\varepsilon 3}$	3.02
		HN	7.43
		N	118.86
95	ILE	H_{α}	3.92
		H_{β}	2.27
		$H_{\gamma 12}$	1.17
		HN	8.35
		N	120.61
		$Q_{\delta 1}$	1.09
		$Q_{\gamma 2}$	1.59
96	GLY	$H_{\alpha 2}$	3.94
		$H_{\beta 3}$	4.05
		HN	8.82
		N	108.05
97	GLU	H_{α}	4.03
		$H_{\gamma 2}$	2.35
		$H_{\gamma 3}$	2.58
		HN	8.94
		N	121.82
98	TYR	H_{α}	4.01
		$H_{\beta 2}$	3.11
		$H_{\beta 3}$	3.15
		$H_{\delta 1}$	6.68
		$H_{\varepsilon 1}$	6.17
		HN	8.17
		N	121.17
99	VAL	H_{α}	3.46
		H_{β}	2.64
		HN	9.00
		N	122.08
		$Q_{\gamma 1}$	1.68
		$Q_{\gamma 2}$	1.28
100	VAL	H_{α}	3.70
		H_{β}	2.08
		HN	7.99
		$Q_{\gamma 1}$	1.01
		$Q_{\gamma 2}$	0.95
101	ALA	HN	8.07
		Q_{β}	2.18
102	SER	H_{α}	3.76
		$H_{\beta 2}$	2.29
		$H_{\beta 3}$	1.57
		HN	7.24
		N	109.51
103	PHE	H_{α}	5.39
		$H_{\beta 2}$	2.85
		$H_{\beta 3}$	2.80
		$H_{\delta 1}$	7.06
		$H_{\varepsilon 1}$	6.50
		HN	6.88
104	PRO	$H_{\delta 2}$	3.45
		$H_{\delta 3}$	3.81

A.3 NMR H and NH assignment of OmcFH47I in the reduced state

Table A.3 – H and NH assignment of OmcFH47I mutant in the reduced state. Samples prepared in 45 mM NaPi pH 7, 100 mM final ionic strength, 25 ºC.

Residue Number	Residue Type	Atom	Chemical Shift (ppm)
21	GLY	$H_{\alpha1}$	4.02
		$H_{\alpha2}$	3.93
		HN	8.77
22	GLY	$H_{\alpha1}$	4.07
		$H_{\alpha2}$	4.01
		HN	8.50
23	SER	H_{α}	4.50
		$H_{\beta2}$	3.96
		HN	8.68
		N	116.64
24	GLY	$H_{\alpha1}$	3.95
		$H_{\alpha2}$	4.07
		HN	8.62
		N	111.05
25	ALA	H_{α}	4.36
		HN	8.17
		N	124.14
		Q_{β}	1.39
26	GLY	$H_{\alpha1}$	4.35
		$H_{\alpha2}$	4.03
		HN	8.60
		N	107.82
27	GLY	$H_{\alpha1}$	3.96
		$H_{\alpha2}$	3.60
		HN	9.00
		N	107.19
28	GLY	$H_{\alpha1}$	3.37
		$H_{\alpha2}$	2.19
		HN	8.71
		N	108.91
29	GLU	H_{α}	4.12
		$H_{\beta2}$	2.07
		$H_{\beta3}$	2.19
		$H_{\gamma2}$	2.30
		HN	7.88
		N	124.86
30	LEU	$H_{\beta2}$	2.16
		$H_{\beta3}$	1.47
		H_{γ}	1.12
		HN	8.22
		N	121.23
		$Q_{\delta1}$	0.97
31	PHE	H_{α}	4.23
		$H_{\beta2}$	2.93
		$H_{\delta1}$	7.33
		$H_{\varepsilon1}$	6.84
		HN	8.72
		HZ	6.71
		N	120.53
32	ALA	H_{α}	4.12
		HN	8.29
		N	123.08
		Q_{β}	1.56
33	THR	H_{α}	3.97
		H_{β}	3.91
		HN	7.92
		N	113.92
		$Q_{\gamma2}$	0.65
34	HIS	H_{α}	5.18
		$H_{\beta2}$	3.43
		$H_{\beta3}$	3.53
		$H_{\delta2}$	7.07
		$H_{\varepsilon1}$	7.89
		HN	8.30
		N	115.97
35	CYS	H_{α}	5.67
		$H_{\beta2}$	0.91
		$H_{\beta3}$	2.06
		HN	8.54
		N	117.81
36	ALA	H_{α}	3.12
		HN	7.27
		N	119.63
		Q_{β}	1.46
37	GLY	$H_{\alpha1}$	3.78
		$H_{\alpha2}$	3.66
		HN	8.46
		N	105.53
38	CYS	H_{α}	4.56
		$H_{\beta2}$	0.59
		$H_{\beta3}$	1.71

		HN	6.24			$H_{\gamma 12}$	1.72
		N	114.62			$H_{\gamma 13}$	1.21
39	HIS	H_{α}	3.48			HN	7.34
		$H_{\beta 2}$	0.99			N	120.45
		$H_{\beta 3}$	1.24	48	PRO	Hα	4.70
		$H_{\delta 1}$	8.93			$H_{\delta 2}$	3.29
		$H_{\delta 2}$	0.48			$H_{\delta 3}$	3.24
		$H_{\varepsilon 1}$	1.15			$H_{\gamma 2}$	2.06
		HN	6.50			$H_{\gamma 3}$	1.96
		N	113.22	49	GLU	H_{α}	4.23
40	PRO	H_{α}	4.18			$H_{\gamma 2}$	2.29
		$H_{\beta 2}$	1.98			HN	8.54
		$H_{\beta 3}$	1.76			N	112.80
		$H_{\delta 2}$	2.67	50	LYS	H_{α}	4.70
41	GLN	H_{α}	3.81			$H_{\beta 2}$	2.20
		$H_{\beta 2}$	2.24			$H_{\beta 3}$	2.14
		$H_{\beta 3}$	1.97			$H_{\gamma 2}$	1.95
		$H_{\varepsilon 21}$	7.51			$H_{\gamma 3}$	1.47
		$H_{\varepsilon 22}$	6.83			HN	7.93
		$H_{\gamma 2}$	2.30			N	122.56
		$H_{\gamma 3}$	2.28			Q_{ε}	2.53
		HN	9.71	51	THR	H_{α}	3.43
		N	122.03			H_{β}	4.64
42	GLY	$H_{\alpha 1}$	2.34			HN	6.87
		$H_{\alpha 2}$	1.75			N	108.91
		HN	7.49			$Q_{\gamma 2}$	1.07
		N	104.69	52	LEU	H_{α}	3.95
43	GLY	$H_{\alpha 1}$	3.68			$H_{\beta 2}$	1.34
		$H_{\alpha 2}$	3.22			$H_{\beta 3}$	0.83
		HN	7.10			H_{γ}	0.03
		N	108.11			HN	8.19
44	ASN	H_{α}	3.93			N	114.51
		$H_{\beta 3}$	2.95			$Q_{\delta 1}$	-0.46
		HN	8.25			$Q_{\delta 2}$	-1.07
		N	119.94	53	ALA	H_{α}	4.02
45	THR	H_{α}	4.49			HN	6.97
		HN	8.26			N	120.70
		N	115.42			Q_{β}	1.34
46	VAL	H_{α}	4.15	54	ARG	$H_{\beta 3}$	1.89
		H_{β}	2.63			$H_{\delta 2}$	3.25
		HN	8.43			H_{ε}	7.57
		N	123.65			$H_{\gamma 2}$	1.42
		$Q_{\gamma 1}$	1.43			HN	7.73
		$Q_{\gamma 2}$	1.36			N	124.55
47	ILE	H_{α}	4.72	55	ALA	H_{α}	4.09
		$H_{\beta 2}$	2.24			HN	9.48

		N	117.65			$H_{\delta 2}$	3.22
		Q_{β}	1.41			$H_{\gamma 2}$	1.81
56	ARG	H_{α}	4.23			$H_{\gamma 3}$	1.68
		$H_{\beta 2}$	1.89			HN	8.02
		$H_{\beta 3}$	1.72			N	117.86
		$H_{\delta 2}$	3.31	67	ASP	H_{α}	4.58
		$H_{\delta 3}$	3.35			$H_{\beta 2}$	2.89
		HN	7.01			$H_{\beta 3}$	3.28
		N	115.64			HN	8.22
59	ALA	H_{α}	4.28			N	120.82
		HN	7.53	68	VAL	H_{α}	3.70
		N	122.87			H_{β}	2.55
		Q_{β}	1.64			HN	8.10
60	ASN	H_{α}	5.10			N	121.76
		$H_{\beta 2}$	3.28			$Q_{\gamma 1}$	1.52
		$H_{\beta 3}$	2.88			$Q_{\gamma 2}$	1.19
		$H_{\delta 21}$	7.87	69	ALA	H_{α}	3.89
		$H_{\delta 22}$	7.57			HN	7.99
		HN	7.39			N	119.48
		N	114.96			Q_{β}	1.42
61	GLY	$H_{\alpha 1}$	4.27	70	ALA	H_{α}	4.13
		$H_{\alpha 2}$	3.75			HN	8.08
		HN	7.84			N	117.03
		N	106.20			Q_{β}	1.51
62	ILE	H_{α}	4.22	71	TYR	H_{α}	3.70
		H_{β}	1.91			$H_{\beta 2}$	2.98
		$H_{\gamma 12}$	0.97			HN	8.22
		$H_{\gamma 13}$	1.46			N	122.35
		HN	8.25	72	ILE	H_{α}	2.61
		N	123.73			H_{β}	1.54
		$Q_{\delta 1}$	0.84			$H_{\gamma 12}$	1.60
		$Q_{\gamma 2}$	0.89			$H_{\gamma 13}$	1.18
63	ARG	$H_{\beta 3}$	1.90			HN	7.09
		H_{ε}	7.43			N	106.13
		$H_{\gamma 3}$	1.61			$Q_{\delta 1}$	0.69
64	THR	H_{α}	4.83			$Q_{\gamma 2}$	0.83
		H_{β}	4.09	73	ARG	H_{α}	3.88
		$Q_{\gamma 2}$	1.30			$H_{\beta 2}$	1.83
65	VAL	H_{α}	3.44			$H_{\beta 3}$	1.77
		H_{β}	2.13			$H_{\delta 2}$	3.31
		HN	8.63			$H_{\delta 3}$	3.08
		N	119.67			H_{ε}	6.95
		$Q_{\gamma 2}$	1.13			HN	6.77
66	ARG	H_{α}	3.93			N	114.57
		$H_{\beta 2}$	1.85	74	ASN	H_{α}	4.47
		$H_{\beta 3}$	1.87			$H_{\beta 2}$	2.25

		$H_{\beta 3}$	2.39			$H_{\varepsilon 1}$	7.09
		$H_{\delta 21}$	7.44			$H_{\varepsilon 2}$	7.08
		$H_{\delta 22}$	6.60			HN	8.10
		HN	6.76			HZ	8.24
		N	112.67			N	122.05
75	PRO	H_{α}	2.78	83	GLY	$H_{\alpha 1}$	4.19
		$H_{\beta 2}$	0.06			$H_{\alpha 2}$	3.83
		$H_{\beta 3}$	-0.28			HN	8.36
		$H_{\delta 2}$	2.63			N	111.50
		$H_{\delta 3}$	2.49	84	GLU	H_{α}	3.94
		$H_{\gamma 2}$	0.33			$H_{\beta 3}$	1.93
		$H_{\gamma 3}$	0.49			HN	8.96
76	GLY	$H_{\alpha 1}$	3.99			N	120.26
		$H_{\alpha 2}$	3.67	85	ALA	H_{α}	4.18
		HN	6.65			HN	8.24
		N	102.99			N	118.78
77	PRO	H_{α}	4.05			Q_{β}	1.38
		$H_{\beta 2}$	2.20	86	MET	H_{α}	4.42
		$H_{\beta 3}$	1.93			$H_{\beta 2}$	2.14
		$H_{\delta 3}$	3.55			$H_{\beta 3}$	2.10
78	GLY	$H_{\alpha 1}$	4.29			$H_{\gamma 2}$	2.61
		$H_{\alpha 2}$	3.74			$H_{\gamma 3}$	2.68
		HN	8.60			HN	7.32
		N	109.42			N	116.37
79	MET	H_{α}	3.81	87	ILE	H_{α}	4.58
		$H_{\beta 2}$	-0.54			H_{β}	1.42
		$H_{\beta 3}$	-2.88			$H_{\gamma 12}$	1.14
		$H_{\gamma 2}$	-1.24			$H_{\gamma 13}$	0.69
		$H_{\gamma 3}$	-3.30			HN	7.90
		HN	7.05			N	115.16
		N	122.84			$Q_{\gamma 2}$	0.70
80	PRO	H_{α}	3.65	88	PRO	H_{α}	5.05
		$H_{\beta 2}$	1.67			$H_{\beta 2}$	2.66
		$H_{\beta 3}$	0.89			$H_{\beta 3}$	2.00
		$H_{\delta 2}$	3.58			$H_{\delta 2}$	4.07
		$H_{\delta 3}$	2.72			$H_{\delta 3}$	3.59
		$H_{\gamma 2}$	1.88			$H_{\gamma 2}$	2.14
		$H_{\gamma 3}$	1.75			$H_{\gamma 3}$	2.05
81	ALA	H_{α}	3.41	89	PRO	H_{α}	4.04
		HN	7.06			$H_{\beta 2}$	2.48
		N	117.99			$H_{\delta 3}$	3.71
		Q_{β}	0.84			$H_{\gamma 2}$	2.30
82	PHE	H_{α}	4.36			$H_{\gamma 3}$	2.02
		$H_{\beta 2}$	2.22	90	ALA	H_{α}	4.15
		$H_{\beta 3}$	2.42			HN	9.10
		$H_{\delta 2}$	6.77			N	118.24

		Q_{β}	1.46
91	ASP	H_{α}	4.50
		$H_{\beta 2}$	2.66
		$H_{\beta 3}$	2.72
		HN	7.23
		N	119.17
92	ALA	H_{α}	3.87
		HN	8.29
		N	124.50
		Q_{β}	1.46
93	LEU	H_{α}	4.04
		$H_{\beta 2}$	1.78
		$H_{\beta 3}$	1.80
		H_{γ}	1.69
		HN	7.64
		N	117.10
		$Q_{\delta 1}$	0.93
		$Q_{\delta 2}$	0.87
94	LYS	H_{α}	4.22
		$H_{\beta 2}$	2.17
		$H_{\delta 2}$	1.67
		$H_{\varepsilon 2}$	3.05
		$H_{\varepsilon 3}$	3.01
		HN	7.43
		N	118.83
95	ILE	H_{α}	3.91
		H_{β}	2.26
		$H_{\gamma 12}$	1.58
		HN	8.35
		N	120.60
		$Q_{\delta 1}$	1.09
		$Q_{\gamma 2}$	1.57
96	GLY	$H_{\alpha 1}$	3.93
		$H_{\alpha 2}$	4.04
		HN	8.81
		N	108.06
97	GLU	H_{α}	4.03
		$H_{\gamma 2}$	2.35
		$H_{\gamma 3}$	2.57
		HN	8.95
		N	121.80
98	TYR	Hα	4.08
		$H_{\beta 2}$	3.07
		$H_{\beta 3}$	3.18
		$H_{\delta 1}$	6.67
		$H_{\varepsilon 1}$	6.16
		HN	8.17
		N	121.14
99	VAL	H_{α}	3.46
		H_{β}	2.63
		HN	9.00
		N	122.09
		$Q_{\gamma 1}$	1.67
		$Q_{\gamma 2}$	1.27
100	VAL	H_{α}	3.64
		H_{β}	2.06
		HN	7.99
		$Q_{\gamma 1}$	1.01
		$Q_{\gamma 2}$	0.95
101	ALA	HN	7.84
		Q_{β}	1.30
102	SER	H_{α}	3.75
		$H_{\beta 2}$	2.27
		$H_{\beta 3}$	1.55
		HN	7.23
		N	109.54
103	PHE	H_{α}	5.39
		$H_{\beta 2}$	2.85
		$H_{\beta 3}$	2.78
		$H_{\delta 1}$	7.04
		$H_{\varepsilon 1}$	6.48
		HN	6.83
		HZ	6.53
104	PRO	$H_{\delta 2}$	3.45
		$H_{\delta 3}$	3.81

A.4 NMR backbone, side-chain and heme assignment of PccH in the oxidized state

Table A.4 – Backbone, side-chain and heme assignment of PccH from *G. sulfurreducens* in the oxidized state. Samples prepared in 45 mM NaPi pH 7.5, 100 mM final ionic strength, 25 ºC.

Residue Number	Residue Type	Atom	Chemical shift (ppm)
2	GLU	CO	175.90
		C_α	56.45
		C_β	30.36
		C_γ	36.01
		H_α	4.39
		$H_{\beta2}$	1.96
		$H_{\beta3}$	2.08
		$H_{\gamma2}$	2.09
		$H_{\gamma3}$	2.27
3	VAL	CO	176.19
		C_α	61.92
		C_β	32.58
		$C_{\gamma1}$	21.60
		$C_{\gamma2}$	21.60
		H_α	4.38
		H_β	1.81
		HN	8.24
		N	123.97
		$Q_{\gamma1}$	0.96
		$Q_{\gamma2}$	0.96
4	THR	CO	175.09
		C_α	58.81
		C_β	72.41
		H_α	5.16
		H_β	4.58
		HN	9.57
		N	116.17
5	TYR	CO	176.27
		C_α	60.87
		C_β	39.28
		H_α	3.47
		$H_{\beta2}$	3.43
		HN	9.31
		N	123.80
6	ARG	CO	177.17
		C_α	59.29
		C_β	31.54
		C_δ	43.60
		C_γ	26.30
		H_α	3.37
		$H_{\beta2}$	1.67
		$H_{\delta2}$	2.93
		$H_{\delta3}$	2.97
		HN	8.23
		N	114.83
7	LYS	CO	176.11
		C_α	57.27
		C_β	32.67
		C_δ	28.74
		C_ε	40.90
		C_γ	23.79
		H_α	4.04
		$H_{\beta2}$	1.49
		$H_{\beta3}$	1.88
		$H_{\delta2}$	1.63
		$H_{\delta3}$	1.75
		$H_{\varepsilon2}$	3.02
		$H_{\gamma2}$	1.24
		$H_{\gamma3}$	1.32
		HN	7.25
		N	113.27
8	ASP	CO	176.01
		C_α	55.13
		C_β	44.40
		H_α	4.73
		$H_{\beta2}$	2.28
		$H_{\beta3}$	2.67
		HN	7.40
		N	113.9
9	ILE	CO	176.57
		C_α	59.57
		C_β	34.72
		$C_{\delta1}$	6.96
		$C_{\gamma1}$	23.29
		$C_{\gamma2}$	15.82
		H_α	3.24
		H_β	1.32
		$H_{\gamma12}$	-0.67
		$H_{\gamma13}$	0.39
		HN	7.01
		N	118.30

		$Q_{\delta 1}$	-0.68			C_{β}	39.59
		$Q_{\gamma 2}$	-0.29			H_{α}	3.15
10	LYS	CO	173.91			$H_{\beta 2}$	2.39
		C_{α}	61.08			$H_{\beta 3}$	3.27
		C_{β}	29.33			HN	8.90
		C_{δ}	29.15			N	121.58
		C_{ε}	42.25	14	ASP	CO	176.70
		C_{γ}	24.78			C_{α}	57.20
		H_{α}	3.57			C_{β}	39.82
		$H_{\beta 2}$	0.66			H_{α}	4.54
		$H_{\beta 3}$	1.58			$H_{\beta 2}$	2.66
		$H_{\delta 2}$	1.00			$H_{\beta 3}$	2.69
		$H_{\delta 3}$	1.08			HN	9.30
		$H_{\varepsilon 2}$	3.20			N	119.28
		$H_{\varepsilon 3}$	3.27	15	VAL	CO	177.05
		$H_{\gamma 2}$	1.25			C_{α}	63.38
		$H_{\gamma 3}$	1.39			C_{β}	33.08
		HN	8.53			$C_{\gamma 1}$	20.99
		N	122.43			$C_{\gamma 2}$	21.03
11	PRO	CO	180.03			H_{α}	4.13
		C_{α}	65.80			H_{β}	1.93
		C_{β}	30.95			HN	6.83
		C_{δ}	49.32			N	114.28
		C_{γ}	28.01			$Q_{\gamma 1}$	0.10
		H_{α}	4.32			$Q_{\gamma 2}$	0.87
		$H_{\beta 2}$	1.61	16	ARG	CO	176.65
		$H_{\beta 3}$	2.28			C_{α}	55.08
		$H_{\delta 2}$	2.85			C_{β}	28.98
		$H_{\delta 3}$	3.22			C_{γ}	24.65
		$H_{\gamma 2}$	1.79			H_{α}	3.945
		$H_{\gamma 3}$	1.88			HN	8.266
12	ILE	CO	177.19			N	115.18
		C_{α}	64.17	17	CYS	CO	175.90
		C_{β}	38.64			C_{α}	52.29
		$C_{\delta 1}$	14.05			C_{β}	34.81
		$C_{\gamma 1}$	27.67			H_{α}	2.14
		$C_{\gamma 2}$	16.59			$H_{\beta 2}$	0.25
		H_{α}	3.62			HN	7.46
		H_{β}	1.58			N	113.58
		$H_{\gamma 12}$	1.67	18	ALA	CO	177.93
		HN	6.50			C_{α}	55.77
		N	115.26			C_{β}	19.17
		$Q_{\delta 1}$	0.67			H_{α}	4.35
		$Q_{\gamma 2}$	0.59			HN	6.95
13	PHE	CO	177.82			N	119.03
		C_{α}	62.49			Q_{β}	1.92

19	GLY	CO	174.83			H_{α}	2.96
		C_{α}	46.44			HN	8.62
		$H_{\alpha1}$	3.66			N	125.29
		$H_{\alpha2}$	4.03			Q_{β}	0.60
		HN	8.60	27	PRO	CO	175.92
		N	105.58			C_{α}	65.53
20	CYS	CO	175.49			C_{β}	32.92
		C_{α}	55.05			C_{δ}	50.83
		C_{β}	34.86			C_{γ}	27.84
		H_{α}	5.31			H_{α}	4.62
		$H_{\beta2}$	0.27			$H_{\beta2}$	2.43
		HN	6.73			$H_{\beta3}$	2.95
		N	114.31			$H_{\delta2}$	3.72
21	HIS	CO	177.73			$H_{\gamma2}$	2.30
		C_{α}	46.81			$H_{\gamma3}$	2.64
		HN	9.24	28	GLU	CO	176.82
		N	117.40			C_{α}	52.73
22	GLY	CO	175.58			C_{β}	35.62
		C_{α}	46.18			C_{γ}	36.64
		$H_{\alpha1}$	5.86			H_{α}	5.49
		HN	10.39			$H_{\beta2}$	0.97
		N	120.82			$H_{\beta3}$	1.02
23	ALA	CO	178.49			HN	6.99
		C_{α}	55.11			N	108.15
		C_{β}	19.14	29	TYR	CO	177.76
		H_{α}	4.65			C_{α}	62.70
		HN	9.26			C_{β}	38.99
		N	127.96			H_{α}	4.075
		Q_{β}	1.86			$H_{\beta2}$	2.51
24	ASP	CO	174.32			HN	9.68
		C_{α}	54.16			N	127.51
		C_{β}	41.83	30	HIS	CO	178.06
		H_{α}	5.24			C_{α}	60.10
		$H_{\beta2}$	2.68			C_{β}	31.26
		$H_{\beta3}$	3.05			H_{α}	4.039
		HN	8.52			$H_{\beta2}$	2.57
		N	115.53			$H_{\beta3}$	3.27
25	ALA	CO	177.32			HN	8.93
		C_{α}	51.42			N	114.73
		C_{β}	20.53	31	ALA	CO	178.90
		H_{α}	4.96			C_{α}	54.24
		HN	7.79			C_{β}	18.34
		N	121.99			H_{α}	4.64
		Q_{β}	2.61			HN	6.71
26	ALA	C_{α}	50.36			N	121.00
		C_{β}	16.91			Q_{β}	1.90

32	PHE	CO	175.81			C_γ	23.81
		C_α	60.94			H_α	3.13
		C_β	38.63			$H_{\beta2}$	1.17
		H_α	3.99			$H_{\delta2}$	1.37
		$H_{\beta2}$	2.83			$H_{\varepsilon2}$	2.74
		$H_{\beta3}$	3.40			$H_{\gamma2}$	0.80
		HN	7.56			$H_{\gamma3}$	0.91
		N	118.12			HN	7.16
33	LYS	CO	178.15			N	122.32
		C_α	57.89	37	GLU	CO	178.82
		C_β	31.51			C_α	59.75
		C_δ	27.96			C_β	28.10
		C_ε	41.44			C_γ	36.46
		C_γ	23.78			H	8.62
		H_α	3.38			H_α	3.70
		$H_{\beta2}$	1.60			$H_{\beta2}$	1.86
		$H_{\beta3}$	1.69			$H_{\gamma2}$	2.18
		$H_{\delta2}$	1.41			HN	8.62
		$H_{\varepsilon2}$	2.70			N	115.58
		$H_{\varepsilon3}$	2.87	38	LYS	CO	177.93
		$H_{\gamma2}$	1.03			C_α	58.51
		HN	7.90			C_β	31.65
		N	113.87			C_δ	29.07
34	ALA	CO	178.30			C_ε	41.58
		C_α	53.87			C_γ	23.88
		C_β	19.28			H_α	3.79
		H_α	4.27			$H_{\beta2}$	1.43
		HN	7.41			$H_{\beta3}$	1.59
		N	117.95			$H_{\delta2}$	1.18
		Q_β	1.69			$H_{\delta3}$	1.27
35	GLU	CO	175.71			$H_{\varepsilon2}$	2.45
		C_α	53.87			$H_{\gamma2}$	0.48
		C_β	30.77			$H_{\gamma3}$	0.98
		C_γ	36.50			HN	7.43
		H_α	4.75			N	119.70
		$H_{\beta2}$	2.04	39	TRP	CO	179.01
		$H_{\beta3}$	2.30			C_α	58.96
		$H_{\gamma2}$	2.38			C_β	29.38
		$H_{\gamma3}$	2.33			H_α	4.34
		HN	7.19			$H_{\beta2}$	2.98
		N	117.23			HN	6.92
36	LYS	CO	177.66			N	120.01
		C_α	60.60	40	LEU	CO	181.20
		C_β	32.32			C_α	57.40
		C_δ	29.38			C_β	40.95
		C_ε	41.48			$C_{\delta1}$	21.68

		$C_{\delta 2}$	21.68			$H_{\beta 3}$	2.67
		C_{γ}	25.24			HN	7.29
		H_{α}	3.60			N	116.27
		$H_{\beta 2}$	1.00	45	GLY	C_{α}	44.71
		$H_{\beta 3}$	1.52			$H_{\alpha 1}$	3.87
		H_{γ}	0.41			HN	8.16
		HN	8.85			N	103.69
		N	119.32	46	MET	CO	178.05
		$Q_{\delta 1}$	0.05			C_{α}	56.88
		$Q_{\delta 2}$	0.05			C_{β}	30.73
		$Q_{\gamma 1}$	0.04			C_{γ}	34.61
		$Q_{\gamma 2}$	0.05			H_{α}	6.32
41	ALA	CO	178.63			$H_{\beta 2}$	2.56
		C_{α}	54.48			$H_{\beta 3}$	2.80
		C_{β}	17.65			$H_{\gamma 2}$	4.01
		H_{α}	4.00			$H_{\gamma 3}$	4.47
		HN	7.62			HN	11.80
		N	121.71			N	122.76
		Q_{β}	1.37	47	ARG	CO	177.90
42	LYS	CO	176.13			C_{α}	60.46
		C_{α}	54.89			C_{β}	31.16
		C_{β}	32.82			C_{δ}	44.22
		C_{δ}	29.23			C_{γ}	28.18
		C_{ε}	41.86			H_{α}	5.59
		C_{γ}	24.40			$H_{\beta 2}$	2.43
		H_{α}	4.39			$H_{\beta 3}$	2.89
		$H_{\beta 2}$	1.84			$H_{\delta 2}$	2.75
		$H_{\beta 3}$	2.11			$H_{\delta 3}$	3.51
		$H_{\delta 2}$	1.62			$H_{\gamma 2}$	2.02
		$H_{\delta 3}$	1.69			$H_{\gamma 3}$	2.32
		$H_{\varepsilon 2}$	2.86			HN	10.38
		$H_{\varepsilon 3}$	2.91			N	127.40
		$H_{\gamma 2}$	1.47	48	MET	CO	174.62
		HN	7.08			C_{α}	56.96
		N	114.68			C_{β}	39.80
43	GLY	CO	173.01			C_{γ}	37.20
		C_{α}	44.96			H_{α}	5.74
		$H_{\alpha 1}$	3.46			$H_{\beta 2}$	3.79
		$H_{\alpha 2}$	2.92			$H_{\beta 3}$	4.28
		HN	7.76			$H_{\gamma 2}$	4.07
		N	109.19			$H_{\gamma 3}$	5.34
44	GLN	CO	173.35			HN	11.25
		C_{α}	53.63			N	125.12
		C_{β}	32.32	49	ASP	CO	175.56
		H_{α}	3.52			C_{α}	55.81
		$H_{\beta 2}$	2.09			C_{β}	41.23

		H_{α}	4.56			$C_{\delta 1}$	13.66
		$H_{\beta 2}$	3.74			$C_{\gamma 1}$	24.01
		$H_{\beta 3}$	3.91			$C_{\gamma 2}$	17.18
		HN	9.11			H_{α}	4.17
		N	120.59			H_{β}	2.31
50	THR	CO	173.86			$H_{\gamma 12}$	1.59
		C_{α}	60.32			$H_{\gamma 13}$	1.65
		C_{β}	72.83			HN	8.56
		H_{α}	5.16			N	110.42
		H_{β}	5.32			$Q_{\delta 1}$	0.63
		HN	7.83			$Q_{\gamma 2}$	0.67
		N	108.94	56	PHE	CO	172.35
51	TYR	CO	176.40			C_{α}	58.71
		C_{α}	62.08			C_{β}	39.96
		C_{β}	38.41			H_{α}	4.41
		H_{α}	3.61			$H_{\beta 2}$	3.09
		$H_{\beta 2}$	2.78			$H_{\beta 3}$	3.24
		$H_{\beta 3}$	2.86			HN	6.86
		HN	9.05			N	125.21
		N	122.05	57	TYR	CO	174.25
52	SER	CO	175.29			C_{α}	57.94
		C_{α}	64.34			C_{β}	37.54
		C_{β}	61.50			H_{α}	4.42
		H_{α}	4.12			$H_{\beta 2}$	2.59
		$H_{\beta 2}$	2.44			$H_{\beta 3}$	2.93
		$H_{\beta 3}$	3.06			HN	7.26
		HN	7.80			N	111.49
		N	112.77	58	THR	CO	173.42
53	HIS	CO	177.81			C_{α}	59.21
		C_{α}	62.31			C_{β}	69.26
		C_{β}	31.04			H_{α}	4.24
		H_{α}	4.47			H_{β}	3.61
		$H_{\beta 2}$	3.26			HN	7.65
		HN	9.00			N	108.72
		N	117.82	59	ALA	CO	175.82
54	LEU	CO	179.62			C_{α}	53.80
		C_{α}	58.19			C_{β}	17.02
		C_{β}	31.87			H_{α}	3.69
		C_{γ}	29.25			HN	8.27
		H_{α}	3.79			N	124.79
		$H_{\beta 2}$	1.44			Q_{β}	-0.57
		HN	8.49	60	TRP	CO	170.87
		N	119.51			C_{α}	54.78
55	ILE	CO	177.50			C_{β}	29.62
		C_{α}	65.72			H_{α}	3.57
		C_{β}	37.64			$H_{\beta 2}$	2.90

		HN	6.06			C_γ	25.68
		N	116.17			H_α	2.28
61	PRO	CO	178.19			$H_{\beta2}$	0.67
		C_α	61.94			$H_{\beta3}$	1.24
		C_β	33.18			$H_{\gamma1}$	0.53
		C_δ	49.50			$H_{\gamma2}$	0.74
		C_γ	24.31			HN	9.12
		H_α	2.74			N	115.90
		$H_{\beta2}$	0.46			$Q_{\delta1}$	-0.58
		$H_{\beta3}$	0.65			$Q_{\delta2}$	-0.58
		$H_{\delta2}$	0.85	67	MET	CO	176.56
		$H_{\delta3}$	2.58			C_α	58.62
		$H_{\gamma2}$	-1.04			C_β	32.26
		$H_{\gamma3}$	0.30			C_γ	36.37
62	ASP	CO	173.42			H_α	2.61
		C_α	49.33			$H_{\beta2}$	0.07
		C_β	34.98			$H_{\beta3}$	1.42
		H_α	4.55			$H_{\gamma2}$	1.30
		$H_{\beta2}$	1.59			$H_{\gamma3}$	1.54
		$H_{\beta3}$	2.43			HN	6.35
		HN	7.36			N	112.58
		N	119.70	68	ARG	CO	180.84
63	THR	CO	177.11			C_α	59.84
		C_α	63.39			C_β	31.11
		C_β	69.78			C_γ	28.73
		H_α	3.30			H_α	3.85
		H_β	3.60			HN	8.38
		HN	6.93			N	115.72
		N	112.67	69	ARG	CO	177.83
64	GLY	CO	173.48			C_α	56.47
		C_α	46.22			C_β	30.23
		$H_{\alpha1}$	3.86			HN	8.063
		HN	9.35			N	110.55
		N	114.30	70	LEU	CO	174.19
65	ALA	CO	179.11			C_α	54.01
		C_α	55.87			C_β	41.66
		C_β	19.88			$C_{\delta1}$	20.86
		H_α	3.58			$C_{\delta2}$	20.88
		HN	7.55			C_γ	24.26
		N	126.99			H_α	4.55
		Q_β	1.34			$H_{\beta2}$	1.42
66	LEU	CO	175.71			$H_{\beta3}$	1.71
		C_α	57.25			H_γ	-0.98
		C_β	41.72			HN	7.24
		$C_{\delta1}$	23.61			N	115.10
		$C_{\delta2}$	23.61			$Q_{\delta1}$	-0.89

		$Q_{\delta 2}$	-0.89			C_{β}	65.41
71	ASP	CO	175.42			H_{α}	4.64
		C_{α}	58.34			$H_{\beta 2}$	4.12
		C_{β}	44.18			$H_{\beta 3}$	4.22
		H_{α}	4.52			HN	7.35
		$H_{\beta 2}$	2.74			N	114.93
		$H_{\beta 3}$	3.67	77	LYS	CO	177.10
		HN	7.25			C_{α}	58.69
		N	115.08			C_{β}	31.97
72	ASP	CO	175.81			C_{δ}	28.92
		C_{α}	53.66			C_{ε}	42.02
		C_{β}	40.34			C_{γ}	24.48
		H_{α}	3.41			H_{α}	4.19
		$H_{\beta 2}$	2.22			$H_{\beta 2}$	1.92
		$H_{\beta 3}$	2.65			$H_{\beta 3}$	1.96
		HN	7.11			$H_{\delta 2}$	1.78
		N	118.57			$H_{\varepsilon 2}$	3.08
73	GLY	CO	175.12			$H_{\gamma 2}$	1.56
		C_{α}	44.10			HN	8.38
		$H_{\alpha 1}$	4.20			N	124.22
		$H_{\alpha 2}$	3.46	78	ASP	CO	175.23
		HN	8.61			C_{α}	53.41
		N	109.48			C_{β}	40.27
74	LYS	CO	177.87			H_{α}	4.68
		C_{α}	58.71			$H_{\beta 2}$	2.78
		C_{β}	32.37			$H_{\beta 3}$	3.04
		C_{δ}	28.67			HN	8.34
		C_{ε}	42.07			N	116.89
		C_{γ}	25.72	79	ALA	CO	176.37
		H_{α}	4.14			C_{α}	52.88
		$H_{\delta 2}$	1.74			C_{β}	16.76
		$H_{\varepsilon 2}$	3.02			H_{α}	4.58
		$H_{\gamma 2}$	1.40			HN	7.88
		$H_{\gamma 3}$	1.60			N	118.33
		HN	8.08			Q_{β}	1.56
		N	120.15	80	LYS	CO	174.81
75	ASN	CO	174.05			C_{α}	53.59
		C_{α}	52.96			C_{β}	32.88
		C_{β}	40.91			C_{δ}	29.17
		H_{α}	5.10			C_{ε}	42.40
		$H_{\beta 2}$	2.89			C_{γ}	24.62
		$H_{\beta 3}$	3.03			H_{α}	5.02
		HN	9.21			$H_{\beta 2}$	1.97
		N	114.18			$H_{\beta 3}$	2.10
76	SER	CO	175.75			$H_{\delta 2}$	1.96
		C_{α}	57.06			$H_{\varepsilon 2}$	3.27

		$H_{\gamma 2}$	1.69			$H_{\beta 2}$	2.52
		HN	7.75			$H_{\beta 3}$	2.64
		N	119.07			$H_{\delta 2}$	4.07
81	PRO	CO	179.11			$H_{\delta 3}$	4.11
		C_{α}	62.72			$H_{\gamma 2}$	1.77
		C_{β}	32.68			$H_{\gamma 3}$	2.91
		C_{δ}	51.02			HN	10.27
		C_{γ}	27.29			N	115.12
		H_{α}	4.55	87	HIS	CO	175.94
		$H_{\beta 2}$	2.53			C_{α}	56.79
		$H_{\beta 3}$	2.69			C_{β}	30.75
		$H_{\delta 2}$	4.05			H_{α}	5.01
		$H_{\delta 3}$	4.24			$H_{\beta 2}$	2.81
		$H_{\gamma 2}$	2.29			HN	8.46
		$H_{\gamma 3}$	2.53			N	116.82
82	GLY	CO	178.25	88	LEU	CO	173.96
		C_{α}	46.21			C_{α}	55.90
		$H_{\alpha 1}$	3.48			C_{β}	42.65
		$H_{\alpha 2}$	5.11			$C_{\delta 1}$	23.50
		HN	9.77			$C_{\delta 2}$	23.50
		N	110.16			C_{γ}	26.40
83	ASN	CO	181.50			H_{α}	3.45
		C_{α}	57.59			$H_{\beta 2}$	1.52
		C_{β}	40.23			$H_{\beta 3}$	1.87
		H_{α}	6.77			H_{γ}	0.97
		$H_{\beta 2}$	4.64			HN	8.25
		$H_{\beta 3}$	5.81			N	117.81
		HN	10.75			$Q_{\delta 1}$	0.14
		N	122.29			$Q_{\delta 2}$	0.14
84	MET	CO	178.55	89	GLY	CO	170.36
		C_{α}	60.71			C_{α}	45.10
		HN	12.38			$H_{\alpha 1}$	3.63
		N	118.40			$H_{\alpha 2}$	3.658
85	TYR	CO	178.15			HN	7.19
		C_{α}	62.43			N	103.37
		C_{β}	39.03	90	ALA	CO	177.32
		H_{α}	4.44			C_{α}	52.83
		$H_{\beta 2}$	3.81			C_{β}	20.10
		$H_{\beta 3}$	3.91			H_{α}	4.58
		HN	9.67			HN	9.14
		N	127.47			N	121.47
86	ARG	C_{α}	57.88			Q_{β}	1.60
		C_{β}	29.63	91	THR	CO	174.64
		C_{δ}	44.32			C_{α}	57.86
		C_{γ}	26.02			C_{β}	73.07
		H_{α}	4.30			H_{α}	4.79

		H_β	4.70			C_δ	43.47
		HN	7.33			C_γ	27.06
		N	105.09			H_α	4.10
92	GLU	CO	177.61			$H_{\beta2}$	1.90
		C_α	59.09			$H_{\beta3}$	2.00
		C_β	28.59			$H_{\delta2}$	3.23
		C_γ	35.36			$H_{\gamma2}$	1.58
		H_α	4.40			$H_{\gamma3}$	1.77
		$H_{\beta2}$	2.27			HN	8.02
		$H_{\gamma2}$	2.51			N	122.11
		$H_{\gamma3}$	2.62	98	ASN	CO	178.12
93	GLU	CO	179.03			C_α	55.14
		C_α	60.11			C_β	37.96
		C_β	28.67			H_α	4.72
		C_γ	36.79			$H_{\beta2}$	2.44
		H_α	3.98			$H_{\beta3}$	2.85
		$H_{\beta2}$	1.91			HN	8.27
		$H_{\beta3}$	2.02			N	117.92
		$H_{\gamma2}$	2.25	99	LEU	CO	177.49
		HN	8.82			C_α	58.15
		N	118.41			C_β	41.30
94	GLU	CO	177.85			$C_{\delta1}$	23.63
		C_α	59.16			$C_{\delta2}$	23.63
		C_β	30.87			C_γ	26.42
		C_γ	36.19			H_α	4.00
		H_α	3.93			$H_{\beta2}$	2.07
		$H_{\beta2}$	2.04			H_γ	1.04
		$H_{\gamma2}$	2.44			HN	9.18
		HN	7.71			N	123.99
		N	121.11			$Q_{\delta1}$	0.69
95	ARG	CO	178.54			$Q_{\delta2}$	0.70
		C_α	59.96	100	ALA	CO	180.44
		C_β	28.45			C_α	55.10
		H_α	3.54			C_β	17.32
		$H_{\beta2}$	2.03			H_α	3.82
		HN	8.37			HN	7.60
		N	117.88			N	118.82
96	GLN	CO	179.31			Q_β	1.52
		C_α	58.61	101	VAL	CO	177.87
		C_β	28.76			C_α	66.48
		H_α	3.92			C_β	31.00
		HN	8.70			$C_{\gamma1}$	21.93
		N	116.10			$C_{\gamma2}$	21.95
97	ARG	CO	178.81			H_α	3.68
		C_α	59.39			H_β	2.08
		C_β	29.96			HN	7.29

		N	119.58			HN	7.46
		$Q_{\gamma1}$	1.11			N	106.78
		$Q_{\gamma2}$	0.61	108	VAL	CO	173.23
102	PHE	CO	178.46			C_α	61.03
		C_α	63.73			C_β	33.38
		C_β	39.30			$C_{\gamma1}$	21.28
		H_α	4.07			$C_{\gamma2}$	21.28
		$H_{\beta2}$	2.84			H_α	4.27
		$H_{\beta3}$	3.11			H_β	2.01
		HN	7.68			HN	7.27
		N	118.27			N	118.85
103	LYS	CO	179.04			$Q_{\gamma1}$	0.99
		C_α	60.29			$Q_{\gamma2}$	0.86
		C_β	32.30	109	TRP	CO	172.57
		C_γ	24.96			C_α	55.06
		H_α	4.12			C_β	28.21
		HN	8.60			H_α	4.61
		N	117.71			$H_{\beta2}$	2.79
104	ALA	CO	179.53			$H_{\beta3}$	3.52
		C_α	54.06			HN	8.74
		C_β	18.32			N	128.78
		H_α	4.21	110	ASN	CO	173.66
		HN	7.65			C_α	52.27
		N	120.97			C_β	39.61
		Q_β	1.58			H_α	4.54
105	TRP	CO	177.56			$H_{\beta2}$	2.23
		C_α	60.39			$H_{\beta3}$	2.57
		C_β	28.74			HN	6.64
		H_α	4.20			N	124.83
		$H_{\beta2}$	3.01	111	LEU	CO	178.25
		HN	8.38			C_α	56.71
		N	118.47			C_β	40.85
106	VAL	CO	175.97			$C_{\delta1}$	26.15
		C_α	65.27			$C_{\delta2}$	24.63
		C_β	31.88			C_γ	30.91
		$C_{\gamma1}$	22.95			H_α	4.06
		$C_{\gamma2}$	22.94			$H_{\beta2}$	1.22
		H_α	3.45			$H_{\beta3}$	2.03
		H_β	2.33			H_γ	1.05
		HN	8.45			HN	8.40
		N	114.28			N	125.51
		$Q_{\gamma1}$	1.30			$Q_{\delta1}$	0.73
		$Q_{\gamma2}$	1.09			$Q_{\delta2}$	0.44
107	GLY	CO	174.27	112	LYS	CO	174.56
		C_α	45.95			C_α	58.37
		$H_{\alpha1}$	3.48			C_β	34.76

		C_{δ}	23.68	117	ILE	CO	173.44
		C_{ε}	42.05			C_{α}	61.67
		C_{γ}	26.58			C_{β}	39.65
		H_{α}	3.86			$C_{\delta 1}$	13.33
		$H_{\beta 2}$	1.48			$C_{\gamma 1}$	31.51
		$H_{\beta 3}$	1.72			$C_{\gamma 2}$	15.84
		$H_{\varepsilon 2}$	2.91			H_{α}	4.14
		HN	8.20			H_{β}	1.31
		N	123.18			$H_{\gamma 12}$	1.43
113	LYS	CO	177.56			$H_{\gamma 13}$	1.48
		C_{α}	54.73			HN	7.12
		C_{β}	34.83			N	122.56
		C_{ε}	41.98			$Q_{\delta 1}$	0.53
		C_{γ}	26.68			$Q_{\gamma 2}$	0.76
		H_{α}	4.40	118	THR	CO	175.53
		$H_{\beta 2}$	2.09			C_{α}	59.99
		$H_{\gamma 2}$	1.58			C_{β}	72.14
		$H_{\gamma 3}$	1.35			H_{α}	4.52
		HN	8.02			H_{β}	4.59
		N	113.91			HN	8.15
114	TRP	CO	174.41			N	116.07
		C_{α}	60.34	119	LYS	CO	176.77
		C_{β}	27.59			C_{α}	58.10
		H_{α}	4.64			C_{β}	32.42
		$H_{\beta 2}$	3.31			C_{γ}	23.60
		$H_{\beta 3}$	3.85			H_{α}	3.88
		HN	8.92			HN	9.31
		N	120.61			N	121.64
115	PRO	CO	176.46	120	GLU	CO	179.57
		C_{α}	65.28			C_{α}	60.14
		C_{β}	30.90			C_{β}	28.84
		C_{δ}	50.21			C_{γ}	36.41
		C_{γ}	28.26			H_{α}	4.05
		H_{α}	4.11			$H_{\beta 2}$	2.14
		$H_{\beta 2}$	2.33			$H_{\gamma 2}$	2.37
		$H_{\delta 2}$	3.47			$H_{\gamma 3}$	2.37
		$H_{\delta 3}$	4.12			HN	8.83
		$H_{\gamma 2}$	2.06			N	117.11
116	ASP	CO	175.62	121	GLU	CO	179.74
		C_{α}	54.09			C_{α}	58.89
		C_{β}	42.87			C_{β}	30.46
		H_{α}	4.65			C_{γ}	38.05
		$H_{\beta 2}$	2.44			H_{α}	3.98
		$H_{\beta 3}$	2.77			$H_{\beta 2}$	1.79
		HN	7.15			$H_{\gamma 2}$	2.21
		N	111.21			HN	7.37

		N	118.69			HN	8.18
122	LEU	C_α	57.80			N	120.19
		C_β	42.73	127	VAL	CO	174.73
		$C_{\delta1}$	25.79			C_α	59.79
		$C_{\delta2}$	25.85			Cβ	32.89
		Cγ	25.86			$C_{\gamma1}$	22.00
		H_α	3.85			$C_{\gamma2}$	19.19
		$H_{\beta2}$	1.44			H_α	2.09
		$H_{\beta3}$	2.33			HN	6.89
		H_γ	0.89			N	110.45
		HN	8.18			$Q_{\gamma1}$	0.84
		N	120.22			$Q_{\gamma2}$	-0.13
		$Q_{\delta1}$	0.75	128	THR	CO	175.86
123	ASN	CO	175.31			C_α	65.56
		C_α	54.78			C_β	69.33
		C_β	38.26			H_α	4.00
		$H_{\beta2}$	2.99			H_β	4.25
		$H_{\beta3}$	3.10			HN	8.74
		HN	8.46			N	118.02
		N	116.94	129	TYR	CO	179.44
124	ALA	CO	176.07			C_α	61.68
		C_α	51.98			C_β	38.62
		C_β	19.24			H_α	3.58
		H_α	4.36			$H_{\beta2}$	2.78
		HN	7.21			$H_{\beta3}$	2.85
		N	119.15			HN	9.06
		Q_β	1.55			N	136.54
125	ILE	CO	176.09		HEME	13^1CH_2	2.10
		C_α	60.58				9.97
		C_β	36.14			17^1CH_2	9.67
		$C_{\delta1}$	12.41				11.89
		$C_{\gamma1}$	27.35			13^2CH_2	-0.89
		$C_{\gamma2}$	17.28				2.55
		H_β	1.96			17^2CH_2	0.61
		$H_{\gamma12}$	1.05				0.37
		$H_{\gamma13}$	1.60			15H	7.25
		HN	7.20			2^1CH_3	15.62
		N	119.63			7^1CH_3	22.97
		$Q_{\delta1}$	0.57			12^1CH_3	18.55
		$Q_{\gamma2}$	0.92			18^1CH_3	25.92
126	THR	CO	175.62			3^2CH_3	0.28
		C_α	63.55			8^2CH_3	1.08
		C_β	68.32				
		C_γ	21.57				
		H_α	4.23				
		H_β	4.17				

A.5 Binding curves for OmcF and PpcA heme methyl groups, in the presence of the other cytochrome.

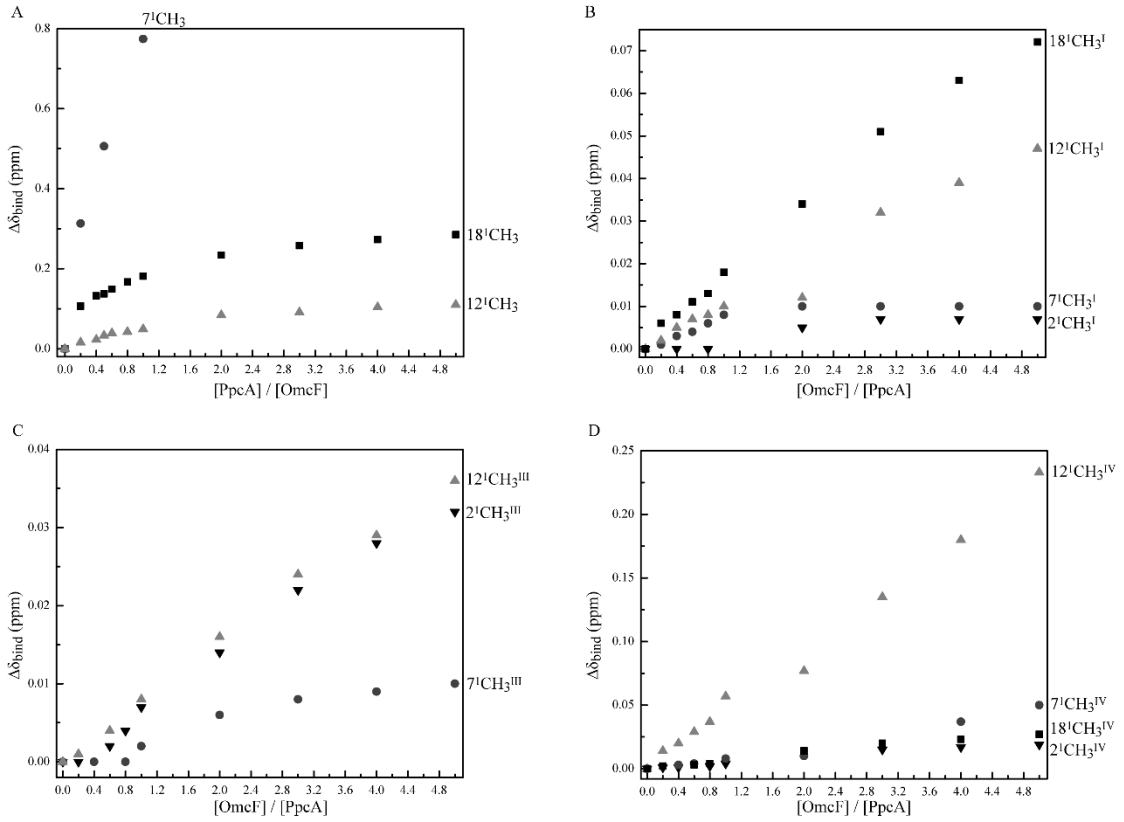

Figure A.1 - Binding curves of the methyl groups of OmcF and PccA (A), and vice-versa (B, C and D for heme I, III and IV, respectively). Comparison of the ^{1}H chemical shifts of the heme methyl groups observed in the 1D ^{1}H NMR spectra of cytochrome OmcF (δ_{OmcF}) and those of PpcA (δ_{PpcA}).

A.6 Binding curves for GSU2515 and PccH heme methyl groups, in the presence of the other cytochrome.

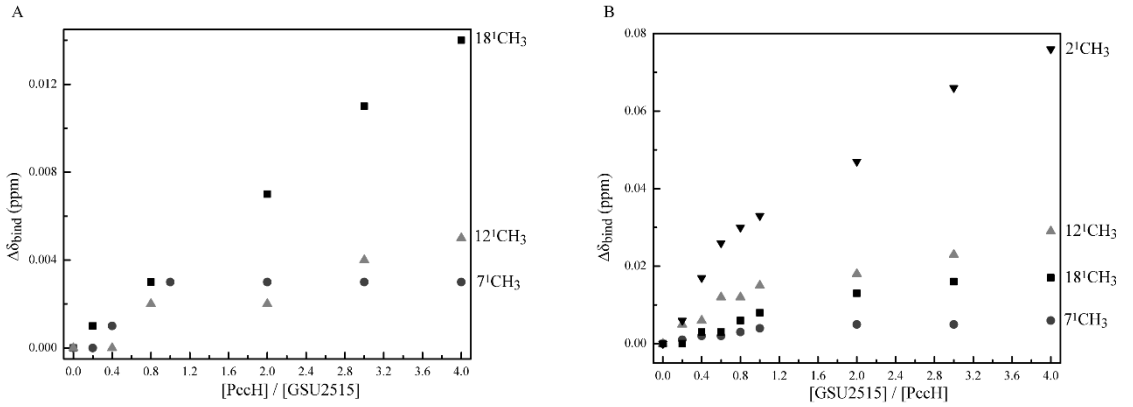

Figure A.2 – Binding curves of the methyl groups of GSU2515 and PccH (A), and vice-versa (B). Comparison of the ^{1}H chemical shifts of the heme methyl groups observed in the 1D ^{1}H NMR spectra of cytochrome GSU2515 ($\delta_{GSU2515}$) and those of PccH (δ_{PccH}).